Investigating the Gasket Function and Perforin Secretion of the Natural Killer Cell Immune Synapse

Adam Cartwright

Imperial College London

Department of Cell and Molecular Biology

Supervised by Professor Daniel M. Davis

Submitted for the Degree of Doctor of Philosophy

2014

Abstract

Natural Killer (NK) cells interact with other cells through a structured interface, the immune synapse (IS). A balance of signals controls NK cell activity through ligation of activating and inhibitory receptors. If signaling favours activation, NK cells mediate the directed secretion of cytotoxic mediators, such as perforin (PFN). To test whether the IS also functions as a gasket to extracellular molecules, fluorescently labeled nanometer-scale dextrans of varying sizes were co-incubated with effector-target cell-cell conjugates. Quantitative fluorescence microscopy of synapses revealed that dextrans with hydrodynamic diameters ≥32 nm were excluded from activating synapses, whilst smaller dextrans could enter. Size-dependent exclusion required an intact filamentous actin scaffold, but not continuous reorganisation following synapse formation. Time-lapse microscopy further revealed that the synapse assembles in a zipper-like manner, clearing larger dextran from the synapse. In addition, monoclonal antibodies and low-density lipoproteins were also excluded from the IS, whereas smaller domain antibodies could penetrate. NK cells can lyse more than one target in series. Whilst it is known that, among other proteins, PFN is secreted to lyse diseased cells, the amount of PFN secreted by NK cells is currently unknown. To quantify PFN release following stimulation through NKG2D or CD16, NK cells were plated on protein-coated surfaces that could capture PFN. Quantification using fluorescence microscopy revealed that PFN secretion was analogue, varying with increased ligand density. Simulating serial killing, repeated stimulation decreased the amount of PFN secreted with sequential activation. Unexpectedly, CD16 stimulation following serial NKG2D ligation recovered this decrease in secretion, however a similar recovery was not seen under reciprocal conditions. These data show that the activating IS clears and excludes extracellular molecules, including antibodies, in a size-dependent manner. Further, NK cell PFN secretion is an analogue response that varies with both ligand density and the receptors ligated in series.

Author declaration

I declare that myself have composed the data and contents of this thesis and the work described is my own, with the following exception:

- In Chapter 3, Stefan Balint measured cell migration speed using Kaleidoscope software and wrote the colour-coded tracking macros

- In Chapter 4, the domain antibody used was purified with the help of Emily Dinley at GlaxoSmithKline, Stevenage, UK.

Adam Cartwright

Copyright declaration

The copyright of this thesis rests with the author and is made available under a Creative Commons Attribution Non-Commercial No Derivatives license. Researchers are free to copy, distribute or transmit the thesis on the condition that they attribute it, that they do not use it for commercial purposes and that they do not later, transform or build upon it. For any reuse or redistribution, researchers must make clear to others the license terms of this work.

Publications

The immune synapse clears and excludes molecules above a size threshold. ***Adam Cartwright***, Jeremy Griggs and Daniel M. Davis*. Nature Communications* (in press)

The central role of the cytoskeleton in mechanisms and functions of the NK cell immune synapse Kathryn Lagrue, Alex Carisey, Anna Oszmiana, Philippa R. Kennedy, David J. Williamson, **Adam Cartwright**, Charlotte Barthen, Daniel M. Davis *Immunological Reviews* (2013) 265(1); 203-221

Acknowledgements

First and foremost I would like to thank my supervisor, Daniel M. Davis. Not only for the opportunity to work in your laboratory, but for your guidance, advice, encouragement and the freedom to investigate and explore. More besides, I would like to thank you for the help you have provided with writing papers, critiquing my work and for reading my thesis. Without your help, I would not be the scientist I am today.

Secondly, I would like to thank Jeremy Griggs, my industry supervisor, who made me feel extremely welcome during my time at GlaxoSmithKline and has provided advice, discussions and comments throughout my PhD in my laboratory work, presentations, publications and thesis. I would also like to thank Thomas Southgate and Simon Chell for their advice and assistance during the final months of the PhD and for reading my manuscript and thesis.

I am thoroughly grateful to the members of the Davis lab, past and present, who have supported me and provided me with engaging discussions, invaluable advice and an excellent and enjoyable environment for conducting research. I would like to give special thanks to Sophie Pageon, Dominika Rudnicka, Anne Aucher and Shaun-Paul Cordoba, and Ania Oszmiana. We have become close friends not only at work, but outside of the lab too and your support during my PhD will never be forgotten. I would also like to thank Stefan Balint, Alex Carisey and Dave Williamson who assisted me with data analysis, and Alice Brown who mentored me during the first year of my PhD.

Thanks to my advisors, Professors Salim Kahkoo and Tony Magee and Doctor Crintina Lo-Celso for your help and support throughout my PhD.

Thank you to my friends from outside the lab. In particular, Jonathan Crowe, without whom, London would not have been the same! Special thanks to my best friends Lee Kearney, Andrew Tombs and Matthew Whittaker, for not only being the greatest friends I have ever had, but for providing an escape from the lab!

I would like to say a special thanks to my girlfriend, Lauren Webb, for assistance with flow cytometry analysis, but, most importantly, you have been a great support and help during the final year of my PhD and the writing of my thesis, respectively. You have been the best girlfriend, friend and scientific companion.

Last, but not at all least, I would like to thank all my family, including my father, Nigel Cartwright; my stepfather, Robert Brasher; and my grandparents, Pat and Ray Williams. Finally, special thanks go to my mother, Debbie Brasher. Visiting home was always a welcome pleasure and your help throughout my PhD in all manners has been truly valued. There is too much that you have done for me to list everything, so I would just like to offer the greatest thanks to you. Unfortunately, I could not possibly list every single person who deserves an acknowledgement, but you will know who you are and know that your presence in my life has been highly valued.

Funding was provided by the Biotechnology and Biological Sciences Research Council (BBSRC) and GlaxoSmithKline (GSK)

Contents

Abstract.....3
Author Declaration.....4
Copyright Declaration.....4
Publications.....4
Acknowledgements.....7
Contents.....9
Abbreviations.....13
List of Figures.....18
List of Tables.....24

1. Introduction.....26
1.1. Natural Killer cells.....26
1.1.1. NK cell development and licensing.....28
1.1.2. Bridging the gap between innate and adaptive immunity.....33
1.2. The immune synapse.....34
1.2.1. The inhibitory synapse.....37
1.2.2. The activating synapse.....41
1.2.3. Polarisation and directed secretion at the immune synapse.....45
1.2.4. The T cell synapse.....51
1.2.5. The size-dependent kinetic segregation model.....54
1.3. Cytotoxic mediators and target cell death.....56
1.3.1. Lytic granules.....56
1.3.2. Perforin.....57
1.3.3. Granzymes.....60
1.3.4. Target cell death by cytotoxic mediators.....62
1.4. NK cells and disease.....66
1.4.1. Anti-tumour therapies.....66
1.4.2. Dysregulation and auto-immunity.....69
1.5. The immune synapse gasket.....71
1.6. Fluorescence microscopy.....73
1.6.1. Basic principles of confocal microscopy.....73
1.6.2. Limitations of confocal microscopy.....79

1.6.3. Basic principles of total internal reflection fluorescence microscopy.....81
1.7. Aims and hypothesis.....83
2. Materials and Methods.....85
2.1. Cells and cell culture.....85
2.1.1. Immortalised cell lines.....85
2.1.2. Primary human NK cells.....86
2.2. Dextran.....87
2.3. Antibodies and proteins.....89
2.3.1. Monoclonal antibodies.....89
2.3.2. F(ab')2 fragments.....90
2.3.3. Domain antibodies.....90
2.3.4. Electrophoresis of antibodies.....91
2.3.5. Proteins.....92
2.4. Flow cytometry.....93
2.5. Microscopy.....94
2.6. Molecule access into the immune synapse.....95
2.6.1. Live cell confocal imaging of molecules within the immune synapse.....95
2.6.2. Time-lapse imaging of molecules within the immune synapse.....96
2.6.3. Time-lapse total internal reflection fluorescence microscopy of molecules clearance from the cell-slide interface.....97
2.6.4. Confocal imaging of antibody access into the cell-slide interface.....97
2.6.5. Cell migration assay.....98
2.7. NK cell activation/degranulation and perforin capture.....98
2.7.1. Perforin capture assay.....98
2.7.2. NK cell serial activation.....99
2.7.3. Estimation of molecule number from fluorescence intensity.....99
2.8. Data analysis.....100
2.8.1. Molecule penetration of the immune synapse.....100
2.8.2. Perforin secretion analysis.....105
2.8.3. Statistical analysis.....108
3. The Immune Synapse Clears and Excludes Molecules Above a Size Threshold.....109

3.1. Introduction.....109
3.1.1. The immune synapse gasket.....109
3.1.2. The physical properties of dextran.....110
3.1.3. Aims.....111
3.2. Results.....112
3.2.1. Dextran access to the NK cell activating immune synapse is
3.2.2. size-dependent.....112
3.2.3. Dextran access to the T cell immune synapse is size-dependent....129
3.2.4. The inhibitory synapse does not exclude extracellular molecules....131
3.2.5. Dextran below the size exclusion threshold moves freely into
and out of the immune synapse.....134
3.2.6. Intact actin is required to exclude dextran from the
immune synapse.....139
3.2.7. Dextran is cleared from the immune synapse during assembly.....149
3.3. Discussion.....155
3.3.1. Summary.....155
3.3.2. Implications of findings.....156
4. Size-dependent Exclusion of Functional Proteins from the Immune Synapse.....166
4.1. Introduction.....166
4.1.1. Antibodies and fragments.....166
4.1.2. Current immunotherapies and their limitations.....168
4.1.3. Aims.....170
4.2. Results.....171
4.2.1. Production of a domain antibody.....171
4.2.2. The NK cell immune synapse restricts the access of antibodies
in a size-dependent manner.....172
4.2.3. Monoclonal IgG antibodies against perforin are unable to
access the immune synapse.....175
4.2.4. Low-density lipoproteins are excluded from the primary
NK cell immune synapse but not from the activating or
inhibitory YTS cell immune synapse.....178
4.3. Discussion.....181
4.3.1. Summary.....181

4.3.2. Implications of findings.....182
5. NK Cell Perforin Secretion Varies with Ligand Density and Serial Stimulation.....186
5.1. Introduction.....186
5.1.1. NK cell serial killing and redirected lysis.....186
5.1.2. Aims.....188
5.2. Results.....189
5.2.1. NK cell perforin secretion begins within three minutes of activation.....192
5.2.2. The amount of perforin secreted by NK cells varies with ligand density.....195
5.2.3. The amount of perforin secreted by NK cells decreases with subsequent serial stimulations.....198
5.2.4. Effective restimulation of NK cells is receptor dependent.....201
5.2.5. Serial stimulation affects the expression of NK cell receptors.....209
5.2.6. Estimation of perforin secretion by NK cells.....215
5.3. Discussion.....217
5.3.1. Summary.....217
5.3.2. Implications of findings.....218
6. Discussion and Conclusions.....230
6.1. Overview.....230
6.2. The immune synapse clears and excludes molecules in a size-dependent manner.....232
6.3. The amount of perforin secreted at the immune synapse is ligand type- and density-dependent.....240
6.4. Future work.....247
6.4.1. Clearance and exclusion from the immune synapse.....247
6.4.2. Perforin secretion at the NK cell immune synapse.....250
6.5. Long term developments.....255
6.6. Concluding Remarks.....258

References.....259

Abbreviations

221	721.221 EBV-transformed B cell line
221-Cw6	221 cells expressing HLA-Cw6
ABC	Antibody binding coefficient
ADCC	Antibody-dependent cellular cytotoxicity
AF	Alexa Fluor
APC	Antigen presenting cell
BM	Bone marrow
Ca^{2+}	Calcium ion
CD	Cluster of differentiation
CM	Conjugation medium
cSMAC	Central supramolecular activation cluster
dAb	Domain antibody
DAP10	DNAX activating protein of 10/12 kDa
DC	Dendritic cell
DM	Diabetes mellitus
DMEM	Dulbecco's Modified Eagle's Medium
DMSO	Dimethyl sulfoxide
DNA	Deoxyribonucleic acid
DNAM1	DNAX accessory molecule 1
dSMAC	Distal supramolecular activation cluster
EBV	Epstein-Barr virus
EEA-1	Early endosomal antigen-1
EGF	Epidermal growth factor
ER	Endoplasmic reticulum
ERK	Extracellular signal-related kinase
F(ab')2	F(ab')2 fragment of IgG antibody
FasL	Fas ligand
FCS	Foetal calf serum
FcγR	Fcγ receptor
FITC	Fluorescein isothiocyanate
FWHM	Full-width half maximum
GPVI	Glycoprotein VI

Gzm	Granzyme
HLA	Human leukocyte antigen
HSC	Haematopoietic stem cells
ICAM-1	Intercellular adhesion molecule 1
IFN-γ	Interferon-γ
IgG	Immunoglobulin G
IL	Interleukin
IS	Immune synapse
ITAM	Immunoreceptor tyrosine-based activation motif
ITIM	Immunoreceptor tyrosine-based inhibition motif
IQGAP1	IQ motif-containing GTPase-activating protein 1
JNK	c-Jun N-terminal kinase
KD	Knockdown
KIR	Killer Immunoglobulin-like receptor
KLRB1A	Killer cell lectin-like receptor subfamily B member 1
KO	Knockout
KS	Kinetic-segregation
LAIR	Leukocyte-associated immunoglobulin-like receptor
LB	Luria Bertani
LFA-1	Leukocyte function-associated molecule 1
LG	Lytic granule
LIR	Leukocyte immunoglobulin-like receptor
LLT-1	Lecitn-like transcript
LN	Lymph node
M6PR	Mannose-6-phosphate receptor
mAb	Monoclonal antibody
MACPF	Membrane attack complex/perforin
MHC	Major histocompatibility complex
MIC	MHC class I chain-related
MMR	Membrane repair response
mRNA	Messenger RNA
MS	Multiple sclerosis
MT	Microtubules
MTOC	Microtubule organizing centre
NA	Numerical aperture

NCR	Natural cytotoxicity receptor
ND	Not defined
NIH	National Institutes of Health
NK	Natural Killer
NKG2D	NK group 2 member D
NS	Non-significant
OD	Optical density
PBMC	Peripheral blood mononuclear cell
PBS	Phosphate buffered saline
PFA	Paraformaldehyde
PFN	Perforin
PFN-SG	Perforin-serglycin complex
PI3K	Phosphoinositide 3-kinase
PKC-θ	Protein kinase C-θ
PKC-ζ	Protein kinase-C-ζ
PLC-γ	Phospholipase C-γ
PLL	Poly-L-lysine
pNK	Primary human NK cell
PSF	Point spread function
pSMAC	Peripheral supramolecular activation cluster
PVR	Poliovirus receptor
QSC	Quantum simply cellular
R10	Supplemented RPMI-1640 (with 10% FCS)
RA	Rheumatoid arthritis
RNA	Ribonucleic acid
RPM	Revolutions per minute
SD	Standard deviation
SG	Serglycin
SH2	Src homology 2
SHIP	SH2 domain-containing inositol phosphatase
SHP-1/SHP-2	SH2 domain-containing tyrosine phosphatases 1 and 2
SIM	Structured illumination microscopy
siRNA	Small interfering RNA
SLE	Systemic lupus erythematous
SLP-76	SH2 domain-containing leukocyte protein of 76 kDa

SMAC	Supramolecular activation cluster
SNARE	N-ethylmaleimide-sensitive protein attachment protein receptor
TCR	T cell receptor
Th1	T helper cell type 1
Th2	T helper cell type 2
TIGIT	T cell immunoglobulin-like receptor
TNF	Tumour necrosis factor
TRAIL	TNF-related apoptosis-inducing ligand
Treg	Regulatory T cell
ULBP	UL16-binding protein
UV	Ultra violet
VAMP7	Vesicle-associated membrane protein 7
WIP	WASp-interacting protein
YTS-KIR2DL1	YTS cells expressing KIR2DL1
ZAP-70	Zeta-chain-associated protein kinase of 70 kDa
$\Delta\Psi_m$	Membrane potential change

.

List of Figures

Figure 1.1 NK cell recognition of target cell health
Figure 1.2. NK cell development
Figure 1.3. NK cell licensing and education
Figure 1.4. The classical structure of the immune synapse
Figure 1.5. The density of MHC class I proteins determines its organisation at the NK cell synapse
Figure 1.6. NK cell integrin signalling pathways
Figure 1.7. NK cell inhibitory signalling pathways
Figure 1.8. NK cell activating signalling pathways
Figure 1.9. Polarisation and directed secretion at the NK cell immune synapse
Figure 1.10. Secretion at the NK cell immune synapse occurs in two modes: Complete and incomplete fusion
Figure 1.11. The structure and organisation of the mature T cell immune synapse
Figure 1.12. T cell activating signalling pathways
Figure 1.13. Size-dependent segregation at the immune synapse
Figure 1.14. The structure and pore formation of perforin
Figure 1.15. Granzyme B initiates apoptosis through both caspase-dependent and caspase-independent pathways
Figure 1.16. Calcium-dependent endosomal uptake of granzyme B into the target cell
Figure 1.17. Schematic diagram of a fluorescence wide-field microscope
Figure 1.18. Schematic diagram of a laser scanning confocal microscope
Figure 1.19. Schematic diagrams of confocal microscope detectors
Figure 1.20. Electronic states of fluorophore excitation and emission
Figure 1.21. The point spread function (PSF) of a microscope
Figure 1.22. Schematic diagram of total internal reflection fluorescence (TIRF) microscopy

Figure 2.1. Analysis of fluorescence intensity within the immune synapse
Figure 2.2. Analysis of Phalloidin-stained actin fluorescence intensity
Figure 2.3. Analysis of fluorescence intensity within the immune synapse at a cell-slide interface

Figure 2.4. Analysis of dextran clearance from the cell-slide interface

Figure 2.5. Analysis of antibody penetration at a cell-slide interface

Figure 2.6. Analysis of perforin secretion by NK cells on activating slides

Figure 2.7. Estimation of number of molecules from fluorescence intensity

Figure 3.1. Dextran entry onto the immune synapse formed by YTS cells is size-dependent

Figure 3.2. Raw intensity profiles of various sized dextran across activating synapses formed by YTS cells

Figure 3.3. Dextran entry onto the immune synapse formed by primary human NK cells is size-dependent

Figure 3.4. Raw intensity profiles of various sized dextran across activating synapses formed by primary human NK cells

Figure 3.5. Dextran entry into the immune synapse is not affected by the degree of labelling

Figure 3.6. Microscope settings do not introduce artefacts for analysis of entry of molecules into the immune synapse

Figure 3.7. Dextran concentration does not affect the analysis of entry into the immune synapse

Figure 3.8. Entry into the immune synapse formed by YTS cells is not affected by dextran charge

Figure 3.9. Entry into the immune synapse formed by primary human NK cells is not affected by dextran charge

Figure 3.10. Dextran entry into the immune synapse formed by primary human NK cells and Daudi target cells is size-dependent

Figure 3.11. Dextran entry into the immune synapse formed by primary human NK cells and K562 target cells is size-dependent

Figure 3.12. Dextran entry into the immune synapse formed by Jurkat T cells and Raji target cells is size-dependent

Figure 3.13. Flow cytometric analysis of YTS cells and 221 cells transfected with KIR2DL1 and HLA-Cw6 respectively

Figure 3.14. Dextran entry into the inhibitory immune synapse formed by YTS/KIR cells and 221/Cw6 cells is not size-dependent

Figure 3.15. Raw intensity profiles of various sized dextrans across inhibitory synapses formed by YTS/KIR cells

Figure 3.16. Dextran is excluded from formed immune synapses in a size-dependent manner

Figure 3.17. Dextran within the immune synapse equilibrates with the concentration in the extracellular solution

Figure 3.18. Dextran can be washed out of the immune synapse formed by YTS cells

Figure 3.19. Dextran can be washed out of the immune synapse formed by primary human NK cells

Figure 3.20. Latrunculin A depolymerises actin in primary human NK cells and 221 target cells

Figure 3.21. Jasplakinolide reduces NK cell migration by stabilising actin filaments

Figure 3.22. Latrunculin A and Jasplakinolide are not detrimental to the health of primary human NK cells, YTS cells or 221 cells

Figure 3.23. Dextran is excluded from the primary human NK cell immune synapse when actin remains intact

Figure 3.24. Dextran is excluded from the YTS NK cell immune synapse when actin remains intact

Figure 3.25. Depolymerisation of actin abolishes the exclusion of dextran from the primary human NK cell immune synapse

Figure 3.26. Depolymerisation of actin abolishes the exclusion of dextran from the YTS cell immune synapse

Figure 3.27. Stabilisation of actin maintains the exclusion of dextran from the primary human NK cell immune synapse

Figure 3.28. Stabilisation of actin maintains the exclusion of dextran from the YTS cell immune synapse

Figure 3.29. Larger dextran is cleared from the YTS cell immune synapse during assembly

Figure 3.30. Larger dextran is cleared from the primary human NK cell immune synapse during assembly

Figure 3.31. The primary human NK cell clears larger dextran from the immune synapse as it assembles in a ‘zipper-like’ fashion

Figure 4.1. Schematic diagrams of the structures of a monoclonal antibody (mAb), a $F(ab')_2$ fragment and a domain antibody (dAb).

Figure 4.2. SDS-PAGE of bacterially expressed anti-glycoprotein VI domain antibodies

Figure 4.3. SDS-PAGE of a goat anti-murine IgG monoclonal antibody, a goat anti-murine IgG $F(ab')_2$ fragment and an anti-glycoprotein VI domain antibody (dAb)

Figure 4.4. Antibody entry into the YTS cell immune synapse is size-dependent

Figure 4.5. Antibody entry into the primary human NK cell immune synapse is size-dependent

Figure 4.6. Perforin secreted by primary human NK cells can be captured on an activating surface

Figure 4.7. The primary human NK cell immune synapse excludes anti-perforin antibodies

Figure 4.8. Low-density lipoproteins (LDL) are excluded from the activating immune synapse but not the inhibitory immune synapse

Figure 5.1. NK cell degranulation is induced through CD16 alone whereas NKG2D requires LFA1 co-ligation

Figure 5.2. NK cells activated though NKG2D/LFA1 secrete perforin within three minutes of activation

Figure 5.3. NK cells activated though CD16/LFA1 secrete perforin within three minutes of activation

Figure 5.4. The amount of perforin secreted by NK cells varies with density of activating ligand MICA-Fc

Figure 5.5. The amount of perforin secreted by NK cells varies with density of activating ligand anti-CD16 antibody

Figure 5.6. NK cells secrete reducing amounts of perforin following serial stimulation through NKG2D/LFA1

Figure 5.7. NK cells secrete reducing amounts of perforin following serial stimulation through CD16/LFA1

Figure 5.8. Serial stimulation through NKG2D/LFA1 does not affect subsequent stimulation though CD16/LFA1

Figure 5.9. Serial stimulation through CD16/LFA1 reduces subsequent stimulation though NKG2D/LFA1

Figure 5.10. Serial stimulation through NKG2D/LFA1 affects continued stimulation though the same receptors but not CD16/LFA1 stimulation

Figure 5.11. Serial stimulation through CD16/LFA1 affects further stimulation through both NKG2D/LFA1 and CD16/LFA1

Figure 5.12. NKG2D expression is not affected by single receptor ligation whereas CD16 is affected by ligation of either MICA-Fc or anti-CD16

Figure 5.13. NK cell surface expression of NKG2D is down regulated following serial stimulation through either NKG2D/LFA1 or CD16/LFA1

Figure 5.14. NK cell surface expression of CD16 is down regulated following serial stimulation through either NKG2D/LFA1 or CD16/LFA1

Figure 6.1. NK cell size-dependent exclusion of dextran molecules of various sizes from the activating immune synapse

Figure 6.2. The NK cell activating immune synapse clears and excludes larger molecules during cell spreading and assembly

Figure 6.3. NK cell size-dependent exclusion of proteins of various sizes from the activating immune synapse

Figure 6.4. Domain antibodies can access the immune synapse and could be used to target proteins secreted across the synaptic cleft

Figure 6.5. NK cells secrete greater amounts of perforin in response to increased ligand density

Figure 6.6. ADCC-mediated cytolysis could be used to promote NK cell-mediated serial lysis efficiency

List of Tables

Table 1.1 NK cell inhibitory receptors

Table 1.2 NK cell activating receptors

Table 1.3. Granzymes expressed within NK cells, their enzyme type and substrates

Table 2.1. Dextran molecular weights, hydrodynamic diameters, fluorophores, excitation/emission maxima, and working concentrations

Table 2.2. Antibodies used for the study of size exclusion and receptor expression and for NK cell activation

Table 2.3. Recombinant and chimera proteins used for perforin quantification and NK cell activation

Table 2.4. The working concentrations of molecules used to assess size-dependent entry into the immune synapse

Table 2.5. Bead populations and their corresponding antibody binding coefficient (ABC)

Table 5.1. Control surface coatings used for protein capture assay (Figure 5.1)

Table 5.2. Pattern of activating surface coating used to test restimulation of NK cells (Figure 5.8)

Table 5.3. Pattern of activating surface coating used to test restimulation of NK cells (Figure 5.9)

Table 5.4. Pattern of activating surface coating used and percentage of total NK cells plated to test restimulation of NK cells (Figure 5.10)

Table 5.5. Pattern of activating surface coating used and percentage of total NK cells plated to test restimulation of NK cells (Figure 5.11)

Chapter 1 – Introduction

1.1 Natural Killer cells

Human Natural Killer (NK) cells are large granular lymphocytes (1, 2), comprising between 2 – 18% of total peripheral blood cells and are phenotypically defined as $CD56^{+}$, $NKp46^{+}$ and $CD3^{-}$ (3-5). Considered part of the innate immune system, NK cells are activated via germ-line encoded receptors, exerting cytotoxicity without prior priming, and secrete cytokines that activate and stimulate other immune cells (6-8). NK cells, and indeed a variety of other immune cells, interact with target cells through an organised, structured interface termed the immune synapse (IS) (9, 10). Through these cell-cell contacts, NK cells can discriminate between healthy or diseased cells via a balance of activating or inhibitory signals, where the dominating signal determines the NK cell response (11, 12). Ligation of inhibitory 'self molecules' on healthy cells instructs the NK cell to not lyse its target, whereas ligation of activating 'stress-induced' or 'non-self' ligands lead to cytolysis of the target cell (9, 13) (Figure 1.1). In addition to the surveying of target cell health, regulatory functions can also be mediated through the IS, termed a regulatory synapse. NK cell interactions with other immune cells, such as T cells and dendritic cells (DC), can mediate cellular proliferation, differentiation and survival (14-16).

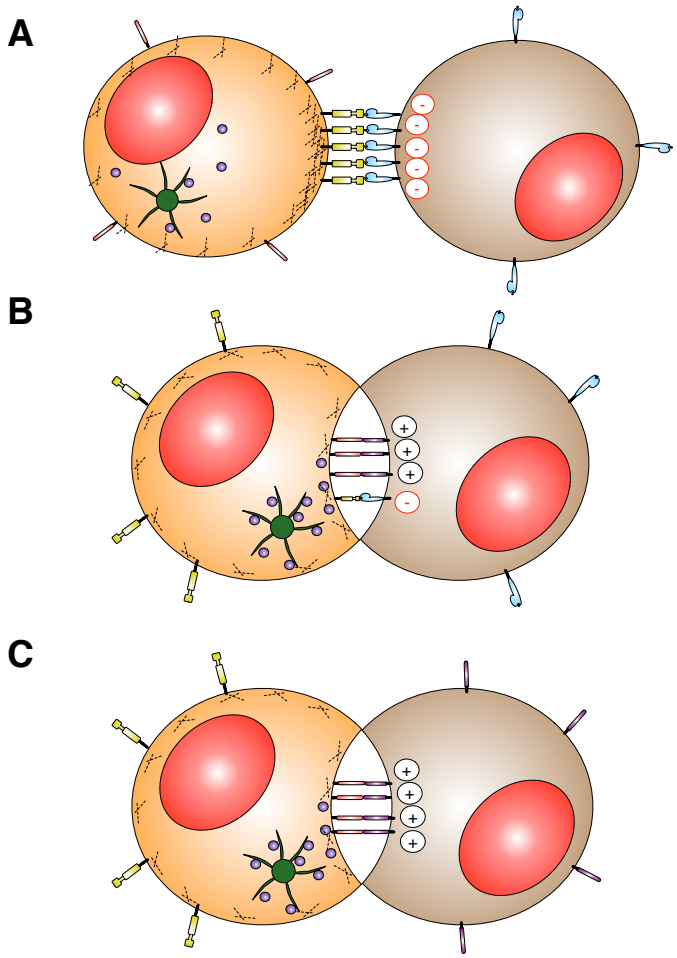


Figure 1.1. NK cell recognition of target cell health. (A) Inhibition – 'Self-recognition'. Interaction between an NK cell and a healthy, autologous cell results in the ligation of inhibitory receptors with their cognate ligands. The NK cell receives inhibitory signals through its receptors, preventing activation and lysis of the target cell. **(B) Activation – 'Induced-self'.** An upregulation of stress induced ligands on the target cell are a result of viral infection or transformation. Interaction with an NK cell enables the binding of these ligands to activating receptors. The balance of signals, activating versus inhibition, favours the former and the target cell is lysed. **(C) Activation – 'Missing-self'.** A target cell can internalise its inhibitory ligands, such as class I MHC molecules, upon viral infection or transformation. Contact with an NK cell results in the ligation of only activating receptors and lysis of the diseased target cell. Adapted from Orange (2008).

The IS forms as a result of the ligation of a combination of integrins and signalling proteins that accumulate at the cell-cell interface (17). NK cells participate in homeostasis by surveying the health of cells. They discriminate between healthy and diseased cells via the ligation of inhibitory ligands (expressed by healthy nucleated cells) and activating ligands (expressed by diseased cells). In the event of dominant activating signals, NK cells secrete a number of different cytotoxic mediators, including perforin (PFN) and granzymes (Gzms) (18, 19). NK cells transport these cytotoxic proteins to the synapse in lytic granules (LG) along microtubules (MT), which direct secretion towards and across the synapse (13, 20). NK cell

communication with other cells is almost wholly governed by receptors recruited to the immunological synapse, utilising a balance between germ-line DNA encoded receptors that activate, inhibit or regulate the response of NK cells (17, 21). Therefore, NK cell development is finely tuned and regulated to ensure that they are fully functional, delivering the correct response.

1.1.1 NK cell development and licensing

NK cell development begins in the bone marrow (BM) microenvironment (22). Stage 1 pro-NK cells, identified phenotypically as $CD34^{+}CD122^{-}$, are NK cell progenitors that give rise to stage 2 pre-NK cells. These second stage cells are sensitive to interleukin (IL)-15-induced differentiation (23), a hallmark characteristic of the pre-NK cells that are defined as $CD34^{+}$, $CD45RA^{+}$, $CD117^{+}$ and $CD94^{-}$ (24). At this stage, pre-NK cells are not yet fully committed to the NK cell lineage, as bulk *in vitro* cultures of these cells can give rise to T cells and myeloid DC (24, 25). The presence of IL-15 drives the development of pre-NK cells into immature NK (iNK) cells, the third stage of NK cell development. These cells lack the plasticity to deviate to other lineages, and are fully committed to an NK cell fate (24). These iNK cells still lack two major features of mature NK cells: the ability to produce interferon gamma (IFN-γ) and to elicit PFN-dependent cytotoxicity against susceptible targets (24). iNK cells also lack expression of mature NK cell markers, including CD94, the receptor natural killer group 2 member D (NKG2D), CD16 and killer immunoglobulin-like receptors (KIR). However, iNK cells have been shown to express NKp44, a receptor responsive to IL-2 stimulation, which is also found uniformly on some mature NK cell subsets (24, 26, 27). The final stage of NK cell development, stage 4, is marked by the expression of CD94-NKG2A, which allows NK cells to detect non-diseased cells (28, 29). Alongside this, CD117, CD33 and CD127 are downregulated, whilst activating receptors are upregulated (such as NKG2D, NKp46). Intracellular PFN stores accumulate and stage 4 NK cells develop the capacity for PFN- and Fas-ligand-mediated killing, as well as IFN-γ production (24). The maturation of NK cells to stage 4 does not signify the end of their development. At this stage, NK cells can differentiate into two distinct subsets, based on their surface expression of CD56. The expression of CD56 gradually increases from stage 2 to 4 to form $CD56^{bright}$ cells (predominantly $CD94^{+}CD16^{-}$) that express high levels of CD56, compared to NK

cells that express lower levels of CD56 ($CD56^{dim}$), which may represent a later, possibly fifth, stage of NK cell development (predominantly $CD94^{+/-}CD16^{+}$) (24, 30) (Figure 1.2).

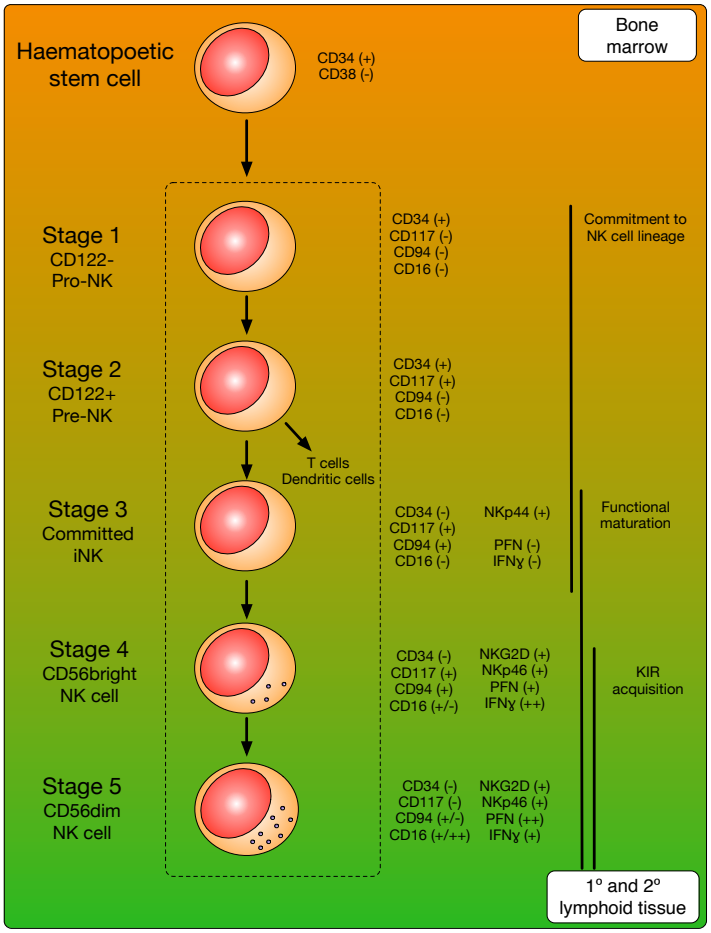


Figure 1.2. NK cell development. NK cell development begins in the bone marrow as haematopoietic stem cell progenitors. As the cells develop, the loss and gain of various surface proteins determines the stage of their development (Stage 1 – 5), as described in the text. Stages 1 and 2 are pro- or pre-NK cells that have the potential to develop into NK cells, T cells or dendritic cells. At stage 3, NK cells are considered committed and will form mature NK cells. NK cells at stages 4 and 5 are fully functioning lymphocytes. Stage 4 $CD56^{bright}$ NK cells lack CD16 and produce significant amounts of cytokines, whereas stage 5 $CD56^{dim}$ NK cells up regulate CD16 expression and gain maximum cytotoxic function.

The control of NK cell development, as with all lymphocytes, is mediated by cytokines. The most significant cytokines involved in the development of NK cells are IL-2 and -15 (31), which not only drive lineage commitment of pre-NK cells, but also stimulate the development of later stage NK cells, such as $CD56^{bright}$ NK cells (26, 30, 32, 33). IL-15 is regarded as the most critical cytokine involved in NK cell development, as demonstrated by a lack of NK cells in IL-15-deficient mice (34). Although soluble IL-15 can promote development of NK cells *in vitro* (32), it is also

physiologically trans-presented by DCs on IL-15 receptors during regulatory synapse formation in the periphery (35).

NK cell development and maturation occur in tissues that provide an environment with both a soluble and membrane-bound milieu of supportive and regulatory factors. Tissue-restricted development of NK cells can then occur without the threat of auto-reactivity to the host. Current data suggests that initial development occurs in the BM, but NK cells undergo their final maturation within secondary lymphoid tissues (SLT) (25, 36). Within the SLT, populations of DCs interact with NK cells through regulatory synapses, driving their differentiation and development through trans-presentation of IL-15 (37, 38). The migration of NK cells through various tissues provides a change in environments that facilitates their development into fully functional, mature cytotoxic lymphocytes.

The development and maturation of NK cells is finely tuned due to the non-specific nature of NK cell cytolysis. For instance, uncontrolled signalling through IL-2/15 receptor *in vivo* can result in the generation of NK cell leukaemia (39, 40) or over-riding of their self-tolerance leads to a hyper-responsive population of cells (41). To ensure a tightly controlled response to target cell interactions, NK cells undergo licensing, or education. Licensing is the process in which NK cells use inhibitory receptors that recognize self major histocompatibility (MHC) class I (MHC-I) molecules on cell surfaces to license, educate or arm themselves for efficient and diseased-cell-selective cytotoxicity (42-45). For instance, NK cells that develop in the absence of MHC-I proteins are unable to kill MHC-I deficient tumour cells (42, 44). In parallel, NK cells lacking the receptors that can bind to MHC-I molecules are also hyporesponsive to *in vitro* stimulation. Therefore, expression and ligation of these MHC-I specific receptors act as a gateway for arming NK cells for effective killing potential (46-48). NK cell licensing requires critical signalling through inhibitory receptors, as mutations in their intracellular signalling domains render these NK cells hyporesponsive (48).

Three major mechanisms have been described by which NK cells may be licensed: arming, disarming or affinity-induced. However, there is some debate as to which of these mechanisms are active *in vivo*. Arming is a mechanism by which primarily unresponsive NK cell inhibitory receptors engage MHC-I proteins, triggering the

initiation of an effector phenotype (48). During the process of disarming, NK cells mature as responsive effector cells but the absence of inhibitory receptors, or MHC-I ligands, the cells are rendered anergic (46) (Figure 1.3A). Affinity-induced licensing of NK cells is a process of fine-tuning effector function, controlled by inhibitory receptor affinity for MHC-I molecules, or the number of inhibitory receptor types expressed on the surface of the educating cell. This is governed by the genotype of the host, specifically by which inhibitory receptors (KIR) and ligand (MHC-I) genes they express (49). The affinity of NK cell inhibitory receptors for their ligands determines the responsiveness of the cell to ligation of activating receptors. This response is both qualitative and quantitative. For example, NK cells that possess two or more inhibitory receptor types respond more frequently and stronger than cells that possess just one type (49, 50) (Figure 1.3B). This suggests that NK cell licensing determines effector function by the recognition and binding of MHC-I molecules.

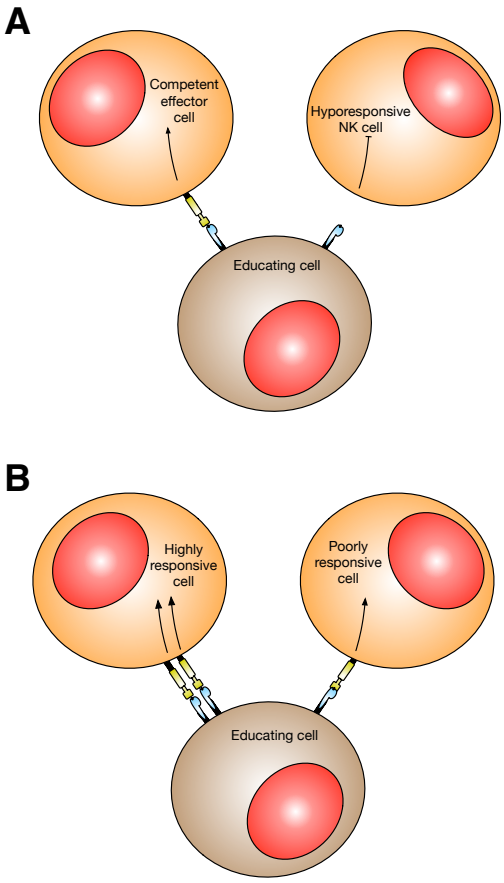


Figure 1.3. NK cell licensing and education. NK cell effector function is mediated or fine-tuned through licensing/education. Licensing of NK cells enables the qualitative and quantitative determine of the eventual effector function of the NK cell. Ligation of MHC class I proteins on 'educating cells' determines the extent to which NK cells become fully competent effector cells. Three modes of licensing have been proposed: arming, disarming and affinity-induced. **(A)** Arming and disarming is the process by which NK cells develop as unresponsive cells. The ligation of MHC class I molecules on the surface of educating cells triggers development into competent effector cells (*left cell*). NK cells that lack KIR expression cannot bind MHC proteins and remain anergic (*right cell*). **(B)** Affinity-induced licensing fine-tunes the NK cell effector response through quantitative ligation of high or low expressed/affinity MHC proteins on the educating cell. NK cells with higher expression of KIR receptors, or those that have a higher affinity to MHC proteins, become highly responsive cells (*left cell*). Low expression, or the expression of low affinity, KIR proteins renders NK cells poorly responsive (*right cell*). Adapted from Orr and Lewis (2010).

1.1.2 Bridging the gap between innate and adaptive immunity

NK cells do not conform to the 'textbook' innate or adaptive bimodal description of the immune system. Classically, innate immunity derives from germ-line encoded receptors and can control, initiate and direct an adaptive immune response (51). The adaptive immune system has high specificity to foreign peptide sequences through somatic recombination (52), requiring various cytokines to initiate but also characterised by long-term 'memory' functions (53, 54).

Innately, NK cells can recognise diseased or healthy cells through the binding of various combinations of germ-line encoded receptors (11). Following activation, NK cells secrete cytokines with inflammatory (55) or immunosuppressive functions (56), through interaction with other immune cells (15, 57, 58). NK cells are activated and elicit their cytotoxicity against target cells through ligation of two types of ligands, either 'stress-induced' proteins expressed on the surface of the target cell or the Fc portions of antibodies that have opsonised a target cell. NKG2D and receptors termed collectively as natural cytotoxicity receptors (NCR) (*e.g.* NKp46) interact with stress-induced ligands and, for example, specific influenza-derived haemagglutinin proteins (59) respectively. Antibody-dependent cellular cytotoxicity (ADCC) is initiated though engagement of the Fc receptor CD16 with the Fc portion of an antibody bound to the surface of a target cell (60). Most recently, NK cells have been shown to have a 'memory-like' function where they display clonal expansion, contraction, persistence and a secondary response to a particular antigen (54, 61), a function previously attributed only to T and B cells of the adaptive immune system.

NK cells display characteristics of both the innate and adaptive immune system. This gives significant advantages to the body, providing responses to a wide variety of pathogens and transformed cells. The varied immunological functions of NK cells are initiated through cell-cell interaction with target cells via the IS. This can stimulate downstream responses within the host that affect other cells and systems in either direct contact or in a paracrine fashion.

1.2 The immune synapse

The IS is an organised cell-cell interaction that forms between cells during direct interaction. Initially described as the site of directed cytokine secretion between T cells and antigen-presenting cells (APCs) (62), the IS is now known to be a micrometer-sized organisation of receptor clusters at the cell-cell interface (10), that can be formed by all lymphocytes. Classically, the structure of the IS was described as supramolecular activation clusters (SMAC) that form distinct rings in a 'bull's-eye' pattern (Figure 1.4). Structured in concentric circles from the centroid of the synapse moving outwards, these are termed the central, peripheral and distal zones (c-, p- and dSMAC respectively) (63, 64). In brief, the activating/inhibitory receptors are located in distinct domains within the cSMAC, segregated from the larger integrins of the pSMAC. These zones are further segregated from glycoproteins, such as CD45, that are located in the dSMAC (65). Segregation of these receptors allows for effective signalling through different phosphatase or kinase cascade pathways following receptor ligation during contact with a target cell (10).

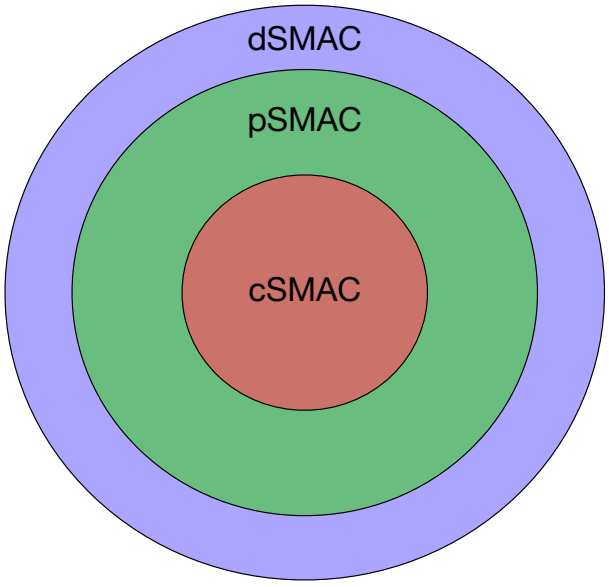


Figure 1.4. The classical structure of the immune synapse. Immune synapses are structured into supramolecular activation clusters (SMAC) composed of distinct domains. These are formed by micro-clusters of similarly sized proteins. The central SMAC (cSMAC) contains activating and inhibitory receptors. The peripheral SMAC (pSMAC) contains mostly integrins. The distal SMAC (dSMAC) contains other large signalling molecules.

The organisation of receptor-ligand complexes at the NK cell IS does not always conform to the bull's-eye structure of the T cell synapse. Whilst the NK cell IS contains regions of activating/inhibitory receptors segregated from integrins, these discrete domains are located throughout the synapse in a variety of configurations (66) (Figure 1.5). These differences may stem from receptor dynamics during the formation of the NK or T cell synapse. The NK cell synapse forms in distinct stages (13), as opposed to the continuous inward movement of the T cell receptors (TCR) towards the cSMAC (67). In brief, NK cell synapse formation consists of adhesion, organisation, polarisation/degranulation and termination.

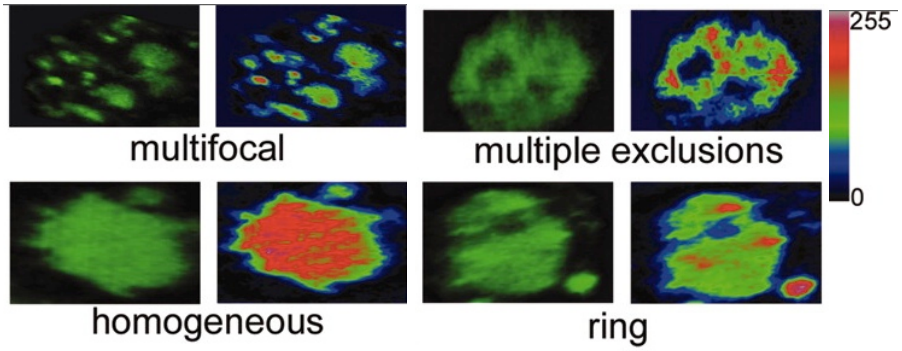


Figure 1.5. The density of MHC class I protein determines its organisation at the NK cell synapse. Panels show 3D reconstructions of 221 target cell-expressed GFP-tagged HLA-C at the synapse formed with YTS cells (*left panel*) and a heat map colour-coded to the fluorescence intniesty of GFP, as shown in the colour scale. Cells were co-incubated for 45 minutes prior to imaging. Images are representative of between 46 and 84 conjugates. Adapted from Almeida and Davis (2006).

Adhesion to the target cell

Adhesion to the target cell is the first step in the formation of an IS. Adhesion molecules such as lymphocyte function-associated antigen (LFA)-1 (β_1, β_2-integrins, CD11a/CD18) bind integrins on the target cell, such as intercellular adhesion molecule (ICAM)-1 and -2 (68). In addition to mediating firm adhesion to the target cell, LFA-1 also plays a role in cellular signalling. The most notable consequence of integrin ligation is LFA-1-mediated polarisation (69, 70). Here, receptor-ligand binding leads to activation of a signalling cascade through PTK2B protein tyrosine kinase 2 beta (Pyk2) and RACK1 (71-74). Pyk2 associates with Vav-1 and this signal further transduces through Ras-related C3 botulinum toxin substrate-1 (RAC1) and p21 protein (Cdc-42/Rac)-activated kinase-1 (PAK1), ultimately leading to cytoskeletal rearrangement at the synapse (72, 75) (Figure 1.6). Stabilisation of adhesion molecules is facilitated by the subsequent rearrangement of the actin cytoskeleton

(13), which is essential for the formation and maintenance of the IS. Once firm adhesion to the target cell has been established, signalling receptors are recruited to the synapse where they bind their respective ligands, either activating or inhibitory (18). The local nature of signalling at the IS means that NK cells can mediate a range of responses to multiple cells simultaneously (76-79). During cell-cell contacts, NK cells can direct cytotoxic responses whilst secreting cytokines including IFNγ, TNFα/β and ILs (80-82).

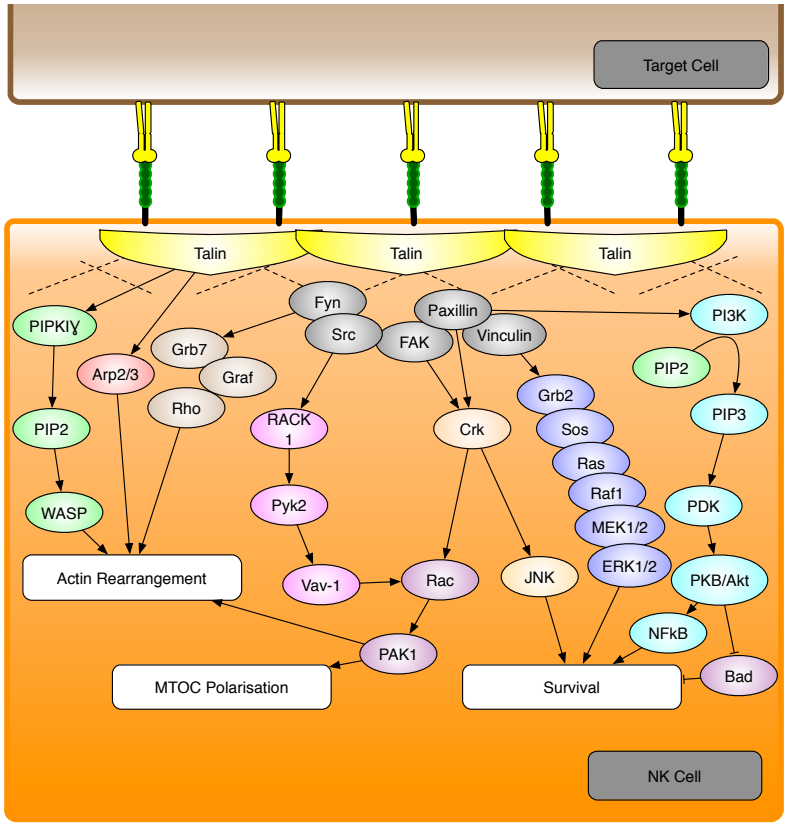


Figure 1.6. NK cell integrin signalling pathways. NK cell adhesion to its target cell is mediated by integrin ligation. Integrin ligation provides both adhesion and initial signalling, priming NK cells for target cell lysis. Once LFA-1 on the NK cell binds ICAM1 on the target cell, a kinase cascade is propagated, as described in the text. Signals result in both the rearrangement of actin at the synapse and polarisation of the MTOC. Adapted from Patsenker and Stickel (2011).

Receptor-ligand binding and subsequent downstream signalling control the response of the NK cell. However, irrespective of the number of synapses formed by one NK cell, at each synapse a balance of activating and inhibitory signals determine the fate of the target cell at that specific interaction. No one single receptor, activating or inhibitory, controls the NK cell response, rather dominance of signals from activating or inhibitory receptors will determine the outcome of the interaction (12). Furthermore, these responses are local, as opposed to global. NK cells in contact with two targets simultaneously can be inhibited at the contact site with a healthy cell, whilst delivering a cytotoxic response to a susceptible target (76).

1.2.1 The inhibitory synapse

NK cells contain pre-formed secretory lysosomes containing cytotoxic mediators that, upon ligation of germ-line encoded receptors, are rapidly released across the synapse, triggering apoptosis of the target cell. Inhibitory receptor ligation can quickly regulate interactions to prevent the inadvertent lysis of healthy cells. Upon contact with a healthy cell, inhibitory receptors bind MHC-I ligands expressed on all healthy, nucleated cells. These interactions form a micro-clustered structure, which was first identified and characterised between NK cells expressing the inhibitory receptor KIR2DL1 and Epstein-Barr virus (EBV)-transformed B cells expressing its cognate ligand, HLA-Cw6 (9).

NK cells express a repertoire of inhibitory receptors that inhibit cytotoxicity by initiating a dominant inhibitory signalling cascade, preventing activating signalling and the release of cytotoxic proteins. KIR receptors recognise MHC-I molecules that are expressed on the surface of all healthy nucleated cells. In humans these are denoted as human leukocyte antigens (HLA). A complex of two non-covalently associated subunits forms MHC-I molecules. These are the polymorphic heavy chain α and the invariant β_2-microglobulin (β_2m) (83). These complexes are recognised by the extracellular domains of KIR receptors. Comprising either two or three immunoglobulin-like domain structural units, these mediate direct contact with the α1 and α2 domains of the HLA-C molecules (84). There are different subsets of MHC-I molecules that are recognised by individual KIR receptors (85). For example, the KIR receptor KIR(2DL1) recognises, amongst others, the MHC-I proteins HLA-Cw4 and –

Cw6, whilst KIR(2DL2) binds HLA-Cw3 and –Cw7. This has been shown by site-directed mutagenesis (86, 87).

Even though binding kinetics have been shown to be rapid (88), intercellular contact lasts for minutes (9). KIR receptors and their ligands accumulate within specific signalling domains, or clusters, that form interspersed within regions of adhesion between LFA-1 and ICAM-1 (78, 89-91). In addition to the KIR receptors, NK cells express a number of other inhibitory receptors that recognise various cognate ligands, summarised below in Table 1.1.

Receptor	Ligand(s)	Reference
KIR	HLA-A, -B, and -C	(92) (93) (94)
CD94/NKG2A	HLA-E	(95) (96)
LIR	A number of MHC class I proteins	(97) (98)
CD66	Non-MHC ligands	(99)
TIGIT	PVR PVR ligand 2	(100)
KLRG1	Cadherins	(101)
LAIR-1	Collagen	(102)
KLRB1A/NKRP1A/CD161	LLT-1	(103)

Table 1.1. NK cell inhibitory receptors. KIR, Killer immunoglobulin receptor; HLA, human leukocyte antigen; NKG2A, natural killer group 2 member A; LIR, leukocyte immunoglobulin-like receptor; MHC, major histocompatibility complex; TIGIT, T cell immunoreceptor with Ig and ITIM domains; PVR, Polio virus receptor; KLRG1, Killer cell lectin-like receptor subfamily G member 1; LAIR, Leukocyte-associated immunoglobulin-like receptor; KLRB1A, Killer cell lectin-like receptor subfamily B member 1; LLT1, Lectin-like transcript-1

Interactions between inhibitory receptors and their ligands do not require reorganisation of the actin cytoskeleton, downstream signalling or the engagement of integrins (9, 78, 104). Importantly, this interaction appears to be a thermodynamic process (9, 66, 90, 105). Rapid ligation of inhibitory ligands effectively overrides any activating signals present at the intercellular contact. Whilst activating receptors have been seen to accumulate at the inhibitory synapse, their proximity to the inhibitory receptors renders them ineffective, as inhibitory signalling is able to terminate activating signals (17). This occurs at a relatively early stage of synapse formation, demonstrated by the lack of cytoskeletal rearrangement, a process involving filamentous (F)-actin that is a hallmark of an activating synapse (106-108).

Inhibitory synapse formation occurs quickly to allow a rapid inhibition of any activating signals that would otherwise prepare the NK cell for a cytolytic attack (F-actin reorganisation, polarisation, *etc.*). Clustering of the inhibitory receptors is ATP-independent (9), yet requires the binding of zinc ions to an extracellular domain (109), which is also required for signal transduction (110). The importance of these ions in the formation of KIR receptor clusters was demonstrated by the loss of KIR function by inhibiting cluster formation, following the addition of metal-ion chelators (9). The micro-scale clusters provide signal-transduction through immunoreceptor tyrosine-based inhibition motifs (ITIM) in the KIR cytoplasmic tail, resulting in the recruitment of tyrosine phosphatases. It is these enzymes that inhibit kinase-dependent phosphorylation of activating cytoplasmic motifs. The dephosphorylation of key activating signalling kinases prevents activating signalling cascades (89, 111-113) and disrupts adhesion to the target cell (111). ITIM are bound by SHP-1 at their conserved sequence V/I/LxYxxL/V (amino acid letter code where x stands for any amino acid) (112). For example, following KIR2DL1 binding to HLA-Cw4/6, two ITIM (one membrane proximal and one distal) are tyrosine phosphorylated. The SH2 domains of cytoplasmic tyrosine phosphatases, SHP-1 and SHP-2, subsequently bind these ITIM phosphotyrosines. The membrane proximal ITIM is sufficient to inhibit NK cell killing through SHP-1 recruitment, whereas the membrane distal ITIM acts in concert with the proximal ITIM to recruit SHP-2 and amplify the signal from SHP-1 (114). It is this SHP-mediated dephosphorylation of key activating signalling proteins, such as Vav1, that mediates the inhibition of NK cells (106) (Figure 1.7).

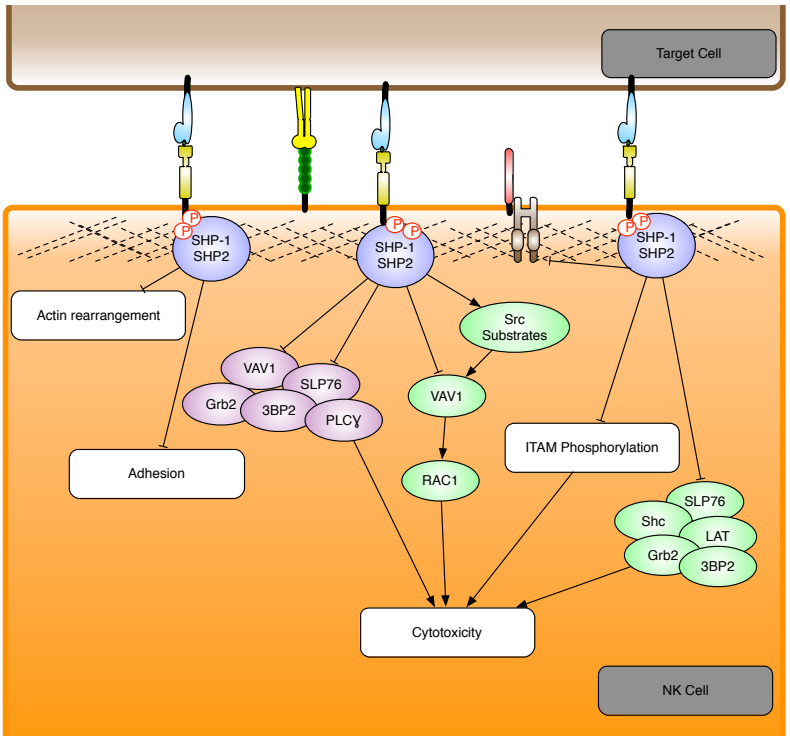


Figure 1.7. NK cell inhibitory signalling pathways. NK cells express inhibitory receptors (such as KIR) that bind MHC class I molecules expressed on healthy nucleated cells. Inhibitory receptors contain intracellular ITIM domains that are phosphorylated on membrane proximal and distal tyrosines following ligation. As described in the text, SHP-1 and -2 are recruited to these domains which then prevent the clearance of actin at the intercellular contact, and dephosphorylate proteins associated with NK cell activation, such as Vav1 and SLP76. This inhibits the activation of NK cells and arrests target cell lysis.

Inhibitory signalling is of a significant importance for regulatory synapses. The target cell must be protected from lysis whilst delivering its modulatory signals to the NK cell. The most well understood regulatory interaction is between NK cells and DC. During this interaction, integrins, inhibitory receptors and cytokine receptors accumulate at the synapse (15). During DC-NK cell interactions, both CD94/NKG2A and KIR2DL1/DL2 have been shown to enrich at the regulatory synapse (15). Most recently, the trans-presentation of IL-15, which is presented to the NK cell bound to the IL-15 receptor, has been reported to confer NK cell proliferation and survival. This is regarded as the mechanism by which NK cells can reach their full functional potential (15, 35, 115). The regulatory synapse has distinct similarities to the inhibitory IS, for instance the recruitment of inhibitory receptors that bind MHC-I proteins at the NK-DC interface, most likely to prevent the lysis of the DC (15). Therefore, the inhibitory synapse is not only essential for the protection of healthy cells during NK cell surveillance, but also has a functional role in facilitating effector functions above and beyond cytotoxicity.

The ligation of inhibitory receptors provides NK cells with a fast and efficient response following cell-cell contact with healthy cells. The clustering of these inhibitory receptor-ligand complexes, in close proximity to activating complexes, facilitates the inhibition of activating kinase cascades. This tightly regulated control of effector functions means that NK cells are able to quickly discriminate the health status of a cell, in addition to mediating regulatory responses with other cells of the immune system.

1.2.2 The activating synapse

NK cell effector functions against diseased cells are crucial in maintaining homeostasis, preventing the persistence of viral infection and tumourgenesis (116). Following contact with a diseased cell expressing ligands for activating receptors, downstream signals result in the polarisation of cellular machinery, including LG, MT and mitochondria (68). Micro-scale clustering of activating receptors on the surface of NK cells (117) skews signaling in favour of activation, leading to the release of cytotoxic proteins onto the target cell.

A diseased cell can be identified by the expression of a range of 'stress-induced' ligands. Therefore, NK cells have evolved to express a vast repertoire of activating receptors (118), summarised below in Table 1.2. Activating receptors are unable to signal intracellularly, instead they signal through immunoreceptor tyrosine-based activating motifs (ITAM) of recruited adaptor proteins. This triggers downstream signalling and results in secretion of cytotoxic proteins and cytokines (119-121). Ligation of activating receptors triggers a phosphorylative signalling cascade of ITAM and ITAM-like motifs encoded within the cytoplasmic domains of activating receptors, or associated adaptor proteins such as the DNAX activating proteins of 10 or 12 kDa (DAP10 and DAP12 respectively) (121). These adaptor proteins carry a negative charge allowing oligomerisation to a variety of receptors. This plasticity allows the same adaptor protein to trigger a response, based on the receptor-ligand complex formed (122-124).

Receptor	Adapter	Ligand	References
NKG2D	DAP10	MICA/B, ULBP1-6	(125)
NCRs			
NKp30	FcRγ/CD3ζ	B7-H6	(126)
NKp44	DAP12	Viral haemagglutinins	(127)
NKp46	FcRγ/CD3ζ	Viral haemagglutinins	(128)
NKp65	-	KACL	(129)
NKp80	-	AICL	(130)
2B4	SLP-76 adapter protein (SAP)	CD48	(131)
DNAM-1	-	PVR (CD155) Nectin-2 (CD226) and nectin-like molecules	(132)
CD16	FcRγ/CD3ζ	Antibody Fc portion	(133)
CD2	CD2BP1	CD58	(134)
CD44	SAP	Hyaluronate	(135) (136)
BY55 (CD169)	DAP10	HLA-C	(137) (138)
CD28		CD80/86	(139)

Table 1.2. NK cell activating receptors. NKG2D, natural killer group 2 member D; DAP10/12, DNAX activating protein of 10 or 12 kDa; MIC, MHC class I polypeptide-related sequence; ULBP, UL16 binding protein; NCR, natural cytotoxicity receptor; FcR, Fc receptor; KACL, keratinocyte-associated C-type lectin; AICL, activation-induced C-type lectin; DNAM-1, DNAX accessory molecule 1; PVR, polio virus receptor; CD2BP1, CD2 cytoplasmic tail-binding protein; HLA, Human leukocyte antigen

One of the most widely studied activating receptors is the evolutionary conserved c-type lectin receptor NKG2D (125). NKG2D is expressed on all NK cells and is fairly promiscuous, recognising as many as 8 ‘stress-inducible’ ligands, such as MICA/B and members of the UL-16 binding protein (ULBP) family (ULBP1-6) (140-143). These proteins are upregulated and expressed on the surface of cells in response to stresses such as UV-induced DNA damage, transformation or viral infection (140, 144). NKG2D is a non-ITAM containing NK cell-activating receptor that is constitutively expressed with DAP10 (121). Ligation of NKG2D causes phosphorylation of the ITAM-like PI3K-binding motif (YxxM) in the cytoplasmic tail of DAP10, in a similar manner to the T cell co-stimulatory molecule CD28 (145), by the Src-kinase Lck (121, 146). This recruits two arms of the NKG2D signalling pathway via PI3K or growth factor receptor-bound protein 2 (Grb2)/Vav1. The importance of Vav1 in activating signalling was demonstrated by the recruitment of SHP-1 during inhibitory signalling, which specifically targets Vav-1, leading to its dephosphorylation and therefore inactivation (106).

In addition to binding cell-expressed ligands, NK cell activation and cytolytic activity can be mediated through ADCC (147). Most hematopoietic cells, except the majority of T cells, express Fcγ receptors (FcγR) (148). There are three types of FcγR and of these, NK cells express the activating low affinity FcγRIIIa (type III receptor for IgG; CD16), which mediates ADCC. This receptor is primarily expressed at high levels on the cytotoxic $CD56^{dim}$ $CD16^{+}$ NK cell subset (149). ADCC is directed towards targets that have been opsonised with IgG_1 and/or IgG_3 antibodies. CD16 binding of Fc domains results in a strong activating signal that initiates cytotoxicity and cytokine release (147, 150). Moreover, co-engagement of other activating receptors has a synergistic effect, enhancing NK cell activation (8).

CD16 also lacks ITAMs, signalling intracellularly through the accessory molecule CD3ζ, which contains the ITAM sequence $YxxL(x)_{1-6}YxxL$ (133). CD16 is thought to signal through the same pathway as some natural cytotoxicity receptors (NCR), such as NKp46 and NKp30 (151). Ligation of CD16, or NCR, recruits and activates the tyrosine kinase Syk and Zeta-chain-associated protein kinase of 70 kDa (ZAP70) (152). However, unlike other NK activating receptors (*e.g.* NKG2D, NKp46 and DNAM-1), specific engagement of CD16 is sufficient to elicit effective killing (8). Specifically, activating receptors such as NKG2D require the co-engagement of LFA-1 and 2B4 to provide a cytotoxic response (153), whereas CD16 ligation alone is sufficient to activate NK cells. Moreover, CD16 is significantly stronger in concert with other receptors, such as NKG2D or 2B4, in resting NK cells (154).

Following ligation of activating receptors, downstream phosphorylation cascades converge through the SH2-domain containing leukocyte protein of 76 kDa (SLP-76), phosphoinosititide 3-kinase (PI3K), phospholipase C-γ (PLC-γ), Rho, Ras, p38 mitogen-activated protein kinase (MAPK) and extracellular signal-regulated kinase (ERK) (122, 152, 155). Regardless of the specific activating receptor-ligand complexes formed at the synapse, activating kinase cascades lead to F-actin polymerisation at the NK-target cell contact site. Parallel polarisation of the microtubule-organising centre (MTOC) (156) prepares the NK cells for secretion of lytic granules containing PFN and granzyme B (GzmB). It is these proteins that enter the target cell and lead to target cell death (121) (Figure 1.8). However, some NK cell lines express and utilize non-classical activating receptors. YTS cells, an NK-like YT sub-clone, uses the activating receptor CD28, utilised by T cells and a small subset of NK cells (157), which signals through PI3K, ERK and JNK in orchestration with LFA-1 to initiate cytotoxic effector functions (20).

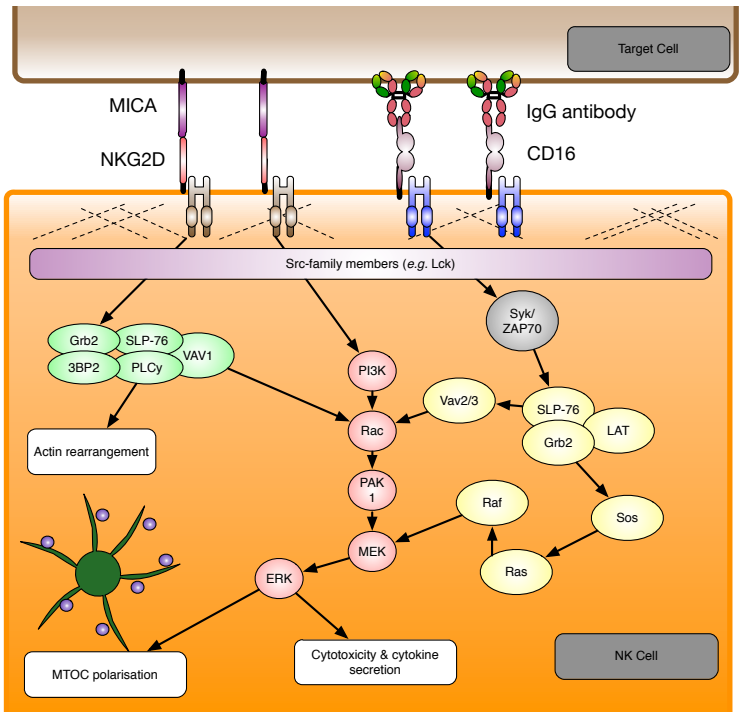


Figure 1.8. NK cell activating signalling pathways. Upon viral infection or transformation, cells up regulate stress-induced ligands and internalise 'self' MHC class I molecules. Viral proteins are also presented on the target cell surface, which can be bound by antibodies. NK cells express activating receptors that recognise up regulated stress induced ligands as well as those that can bind the Fc portion of an IgG antibody. As described in the text, ligation of activating receptors to their cognate ligands results in the tyrosine phosphorylation of the intracellular ITAM on adapter proteins. These kinase cascades result in the activation of NK cells where its MTOC is polarised to the synapse as actin is cleared form the interface to allow the release of cytotoxic mediators. Adapted from Vivier *et al* (2004)

The IS is a highly responsive interaction, which utilises a wide range of receptors that allow NK cells to quickly and efficiently survey target cells. The formation of this complex, dynamic interface is crucial for the function and execution of NK cell interactions, directing cytolysis and mediating regulation. Through an array of activating and inhibitory receptors, NK cells are primed and prepared for a strong and efficient cytolytic response to infected or transformed cells. Despite the lack of somatic recombination of receptor genes, NK cells can effectively discriminate between 'self', 'non-self' and opsonised targets, resulting in signalling cascades to polarise and release cytotoxic mediators through the IS to diseased targets only.

1.2.3 Polarisation and directed secretion at the immune synapse

The polarisation of NK cells prior to degranulation is critical for the lysis of target cells (158). The mechanism by which NK cells polarise their LG to the synapse and release their cytolytic contents has been intensively investigated. The most critical factor in assembling a mature, cytolytic synapse and delivering a cytotoxic response is the proper functioning of the cytoskeleton (Figure 1.9). Numerous groups have dissected this through depletion/inhibition of proteins key to the cytoskeleton through knockdown (KD), knockout (KO) or pharmacological inhibition.

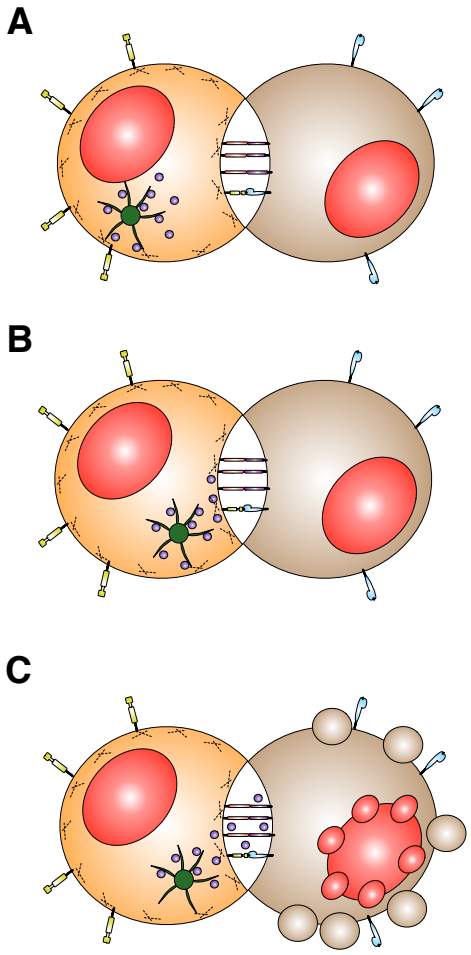


Figure 1.9. Polarisation and directed secretion at the NK cell immune synapse. Virally infected or transformed cells up regulate stress-induced ligands or are opsonised by antibodies. **(A)** NK cell contact with diseased cells engages activating ligands, where signals from activating receptors dominate over inhibitory signals. **(B)** Activating kinase cascades and signalling pathways cause polarisation of the MTOC (green) and its bound LG (purple), in addition to other cellular machinery, towards the synapse. **(C)** Once LG have reached the synapse, their membranes fuse with the cell membrane and release their cytolytic contents into the synaptic cleft. These trigger apoptosis in the target cell, identified by hallmarks such as membrane blebbing and DNA fragmentation. Adapted from Orange (2008).

For instance, March and Long showed that by KD of paxillin, a signal transduction adapter protein known to be associated with LFA-1 signalling and actin regulatory functions (159), NK cell polarisation was significantly inhibited (160). Paxillin associates with Pyk2 (161), which is tyrosine phosphorylated downstream of LFA-1 ligation. They conclude that by siRNA-mediated KD of paxillin, further signal transduction that localizes the MTOC to the synapse is lost, reducing NK cell cytotoxicity. In addition, Butler and Cooper demonstrated that following shDNA KD of Arp2/3, a protein complex required for actin nucleation, NK cells exhibited a reduced capacity to lyse target cells (162). Similarly, Mace *et al.* showed that the ligation of LFA-1 by NK cells from both talin- and Wiskott-Aldrich syndrome protein (WASp)-KO

mice were unable to induce localised actin polymerisation (163). Talin and WASp are both signal transduction proteins, required for the organisation of actin at the cytoskeleton following LFA-1 ligation, and prerequisites for the reorientation of NK cells to dock LG at the synapse (70). Finally, the pharmacological inhibition of NK cell F-actin dynamics disrupts the accumulation of actin and the assembly of a functional IS. Actin targeting drugs, such as cytochalasin (164, 165), Latrunculin A (166), and Jasplakinolide (167), have all been shown to inhibit cytotoxicity.

Cytoskeleton-dependent polarisation

Polarisation of NK cells is critical for efficient target cell lysis (168). Prior to the movement of the MTOC, WASp facilitates F-actin rearrangement at the synapse. Following binding of the Rho GTPase Cdc42, Arp2/3 mediates the movement of actin in waves from the centroid of the synapse towards the periphery (169-171). This polymerisation and rearrangement of F-actin functions to stabilise the synapse, generating forces to tether the NK cell to its target, demonstrating the crucial role of integrin signaling for this process (166).

Following the rearrangement of F-actin at the synapse, MT movement facilitates the reorientation of the MTOC – including its associated LG – towards the synapse. The relationship between F-actin reorganisation and movement of the MTOC has been demonstrated by the disruption of actin, causing the arrest and impairment of MTOC polarisation (172). Upon ligation of activating ligands, LG first rapidly move along MT towards the MTOC in a minus-end direction (173). LG interaction and movement along MT is facilitated by a combination of Rab7, vesicle-associated membrane protein (VAMP)-4 and VAMP7 expressed on the granule surfaces in both T cells and NK cells (174, 175).

Studies using NK cells have shown that lysosomal-associated membrane protein (LAMP)-1 (CD107a) may also be a key factor in LG movement. Silencing CD107a impaired initial LG movement towards the MTOC, suggesting that proteins on the surface of granules are important in their trafficking (176). As LG move towards the MTOC, NK cells undergo a massive rearrangement of organelles required for cytolysis. The specific cell machinery for secretion (MTOC, Golgi apparatus, and mitochondria) moves towards the synapse, and those not required are trafficked

towards the posterior of the cell (177). A large number of factors are required for MTOC polarisation including Pky2, ERK2, CIP4 and Vav-1 (156, 172, 178). The major motor protein involved in the polarisation of NK cells is kinesin-1 that interacts with the small GTPase Arl8b (179). It is thought that the movement of the MTOC towards the synapse is facilitated by pushing and pulling forces generated by growth or shrinkage, respectively, at the sites where MT are anchored into the cortical actin (180, 181). At these junctions, IQ motif-containing GTPase-activating protein-1 (IQGAP1) may act as a linker between CLIP-170 at the ends of the MT and the actin mesh (182). Once the MTOC has polarised to the synapse, LG are then trafficked along MT in a plus-end direction facilitated by WASp-interacting protein (WIP) (183). The physical docking of the MTOC at the synapse has been observed in T cells (184), but such close proximity has not been reported in NK cells. At this point, NK cells may simply traffic their LG along MT towards and onto the actin at the synapse for directed secretion into the synaptic cleft.

Directed secretion

NK cells use directed secretion to release potent cytotoxic mediators within the synaptic cleft onto their target. To facilitate this, in parallel with MTOC polarisation, F-actin continues to undergo rearrangement at the synapse. This was originally thought to be a large-scale clearance of actin to permit the access of LG to the membrane (13, 185). However, recent advances in microscope techniques, primarily super-resolution microscopy, have revealed that ligation of activating receptors creates a hypo-dense mesh of actin, punctuated with holes, or pores, that allow the passage of LG through to the membrane (117, 186, 187). The diameters of the holes within the mesh are sufficiently large to allow the passage of LG. Whilst LG appear to be polarised towards the vicinity of these holes, data from Mace *et al.* suggest that motor protein-based mechanisms (possibly through myosin IIA) could facilitate the final movement of LG along F-actin. Through this process, LG could migrate to, and through, these areas of increased periodicity for fusion with the NK cell membrane and the release of their cytotoxic contents (188). Conversely, inhibitory signalling does not produce an increased periodicity in the mesh and therefore may prevent the access of LG to the synapse (117).

The fusion of the cell and granule membranes to release the cytotoxic payload into the synaptic cleft is a multistep process, involving the initial vesicle tethering, membrane fusion and finally, the release of cytolytic contents. The N-ethylmaleimide-sensitive protein attachment protein receptor (SNARE) proteins regulate the fusion of the LG with the NK cell membrane, directing the granules to the secretory zones of the synapse for intra-synaptic release. These regions are rich in proteins such as VAMP7, syntaxin-11 and Munc18-2. Interaction of these proteins drives membrane fusion for the release of cytotoxic contents (175) (158). Secretion occurs across the synaptic cleft, the gap formed between the effector and target cell, which varies between 15-55 nm (65, 189), focusing these cytotoxic mediators towards the target cell (190).

It has been shown that degranulation occurs in two modes: complete and incomplete fusion (Figure 1.10). This was revealed by the use of a pH-sensitive fluorophore, pHluorin, where fluorescence is suppressed in acidic compartments, such as LG lumen. Firstly, LG were shown to fuse with the NK cell membrane in a slow (complete) manner. Upon contact and fusion of the LG and cell membranes, pHlurin entered a neutral pH and emitted fluorescence. This signal then dispersed across the cell membrane, away from the initial point of membrane fusion. This demonstrated that the LG, after releasing its contents, completely fused with the membrane. This mode of degranulation is also demonstrated, and used as an assay for NK cell degranulation, by the presence of the LG membrane protein CD107a on the NK cell surface (191). Fast (incomplete) fusion is the partial release of cytotoxic mediators, without complete fusion of the LG and NK cell membranes. This is thought to be via the formation of ‘fusion pores’ through which cytotoxic proteins are briefly released through areas of partial fusion. This is then followed by granule recession back into the NK cell cytoplasm. This was demonstrated by the appearance then disappearance of pHluorin fluorescence without any dispersion into the NK cell membrane (192). Based on the differential timing of these modes of degranulation, the mode of degranulation may depend on the signals received and the speed of kill required, however, the exact mechanisms that result in these modes of action have not been elucidated.

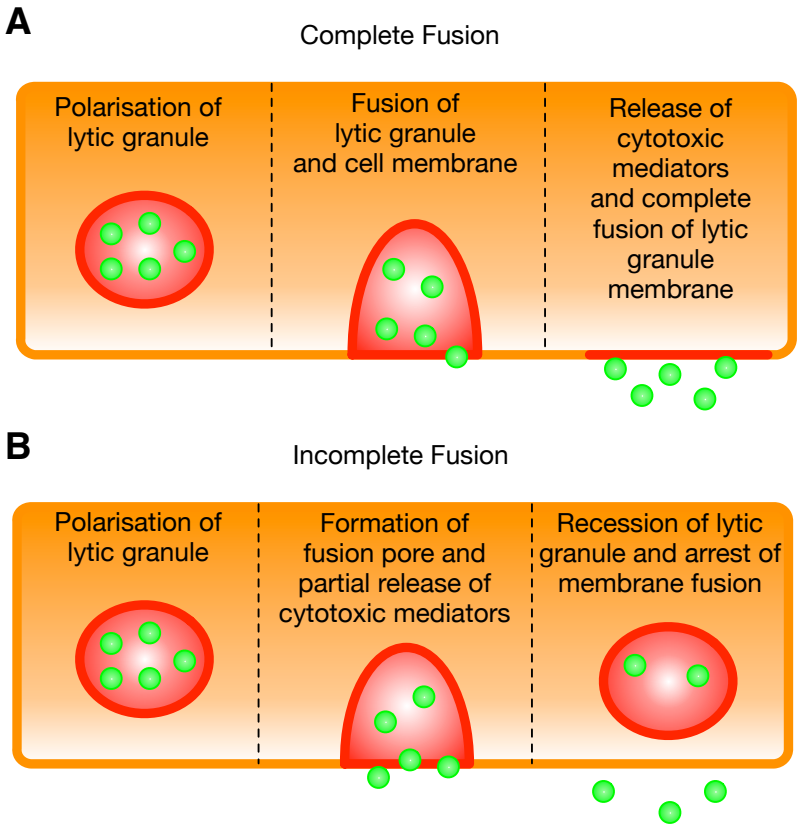


Figure 1.10. Secretion at the NK cell immune synapse occurs in two modes: Complete and incomplete fusion. Following activation and polarisation of the MTOC to the intercellular contact. LG fuse with the cell membrane to release their cytolytic contents. Using pH-sensitive proteins, this has been shown to be achieved by either slow, complete fusion or fast, incomplete fusion. **(A)** Complete fusion occurs in three stages. (*Left segment*) LG (red) containing cytotoxic mediators (green) move towards the cell membrane (orange) at the synapse. (*Central segment*) The LG membrane fuses with the cell membrane and its contents are released. (*Right segment*) The LG completely fuses with the cell membrane, dissipating into the membrane. **(B)** Incomplete fusion occurs in three stages. (*Left segment*) The LG containing cytotoxic mediators moves towards the cell membrane at the synapse. (*Central segment*) The LG membrane fuses with the cell membrane and some of its contents are released. (*Right segment*) The LG then recedes back into the cytosol, retaining some of its contents within the LG lumen.

In contrast, a study by Bertrand *et al.* showed that polarisation of the MTOC in cytotoxic lymphocytes (CTL) does not necessarily precede LG secretion. In this setting, it was shown that the accumulation of LG at the synapse occurred before MTOC polarisation in up to 50% of cells (193). Furthermore, partial inhibition of MTOC polarisation using a PKCζ inhibitor did not impede secretion of cytotoxic mediators at the synapse. This indicates that there may be a separate mechanism employed by CTL that can facilitate the rapid secretion of cytotoxic mediators.

1.2.4 The T cell synapse

T cells are crucial players in the adaptive immune system, orchestrating immune responses by amplification ($CD4^+$ T cells) and suppression (regulatory T cells; Treg) of immune responses or cytolysis of target cells bearing cognate antigens for antigen-specific receptors ($CD8^+$ T cells). The T cell synapse was first described between T- and B-cells (194, 195) and has been demonstrated both *in vitro* (196) and *in vivo* (197-199). The T cell synapse is crucial for the proper functioning of T cells where antigen-specific TCR engage antigenic peptide fragments presented on the surface of APC by MHC-I or -II proteins (200, 201).

The T cell synapse is organised in a spatio-temporal manner. The initial visualisation of the T cell synapse found that protein-protein complexes at the interface of a T cell and B cell were organised into segregated micrometer-scale domains, termed SMACs (196). T cells form synapses that are structured in SMACs, organised into concentric rings of receptors and adhesion proteins, determined by their extracellular domain length (10, 196), termed the mature T cell synapse (Figure 1.11). This is in contrast to the NK cell synapse, which conforms to a number of configurations consisting of punctate domains of activating/inhibitory receptors, surrounded by a mesh of integrin-ligand complexes (9, 66, 124).

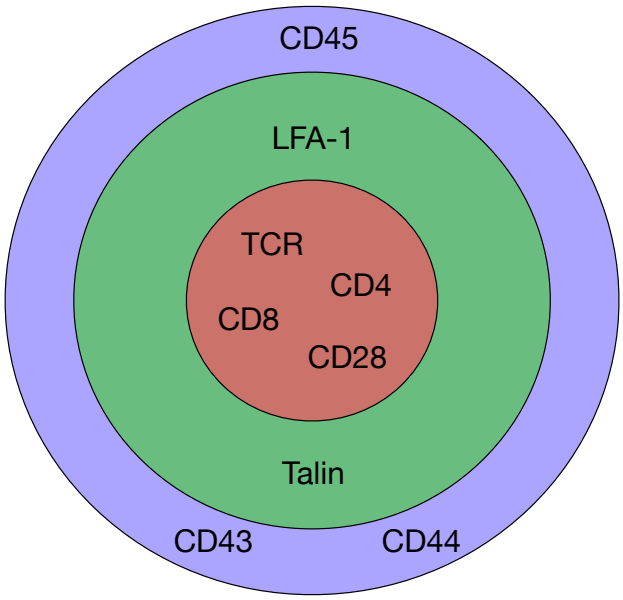


Figure 1.11. The structure and organisation of the mature T cell immune synapse. An *en face* view of the mature T cell immune synapse. The structure is characterised by its 'bull's eye' pattern, comprised of the dSMAC (blue), pSMAC (green) and the cSMAC (red). The cSMAC contains signalling proteins such as the TCR and CD28. The pSMAC contains integrins and integrin-associated proteins such as LFA_1 and Talin. The dSMAC contains larger signalling molecules such as CD45.

The key receptors involved in T cell activation are located in the central region of the synapse or cSMAC. The somatic, multimeric TCR signals through Lck/ZAP70 and the co-stimulatory molecule CD28, which suppresses inhibitory E3 ubiquitin ligases (202) (Figure 1.12). A ring of LFA-1 adhesion molecules and talin, the pSMAC, surrounds this central region. Finally, larger molecules, such as CD43 and CD45, are segregated from the central and peripheral regions of the synapse, located in a distal region at the edge of the intercellular interface, the dSMAC (196, 203). The dynamic organisation of the T cell synapse was imaged in real-time using lipid bilayers incorporated with fluorescently labelled peptide-loaded MHC (pMHC) proteins (10). These studies showed that at the point of cell-cell contact, the TCR-pMHC complexes were first accumulated at a peripheral ring surrounding central integrin receptor-ligand complexes, termed the immature T cell synapse. Within a short space of time, in the order of a few minutes, the organisation of the synapse was reversed to form a mature synapse (10, 196, 203). More recently, improved imaging techniques have shown that the T cell synapse is formed with small aggregations of proteins within the interface, termed micro-clusters (204-206). The TCR mediates this initial signalling at the peripheral region of the synapse, migrating to the central zone, where signalling is terminated (205-207). This continuous dynamic movement of

micro-clusters, of up to 100 TCR molecules (207), is critical for sustained TCR signalling (206) where the density of pMHC is proportionate to the micro-cluster size (207).

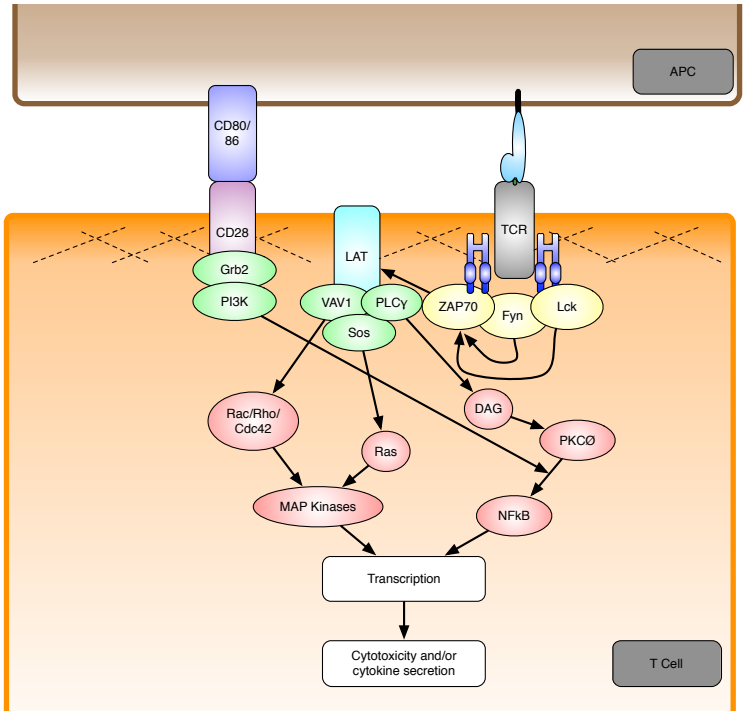


Figure 1.12. T cell activating signalling pathways. Upon engagement with an antigen presenting cell, TCR engagement of specific peptides presented on MHC proteins triggers activating signalling pathways. Initially bound at the periphery of the synapse, the TCR moves into the central region as the synapse matures. As the TCR moves centrally, phosphorylation cascades, as described in the text, initiate gene activation and transcription. These pathways result in the secretion of cytokines and/or cytotoxic proteins, activating other branches of the adaptive immune system or lysing their target, respectively. Adapted from Fathman and Lineberry (2007).

The segregation and resulting dynamics of extracellular receptor-ligand complexes that control immune cell signalling are not controlled by receptor ligation alone. In synapses formed by both T cells and NK cells this has been consistently observed. Specifically, the extracellular domains of activating receptors of both cell types are of similar dimensions (84, 208-210), with the crystal structures of TCR-pMHC, NKG2D-MICA and LFA-1-ICAM-1 receptor-ligand complexes already elucidated. The signalling receptor-ligand complexes of both T cells and NK cells are ~15 nm (84, 208, 209, 211), whereas adhesion complexes are ~50 nm (212). This suggests that the receptor organisation is dependent on the extracellular span of the receptor-ligand complexes that form and accumulate at the intercellular interface.

1.2.5 The size-dependent kinetic segregation model

The kinetic segregation (KS) model proposes that receptors at the IS are spontaneously segregated according to their extracellular domain lengths (213). Described as early as 1992 (214), it has been thought, specifically for T cell-APC interactions, that extracellular domain size is a major contributor in the final outcome of signalling at the IS. This size-dependent segregation has also been confirmed for NK cell synapses (65, 124, 189).

The extracellular domains of activating and integrin receptor-ligand complexes have been shown to be around 15 – 25 nm and 45 – 50 nm, respectively (65). The difference in extracellular length of proteins within such close cell-cell interactions would result in a significant bending of the cell membrane, which would be at a high energy cost to the cell (189). To overcome this, immune cells segregate their receptors according to size (215) (Figure 1.13). Larger integrins are segregated from the smaller activating and inhibitory signalling receptor-ligand complexes. Recently in NK cell systems, both experimental data and mathematical modelling have addressed this segregation in accordance with the KS model.

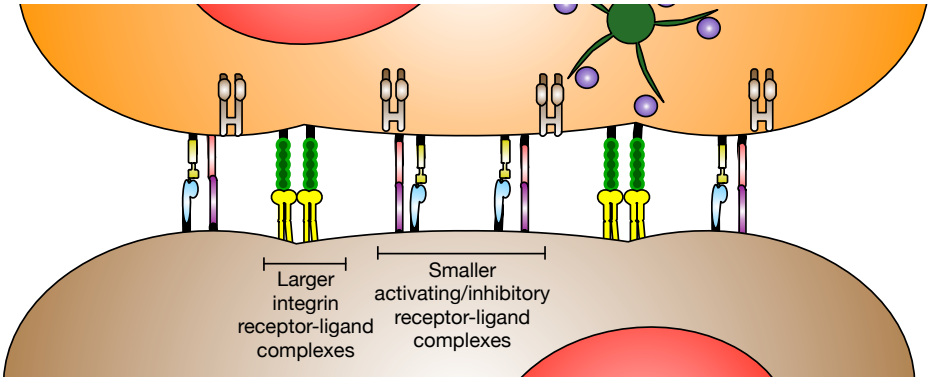


Figure 1.13. Size-dependent segregation at the immune synapse. Receptor-ligand complexes are segregated at the synapse depending on their size. Smaller signalling proteins (NKG2D-MICA (red and purple), KIR-HLA (Blue and yellow) and CD16-Fc fragment (purple and pink)), around 15 – 25 nm, are clustered between complexes of larger span, around 45 – 50 nm, such as LFA1-ICAM1 (green and yellow). The segregation of these proteins is known as the kinetic segregation model. Diagram not to scale.

Köhler *et al*. demonstrated that elongation of the extracellular domains of MICA or HLA-Cw6 drove segregation of differently sized proteins within the synapse. The addition of 2, 3, or 4 Ig domains into the extracellular portion of the protein segregated receptor-ligand complexes from the shorter wild-type (WT) form. However, matched sizes, either long (4 additional Ig domains) or short forms (no additional domains), were clustered together within the synapse. Secondly, they showed that elongation of MICA decreased NK cell-mediated lysis, but the co-expression of a shorter Cw6 protein did not decrease killing any further. Only the expression of a matched-size inhibitory receptor had any further effect. Pearson's co-localisation analyses confirmed that only matched sizes are able to cluster together in the synapse ($r \geq 0.5$), whereas mismatched sizes were segregated ($r \leq 0$). This is most likely due to the inability of the receptors to co-localise within the synapse. Functionally, this lack of co-localisation abrogated the ability of inhibitory receptors to efficiently dephosphorylate the activating receptors, resulting in the diminished signalling reported (124).

To address size segregation at the synapse by a different means, Alakoskela *et al*. inserted lipid anchors into NK cell membranes that could bind quantum dots (QD) of a range of sizes via a biotin-streptavidin bond. These data demonstrated that the exclusion of QD was proportional to their size. Those of diameter below the span of signalling receptor-ligand complexes were included within the central regions of the synapse, whereas those larger were excluded to the periphery (189).

Together, these studies show the importance of extracellular domain size at the IS, influencing both the organisation and proper function of the synapse. More importantly, the extracellular dimensions of these receptors will have a profound effect on the cell-cell membrane proximity, thus influencing where cell-bound proteins are located within the synapse. Whilst these studies do not address the effect size has on extracellular proteins, they confirm the importance of size at the IS.

1.3 Cytotoxic mediators and target cell death

Cytotoxic proteins, stored in pre-formed LG, facilitate NK cell-mediated cytolysis. These lysosome-like organelles are polarised to the IS and their cytotoxic contents are secreted across the synaptic cleft following activating signal cascades. The polarisation and release of these mediators activates various pathways that induce apoptosis of the target cell. The major proteins expressed by NK cells that are involved in cytolysis are PFN (216-218) and Gzms (219-222).

1.3.1 Lytic Granules

LG are considered to be 'secretory lysosomes' based on their similarities to conventional lysosomes (223-225). They are classed as 'dual-functional' organelles, exhibiting both degradative activity, as well as trafficking and membrane fusion, which facilitates release of granule contents during secretion (226). A lipid bilayer separates LG contents from the cytoplasm. This membrane also contains various proteins required for transport within the NK cell (227).

Mature LG membranes contain a number of proteins required for fusion, trafficking and secretion, including CD63, the LAMP family of proteins (LAMP-1, -2 and -3), Munc13-4 and Synaptobrevin-2, a vesicular SNARE protein (223, 228, 229). Diseases associated with the loss of function of these molecules demonstrate the importance of the surface proteins required for LG trafficking and secretion. For example, individuals suffering from diseases such as Chédaik-Higashi syndrome and Griscelli syndrome have impaired secretory lysosome function. This is due to a mutation in the gene LYST, which encodes the protein lysosomal trafficking regulator (230-232). These diseases are associated with both severe immunodeficiencies, due to a lack of LG secretion, as well as hypopigmentation, caused by defects in the melanosome formation. These findings show that LG are an integral part of a system that is employed by a range of cells in the human body to release proteins in a secretory manner (233). Similarly, familial heamophagocytic lymphohistocytosis type 3 (FHL3) manifests in patients with defects in the gene UNC13D, which encodes Munc13-4. This leads to a disruption in LG exocytosis and abrogation of cell-

mediated cytolysis, demonstrating the essential requirement for exocytosis in NK cell-mediated effector function (234).

Whilst diseases such as these have highlighted proteins critical for correct sorting and trafficking of LG, the exact mechanisms behind these processes are currently unknown (226). Traces of proteins from LG can be found across the rough endoplasmic reticulum and trans-Golgi network (TGN), but not of endosomal compartments, which indicate that the dense cores of LG are derived directly from the TGN, with little or no involvement of endosomes (235, 236). Previous groups have attempted to characterise LG, detailing their formation through fusion of multivesicular bodies (223). However, recent EM cryosections, which preserve intracellular organelles, have identified that there are a number of different structures that resemble LG. This makes following the maturation of LG and their identification particularly difficult (237).

The LG lumen contains an array of unique enzymes and those typical of lysosomes. These unique proteins include PFN, Gzms, Fas ligand (FasL; CD178), TNF-related apoptosis-inducing ligand (TRAIL; CD253), and granulysin (223, 238). The identification of PFN and Gzms within the LG lumen is currently the most reliable indicator of a mature LG (224). Within the multivesicular bodies of fully developed LG, cathespins and other lysosomal hydrolases (*e.g.* acid phosphatase) exist in areas devoid of cytotoxic enzymes. The dense cores of LG are where cytotoxic proteins (such as PFN and Gzms) are held in lattices by a chondroitin-sulfate proteoglycan, serglycin (SG) (223). Furthermore, the deficiency of SG in CTL has been shown to affect the maturation and storage of GzmB, suggesting a critical role in LG formation and processing of granule contents (239).

1.3.2 Perforin

PFN is the major cytotoxic protein expressed by CTL and has been the subject of many studies since its discovery in LG (240, 241). PFN is a multi-domain protein, named for its ability to form pores within a membrane. It is constitutively expressed in NK cells (at greater levels in $CD56^{dim}$ compared to $CD56^{bright}$) (242-245). PFN is transcribed as a 65 kDa protein that consists of a 21 amino acid signalling peptide, a highly conserved membrane attack complex/PFN (MACPF) domain (246), a four-

stranded β-sheet flanked by two clusters of α-helices (CH1 and CH2) (247), an epidermal growth factor (EGF)-like domain and a C2 domain at its extreme C-terminal end (248) (Figure 1.14A and B). The MACPF domain has homology with many other pore-forming proteins such as complement C9 (249, 250) and distinct functional similarities to bacterial pore-forming toxins (251). Once transcribed, PFN is transported from the ER to the Golgi apparatus via its C2 domain, then via N-glycosylation sites to the LG (252). Whilst these trafficking mechanisms have not been fully elucidated, the mannose-6-phosphate receptor (M6PR) pathway is thought to be involved, similar to neuraminidase transport to lysosomes (253). Once located within LG, PFN is modified by cathespin-L, undergoing proteolytic cleavage to remove the signal peptide at the N-terminal, resulting in a mature, active PFN protein (254). Once active, PFN activity is controlled and inhibited by a combination of the acidic LG lumen, calreticulin/calreticulin-mediated resistance to lysis and interaction with SG (255, 256).

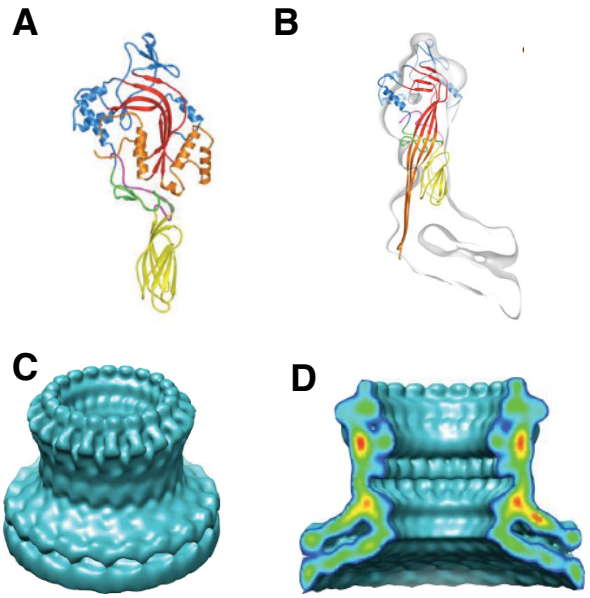


Figure 1.14. The structure and pore formation of perforin. The structure and domains of perforin facilitate its membrane binding and insertion, and pore-formation. **(A)** Crystal structures of perforin monomers show a 'key-shaped' protein containing a MACPF domain with a central β-sheet (blue and red respectively), amphipathic CH1 and CH2 domains (orange), an EGF-like domain (green) and a C2 domain (yellow). **(B)** Once in a neutral pH, perforin can extend its CH1/CH2 domains into β-hairpins that facilitate membrane insertion. **(C)** Surface and **(D)** cut-away views of a cryo-electron microscopy reconstruction of a perforin pore with 20-fold symmetry. The cut away image is rainbow coloured by density, where red to green represent high- to low-density regions, respectively. Images taken from Law *et al.* (2010)

Even a small decrease in PFN expression can have an impact on the cytolytic capacity of NK cells (257). Studies using NK cells or CTL cells from PFN (258, 259) or Gzm (260) KO mice have shown that PFN is critical for GzmB-mediated apoptosis. PFN alone is insufficient to mediate effective cytolysis, demonstrated in KO mouse studies and using *in vitro* cell cultures with the addition of PFN in the presence or absence of Gzms (258, 261). A later study by Smyth *et al.* investigated the lytic ability of *in vivo* NK cells from WT and PFN KO mice to clear tumour cells (222). The absence of PFN markedly reduced, or abolished, NK cell-mediated lysis. Furthermore, PFN-deficient NK cells have been shown to lack lytic capacity following activation by IL-2 or polyI:C (258). These studies demonstrate the essential role of PFN in NK cell-mediated lysis. In a more recent study, Krzewski *et al* demonstrated that depletion of LAMP1, a surface protein expressed on the surface of PFN-containing LG, inhibited both the trafficking of PFN to the LG and the fusion of LG with the cell membrane, ablating the cytotoxicity of NK cells. (176). These findings further highlight the critical role of PFN in NK cell-mediated lysis. However, the amounts of PFN that are secreted by NK cells remain unknown.

The critical role of PFN in immune regulation of tumour cells is demonstrated by the increased susceptibility to tumourgenesis in PFN KO mouse models (262). Whilst there have been significant advancements in our understanding of the modes of action of these proteins, the physiological amounts secreted and the exact mechanism of entry are contentious. Indeed, if a sufficient amount of PFN is added to an *in vitro* cell culture, cell death is initiated, however in the absence of GzmB, cells undergo necrotic cell death rather than apoptosis (248, 261). These studies are not representative of the physiological secretion of PFN, which is secreted by CTL into a micrometer-sized cleft. These *in vitro* studies involved the addition of extracted or recombinant protein to culture medium. Moreover, amount of PFN capable of initiating 50% lysis of cells in culture varied by an order of magnitude – 175 pM and 1.27 nM. This could well have been due to cell types or the source of PFN (recombinant or extracted from granules). These experiments did not take into account the effect that PFN has over the entire surface of the cell body, which may require more or less PFN than is released across the synapse. Therefore, the physiological amounts of PFN released by CTL to initiate cytolysis remain unknown.

1.3.3 Granzymes

Gzms are a group of five serine proteases that are constitutively expressed in NK cells (245, 263) and are classified based on the residues at which they cleave their substrates (263-266), as summarised below in Table 1.3. Gzms are synthesised as pro-enzymes and are transported to LG through the M6PR pathway (267). Once within LG, Gzms are processed into an active form by cathespin-C (Gzms A, H, K and M) or -H (GzmB) (222, 268, 269) and packaged in complexes with SG and PFN (256, 270). Studies in SG-deficient mice demonstrate that CTL have significantly lower intracellular levels of GzmB, but not GzmA, compared to WT mice, suggesting that whilst these proteases are required for effective induction of apoptosis, they use distinct transport mechanisms to traffic from the Golgi to the LG (239).

Granzyme	Enzyme Type	Substrate cleavage	Reference
A	Tryptase	After arginine or lysine residues	(266)
B	Asp-ase	After aspartic acid residue	(264)
H	Chymase	At hydrophobic residues – Phe, Tyr or Trp)	(265)
K	Tryptase	After arginine or lysine residues	(263)
M	Met-ase	At methionine or leucine residues	(263)

Table 1.3. Gzms expressed within NK cells, their enzyme type and substrates.

One of the most widely studied Gzms is GzmB. This protein has been shown to initiate apoptosis via two mechanisms: caspase-dependent or caspase independent pathways (271) (Figure 1.15). The key features of granule-mediated apoptosis are DNA fragmentation, phosphatidylserine (PS) externalization, cytoskeletal breakdown and the loss of inner mitochondrial transmembrane potential ($\Delta\Psi_m$) resulting in the release of cytochrome c (272).

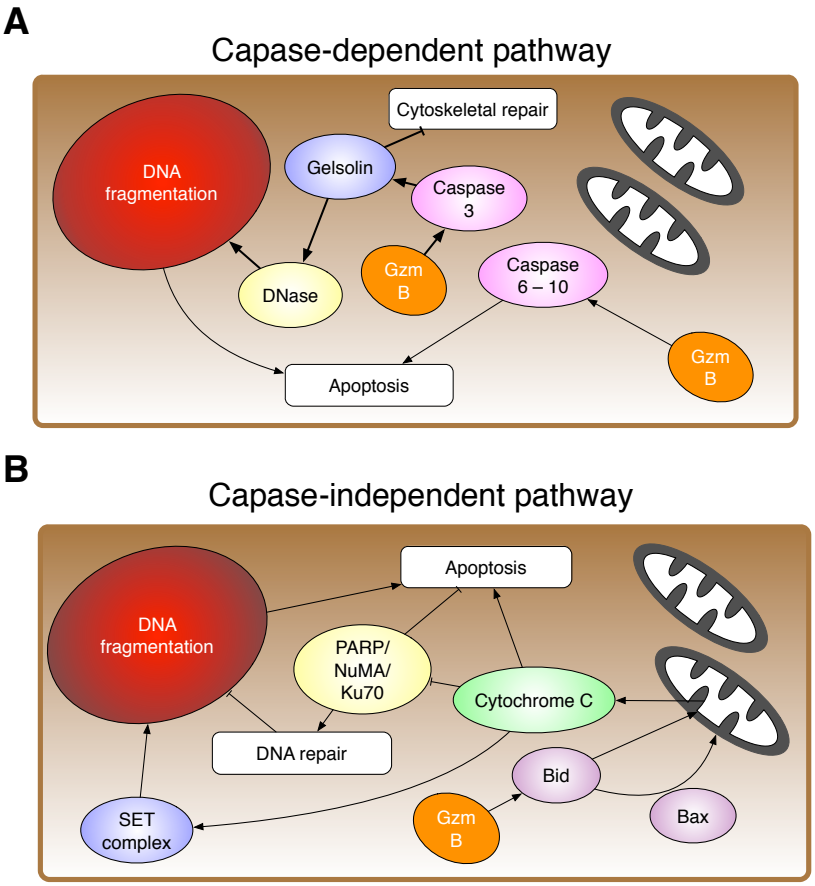


Figure 1.15. Granzyme B initiates apoptosis through both caspase-dependent and caspase-independent pathways. (A) Upon entry into the target cell cytosol, Granzyme B cleaves and activates caspases 3 and 6 – 10. These activated caspases then deactivates gelsolin, a protein that maintains cytoskeletal repair and inhibits DNase. Uninhibited DNase moves into the nucleus and fragments the DNA. **(B)** In the absence of caspases (*e.g.* following inactivation of caspases through transcribed viral proteins), granzyme B can initiate apoptosis independently. Cleavage and truncation of Bid, which moves to the mitochondrial membrane, recruits Bax. These proteins form pores within the outer mitochondrial membrane, resulting in the release of cytochrome c. Cytochrome c both inhibits DNA repair mechanisms and activates the SET complex that performs single-stranded DNA damage.

Caspase-dependent pathway (Caspase-3)

Caspase-dependent cell death is induced through activation of caspase-3 (273), demonstrated in GzmB deficient murine cells, where DNA fragmentation in target cells was significantly reduced during *in vitro* assays of cytolysis (274). Caspases 6 – 10 are also substrates for GzmB, but caspase-3 appears to be the most important (275). Activation of caspase-3 leads to the cleavage of gelsolin, a cytoskeletal maintenance protein and an inhibitor of caspase-activated DNase, inducing apoptosis in target cells. Cell death is demonstrated by the hallmark cellular changes, such as cytoskeleton breakdown and DNA fragmentation (276, 277). However, other

studies have demonstrated that in addition to caspases, there are additional substrates for GzmB activity (278).

Caspase-independent pathway (Bid)

Whilst caspase inhibition was able to inhibit DNA fragmentation, the loss of $\Delta\Psi_m$ and cytochrome c release still occurred. This resulted in the necrosis of target cells as opposed to regulated cell death via apoptosis (272). This may be an evolutionary advantage so that viral inhibition of caspases would not prevent the death of infected cells. The loss of $\Delta\Psi_m$ has been demonstrated to be a result of GzmB-mediated Bid cleavage, which translocates to the mitochondria upon truncation (279). The truncated Bid protein recruits the pro-apoptotic B-cell lymphoma protein (Bcl)-2 family member, Bax, to the membrane of the mitochondria, forming pores in the outer mitochondrial membrane and causing the release of cytochrome c (280). In addition, Gzms B and K abrogate DNA repair and spindle stabilisation by inhibiting proteins essential for these processes (poly APD ribose polymerase (PARP), DNA-PKc, nuclear mitotic apparatus (NuMA) and Ku70 (278, 281, 282). In addition, these Gzms activate nucleases that induce single-stranded DNA damage, such as the SET complex (283). In concert, the cleavage of DNA related enzymes and the loss of mitochondrial membrane integrity prevent the repair of the target cell and increase the amplitude of the pro-apoptotic effect of Gzms.

1.3.4 Target cell death by cytotoxic mediators

Target cell lysis, mediated through apoptosis, is initiated by a combination of pore-forming PFN and the apoptosis-triggering factors, Gzms. Once released into the synaptic cleft, physiological calcium (Ca^{2+}) levels and a neutral pH facilitate PFN membrane binding via the calmodulin-based C-terminal C2 domain (248). Up to 4 Ca^{2+} ions bind the C2 domain within Ca^{2+}-binding loops, possibly via lipid head groups (284, 285). Once bound to the target cell membrane, extension of the amphipathic CH1 and CH2 regions facilitate insertion into the membrane. These PFN monomers then oligomerise to form pores within the target cell membrane (Figure 1.14C and D). PFN pore diameters range between 5 – 30 nm, with most formed of 19 – 24 subunits corresponding to lumen diameters 13 – 20 nm (286). These diameters

are of sufficient dimensions to allow typical GzmB monomers or dimers (5 and 9 nm in their longest dimensions respectively (286)) to pass through the lumen into the target cell cytosol. However, it has been shown that they are unable to enter the target cell cytosol by diffusion alone (261, 287). Gzms are held within complexes formed with SG and PFN. This may impede their diffusion through the PFN pore lumen as these complexes can consist of up to 20 GzmB molecules interacting with a single SG (256). Instead, Gzms require mechanisms that are initiated by PFN to enter the target cell (256). Insertion of the PFN-SG-GzmB complexes into the target cell membrane form invaginations and facilitate GzmB entry. Studies have shown that in concert with PFN-SG, GzmB delivery to cells was markedly improved, when compared to PFN proteins alone, suggesting that this complex enhances the entry of Gzms into the target cell (256). GzmB is thought to enter cells through one of two mechanisms: diffusion or endosomal uptake.

Diffusion of GzmB into the target cell cytosol may require PFN-generated pores within the membrane that allow the diffusion of Gzms into the cytosol (242, 288, 289). Studies have demonstrated that PFN added to *in vitro* cell cultures with and without GzmB can induce cytolysis. Whilst PFN alone induces necrosis, the addition of GzmB facilitates the initiation of apoptotic cell death. In addition, a study by Gross *et al.* demonstrated a PFN-independent entry of GzmB into the cytosol. Heat shock protein (HSP)-70, expressed by a human colon carcinoma cell line, was shown to facilitate the uptake of GzmB into the cells (290). Whilst this uptake indeed induced apoptosis in the cells, the effect was observed over a 24-hour period of GzmB exposure to the cells. An unexpected finding of this study was that the high expression of HSP-70 on the surface of cancer cells increased cell-mediated lysis. This demonstrates that there are proteins, in addition to PFN, that can facilitate the entry of GzmB into the target cell.

The endosomal route of PFN, Gzms and SG uptake is a mechanism facilitated via invagination and disruption of the target cell membrane, demonstrated by a number of groups (261, 287, 288) (Figure 1.16). Collectively, these studies have shown that the binding of PFN to the target cell membrane caused ruptures that allowed Ca^{2+} entry into the cytosol (291). This triggered a membrane repair response (MRR) mechanism, by which the damaged membrane was endocytosed in a clathrin- and dynamin-dependent manner (261, 265, 292, 293). As a result, PFN-GzmB-SG

complexes bound to the target cell membrane via PFN were endocytosed into the target cell in a number of early endosomal antigen (EEA)-1 positive endosomes. The fusion of these endosomes forms larger vesicles, termed gigantosomes (294). The neutral pH within the lumen of these gigantosomes causes the gradual dissociation of PFN-GzmB-SG complexes. PFN monomers insert into the gigantosome membrane, oligomerise into pores, and disrupt the structural integrity of the membrane. PFN-mediated pore-formation at this stage facilitates the gradual release of free Gzms into the cytosol until the collapse of the gigantosome, providing the full release of GzmB, and the death of the target cell. This growing body of evidence suggests that it is most likely that this mechanism is used by GzmB to access the target cell cytosol. These findings demonstrate the necessary role of both PFN and GzmB to act in concert to initiate apoptosis, driving cytolytic effector functions.

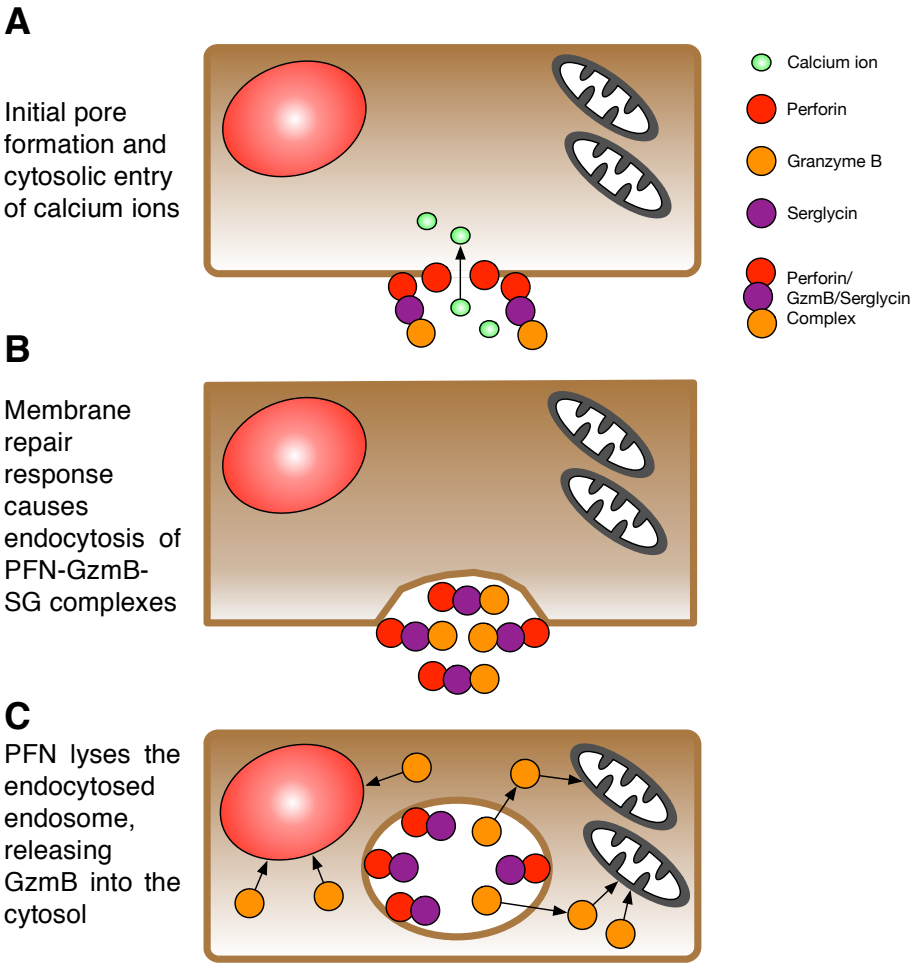


Figure 1.16. Calcium-dependent endosomal uptake of granzyme B into the target cell. Recent data suggests that granzyme B enters the target cell through endosomal uptake. **(A)** Perforin (red) binds to the cell membrane (brown), creating small pores that allow the influx of calcium ions (green). **(B)** Calcium ions within the target cell trigger the membrane repair response, a mechanism by which the cell tries to repair damage via endocytosis of the damaged membrane. **(C)** Endosomal uptake of the damage membrane internalises perforin, granzyme B (orange) and serglycin (purple) complexes. Under neutral pH, perforin dissociates from the complex, creating pores within the endosome. Granzyme B gradually leaks out of the endosome until sufficient pores cause a collapse of the endosomal and a full release of granzyme B and perforin initiate apoptosis. Cell death is mediated through binding to the mitochondria (black) and fragmenting DNA within the nucleus (red).

1.4 NK cells and disease

A significant proportion of NK cell research is focused towards their ability to lyse virally infected or transformed cells. As a result, therapies to increase NK cell lytic capacity against tumours have been extensively researched and there are various therapies emerging that employ redirected lysis to aid the clearance of transformed cells. However, research into the role of NK cells in autoimmunity has not been widely studied and hence, few therapies are available to modulate their role in these diseases.

1.4.1 Anti-tumour therapies

Despite the evolution of a range of receptors to recognise and exert cytotoxic function towards transformed or infected cells, flaws in the system, mostly due to immune escape or evasion, can lead to the development of long-term, terminal cancers (295-297) or persistent viral infections (298-300). Therefore, therapeutic manipulation of NK cells, both *in vitro* and *in vivo,* to augment the clearance of pathogenic agents within the body is an area of ongoing research.

There have been a number of methods developed to enhance NK cell-mediated cytolytic functions against tumours. The first trials in humans made use of *ex vivo* IL-2 expanded NK cells. Recent work using such methods have shown NK cell cytolytic capacity to increase 5-fold and resulted in remission in a number of patients treated (301). More recently, *ex vivo* NK cells have been expanded with other cytokines such as IL-15, or EBV-transformed lymphoblastoid feeder cells. These studies have both shown promising results. IL-15 expansion of NK cells increased cytotoxicity by 40-fold, prolonging one- and two-year patient survival rates by 20% and 30% respectively (302). EBV-transformed feeder cells have been shown to increase NKG2D expression on NK cells, in addition to increasing cytotoxic capacity and expanding cell numbers up to 850-fold over three weeks (303). In addition to the *ex vivo* expansion of NK cells, clinical researchers are using novel methods of amplifying the NK cell response against tumour cells. In a very recent trial by Guma *et al.*, IL-2 in an aerosol form was administered intranasally (304). They reported an increase in the numbers of NK cells in metastatic nodules, but not in other organs.

Encouragingly, the application of aerosol IL-2 decreased nodule size in the lung and the further addition of expanded NK cells was able to decrease the number of lung nodules by up to 6-fold.

Unfortunately, such therapies are not all successful in the long term. This is due to numerous factors including autologous inhibition by MHC-I and immunosuppression by tumour-derived factors and regulatory T cells (Treg). To overcome this, the transfer of tissue-typed NK cells from healthy related donors was trialled (305). A number of factors must be considered prior to the allogenic transfer of NK cells. These include KIR/HLA expression profiles of both the donor and recipient to ensure tissue compatibility and to improve the outcomes of adoptive transfer-based therapies (306-308). Nonetheless, IL-2-activated-NK-cell transfer resulted in successful expansion of NK cells and up to 66% of patients cleared leukaemias – significantly more than patients whose NK cell transfers failed to expand. Unfortunately, despite this success, IL-2 expansion of NK cells can also be associated with life-threatening toxicity (309), as well as an increase in NK cell susceptibility to apoptosis following contact with vascular endothelium (310).

The expansion of NK cells using IL-15, a cytokine paramount to NK cell development, is possible without some of the caveats of IL-2 activation (32, 310, 311). IL-15 has been shown to be more efficient than IL-2 for expanding NK cells, promoting their survival and protecting them from IL-2 associated-induced cell death (AICD) (310, 311). The limitation of this therapy is that large quantities of IL-15 are required to provide a significant effect. For this reason, the use of DC-mediated IL-15 trans-presentation has been proposed (312). Further studies have also focused on the use of IL-12 and IL-18 for augmentation of NK cell function. Aside from increased cytotoxicity and lysis of tumour cells, both IL-12 and IL-18 have been shown to increase IFNγ production from NK cells through the upregulation of the IL-12 receptor in response to IL-18 (38, 313-316). This enhanced IFNγ production promotes a type I immune response that can counteract the immune escape mechanisms employed by tumour cells or immune suppression mediated by Tregs (317-319). These findings show that NK cell-based immunotherapies can be used to efficiently modulate cytolysis, improving the eradication of tumour cells.

Another NK cell-based therapy that has been trailled is use of antibodies to direct ADCC against transformed cells (320). A successful and well-studied example is Rituximab. Rituximab is a monoclonal IgG antibody against CD20, expressed on mature B cells, and is currently used to treat non-Hodgkin's lymphoma (321, 322). Increased efficacy of this antibody has been attributed to both the high affinity CD16 F/F genotype (a homozygous polymorphism at position 158 of Phe instead of Val) (323) and the alteration of the phenotype of the B cell itself (CD20 capping), increasing its susceptibility to killing (324). The use of antibodies to target NK cells towards tumours provides a useful tool for combating tumour cell growth. Other monoclonal antibodies that promote NK cell ADCC have been successful, including Trastuzumab (breast cancer) (325), Alemtuzumab (chronic lymphoid leukaemia) (326) and Cetuximab (colorectal cancer) (327).

In combination with therapies promoting ADCC, blocking antibodies against the KIR inhibitory receptors have also been developed. Specifically, an antibody that targets KIR2DL1/2/3 has been shown to increase the lysis of acute myeloid leukaemia cells and clinical trials are currently underway (328). Finally, antibodies to promote cytokine secretion and cell-mediated cytolysis have also been developed. Trastuzumab-mediated ADCC was found to upregulate CD137 on the NK cell surface. CD137, a co-stimulatory molecule of the TNF receptor family, is normally expressed at low levels on NK cells prior to CD16 ligation. Whilst the mechanism is unknown, the addition of anti-CD137 antibodies along with Trastuzumab increased both IFNγ and ADCC-mediated cytolysis of $HER2^+$ breast cancer cells, both *in vitro* and *in vivo* (325). Antibodies against CD137 have been used in combination with Rituximab and increased both NK cell degranulation and IFNγ production. Other treatments include the co-administration of antibody-based therapies that target cancer cells or NK cell receptors with drugs. One such drug is Lenolidamide that enhances ADCC in the treatment of multiple myelomas (329). In addition, cytokine-based stimulation (IL-2, -12, -15, and -21) has also been shown to increase NK cell-mediated ADCC against tumour cells (330-333).

These findings demonstrate that there is a vast amount of work focused on enhancing NK cell-mediated tumouricidal functions. The expansion, manipulation, and direction of the immune system towards evasive targets have shown promising results. Whilst the exact mechanisms of some therapies remain unknown, it is clear

that NK cells play a pivotal role in protection against virally infected and transformed cells.

1.4.2 Dysregulation and auto-immunity

Autoimmune diseases can be divided into two types: tissue-specific (*e.g.* diabetes mellitus (DM) or multiple sclerosis (MS)) or systemic (*e.g.* systemic lupus erythematous (SLE)) (334). The majority of studies on autoimmune diseases have focused on inappropriate T- and B-cell-mediated reactions to 'self', which can be a multi-step process over a number of years (335). The inclusion of NK cells to autoimmune studies most commonly arises following the onset of symptoms and thus their contribution to autoimmune diseases remains poorly investigated (334).

Several studies have shown an elevated number of NK cells in tissues affected by autoimmune diseases, such as the pancreas of type 1 DM patients (336), the hair follicles of alopecia areata patients (337) and the muscle tissues of jeuvenile dermatomytosis affected individuals (338). The roles of NK cells in the progression of these diseases is not fully understood, but studies in both mouse models and human patients have shown that increased numbers of NK cells are located within the islets of Langerhans during the early stages of type 1 DM, whereas late-term diseased tissues show a reduced number (336, 339). Other studies have shown a role of ADCC in SLE nephritis. The high expression of CD16 by NK cells, in combination with a high-affinity F/F homozygous polymorphism, renders the patient susceptible to severe cytolysis of kidney tissue (340) following the production auto-reactive antibodies by plasma cells (341). These findings suggest that NK cells may contribute to the onset and initial progression of autoimmune conditions, whereas later stages of disease may not involve NK cells.

Conversely, in some autoimmune diseases, NK cell numbers are severely reduced and those that are present lack cytolytic capacity (342-344). Various studies have shown that NK cell involvement in autoimmunity can be tissue specific, a reflection of their varied functions within different tissues (345). For instance, rheumatoid arthritis (RA) patients have been shown to elevate levels of IFNγ-producing $CD56^{bright}$ NK cells in their joint synovia (343, 346), whilst peripheral blood NK cells are depleted

and those remaining have a reduced function. Functionally, the increased production of IFNγ by NK cells has a direct effect on DCs, promoting disease progression in this setting (343, 344).

NK cells have been shown to have simultaneously exacerbating and ameliorating roles in a range of autoimmune diseases. This dichotomy may depend on NK cell interactions with other immune cells. MS, an inflammatory disease that affects the central nervous system (CNS), is thought to be a case where NK cells have bi-modal roles. An immunoregulatory role has been demonstrated by lysis of alloreactive T cells by NK cells (347). In contrast, oligodendrocytes, astrocytes and microglia in the CNS are directly lysed through the recognition of NKG2D ligands (348, 349). However, monoclonal antibody therapies, such as daclizumab (a humanized anti IL-2Rα antibody), significantly increase the number of $CD56^{bright}$ NK cells leading to a decrease of infiltrating $CD4^{+}$ T cells in the CNS (350, 351). This demonstrates that whilst NK cells may well play a role in disease progression, NK cell directed therapeutics may increase their capacity for an immunoregulatory, protective role.

Studies of SLE, a disease associated with immune complex-mediated destruction and dysfunction of a number of organs, have indicated that NK cells may inhibit the development of B-cell-derived autoantibodies, a hallmark of SLE (352). Specifically, NK cell depletion leads to the development of autoantibody-secreting B cells, whilst adoptive transfer of NK cells delayed the onset of antibody production (353). Furthermore, *in vitro* differentiation of haematopoietic stem cells (HSC) taken from SLE patients generated lower proportions of NK cells that expressed reduced amounts of PFN (344). These findings suggest that NK cells have both 'central' and 'peripheral' roles in the development of SLE. Further, NK cells in SLE are $CD56^{bright}$, producing excess amounts of IFNγ. This results in a severe dysregulation of the adaptive immune system (354). There also appears to be a genetic component to the role of NK cells in SLE. Studies have shown that the CD16 F/F genotype, as discussed above, has been strongly correlated with increased IgG_1 binding. This leads to improved ADCC, but increased pathogenicity of nephritic SLE (341). Potentially, this could result in a greater capacity for NK cell-mediated lysis. This double-edged sword could predispose NK cells to more efficient clearance of opsonised targets, but may also have the consequence of increased lysis of healthy cells in autoimmune diseases.

As of yet, NK cells are not direct therapeutic targets for autoimmune conditions (334). This is primarily due to a lack of knowledge of the specific roles of NK cells within each disease setting. The studies detailed above have demonstrated that NK cell depletion or loss/gain of functions could be associated with the development of some autoimmune diseases. NK cells have various roles within the development of autoimmune disorders, associated with both cell-mediated lysis and cytokine production. The treatment of the immune dysregulation associated with autoimmunity is currently confined to targeting proteins expressed on cell surfaces or secreted into the serum. However, dysregulation of the immune system can also occur at the cell-cell level, mediated by intercellular contacts like the IS (355). Currently, no therapies that target proteins secreted across the IS have been developed, possibly because antibodies targeting these molecules are unable to penetrate the interface formed between interacting cells. Therefore, the development of antibody-based therapies capable of penetrating the IS may provide novel methods to augment or inhibit the immune response.

1.5 The immune synapse gasket

A relatively unexplored function of the IS is to form a gasket, or seal, around its secretory domains. This may be formed by both inhibitory, *e.g.* KIR-HLA, and activating, *e.g.* NKG2D-MICA, complexes that possess small extracellular domains, spanning only ~15 nm. This has been confirmed by receptor-ligand crystal structure analysis (356, 357) and electron microscopy of the IS (65). These complexes segregate within the IS away from the larger, ~50 nm, LFA-1-ICAM-1 complexes (65, 124, 189). Molecular ruling with QD of known diameters has also confirmed the distance of the inter-membrane span at the IS. These QD were sized to match or exceed extracellular receptor-ligand complex dimensions, and as a result were included or excluded from the synapse, respectively (189). As signalling is achieved by tyrosine-phosphorylation, similar receptor sizes allow clustering (9, 66) and co-localisation of the receptors within the IS (124) along with associated adaptor proteins such as DAP10, DAP12 and CD3ζ (17). These data have conclusively shown that receptor size is crucial at the IS, however, how soluble extracellular

molecules are affected by this, or indeed could affect synapse formation, has not yet been investigated,

The structure of the synapse, specifically with respect to the extracellular domains of receptor-ligand complexes, results in NK and target cell membranes coming into extremely close contact, within tens of nanometers. Following the binding of activating receptors, PFN and Gzms are released across the IS cleft – yet no bystander-cell death occurs (358). It has been hypothesised that this is due to the structure of the IS forming a gasket, or seal, around the signalling and secretory domains (68, 359-364). This gasket may consist of membrane ruffles (123, 363), adhesion molecules (365), activating and inhibitory complexes (19, 90) and distal CD45 (65). The crystal structures of ICAM-1 (356) and LFA-1 (212) suggest that the extracellular receptor contours would be unable to perfectly align, resulting in small nanometer spaces around the receptor-ligand complexes. Whilst this may prevent receptors forming a tight seal as they accumulate at the synapse, the close proximity of the cell membranes may contribute to forming this gasket.

To function as a gasket, the extracellular domains of the receptors at the synapse may cause both the inclusion of secreted proteins and the exclusion of extracellular molecules from the synapse. Should PFN and Gzms leak from the synapse, this could lead to collateral damage to neighbouring cells. Gasket formation may act to prevent leakage of cytotoxic mediators at the synapse. In addition, the inclusion of extracellular molecules within the synapse could affect the efficacy of cytotoxic proteins secreted by NK cells, either interfering directly with their function or decreasing PFN/Gzm concentration within the synapse. Studies using monoclonal IgG antibodies demonstrated the inability of these large molecules to block proteins, either cytotoxic mediators or cytokines, secreted at the synapse (366) (367). This suggests that the IS is able to restrict the entry of molecules into the synapse, but the extent to which this occurs, specifically regarding a range of molecular sizes, and whether this is directly determined by molecule size alone, has not been investigated.

A gasket function of the IS would be beneficial to the immune system, maintaining cytolytic proteins within the synaptic cleft to provide the most efficient response. However, exclusion of molecules from the synapse may also restrict the ability to target these proteins and influence their function for therapeutic purposes. Most

importantly, many autoimmune diseases are associated with dysregulation at the synapse, either from signalling or secretion of cytotoxic proteins and cytokines (368). Any dysregulation at the synapse may lead to unnecessary attack on the body's healthy cells. This can ultimately result in a range of diseases that are, at present, difficult to treat. Therefore, to determine whether – or to what extent – the IS functions as a gasket to exclude extracellular molecules, would provide a basis for the engineering of novel antibody-based therapies. Subversion of this gasket by antibody-based therapies could allow targeting of secreted proteins that are currently inaccessible to existing therapeutics. This could provide a novel treatment for autoimmune disorders.

1.6 Fluorescence Microscopy

Many major discoveries regarding dynamics and functions of the IS have been revealed using fluorescence microscopy. Our understanding of IS structure, such as the identification of protein segregation (10) (9) (369), and the dynamics of receptors (196) (13) and signalling proteins (370) (203) (371), is entirely dependent on this technique. Fluorescence microscopy is now an essential tool to study cellular structures and functions – including at the IS – in real-time. The ability of this technique to accurately visualise fluorescent labels, tags and proteins enables biologists to watch cell functions unfold before them. Furthermore, the quantification of images allows the generation of readable information that can describe, in detail, numerous cellular processes. Most importantly, fluorescence microscopy facilitates the study of processes and mechanisms, such as the IS, that cannot be visualised or investigated by other means.

1.6.1 Basic principles of confocal microscopy

Confocal microscopy is an imaging technique that is based on wide-field fluorescence microscopy. In this technique, the entire sample is illuminated and all photons emitted are collected at the same time to create an image. As the same lens is used for illumination of the entire sample and signal collection, this results in a significant amount of background noise from out-of-focus light reflected from the sample (Figure 1.17).

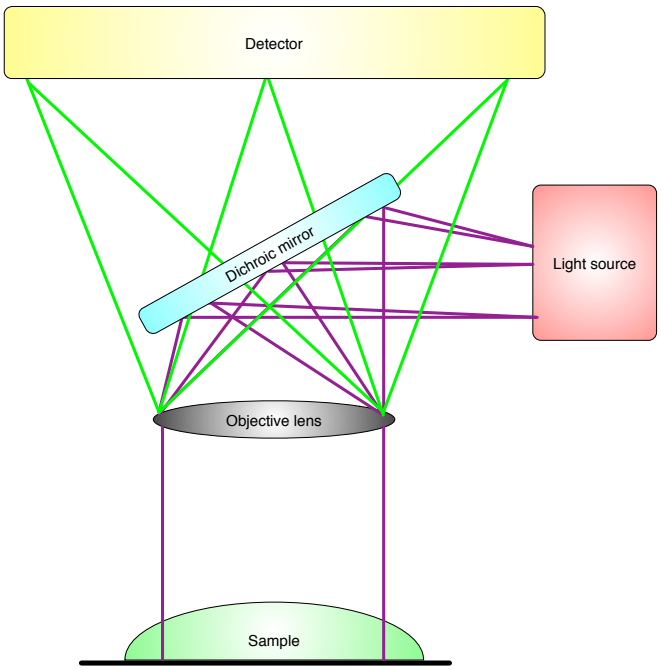


Figure 1.17. Schematic diagram of a fluorescence wide-field microscope. A wide-field microscope uniformly illuminates the sample at a specific wavelength (purple). The light emitted from the sample (green) is collected on a wide-field detector, producing an image of the entire sample.

This was overcome by optically sectioning the sample, building up an image from multiple images taken horizontally along the xy-axis and vertically through the z-axis. This led to the development of the laser scanning confocal microscope (372), providing an increase in optical resolution and contrast. This technique uses a laser that is passed through a light source aperture and is then focused by an objective lens into a small focal volume, either within or on the surface of the sample. As the light reflects off the sample, a beam splitter separates a portion of light and a pinhole is used to prevent any out-of-focus light from reaching the photo-detection device (Figure 1.18). Detectors are usually a photomultiplier tube (PMT), avalanche photodiode (APD) or a combination of both, termed Hybrid Detectors (HyD) (373).

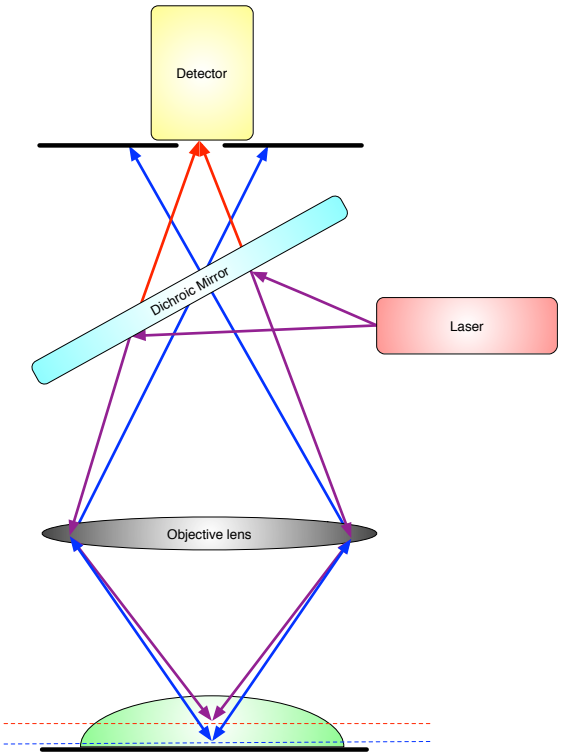


Figure 1.18. Schematic diagram of a laser scanning confocal microscope. A laser beam at a specific excitation wavelength (purple) is focused onto the sample. This creates an excitation spot across a specific plane of the sample (red dotted). The emitted light is focused through a pinhole towards the detector. In-focus light (red) is captured by the detector, and out-of-focus light (blue) is blocked around the periphery of the pinhole. The laser line is then scanned across the sample to generate an image. The focal plane of the microscope can be adjusted throughout the sample (along the z-axis) to generate multiple slices and a computer can reconstruct these into a 3D image.

PMT detectors consist of a vacuum tube that detects low amounts of photons, converting the signal into an analogue electron flow. The electron flow is then amplified over a series of dynodes before arriving at the anode. This continuous signal is sampled at separate time points and then digitised into a discrete signal by an image processor, pixel-by-pixel, into the image displayed by a computer. If signals are fast enough, PMT can measure single photons as electric pulses. However, due to the nature of electron amplification employed by PMT, images produced can contain a significant level of noise (Figure 19A).

APD are highly sensitive semiconductor devices that use the photoelectric effect to convert light into an electrical signal. These detectors use a voltage to drive an avalanche amplification of electron signals. Starting from electron pairs, waves of electrons move through a multiplication zone where they are amplified by impact ionisation. The amplification of signals within an APD allows the signal to be

measured without additional circuitry, resulting in very low noise. Despite a low dynamic range, APD provide a better sensitivity in the red range of wavelengths. (Figure 19B).

HyD are a combination of both PMT and APD detectors, allowing precise and fast measurements over a wide dynamic range. HyD use a photocathode for light conversion, similar to the PMT. Electrons within the PMT component are accelerated by a high voltage, which is dissipated in a semiconductor almost instantly. The initial high voltage acceleration increases the signal 500-fold and the straight movement of the accelerated photon means that there is no variation in the time that the individual electrons hit the semiconductor. This provides a higher frequency of photon counting, which directly translates into a higher dynamic range. This also reduces the instrument time constant, improving the lifetime of the detector. Once electrons have reached the semiconductor, avalanche gain increases the count and they are converted to an electronic digital signal (Figure 19C).

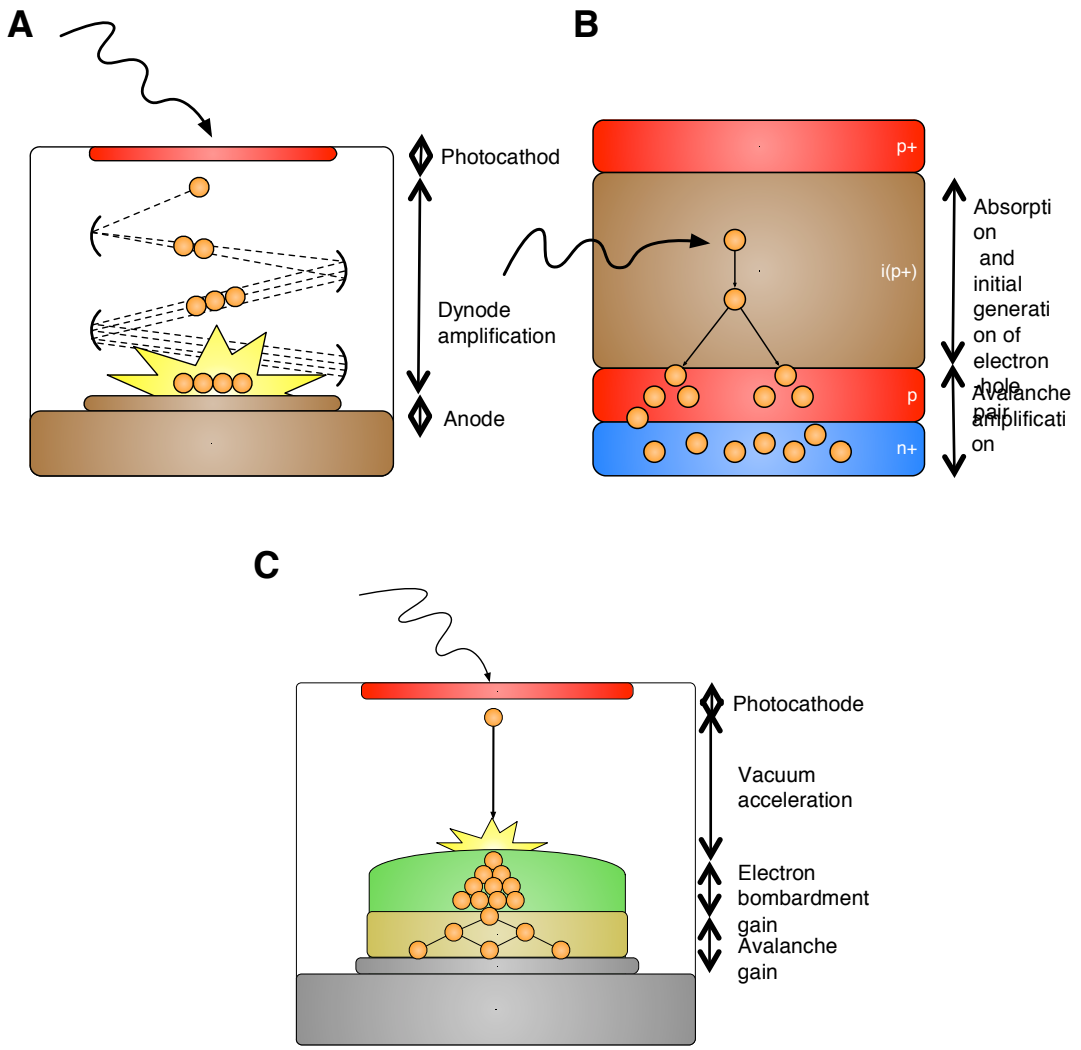


Figure 1.19. Schematic diagrams of confocal microscope detectors. Confocal microscopes use a number of detectors to convert light energy into an electrical signal. Each detector type has advantages and limitations, as described in the text. **(A)** A photomultiplier tube (PMT) detector converts photon energy into accelerated electrons at the photocathode. Subsequent collisions with dynodes multiply the photoelectrons by secondary emission. The potential difference between the dynodes determines the multiplication of photons. **(B)** An avalanche photodiode (APD) absorps photons in an intrinsic layer, where an electron-hole pair is generated. Within a multiplication zone, an electron avalanche is created by impact ionisation. **(C)** A hybrid detector (HyD) is a combination of PMT and APD detectors. HyD firstly uses PMT technology to accelerate the electrons through a vacuum, the accelerated electrons then strike an APD where the electron signal multiplies. Adapted from Borlinghaus, Birk and Schreiber (2012).

The laser beam of a confocal microscope can be focused throughout the sample, which enables the imaging of a number of confocal planes, which can then be reconstructed into a three-dimensional (3D) image. This technique provides a method for studying biological structures, either live or following fixation, in details that surpass previous microscope techniques (374).

Lasers of specific wavelengths can be used to illuminate the sample. This allows the use of fluorophores that are bound to individually dyed or labelled samples. Use of

fluorophores enables identification or localisation of specific proteins or structures throughout a sample. Fluorophores are molecules that are excited by a particular wavelength, providing energy that moves electrons to a higher energy state. A loss of energy through a nonradiative transition (internal conversion) then occurs due to a relaxation of the molecule to its lowest vibrational level (termed vibrational relaxation), a process involving dissipation of the electron's energy to its surroundings. This is followed by the loss of energy that is then emitted as light (a photon) at a longer wavelength than that used for excitation, specifically the difference in energy between the first excited state and the internal conversion. These photons can then be collected to image labelled areas within a sample (Figure 1.20). Following the identification of the genetic sequence for fluorescent proteins, such as green fluorescent protein (GFP) (375), this allowed for endogenous proteins within cells (or whole organisms) to be fused in tandem at the C- or N-terminal with GFP. These constructs can be used to identify specific protein locations, interactions and dynamics in real-time.

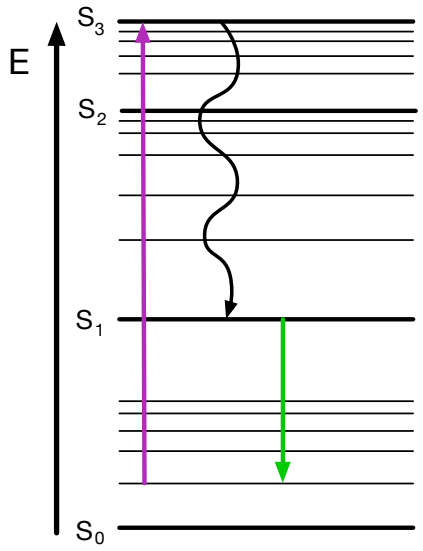


Figure 1.20. Electronic states of fluorophore excitation and emission. Molecule electrons can emit energy as a photon. This occurs though excitation and relaxation (gain and loss of energy) across higher energetic vibrations states (S_{0-3})**.** The electrons of a resting fluorophore populate the ground state (S_0). When excited by light of the appropriate wavelength, the fluorophore will absorb the photon and be promoted to a higher energy and vibrational state (S_3) (*purple arrow*). A loss of energy through internal conversion (*black arrow*) dissipates the electron's energy into its surroundings, termed vibrational relaxation. Finally, the further loss of energy is then emitted as a photon at a longer wavelength than used for excitation – the difference between the energy of the excited state and the internal conversion (*green arrow*).

1.6.2 Limitations of confocal microscopy

Despite the vast improvements of confocal microscopy over previous imaging techniques, there still remain some limitations. For instance, when imaging smaller structures (at the micro- or nanometer scale), resolution and diffraction become limiting factors on the size of structures that the microscope can discriminate between. Optical resolution is defined as the minimal distance at which two separate structures can be identified as individual objects. This is heavily dependent on the signal-to-noise (SNR) ratio and the point spread function (PSF) of the microscope. SNR is the ratio at which the signal strength from the sample can be measured over the background levels. This can be affected by the fluorophore brightness, density or specificity within a sample. SNR can also be exacerbated by increased laser power but ameliorated by reducing the size of the pinhole through which photons reach the detector. However, this reduction in photon numbers produces a dimmer image. This can be partially corrected by altering the gain (based on the voltage) of the detector. Extremely high or low values of gain, however, result in a non-linear increase or decrease of signal, affecting quantitative analysis of the image. The PSF is the response of an imaging system to a point source or object. This is usually a spatial domain that is occupied by each fluorophore and is determined by the imaging system (Figure 1.21). The PSF plays a key role in optical resolution as the overlap of two adjacent fluorophores prevents the resolution of those two independent objects.

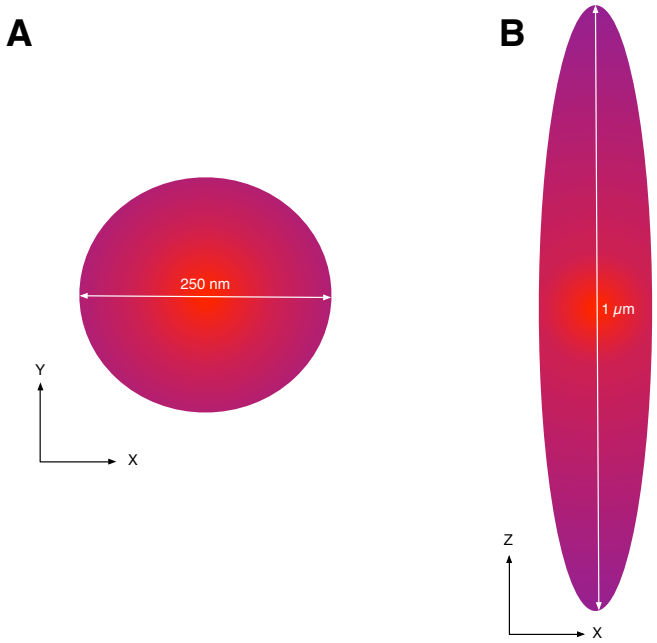


Figure 1.21. The point spread function (PSF) of a microscope. The PSF is the response of a microscope system to a point object. This is the smallest representation of a single object that the imaging system can achieve. The PSF can be measured in the **(A)** xy-axis, averaging around 250 nm, and the **(B)** xz-axis, averaging around 1 µm. The PSF can vary depending on the microscope system and the fluorophore.

Diffraction is the consequence of varying refractive indexes (the ratio of the speed of light in a vacuum to the speed of light within a substance) on the path of a wave. Some diffraction is overcome by the use of a medium, usually water or oil, between the objective lens and the cover glass. The refractive index of the medium is matched to the lens and cover glass so that when the light exits the objective, the diffraction is almost entirely eliminated, as compared to if it was passing through air. However, as light travels through a sample, there are numerous refractive indexes (a change of sample composition, proteins, *etc.*), which diffract the light. This can limit the detail of cellular structures, proteins and imaging dynamics when using confocal microscopy.

1.6.3 Basic principles of total internal reflection fluorescence microscopy

Total internal reflection fluorescence (TIRF) microscopy is based on conventional wide-field techniques, similarly to confocal microscopy. This technique is able to selectively excite fluorophores within a small (~100 nm) region adjacent to the coverglass, known as the evanescent field, minimizing the background fluorescence from the intracellular regions. For this reason, TIRF microscopy as also known as evanescent wave or evanescent field microscopy.

TIRF microscopy takes advantage of the effect of total internal reflection. When the incidence angle of the light source is irradiated at above the 'critical angle', almost all photons are reflected from the surface at the same angle. Instead of directly illuminating the sample, an evanescent wave is created on the opposite side of the coverglass, penetrating approximately 100 nm into the sample. This allows improved sample sectioning compared to confocal microscopy. Only fluorophores within the range of this evanescent field, which decays exponentially into the sample, are excited. This minimises the background fluorescence and creates an image of the sample immediately in contact with the coverglass surface (Figure 1.22). Optimal TIRF is achieved by creating a uniform angle of illumination. This is achieved by focusing the laser beam on the back focal plane of the objective. Here, the light is collimated and exits the objective in a coherent beam, all rays parallel, at the same angle, and in phase. Practically, the illumination angle of a TIRF microscope cannot be 'set' at a predefined angle, but rather evaluated for each sample type, as the critical angle will change depending on the refractive index of the sample.

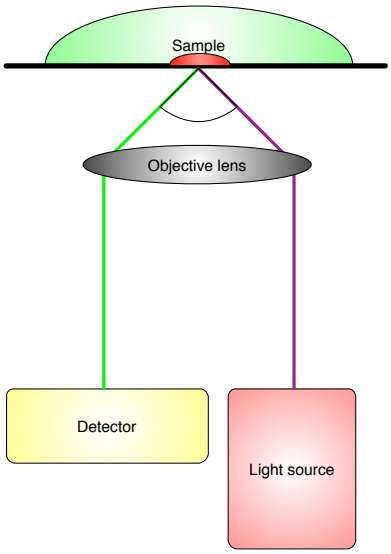


Figure 1.22. Schematic diagram of total internal reflection fluorescence (TIRF) microscopy. A laser beam at a specific excitation wavelength (purple) is focused onto the sample above the critical angle to give total internal reflection. This creates an evanescent wave (red) that decays exponentially from the sample-slide interface, selectively exciting fluorophores within a restricted region of the sample adjacent to the coverglass (black). The microscope optics then collect the light from these excited fluorophores (green) creating an image with a z-axial depth of ~100nm.

TIRF microscopy has both advantages and disadvantages compared to confocal microscopy. Whilst confocal microscopy provides optical sections from almost any plane within a specimen, unlike the narrow ~100 nm imaging depth of TIRF microscopy, the optical sections generated by a confocal microscope can be 6-fold greater in depth. Consequently, the application of either technique is governed by the experiment and exactly what is being imaged. TIRF microscopy has been utilised for a wide range of studies investigating processes close to the cell-slide interface, including cytoskeleton structure and dynamics, endocytosis, cell-substrate contact regions and intracellular signalling (376). A number of significant membrane-proximal events regarding the IS have been revealed and studied using TIRF microscopy with the addition of tools such as supported planar bilayers (377). TIRF microscopy is therefore an extremely powerful technique for imaging samples at or within extremely close proximity to the coverglass.

Fluorescence microscope offers insights into biological functions that cannot be addressed by other means. The dynamic movement of molecules, the organisation of cellular structures, and mechanisms of cellular functions has all been revealed through this technique. There remain many questions regarding NK cell function, but microscopy promises to be an indispensible tool to address these issues.

1.7 Aims and hypothesis

The IS is a complex, ordered and dense meshwork of protein-protein interactions comprised of integrin, activating and inhibitory receptor-ligand complexes. A balance of signals in favour of activation results in NK cells directly secreting cytotoxic mediators, primarily PFN and Gzms, across the synapse to initiate apoptosis and clearance of diseased cells.

Close, but variable, proximity of the NK and target cell membranes occurs at the IS. This results in not only the size-dependent segregation of receptor-ligand complexes, but may also form a gasket, or seal, around the synapse. This gasket could prevent both the leakage of cytotoxic mediators but could also limit the entry of extracellular proteins, including antibody-based therapies. Some anecdotal evidence exists that supports this theory, however, it has not been directly tested. This may explain why there are currently no antibody-based therapies that target these secreted proteins. Development of an appropriately sized antibody may be able to access the synapse and block secreted proteins.

Much is still unknown about the nature of the cytolytic response initiated by NK cells across the IS. Before the development of therapies to block NK cell effector proteins can occur, the concentrations at which they are released across the synapse must be elucidated. Given that any cytolytic activity of Gzms is wholly dependent on the presence of PFN, a better understanding of the nature of the PFN response is crucial. In particular, NK cells recognise a number of ligands, yet the effects of these different ligands and their density on the amount of PFN secreted have not yet been directly investigated. Further to this, the impact of serial stimulation of NK cells by activating ligands has not been addressed, with regards to the effect on PFN secretion.

The aims of this thesis were to establish to what extent the IS functions as a gasket to extracellular molecules and to quantify PFN secretion at the synapse.

The specific objectives of this thesis were:

1. To investigate the extent to which the IS functions as a gasket to various nanometer-scale sized molecules (Chapter 3)

2. To investigate the extent to which the NK cell IS acts as a gasket against functional proteins (Chapter 4)

3. To quantify the amount of PFN secreted by NK cells following activation and degranulation (Chapter 5).

To address these aims, fluorescence microscopy was utilised. In addition, cell responses were measured using flow cytometry, molecular biology techniques and other cell assays.

Chapter 2 – Materials and Methods

2.1 Cells and cell culture

2.1.1 Immortalised cell lines

A variety of immortalised cell lines were used throughout this study. All cell lines were maintained in RPMI-1640 supplemented with 10% heat-inactivated foetal calf serum (FCS), 2 mM L-glutamine, and 1 mM penicillin/streptomycin (hereon referred to as R10) (all Gibco, Life Technologies, USA). Cells were incubated at 37ºC in a 5% (vol/vol) CO_2 atmosphere.

Effector cell lines

Effector cell lines used in this study were the YT sub-clone, YTS (378), and the leukaemic T cell line, Jurkat (379). To form inhibitory synapses, YTS cells expressing KIR2DL1 (YTS/KIR) (380) were available in the lab.

Target cell lines

The target cell lines used in this study were as follows. The human EBV-transformed B cell line 721.221 (hereon referred to as 221), which lacks endogenous class I HLA-A/B/C, was used as the main NK cell target (381). This was due to their specific lysis by both YTS and primary NK cells. For inhibitory synapse studies, 221 cells transfected with HLA-Cw6 (221/Cw6), the cognate ligand for KIR2DL1, were available in the lab (89). In addition, the B cell lymphoblastic cell line, Daudi (382) and the myeloid leukaemia cell line, K562 (383), were used as additional targets for primary NK cells. To study the T cell synapse, Raji cells (384) were loaded with superantigen Enterotoxin E (SEE) from *Staphylococcus aureus* (Sigma Aldrich, UK). To load Raji cells, 5 x 10^6 cells were centrifuged (353 *g*, 5 minutes) and resuspended in 1 mL R10. One microlitre of SEE was added to the suspension to a final concentration of 10 ng/mL and incubated at 37ºC 5% (vol/vol) CO_2 for 1 hour. Cells

were then washed 3 times with conjugation medium (0.5% FCS in RPMI-1640) by centrifugation (353 *g*, 5 minutes) and resuspended in 1 mL R10.

2.1.2 Primary human NK cells

Primary human NK (pNK) cells were isolated from peripheral blood mononuclear cells (PBMC) from normal healthy donors by negative selection using an NK isolation kit (Mitlenyi Biotec, Germany) as previously described (90). Briefly, human blood from a leukocyte cone was poured in to a 250 mL flask and 50 mL RPMI 160 (equilibrated to room temperature) was then added (Sigma-Aldrich). In 50 mL tubes, 15 mL Ficoll-Pacque (GE Healthcare) was added and an equal amount of the blood/RPMI 1640 mixture was added drop by drop. This was then centrifuged at 535 *g* for 40 minutes at 20ºC without a brake applied. Using a sterile plastic Pasteur pipette, the lymphocyte layer (second from top) was removed and placed into 50 mL tubes. The cells were then washed twice, adding RPMI 1640 to the lymphocytes to a final volume of 50 mL and centrifuged at 301 *g* for 10 minutes at room temperature. The supernatant was then decanted and cells were resuspended in 10 mL RPMI 1640, counted, and 10^8 cells were taken and RPMI 1640 added to a final volume of 5 mL. Tubes were then centrifuged at 301 *g* for 10 minutes at 4ºC and the supernatant removed completely. The pellet was then resuspended in 400 µL MACS buffer (PBS, 2mM EDTA (Sigma) and 0.5% BSA (Sigma); sterile filtered) and to this, 100 µL biotin-antibody cocktail (Product code: 130-092-657; Miltenyi Biotec) was added, mixed, and incubated for 5 minutes at 4ºC. After incubation, 300 µL MACS buffer and 200 µL anti-biotin microbeads (Miltenyi Biotec) were added, mixed and incubated for 10 minutes at 4ºC. Cells were then washed by centrifugation at 301 *g* for 10 minutes at 4ºC and the supernatant removed. Cells were then resuspended in 500 µL MACS buffer and placed in a prepared (rinsed with 3 mL MACS buffer, placed in a magnetic stand (Miltenyi Biotec)) LS column (Product code: 130-042-401; Miltenyi Biotec) over 15 mL tubes. The column was then washed 3 times with 3 mL MACS buffer, allowing column to dry between each wash. The cells were then counted, pelleted by centrifugation at 301 *g*, 4ºC and resuspended in clone medium (described below) to a final cell density of 10^6/mL.

Human biological samples were sourced ethically and their research use was in accord with the terms of the informed consents. Blood collection approved for Imperial College London by the Riverside Research ethics committee (05/Q0401/108) and for the University of Manchester by the University Research Ethics Committee (12295).

Primary NK cells were maintained in Dulbecco's Modified Eagle's Medium (DMEM) supplemented with 10% human serum, 2mM L-glutamine, 1mM sodium pyruvate, 1mM penicillin/streptomycin and 1 mM non-essential amino acids (all from Gibco, Life Technologies, USA) (hereon referred to as clone medium). Cells were incubated at 37ºC in a 5% (vol/vol) CO_2 atmosphere. Following isolation, pNK cells were expanded using 150 U/mL recombinant interleukin (IL)-2 and 6 day rested prior to use.

2.2 Dextran

Dextran (Molecular Probes, Life Technologies, USA) is a hydrophilic, complex branched glucan (a polysaccharide comprised of glucose molecules). Molecules of varying molecular weights are synthesised from sucrose by certain lactic-acid bacteria (385). Dextran can be bound to different fluorophore dyes to allow visualisation using a fluorescence microscope. Dextran has been previously measured by dynamic light scattering to give nominal values of the hydrodynamic radii for each molecular weight available (386, 387). The dextrans used in this study including molecular weights, hydrodynamic radii, fluorophore conjugations, excitation and emission maxima and working concentrations are detailed in Table 2.1 below. Stock solutions were prepared in phosphate buffered saline (PBS) to maintain physiological salt concentrations. Working concentrations were prepared by further dilution of stock solutions in R10 medium.

Molecular Weight (kDa)	Hydrodynamic Diameter (nm)	Fluorophore	λ_{ex}, λ_{em} (nm)	Working Concentration (μM)	Reference
3 000	3	Fluorescein	494/ 521	50	(387)
10 000	4	Biotin Fluorescein Texas Red Alexa Fluor 647	N/A 494/ 521 595/ 615 650/ 668	50	(386)
40 000	10	Fluorescein	494/ 521	50	(386)
70 000	13	Fluorescein	494/ 521	50	(386)
500 000	32	Biotin Fluorescein	N/A 494/ 521	20	(386)
2 000 000	54	Fluorescein	494/ 521	2.5	(386)

Table 2.1. Dextran molecular weights, hydrodynamic diameters, fluorophores, excitation/emission maxima, and working concentrations.

2.3 Antibodies and proteins

2.3.1 Monoclonal antibodies

The monoclonal antibodies used in this study are summarised in Table 2.2. Specific methods are outlined below in the relevant experimental procedures.

Antigen	Clone or Product No.	Host	Isotype	Fluorophore	Source
Murine IgG	A-11001	Goat	(H + L)	Alexa Fluor 488	Molecular Probes, USA
Human	CE2.10	Mouse	IgG2a	Unconjugated	Abcam, UK
Human	dG9	Mouse	IgG2b, κ	Alexa Fluor 488	Biolegend, USA
CD16	3G8	Mouse	IgG1, κ	Purified	BD Pharmingen, UK
HLA Class I	W6/32	Mouse	IgG2A	Alexa Fluor 488	R&D Systems, UK
KIR2DL1	143211	Mouse	IgG1	FITC	R&D Systems, UK
Isotype Control	20102	Mouse	IgG2A	Alexa Fluor 488	R&D Systems, UK
Isotype Control	11711	Mouse	IgG1	FITC	R&D Systems, UK
CD56	B159	Mouse	IgG1, κ	Alexa Fluor 488	BD Biosciences, USA
CD3	SP34-2	Mouse	IgG1, λ	PE-Cy7	BD Biosciences, USA
NKG2D	1D11	Mouse	IgG1, κ	BV510	BD Biosciences, USA
CD16	B73.1	Mouse	IgG1, κ	APC	BD Biosciences, USA

Table 2.2. Antibodies used for the analysis of size exclusion and receptor expression and for NK cell activation.

2.3.2 F(ab')$_2$ fragments

Antibody fragments can be generated by digestion of IgG molecules (388). To study access of the immune synapse by antibody fragments, F(ab')$_2$ fragments conjugated to Alexa Fluor 488 were used (A-11070, Life Technologies). The fragments were generated from a goat anti-rabbit IgG that contained both heavy and light chains. The F(ab')$_2$ fragment was supplied at 2 mg/mL and used as described in the relevant methods section.

2.3.3 Domain antibodies

Domain antibodies (dAb) are single domain antibody fragments that comprise of a single monomeric variable heavy chain antibody domain (389). To investigate the ability of dAb to penetrate the immune synapse, a previously published dAb against glycoprotein VI (GPVI) was produced (390). HB2151 E. *coli* were electroporated to take up a pDOM5 expression vector containing the sequence for the BLO8-1dAb and a 5ml starter culture was grown in LB broth supplemented with 100 µg/mL carbenicillin (Sigma), incubated at 37ºC with 220 RPM shaking overnight. Then, 1 mL of the starter culture was used to inoculate a 1 L ONEX media broth culture (Merck Millipore, Germany) supplemented with 100 µg/mL carbenicillin and incubated at 37ºC with 220 RPM shaking overnight. The culture supernatant was harvested by centrifugation in a bench-top centrifuge for 30 minutes at 6800 *g* and decanted into fresh flasks. To the supernatant, 20 mL of PBS washed sedimented protein L (Life Technologies), a bacterial protein that binds immunoglobulin, was added and rotated at 4ºC overnight. The solution was allowed to settle and the supernatant was removed (leaving about 20 mL for resuspension of the protein L). The solution was transferred to a PD10 column (GE Healthcare, UK) and washed, twice using 3 resin bed volumes of PBS and twice using 2 resin bed volumes of 10 mM Tris pH 7.4, to remove any remaining salts and precipitation. The dAb was then eluted from the matrix using 2 rounds of 2 resin bed volumes of 0.1 M glycine pH 2. Neutralisation of the elution buffer was performed using 0.2 volumes of 1 M Tris pH 8. Precipitation was removed by centrifugation at 6800 *g* for 2 minutes. Once precipitates had been removed, the dAb was concentrated using an ultra centrifugal filter (Millipore, USA)

by centrifugation at 6800 *g* for 10 minutes. Spins were repeated (times adjusted accordingly) until 1 mL of solution was remaining.

As dextran has been prepared in PBS, a Slide-A-Lyser dialysis cassette (Thermo Scientific, USA) was used to transfer the dAb into PBS buffer. To achieve this, the dAb was placed in a PBS hydrated cassette by hypodermic needle, which was then placed in 2 L PBS and incubated at 4ºC overnight with stirring. PBS was then replaced and the cassette was incubated at 4 ºC with stirring for a further 2 hours. The dAb was then run on a 12% polyacrylamide gel at 165V for 45 minutes under reducing and non-reducing conditions to confirm its monomeric structure.

For identification using a confocal microscope, the dAb was labelled using a Texas Red protein-X labelling kit (Molecular Probes, Life Technologies, USA) according to the manufacturer's instructions. Briefly, 50 µL 1 M sodium bicarbonate solution was added to 0.5 mL of dAb solution. This was then placed in a 2 mL tube containing a metallic stirrer and DMSO-hydrated Texas Red dye. To label the dAb, this solution was then stirred at room temperature for 1 hour. The labelled protein was then placed in a column loaded with a purification resin and eluted into fractions. The most concentrated fraction was then measured by spectrometry to determine the final concentration and degree of labelling.

2.3.4 Electrophoresis of antibodies

To confirm that the dAb had a monomeric structure, dAb samples prior to and following protein L purification were boiled for 20 minutes under reducing and non-reducing conditions. Thirty microlitres of each sample and 5 µL of protein ladder (SeeBlue II, Life Technologies) was then loaded into a 12% polyacrylamide gel (Life Technologies) and ran at 145 V for 45 minutes using a NuPAGE SDS-PAGE Gel system (Life Technologies). To confirm the molecular weights of each antibody used in size-exclusion experiments (rabbit IgG, $F(ab')_2$ and dAb), 5 µL of each antibody and 5 µL of protein ladder (Precision Plus, BioRad, USA) were loaded into a 12% polyacrylamide gel and ran at 145 V for 45 minutes.

The gels were then fixed (50% methanol, 10% glacial acetic acid) for 1 hour at room temperature, stained (0.1% Coomassie Brilliant Blue (Sigma) for 20 minutes at room temperature, 50% methanol, 10% glacial acetic acid), then distained (40% methanol, 10% glacial acetic acid) by 3 washes for 20 minutes, until the background of the gel was fully distained. Gels were then imaged using a GelDoc XR+ System (BioRad, USA).

2.3.5 Proteins

Recombinant and chimera proteins

Recombinant and chimera proteins used in this study are detailed below in Table 2.3.

Protein	Concentration	Source and Product Number
Recombinant	0.05 mg/mL	Abcam, UK; ab114201
MICA-Fc	100 µg/mL	R&D Systems, UK; 1300-MA-050
ICAM1-Fc	100 µg/mL	R&D Systems, UK; 720-IC-050
Noggin-Fc	100 µg/mL	R&D Systems, UK; 3344-NG-050

Table 2.3. Recombinant and chimera proteins used for quantification and NK cell activation. MICA, MHC class I polypeptide related sequence A; ICAM1, intercellular adhesion molecule.

Low-density lipoprotein (LDL)

LDL is a large protein complex (~500 kDa) that can bind to a specific receptor on the surface of vertebrate cells (391). An acetylated LDL conjugated to Alexa Fluor 488 (Molecular Probes), supplied at 1 mg/mL, was used to assess its ability to enter the immune synapse. Acetylated LDL was used to reduce/prevent binding to LDL receptors expressed on cells. LDL was used as described in the relevant methods section.

2.4 Flow Cytometry

Surface Receptor Expression

NK cells were analysed for their surface expression of various receptors by flow cytometry. YTS/KIR and 221/Cw6 cells were assessed for their expression of KIR2DL1 or HLA-Cw6 respectively. Primary human NK cells were assessed for their expression of CD56, CD3, NKG2D and CD16 (see Table 2.2 for antibodies used).

Briefly, 10^6 cells (or all cells from slide surface following stimulation) were collected and then resuspended in 1 mL flow buffer (0.1% FCS in PBS). The cells were incubated with primary conjugated antibodies at a dilution of 1:100 for 45 minutes at 4ºC. Samples were then washed 3 times with FACS buffer and resuspended in 4% PFA for fixation at 4ºC for 20 minutes. Samples were then washed 3 times in flow buffer and transferred to FACS microtubes. Data was acquired on a FACSCanto II flow cytometer (Becton Dickinson, USA). 10 000 intact events, as determined in forward scatter/side scatter plots, were collected for each condition and data analysis was performed using FlowJo software version 9.7.6 (TreeStar).

Cell Viability

Primary human NK cells, YTS cells, and 221 cells were assessed for their viability after incubation with actin depolymerizing or stabilising drugs. Treated cells were washed and resuspended in flow buffer, before staining with DAPI (Molecular Probes) according to the manufacturer's instructions, washed and resuspended in flow buffer prior to acquisition on the LSRFortessa, as described above for assessment of surface receptor expression.

2.5 Microscopy

Confocal microscopy

Confocal imaging was performed using commercially available laser scanning confocal microscopes (TCS SP5 RS and TCS SP8 CW; Leica, Germany) equipped with 63x and 100x oil immersion objectives (N.A. = 1.2 or 1.47 respectively. Nuclei of the cells were imaged using NucBlue (Hoechst 33342) (Molecular Probes) (λ_{ex} = 405, λ_{em} = 415-450). Dextran was imaged depending on its specific dye: fluorescein (λ_{ex} = 495, λ_{em} = 505-560), Texas Red (λ_{ex} = 595, λ_{em} = 605-660) and Alexa Fluor 647 (λ_{ex} = 647, λ_{em} = 657-700). Antibodies and LDL were imaged depending on their specific dye: Alexa Fluor 488 (λ_{ex} = 488, λ_{em} = 498-560) or Texas Red (λ_{ex} = 595, λ_{em} = 605-660). All live cell-imaging experiments were performed at 37ºC. Fixed cells and immunostained PFN were imaged at room temperature. Time-lapse images were acquired every 60-100 seconds over 15-20 minutes.

Total internal reflection fluorescence (TIRF) microscopy

TIRF microscopy imaging was performed using a commercially available widefield fluorescence inverted microscope (SR GSD 3D; Leica, Germany) in TIRF illumination mode with an HC PL APO 160x oil immersion objective (N.A. = 1.43) using an Andor iXon3 EMCCD camera. Dextran was imaged using either a 488 nm or 532 nm laser, depending on its specific dye: fluorescein (λ_{ex} = 488) and Texas Red (λ_{ex} = 532).

Images were analysed using ImageJ software (ImageJ; National Institutes of Health (NIH), USA). Brightness and contrast were altered in some images to make the intensity within the synapse visible in the figures shown, but analyses were performed on raw images and datasets.

2.6 Molecule access into the immune synapse

2.6.1 Live cell confocal imaging of molecules within the immune synapse

To assess the ability of molecules to penetrate the immune synapse, fluorescently labelled dextran of varying diameters or fluorescently labelled antibodies/low-density lipoproteins (LDL) were used at the concentrations detailed in table 2.4 below, unless otherwise indicated. Target cells were labelled with NucBlue (Molecular Probes) according to the manufacturer's instructions. Briefly, 10^6 cells were collected and resuspended in 1 mL R10. Two drops of NucBlue were added to the medium and cells were incubated for 20 minutes at 37ºC. Cells were then washed 3 times and resuspended in phenol-red free R10 medium.

NK cells and target cells were mixed at a total density of 10^5 cells/mL with dextran, antibodies or antibody fragments in 0.2 mL microcentrifuge tubes. Dextran final concentrations are detailed in Table 2.4 below, unless otherwise indicated in results. Conjugates were then plated in eight-well chambered borosilicate coverglasses (coated with 0.01% poly-L-lysine according to the manufacturer's instructions, where indicated in results) and incubated at 37ºC for 5 minutes to allow the cells to settle and form synapses. Conjugates were then imaged by confocal microscopy, taking image stacks with a z-axial step size of 500 nm during a period of 15 – 30 minutes, to ensure that no synapse had been formed longer than this. Molecule penetration of the synapses was then analysed using ImageJ software.

Molecule	Final Concentration (μM)
Dextran – 3 kDa	50
Dextran – 10 kDa	50
Dextran – 40 kDa	50
Dextran – 70 kDa	50
Dextran – 500 kDa	5
Dextran – 2, 000 kDa	2.5
IgG monoclonal antibody	3.25
F(ab')2 fragment	4.5
Domain antibody	3
Low-density lipoprotein	1

Table 2.4. The working concentrations of molecules used to assess size-dependent entry into the immune synapse.

For experiments with Latrunculin A (Lat A, Sigma) and Jasplakinolide (Life Technologies), 1 μM or 0.5 μM, respectively, was added to the cells after 5 minutes incubation on PLL-coated slides. Conjugates were then imaged every minute following addition of the drug for a total of 5 minutes.

2.6.2 Time-lapse imaging of molecules within the immune synapse

To assess the entry of molecules into the immune synapse formed by effector and target cells over time, time-lapse confocal microscopy was used. Target 221 cells were labelled with NucBlue as described above. YTS and 221 cells were plated at a total density of 10^5 cells/mL on 0.01% poly-L-lysine- or 1 μg/mL fibronectin-coated slides (both according to the manufacturer's instructions) and incubated at 37ºC for 5 minutes prior to imaging to allow cells to settle. Dextran was added prior to or following plating on slides, as indicated in results. Conjugates or conjugate formation were imaged using a z-axial step size of 500 nm, taking stacks every 60 – 100 seconds for 15 – 20 minutes.

To assess the entry of molecules into the immune synapse formed with coated glass slides, cells were imaged using interference reflection microscopy (IRM) to visualize contact with the slide and by fluorescence microscopy to visualize dextran within the cell-slide interface. Primary human NK cells were plated with dextran on activating slides coated with 2 μg/mL MICA-Fc and 0.5 μg/mL ICAM1-Fc (both R&D Systems, UK) at a density of 10^5 cell/mL.

2.6.3 Time-lapse total internal reflection fluorescence microscopy of molecule clearance from the cell-slide interface

To assess the clearance of molecules from the immune synapse, TIRF microscopy was used. Primary human NK cells were plated at a total density of 10^5 cells/mL on eight-well chambered borosilicate coverglasses coated with MICA-Fc and ICAM1-Fc, as previously described. Cells were imaged using a penetration depth of 110 nm in both the 488 nm and 532 nm laser channels. Time-lapse images were taken sequentially in either channel at intervals of 20 seconds from the initial moment of cell-slide contact for 5 minutes.

2.6.4 Confocal imaging of antibody access into the cell-slide interface

To assess the entry of antibodies into a synapse formed at the cell-slide interface, pNK cells were plated at a total cell density of 10^5 cells/mL on slides coated with 2 µg/mL MICA-Fc, 0.5 µg/mL ICAM1-Fc and 5 µg/mL anti- antibody (Clone CE2.10). Cells were then incubated at 37ºC, 5% CO_2 for 30 minutes. To confirm NK cell activation and PFN secretion, capture and staining, cells were removed and slides were incubated with fluorescent anti- antibodies [1]. To assess the access of fluorescent anti- antibodies into the synaptic cleft, primary cells were either fixed then incubated with fluorescent anti- antibodies [2] or incubated with anti- antibodies then fixed [3]. Specific methods are described below:

1. Cell were removed from slides using 1x non-enzymatic cell dissociation buffer (Sigma-Aldrich, UK) for 20 minutes at 37ºC. Slides were washed 3 times with PBS and captured PFN was stained using a anti- antibody (Clone dG9) conjugated to Alexa Fluor 488 (α--488) for 1 hour at 37ºC.

2. Cells were fixed with 4% paraformaldehyde (PFA) for 20 minutes at room temperature, then permeabilised using 0.2% Triton-X (Sigma) and stained for actin and PFN using Phalloidin conjugated to Alexa Fluor 647 (Molecular Probes) and anti-perfrorin-488 in a blocking buffer (3% BSA in PBS) for 1 hour at room temperature.

3. Cells were fixed using 4% PFA then stained for PFN using anti-PFN-488 for 1 hour at 37ºC.

Cells/ were then imaged by interference reflection microscopy and confocal microscopy.

2.6.5 Cell migration assay

To analyse cell migration ability and speed, a cell migration assay was used. Firstly, 3 x 10^6 primary human NK cells were stained with NucBlue according to the manufacturer's instructions. Cells were then washed 3 times, resuspended in 3 separate 1.5 mL microcentrifuge tubes in 1 mL of clone medium each. Then, either 1 µL R10 medium, 1 µL DMSO or 1 µL Jaspalinolide (1 mM stock) was added to 10^6 primary human NK cells resuspended in 1 mL clone medium and incubated for 5 minutes at 37ºC 5% (vol/vol) CO_2. Cells were then washed with clone medium, resuspended in 1 mL clone medium and 2 x 10^5 cells were plated in eight chambered borosilicate coverglasses and imaged by confocal microscopy. Single plane images were taken every 3 seconds for 10 minutes. Cell migration speed was measured using automated tracking software (Kalaimoscope; Transinsight).

2.7 NK cell activation/degranulation and perforin capture

2.7.1 Perforin capture assay

To analyse PFN secreted by primary human NK cells, a protein capture assay was used. Eight-well chambered borosilicate coverglasses were coated with 0.01% PLL followed by MICA-Fc or anti-CD16 (Clone 3G8, BD Biosciences) (at amounts indicated in results section), 0.5 µg/mL ICAM1-Fc and 5 µg/mL anti-PFN (Clone CE2.10, Abcam) at 4ºC overnight. Slides were then washed 3 times with PBS and blocked for 20 minutes at 37ºC with R10 medium. Cells were plated on coated slides at a total density of 10^6 cells/mL and incubated for 1 hour (unless otherwise indicated) at 37ºC, 5% (vol/vol) CO_2, then removed using 1x non-enzymatic cell dissociation solution (Sigma-Aldrich, UK) at 37ºC for 20 minutes. Slides were washed 3 times with PBS and captured PFN was immunostained with anti-PFN-488 at 4ºC

overnight. Slides were washed 3 times with PBS and imaged by confocal microscopy.

2.7.2 NK cell serial activation

To analyse serial activation of primary human NK cells, the protein capture assay was performed in the following way. Eight-well chambered borosilicate coverglasses were coated with 0.01% PLL, then 2 µg/mL MICA-Fc or anti-CD16 (Clone 3G8) (where indicated in results section), 5 µg/mL ICAM1-Fc and 5 µg/mL anti-PFN (Clone CE2.10) at 4ºC overnight and blocked for 20 minutes at 37ºC with R10 medium. Cells were plated on coated slides at a total density of 10^6 cells/mL and incubated for 1 hour at 37ºC, 5% (vol/vol) CO_2, then removed using 1x non-enzymatic cell dissociation solution at 37ºC for 20 minutes and the slide was washed 3 times with PBS. Removed cells were then centrifuged at 956 *g* for 5 minutes, resuspended in clone medium, plated on a new slide surface (coated as indicated in results section) and incubated for 1 hour at 37ºC, 5% (vol/vol) CO_2. This was repeated until cells had been activated as identified in the results sections. Captured PFN was immunostained with an anti-PFN-488 at 4ºC overnight. Slides were washed 3 times with PBS and imaged by confocal microscopy.

2.7.3 Estimation of molecule number from fluorescence intensity

To quantify the number of PFN molecules from the mean integrated intensity, Quantum Simply Cellular (QSC) beads (Bangs Laboratory Inc., USA) were used. QSC beads are provided in 4 populations of known surfaces densities of anti-murine IgG antibodies, termed the antibody-binding coefficients (ABC). The ABC values assigned to each bead are presumed to be monovalent antibody-to-surface receptor binding. Therefore, the ABC given is the number of antibodies that bind to the bead surface. The ABC of each population is detailed in Table 2.5 below.

Bead Population	ABC
1	3258
2	35150
3	145457
4	371766

Table 2.5. Bead populations and corresponding antibody-binding coefficients (ABC).

Beads were prepared using a modified version of the manufacturer's instructions. A drop (~50 µL) of each bead population was placed in 1.5 mL tubes and 50 µL PBS was added. Beads were then incubated at room temperature for 20 minutes with 1 µL of murine anti-PFN antibody (clone CE2.10), and then washed 3 times in PBS by centrifugation at 17949 *g* for 5 minutes. Beads were then incubated at room temperature for 20 minutes with 5 µL of recombinant PFN (rPFN), and then washed 3 times in PBS with centrifugation at 17949 *g* for 5 minutes. Finally, beads were incubated at room temperature for 20 minutes with an anti-PFN-488, then washed 3 times in PBS with centrifugation at 17949 *g* for 5 minutes and resuspended in 200 µL PBS. Confocal microscopy was then used to image the labelled QSC beads, taking image stacks with a 0.34-µm z-axial step size.

2.8 Data Analysis

2.8.1 Molecule penetration of the immune synapse

Confocal microscope images were analysed using ImageJ software with additional plugins where indicated. Brightness and contrast levels of images were altered and adjusted in Photoshop (Adobe, USA) to improve visualization and printing. However, raw data was used for analysis.

Molecule entry into effector-target cell conjugates

Fluorescence intensity of molecules within the synapses formed by effector and target cells in conjugate was measured and analysed as follows. At the imaging plane located at centre of the synapse in the z-axial direction, a 50-pixel-wide line was drawn across the conjugate, perpendicular to the synapse, from the extracellular solution across the cell bodies and synapse to the extracellular solution on the

opposite side of the conjugate. The centre of the line was placed at the synapse (Figure 2.1A). The mean fluorescence intensity was then measured as a profile plot (Figure 2.1B). One-micron-wide boxes were then drawn over the intensity profile at the synapse and extracellular solution (Figure 2.1C). The areas under the curve (corresponding to the integrated intensity at each point) were measured and the synapse intensity was divided by the extracellular solution intensity to give intensity at the synapse relative to the extracellular solution.

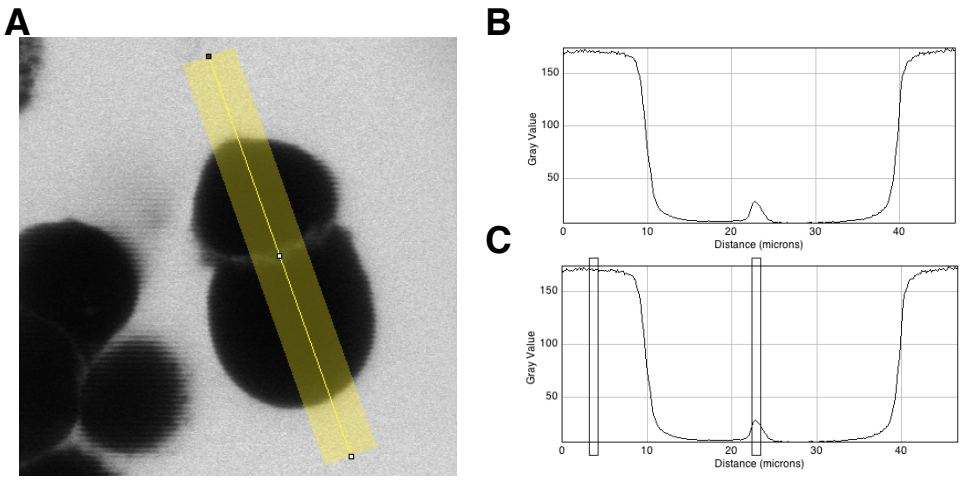


Figure 2.1. Analysis of fluorescence intensity within the immune synapse. Molecule entry into the immune synapse was measured as the intensity at the synapse relative to the extracellular solution. **(A)** A 50-pixel-wide line (*yellow bar*) was first drawn across the conjugates. **(B)** A profile plot was then measured taking the mean intensity across the width of the line drawn. **(C)** One micron boxes were drawn at the synapse (centre of the line) and the solution. The area under the line was measured to give the integrated intensity at each point. The area under the curve at the synapse was divided by the area under the curve at the solution to give the relative intensity.

Actin depolymerisation

To analyse the effect that pharmacological agents had on actin, specifically depolymerisation or stabilisation compared to the DMSO vehicle control, ImageJ was used. A rectangular region of interest (ROI), ~50 μm^2, was drawn across the cell membrane (Figure 2.2). The total raw intensity within the ROI was then measured for each condition.

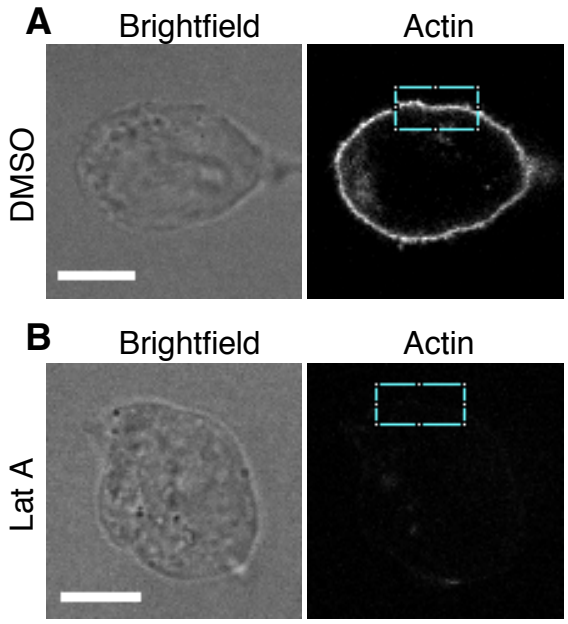


Figure 2.2. Analysis of Phalloidin-stained actin fluorescence intensity. The change in actin compared to a DMSO vehicle control was measured at the cell periphery. An ROI of ~50 μm^2 was drawn across the cell membrane (*blue box in fluorescence panel*). The total raw intensity within this region was then measured for each cell under each condition. **(A)** Panels show brightfield and corresponding fluorescence image of YTS cell stained for actin after 5 minutes DMSO treatment. **(B)** Panels show brightfield and corresponding fluorescence image of YTS cell stained for actin after 5 minutes Lat A treatment. Scale bars; 10 µm.

Molecule clearance from cell-slide interfaces

To analyse fluorescence intensity at the cell-slide interface when using confocal microscopy, the ImageJ plugin 'Time Series Analyzer, Version 4_H' (http://rsb.info.nih.gov/ij/plugins/time-series.html) was used. An ROI was drawn over the region where the cell made contact with the slide (Figure 2.3A – C). The mean intensity at the cell-slide interface within the ROI was then measured at each time point prior to initial cell-slide interaction until the end of the time-lapse imaging. To measure the intensity of the extracellular solution, this was repeated using the same size ROI in a region where no cells came into contact with the slide (Figure 2.3D – F). The synaptic intensity was then divided by the extracellular solution intensity at the corresponding time points to give intensity at the synapse relative to the extracellular solution.

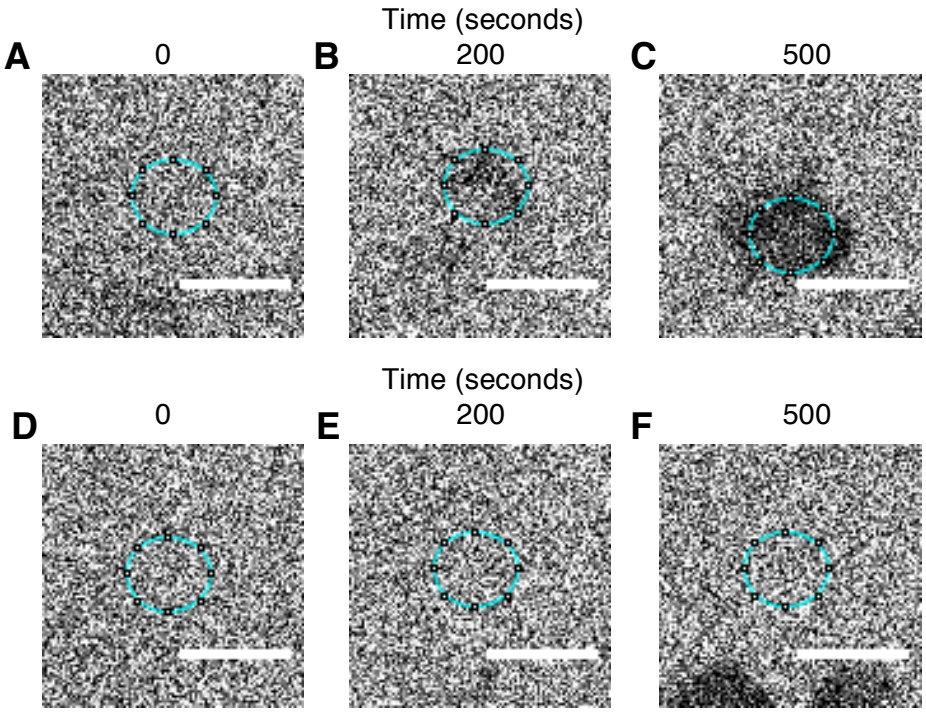


Figure 2.3. Analysis of fluorescence intensity within the immune synapse at a cell-slide interface using confocal microscopy. Molecule entry into the immune synapse was measured as the intensity at the synapse relative to the extracellular solution using the 'Time Series Analyzer' plugin. The synapse and solution fluorescence intensities of dextran were measured at each time point within a region of interest (ROI). **(A)** A ROI used to measure fluorescence intensity at the synapse prior to cell-slide contact at time = 0 seconds. **(B) A** ROI measuring fluorescence intensity within the synapse at the point of cell-slide contact at time = 200 seconds. **(C) A** ROI measuring the fluorescence intensity of dextran within the synapse following synapse formation at time = 500 seconds. **(D – E)** A ROI measuring fluorescence intensity of dextran within the solution where no cell contacts the slide surface at time = 0, 200 and 500 seconds respectively. Scale bars, 10µm.

To analyse dextran clearance from the cell-slide interface, a threshold was applied to TIRF images to first obtain the peripheral outline of the cell-slide interface (Figure 2.4A). The area of the interface was then measured (Figure 2.4B). Raw images were then converted to 8-bit format. On these images, a threshold between 32 – 223 AU was applied (Figure 2.4C and D for images of 4 nm and 32 nm dextran respectively). Images were inverted and using an ROI, the area of pixels below 32 AU was measured in images of 4 nm and 32 nm dextran (Figure 2.4E and F for images of 4 nm and 32 nm dextran respectively). The ratio of the pixels below 32 AU and the area of the cell interface were then used to calculate the percentage of the cell-slide interface occupied by pixels below 32 AU.

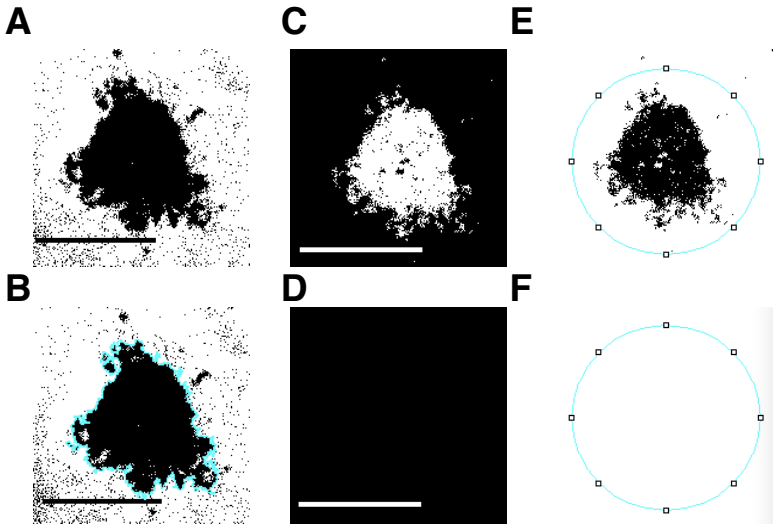


Figure 2.4. Analysis of TIRF imaging of dextran clearance from the cell-slide interface. Dextran clearance from the cell-slide interface was identified as pixels below 32 AU in 8-bit TIRF images **(A)** The area of the cell-slide interface was determined using a threshold applied to TIRF images of 32 nm dextran. **(B)** The area of the cell slide interface was then measured. **(C and D)** TIRF images were converted to 8-bit format and a threshold of 32 – 223 AU was then applied to images of **(C)** 4 nm dextran or **(D)** 32 nm dextran . **(E and F)** Images were then inverted and the area of pixels below 32 AU was measured using an ROI around the cell-slide interface of images of **(E)** 4 nm dextran and **(F)** 32 nm dextran. Scale bars; 10 µm)

Antibody penetration of cell-slide interfaces

To analyse the entry of anti-PFN-488 into the immune synapse formed by primary human NK cells with an activating surface, cells were scored on the staining of PFN at the cell-slide interface. The cell-slide interface was identified using the IRM image (darker regions). The presence of PFN was scored at positive (Figure 2.5A) and a lack of fluorescence signal was scored as negative (Figure 2.5B).

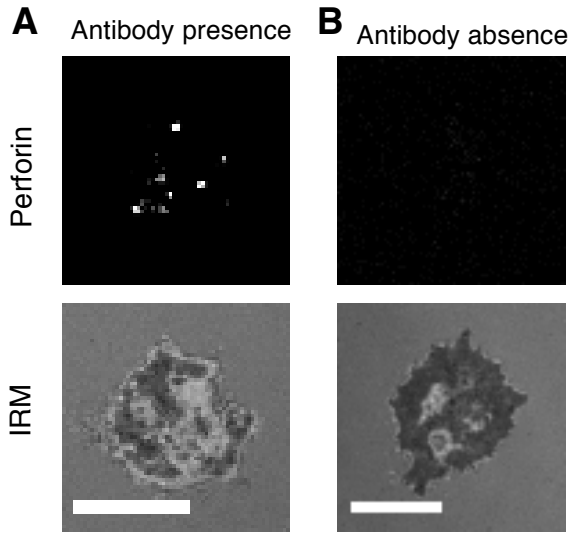


Figure 2.5. Analysis of antibody penetration at a cell-slide interface. Primary human NK cells were incubated on slides coated with MICA-Fc, ICAM1-Fc and anti-perforin. Cells were either fixed and incubated with fluorescent anti-perforin antibodies or incubated with fluorescent anti-perforin antibodies then fixed. Cells were then assessed for access of antibodies into the synapse by the **(A)** presence or **(B)** absence of fluorescence signal within the synapse at the cell-slide interface. Cell contact and synapse formation was determined by the presence of darker regions on the interference reflection microscopy (IRM) images (*lower row*). Scale bars; 10 µm.

2.8.2 Perforin secretion analysis

Confocal microscope images were analysed using ImageJ software. Brightness and contrast levels of images were altered and adjusted in Photoshop to improve visualization and printing. However, raw data was used for analysis.

Integrated intensity of immunostained

Secreted PFN was measured on a 'per cell' basis where isolated clusters of PFN spots were assumed to have been secreted from one cell (Figure 2.6A). A default auto-threshold mask was selected to threshold images to remove any background fluorescence (Figure 2.6B). The threshold was first applied to images to isolate secreted PFN. A ROI was then drawn around each cluster of PFN spots and the integrated intensity was measured (Figure 2.6C).

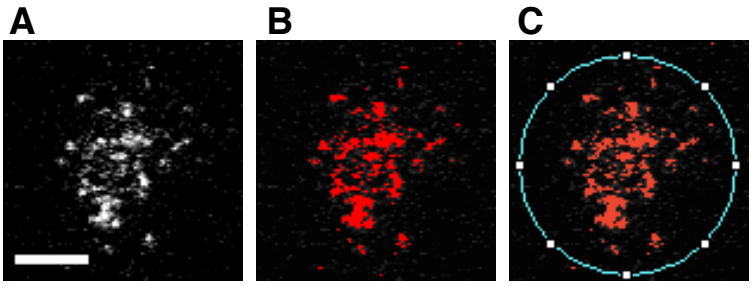


Figure 2.6. Analysis of perforin secretion by NK cells on activating slides. Perforin secretion was measured as the integrated intensity per cell. **(A)** Representative confocal image of captured perforin. **(B)** A default threshold was applied to the image to remove background. **(C)** A region of interest was drawn around perforin to measure the total integrated intensity. (Scale bar, 5 μm)

Estimation of number of molecules from integrated intensity

Imaging data from bead populations coated with an anti-PNF antibody, rPFN and anti-PFN-488 were used to estimate the number of molecules from integrated intensity (Figure 2.7A). Firstly, the upper most plane of an image stack that contained the top of the bead was isolated. A default auto-threshold was then applied to the image. The integrated intensity was then measured of each bead population and mean integrated intensity was plotted against the number of molecules per micron squared of the bead that was analysed (Figure 2.7B). The number of binding sites on the bead was given as the antibody-binding coefficient (ABC). As anti-PFN antibodies bound to the beads could bind 0, 1 or 2 rPFN proteins, the mean was assumed to be 1. These proteins would then be bound by an average of 1 fluorescently labelled anti-PFN-488 antibody. Therefore, the ABC indicated the number of rPFN proteins bound to the bead surface and the integrated intensity would indicate a number of rPFN proteins per area. With this assumption, a line of best fit was plotted to give the relationship between number of molecules and integrated intensity (Figure 2.7C). This line gave the relationship between integrated intensity (y) and number of molecules (x), shown below.

$$x = \frac{y - 1.049}{4.99 \times 10^{-4}}$$

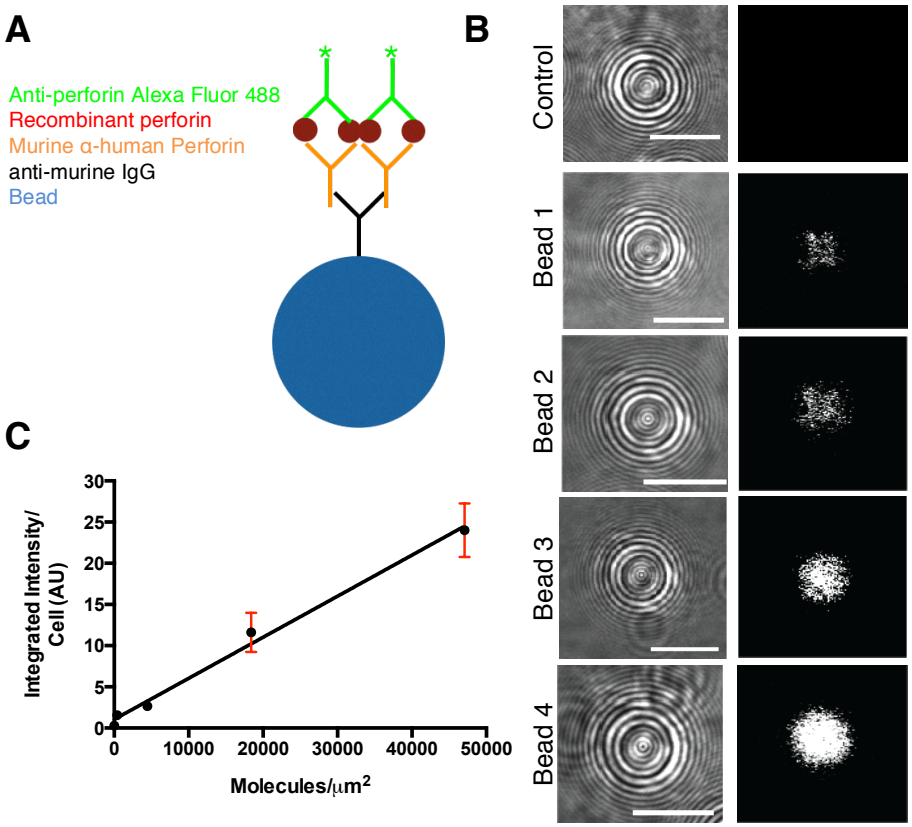


Figure 2.7. Estimation of number of molecules from fluorescence intensity. (A) Bead populations of increasing surface anti-murine IgG antibodies were sequentially bound with murine anti-human perforin antibodies, recombinant perforin and murine α-human perforin antibodies conjugated to Alexa Fluor 488. **(B)** Bead populations were imaged by confocal fluorescence microscopy. Panels show brightfield images (*left column*) and the corresponding fluorescence image (right column). Scale bars; 10 μm. **(C)** Integrated fluorescence intensity of each bead population was measured. Graph shows the mean intensity of each population and a linear line of best fit (R^2 = 0.9488).

To then quantify the number of molecules secreted by NK cells, the mean integrated intensities could be placed into the equation to provide an estimate.

The estimated amounts of PFN were then used to calculate the concentration at which PFN would be at within the synapse. The diameter and depth of the IS (including all signalling and integrin receptor/ligand complexes) have been estimated to be ~16 μm (117, 123) ~32.5 nm (65) respectively. Based on these dimensions, the volume of the IS was estimated to be ~5 μm^3, and therefore contains ~5 fL of fluid. The number of molecules of PFN could then be used to calculate the concentration of PFN in the volume of fluid at the synapse using the equations outlined below (equations 5.1 – 5.3).

Equation 5.1:

$$Quantity\ of\ protein\ (moles) = \frac{number\ of\ molecules}{Avagadro's\ number}$$

Equation 5.2:

$$mass\ (g) = quantity\ of\ protein\ (moles) \times molecularweight\ (Daltons)$$

Equation 5.3:

$$Concentration\ (Molar) = \frac{Qquantity\ of\ protein\ (moles)}{volume\ (litres)}$$

Using these equations, the molar concentrations of PFN at the synapse in each condition were calculated.

2.8.3 Statistical analysis

Significance of the data was determined by one-way ANOVA with Tukey multiple comparisons, Student's t-test with Welch's corrections or 95% confidence intervals (where indicated in figure legends). Error bars shown indicate mean ± standard deviation (SD). In the statistical analyses, differences were defined as non-significant (NS) where $p \geq 0.1$ and statistically significant where $p < 0.1$ (indicated by a single asterisk *), $p < 0.01$ (**), $p < 0.001$ (***) and $p < 0.0001$ (****). All graphs were prepared and statically analysed using Prism (GraphPad, USA).

Chapter 3 – The Immune Synapse Clears and Excludes Molecules Above a Size Threshold

3.1 Introduction

3.1.1 The immune synapse gasket

A relatively unexplored function of the IS is to form a gasket, or seal, around its secretory domains. This gasket may prevent the leakage of cytotoxic proteins from the synapse, protecting neighbouring cells from collateral damage during the lysis of diseased cells. In addition, this gasket could restrict the access of extracellular molecules into the synapse, preventing interference with proteins secreted across the synapse.

A gasket may be formed by the dense accumulation of receptor-ligand complexes, as well as the close proximity and inter-digitation of the NK cell membranes (392). Previous measurements of the extracellular domains of receptor-ligand complexes and synaptic cleft distances have shown the membranes at the IS to be ~15-20 nm apart, with some areas of larger spacing, up to 50 nm, where integrin receptor-ligand complexes bind. The extracellular domain sizes of the receptor-ligand proteins at the synapse can influence both the clustering of similarly sized receptors and segregate larger membrane-bound particles (greater than the receptor-ligand complex spans) from the cell-cell interface (65, 189, 208). These complexes ensure close proximity of the cell membranes, within tens of nanometers. Such a tight interface may be essential in forming a gasket around the synapse. Previous studies have indirectly shown that proteins, such as monoclonal antibodies, are unable to access the IS (366, 367). Despite this anecdotal evidence, whether or not the IS forms a gasket has not been tested directly.

3.1.2 The physical properties of dextran

Dextran is a soluble, hydrophilic, complex branched glucan (a glucose polysaccharide), which can be produced at varying molecular weights, with a range of sizes from 3 to 2, 000 kDa. Synthesised from sucrose by *Leuconostoc mesenteroides* and *Streptococcus mutans (385)*, it is one of the main constituents of dental plaque (393) and was discovered by Louis Pasteur as a microbial product in wine (394). Dextran has many medical uses including an antithrombotic agent to reduce blood viscosity (395), an inhibitor of bacterial growth (396), and as a volume expander to treat anemia (397).

Dextran can be conjugated to a range of fluorophores, enabling its visualisation using a fluorescence microscope. Fluorophores are conjugated to dextran using the reaction between a water-soluble amino dextran with the succinimidyl ester derivative of the dye followed by capping of any free amides with acetic anhydride. Depending on the dye being conjugated, this leads to different overall charges of the dextran; anionic, neutral (zwitterionic) and cationic. As dextran labelling uses free amide groups, the size of the molecule will determine the number of binding sites available and thus, larger dextrans have a greater number of fluorophores bound to their surface. Fluorophores (*e.g.* fluorescein) are around 1 nm in their longest dimension (398), and the dimensions of dextran provided in the literature are of dextrans labelled with this fluorophore.

Dextran molecules have previously been measured to ascertain their hydrodynamic radii (386, 387) using dynamic light scattering (399). A hydrodynamic radius is the effective hydrated radius of a particle in solution. Due to the branched nature of dextran, the sizes given are nominal hydrodynamic radii. This can be measured by dynamic light scattering (DLS), which is commonly used to determine the distribution profile of small particles in suspension or polymers in solution. Expressing dextran sizes as a hydrodynamic radius (or diameter) allows the assumption of the size of the molecule, were it to exist as a sphere. Spatially, dextran exists as a dense coiled chain, whilst not an exact sphere, the larger molecules, which coil significantly more than smaller molecules, forming a spherical shape of which the hydrodynamic radius

is a sufficient measurement of size and commonly used in many studies where the particle size needs to be known (400). In addition, the biologically uncommon α-1,6-glycosidic linkages between dextran chains are resistant to cleavage by most endogenous glucosidases, thus dextran molecules are not easily degraded. For this reason, dextrans have routinely been used for imaging cell loading of macromolecules, vesicular fusion and electroporation. Fluorescently labelled dextrans of varying sizes are commercially available. Based on these favourable properties, dextrans were used as a model of extracellular proteins in this study to investigate the IS gasket.

3.1.3 Aims

The IS is an organised cell-cell interface composed of a dense mesh of receptor-ligand complexes and membrane inter-digitation that may form a gasket, or seal, to prevent the entry of extracellular molecules. However, the extent to which extracellular molecules can access the IS has yet to be investigated. The specific aims are as follows:

i. To investigate the extent to which the IS functions as a gasket

ii. To investigate the mechanism by which this occurs

iii. To investigate how synapse formation affects molecules within the synaptic cleft during assembly

3.2 Results

3.2.1 Dextran access to the NK cell activating immune synapse is size-dependent

The ability of small molecules to access the immune synapse was investigated using fluorescently labelled dextran. As discussed above, dextran, a coiled branched glucan, is available in a range of sizes conjugated to a wide variety of fluorophores. To assess whether differently sized dextrans have a differential capacity to access the IS, effector and target cells were co-incubated with fluorescently labelled dextrans of known sizes, then imaged by confocal microscopy. Dextran penetration of the synapse was measured relative to the extracellular solution, as described in the methods (Chapter 2, Section 2.8.1; Figure 2.1), to directly compare the access of differently sized dextrans into the synaptic cleft.

The activating immune synapse excludes extracellular molecules in a size-dependent manner

To test the whether or not differently sized dextran can access the IS, YTS cells (a human NK cell line) and 221 cells, which are well-established sensitive targets for YTS cells (381, 401), were co-incubated with fluorescein labelled dextrans of diameters 3 – 54 nm. YTS-221 cell conjugates were then imaged by confocal microscopy. Imaging showed that as dextran size increased, its ability to access the IS decreased, with 54-nm-sized dextran completely excluded from the IS (Figure 3.1A). The raw fluorescence intensity of dextran was measured across the solution, cell bodies and synapse (Figure 3.2). Dextran within the synapse was identified as a peak in the signal over the background fluorescence within the cell body. The peak in raw dextran fluorescence intensity within the synapse decreased as dextran size increased (Figure 3.1B and Figure 3.2). Importantly, the intensity of the 54 nm dextran within the synapse was consistent with the background measurement within the cell bodies (where there was no dextran), showing that the 54 nm dextran was completely excluded from the synapse. Quantitatively, access to the synapse was measured relative to the extracellular solution (Figure 3.1C). This was to correct for

any fluctuations in laser power and allow comparison between the various dextran sizes. Dextrans sized 3 and 4 nm were able to enter the synapse comparably (synapse intensity relative to the extracellular solution 0.09 ± 0.04 and 0.09 ± 0.05 respectively). A decrease of almost 40% in fluorescence intensity was measured for dextran sized 10 nm (0.06 ± 0.03) compared to 3 or 4 nm dextrans, and an even greater reduction (~60%) was seen with dextran sized 13nm (0.04 ± 0.03). Dextran sized 32 nm was the largest molecule able to enter the IS formed by YTS cells (0.03 ± 0.02) and 54-nm-sized dextran was entirely excluded (0.01 ± 0.01). These data show that the IS excludes extracellular molecules in a size-dependent manner.

Due to its physical properties, larger sized dextran has lower maximum solubility and a higher degree of labelling, resulting in greater brightness at lower concentrations. To compensate and increase relative brightness, smaller dextrans were added to cell conjugates at higher concentrations to improve their visualisation during microscopy. To test whether the differences seen were influenced by dextran concentration, YTS and 221 conjugates were co-incubated with both Texas Red-labelled 4 nm dextran and fluorescein-labelled 54 nm dextran at the same concentration (2.5 μM), and relative fluorescence intensities within the IS was measured for each dextran in the same synapse (Figure 3.1D). These data show that even at the same concentration, 54 nm dextran is excluded from the IS whereas the 4 nm dextran remains able to access the synaptic cleft. Taken together, these data show that the IS indeed excludes extracellular molecules, but only those above a size threshold. Molecules below this threshold are able to access the synapse.

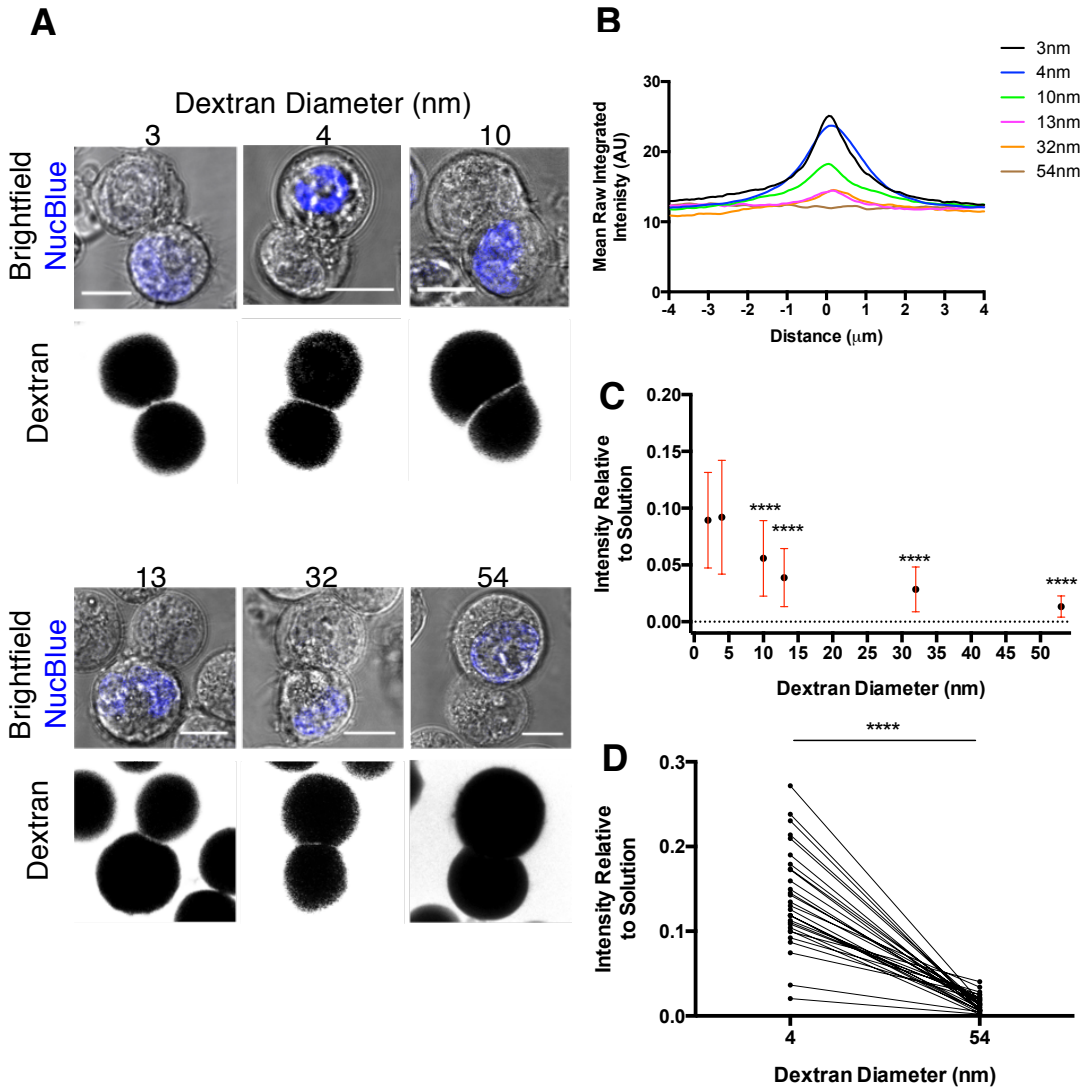


Figure 3.1. Dextran entry into the immune synapse formed by YTS cells is size-dependent. **(A)** Representative images of YTS and 221 conjugates co-incubated with fluorescein-labelled dextrans of various sizes, as indicated. Images show brightfield overlaid with target cell nuclear staining (*upper rows*) and the corresponding fluorescence images of dextran (*lower rows*). Scale bars; 10 μm. **(B)** Graph shows the mean raw intensities of differently sized dextrans, as indicated, across the synapse. **(C)** Dextran fluorescence intensity within the synapse was measured relative to the intensity of the extracellular solution for each dextran. Graph shows the mean ± SD. Data were analysed by one-way ANOVA with Tukey corrections (n = 49, 42, 47, 53, 39 and 39 for 2, 4, 10, 13, 32 and 54 nm dextran respectively) **(D)** YTS and 221 cells were co-incubated with 4 and 54 nm dextrans labelled with Texas Red or fluorescein respectively. Fluorescence intensity within the same synapses was measured for each dextran relative to the extracellular solution of the corresponding dextran. Graph shows the relative intensity of each dextran size within the same synapse (*connecting lines*). Data were analysed using a Student's t-test with Welch's corrections (n = 30). All data are from 3 independent experiments. ****p<0.0001

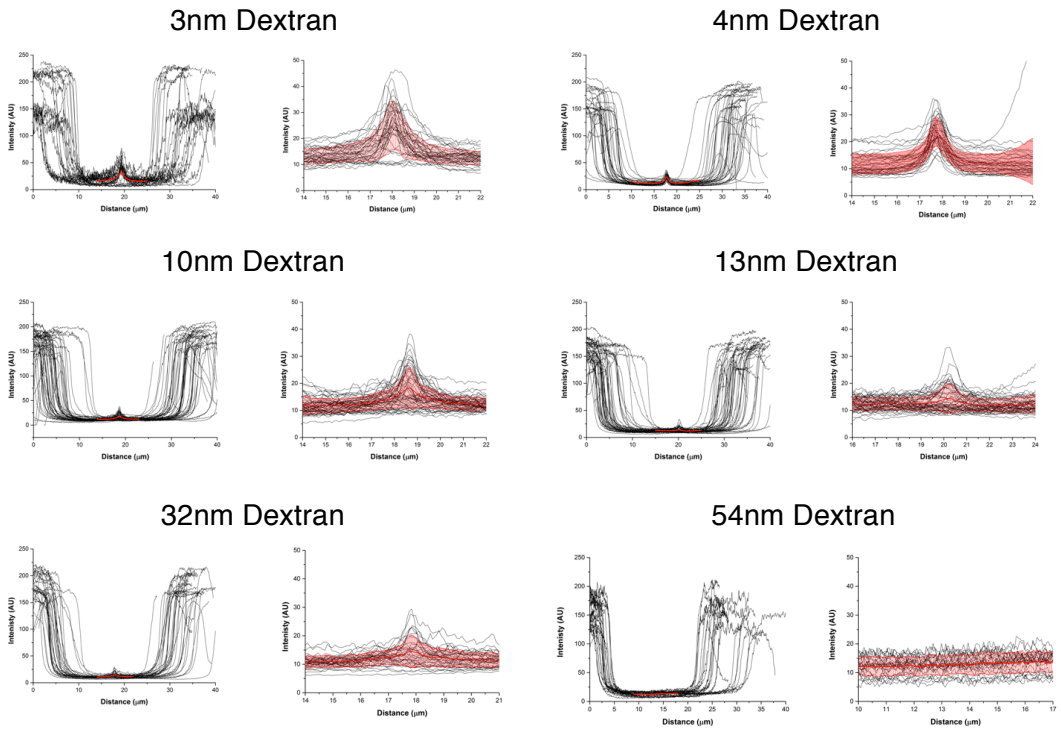


Figure 3.2. Raw intensity profiles of various sized dextrans across activating synapses formed by YTS cells. Dextran raw integrated intensity was measured using a 50-pixel-wide line across the solution, cell body (*e.g.* YTS cell), synapse, cell body (*e.g.* 221 cell) and solution. Graphs show either the raw intensity across the solution, cell bodies and synapse (*left graph*) or zoomed in the synapse (*right graph*) for each dextran size as indicated. Red lines show the mean intensity ± SD (n = 49, 42, 47, 53, 39 and 39 for 2, 4, 10, 13, 32 and 54 nm dextran respectively).

The reason that the value for 3 and 4 nm dextrans is lower than 1 (which would suggest equal concentrations of fluorophore within the synapse and solution) is due to the point spread function (PSF) of the microscope capturing a larger volume of fluorescence in the solution, compared to the fluorescence in the narrow synaptic cleft. The theoretical spatial resolution, or PSF, of the objective and wavelength used to excite fluorescein molecules is 280 nm in the x- and y-axes and 1086 nm in the z-axis, significantly larger than the 55 nm maximum intermembrane distance across the synapse (65). Therefore, intensity within the synapse appears dimmer than in the solution.

Importantly, the cells imaged were known to be viable as cytoplasmic entry of dextran occurs following cell death. When a cell is undergoing apoptosis, the resultant breakdown of membrane integrity led to in an influx of dextran into the cell

body (data not shown). Therefore, a defined outline of the cells within the fluorescence images indicates that the cells are viable.

The ability of dextrans sized 3 – 54 nm to access the IS was then assessed using primary human NK (pNK) cells and 221 target cells. Confocal imaging showed that dextran was also excluded from the pNK IS in a size-dependent manner (Figure 3.3A). The raw fluorescence intensity of dextran was measured across the solution, cell bodies and synapse (Figure 3.4). The peak in raw dextran fluorescence intensity within the synapse decreased as dextran size increased (Figure 3.3B and Figure 3.4), consistent with previous data from NK cell lines (Figure 3.1 and 3.2). This shows that the synapse formed by pNK cells also restricts the access of dextran into the cleft in a size dependent manner. In this instance, the intensity of both the 32 nm and 54 nm dextrans within the synapse were consistent with the background measurements within the cell bodies. This shows that dextrans 32 nm and larger are excluded from the pNK cell synapse. As before, dextran within the IS was measured relative to extracellular solution. This indicated that 3 and 4 nm-sized dextrans were able to penetrate the pNK IS to the same degree (0.09 ± 0.05 for both). This reflected the findings from our experiments using YTS cells.

As seen in the YTS cell synapses, dextran access into the synaptic cleft decreased as dextran sized increased. However, an almost 50% decrease in relative fluorescence intensity was measured for the 10 nm dextran (0.05 ± 0.03) and ~70% for the 13 nm dextran (0.03 ± 0.02). Dextran sized 32 nm was excluded from the pNK synapse (0.01 ± 0.02), as was dextran sized 54 nm (0.01 ± 0.01) (Figure 3.3C). These data show that the pNK cell synapse excludes dextrans ≥32 nm. Unexpectedly, the size exclusion thresholds of synapses formed by YTS cells and pNK cells were not the same. Whilst the synapses formed by YTS cells were only able to exclude 54 nm dextran, the pNK cell synapse excluded those with a diameter of 32 nm and 54 nm. This suggests that the synapse formed by YTS cells is not as tight as pNK cells, possibly due to receptor-ligand complexes at the synapse. In support of this theory, the YTS cell primarily uses CD28 for activation (20), whereas pNK cells utilise a variety of receptors (118). These differences in synaptic structure could impact on the ability of the synapse to exclude extracellular molecules.

To test whether or not this size exclusion was due to the difference in molecule concentrations and/or dimensions, pNK-221 conjugates were also co-incubated with both Texas Red-labelled 4 nm dextran and fluorescein-labelled 54 nm dextrans at the same concentration (2.5 μM) (Figure 3.3D). Analysis of dextran access to the same synapses (relative to the extracellular solution) by 4 nm or 54 nm dextrans demonstrated that the 54 nm dextran was still unable to access the IS, whereas the 4 nm dextran penetrated at a comparative level to higher concentrations in previous experiments. Therefore, both the YTS NK cell line and pNK cell IS are able to exclude extracellular dextran in a size-dependent manner. Whilst the exclusion threshold is lower for synapses formed by pNK compared to YTS cells, both synapses are able to restrict the entry of extracellular molecules below a defined size threshold.

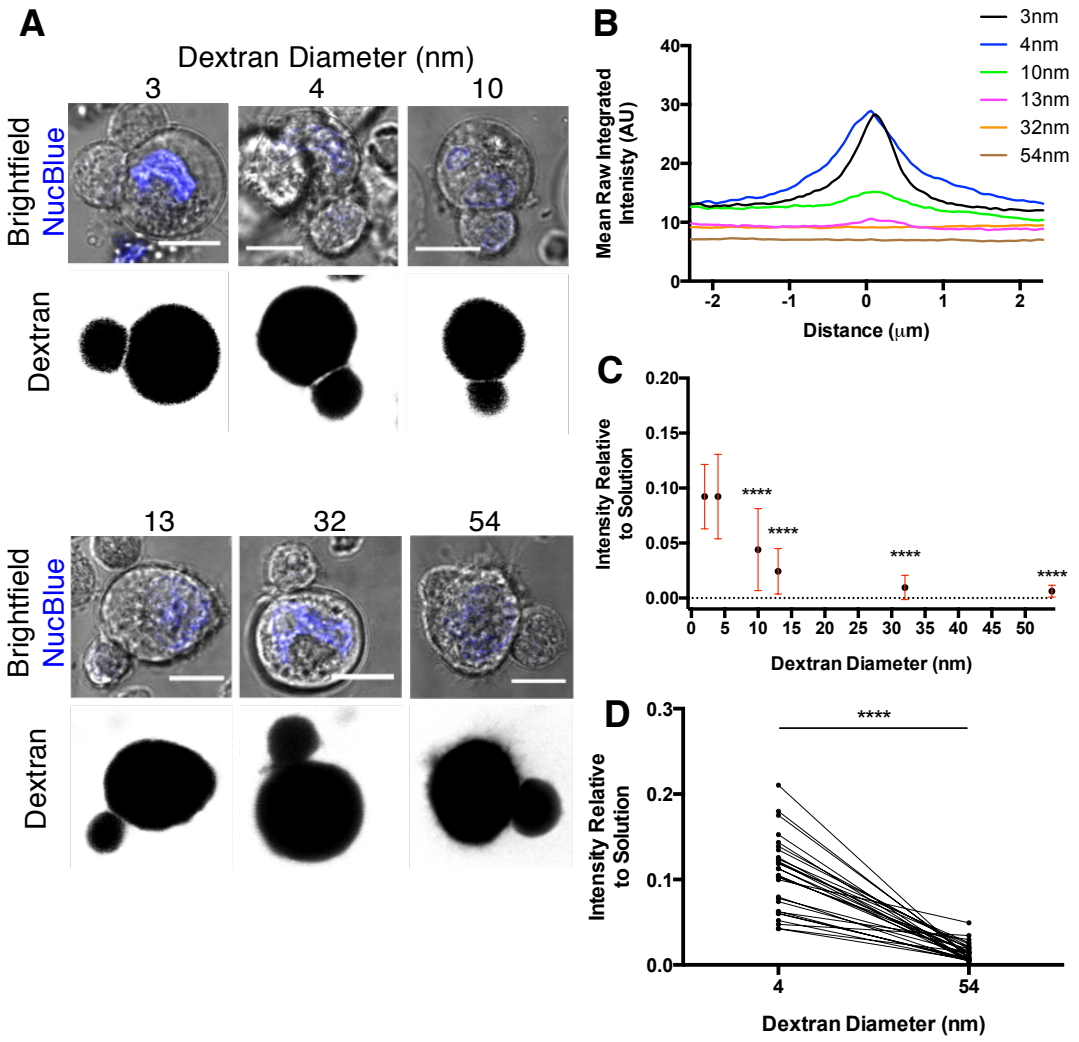


Figure 3.3. Dextran entry into the immune synapse formed by primary human NK cells is size-dependent. (A) Representative images of primary human NK cells and 221 conjugates co-incubated with fluorescein-labelled dextrans of various sizes. Images show brightfield overlaid with target cell nuclear staining (*upper*) and the corresponding fluorescence images of dextran (*lower*). Scale bars; 10 μm. **(B)** Graph shows the mean raw intensities of differently sized dextrans, as indicated, across the synapse. **(C)** Dextran fluorescence intensity within the synapse was measured relative to the intensity of the extracellular solution for each dextran. Graph shows the mean ± SD. Data were analysed by one-way ANOVA with Tukey corrections (n = 38, 32, 33, 31, 38 and 35 for 2, 4, 10, 13, 32 and 54 nm dextran respectively) **(D)** YTS and 221 cells were co-incubated with 4 and 54 nm dextrans labelled with Texas Red or fluorescein respectively. Fluorescence intensity within the same synapses was measured for each dextran relative to the extracellular solution of the corresponding dextran. Graph shows the relative intensity of each dextran size within the same synapse (*connecting lines*). Data were analysed using a Student's t-test with Welch's corrections (n = 29). All data are from 3 independent experiments. ****p<0.0001

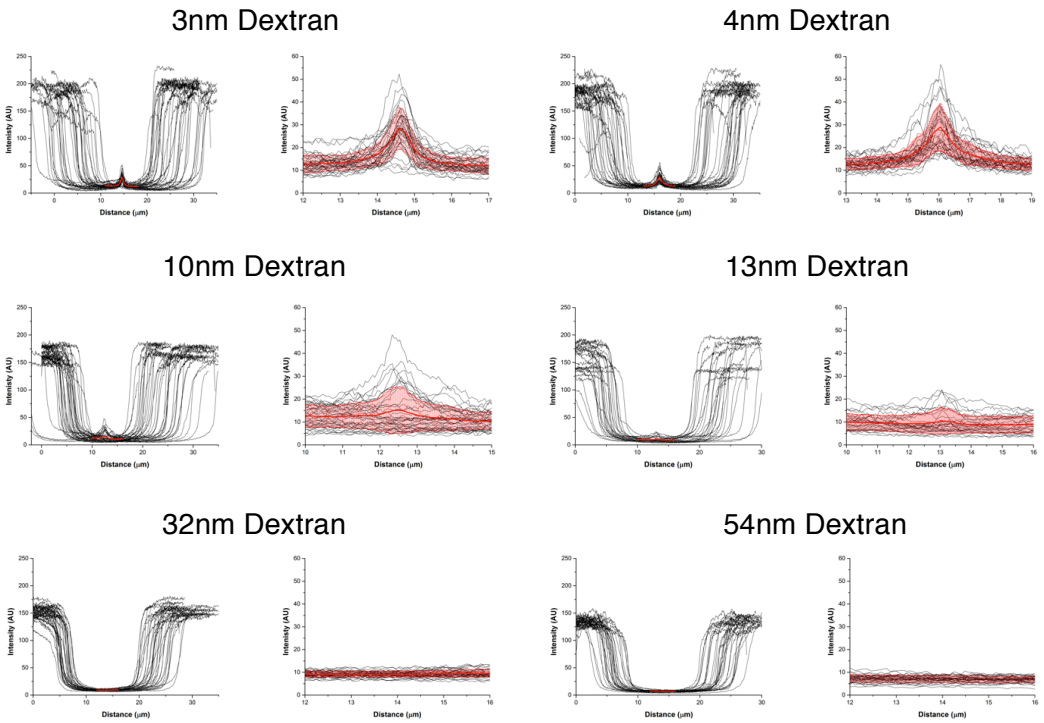


Figure 3.4. Raw intensity profiles of various sized dextrans across activating synapses formed by primary human NK cells. Dextran raw integrated intensity was measured using a 50-pixel-wide line across the solution, cell body (*e.g.* pNK cell), synapse, cell body (*e.g.* 221 cell) and solution. Graphs show either the raw intensity across the conjugate (*left graph*) or zoomed in across the synapse (*right graph*) for each dextran size as indicated. Red lines show the mean intensity ± SD (n = 38, 32, 33, 31, 38 and 35 for 2, 4, 10, 13, 32 and 54 nm dextran respectively).

A caveat to the data analysis was that the labelling density and maximum solubility increased or decreased respectively as dextran size increased. Therefore, concentrations and microscope settings were adjusted accordingly to visualize the dextrans. For example, 32 nm dextran has up to 10-fold greater labelling denisty than 4 nm dextran. In order to ensure that these factors did not introduce artefacts, fluorescein-labelled dextrans were mixed with unlabelled dextrans of the same molecular weight. This served to decrease the fluorescence intensity, but not the total amount of dextran within the solution. Dextrans sized 4 nm and 32 nm were mixed with YTS and 221 conjugates at labelled:unlabelled dextran ratios of 1:0, 1:1 and 1:10 at a final dextran concentration of 2.5 μM. Conjugates were then imaged by confocal microscopy using the same settings optimised for the brightest dextran mixed at a 1:0 ratio. The results show that access to the synapse by the 4 nm (Figure 3.5A and B) and 32 nm (Figure 3.5C and D) dextrans were not significantly different for all ratios of either dextran size. Further, relative intensities were comparable to

previous experiments using unmixed dextrans at higher concentrations (Figure 3.1). Thus, the size-dependent access of dextran into the synapse remains similar, irrespective of the ratio of labelled to unlabelled dextrans. These data show that the access of dextran into the synapse is dependent on their physical dimensions, and the adjustment of microscope settings, based on the dextran brightness, did not affect their quantification.

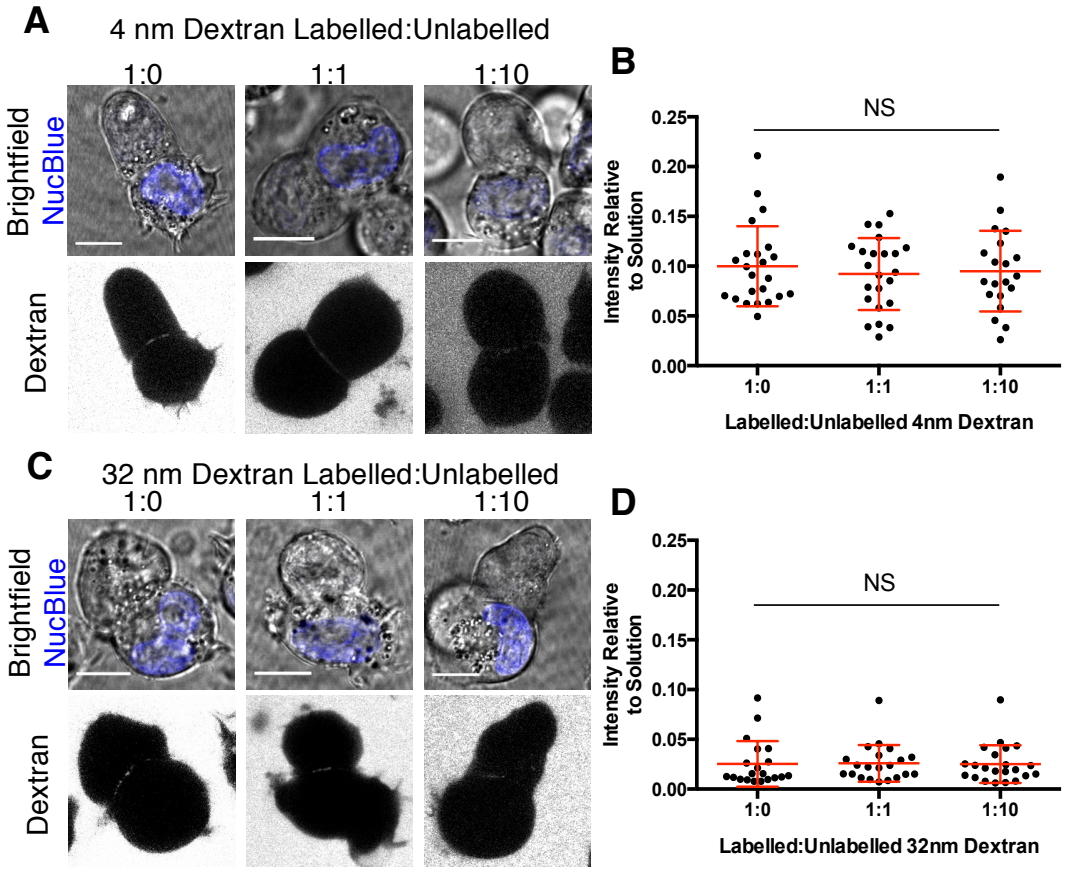


Figure 3.5. Dextran entry into the immune synapse is not affected by the degree of dextran labelling. (A) YTS and 221 conjugates were co-incubated with fluorescein-labelled and unlabelled 4 nm dextran at the ratios indicated and imaged by confocal microscopy using the same settings optimised to the labelled only (1:0) dextran. Panels show brightfield images overlaid with target nuclear staining (*upper row*) and the corresponding fluorescence image. Scale bars; 10 µm. **(B)** Dextran fluorescence intensity within the synapse was measured relative to the intensity of the extracellular solution for each dextran. Bars show the mean ± SD. Data were analysed by one-way ANOVA with Tukey corrections. (n = 25, 23 and 20 for 1:0, 1:1 and 1:10 labelled:unlabelled dextran mixtures). **(C)** YTS and 221 conjugates were co-incubated with fluorescein-labelled and unlabelled 32 nm dextran at the ratios indicated and imaged by confocal microscopy using the same settings optimised to the labelled only (1:0) dextran. . Panels show brightfield images overlaid with target nuclear staining (*upper row*) and the corresponding fluorescence image. Scale bars; 10 µm. **(D)** Dextran fluorescence intensity within the synapse was measured relative to the intensity of the extracellular solution for each dextran. Bars show the mean ± SD. Data were analysed by one-way ANOVA with Tukey corrections. (n = 20, 21 and 22 for 1:0, 1:1 and 1:10 labelled:unlabelled dextran mixtures). All data from 3 independent experiments. NS = no significance.

Next, to test whether different sized dextrans could be imaged using the same settings and yield similar findings, 4 nm and 32 nm dextran were mixed at labelled:unlabelled ratios of 1:0 and 1:10 respectively. These were then co-incubated with YTS and 221 cells and imaged by confocal microscopy, with microscope settings optimised for the intensity of the 4 nm dextran (Figure 3.6A). The 4 nm dextran was able to access the synapse more effectively than the 32 nm dextran (0.8 ± 0.04 and 0.03 ± 0.03 respectively) (Figure 3.6B), at comparable levels shown in the previous data (Figure 3.1). This further demonstrates that microscope settings do not skew relative intensities within the synapse and penetration is governed by dextran size alone.

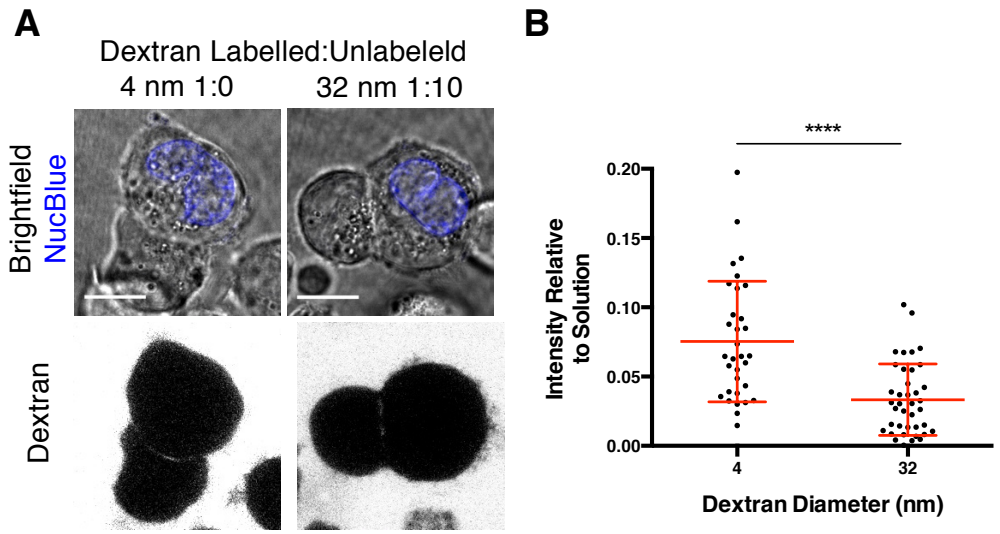


Figure 3.6. Microscope settings do not introduce artefacts for analysis of entry of molecules into the immune synapse. (A) YTS and 221 conjugates were co-incubated with fluorescein-labelled 4 nm dextran or a mix of fluorescein-labelled and unlabelled 32 nm dextran at a ratio of 1:10 and imaged by confocal microscopy using the same settings optimised to 4 nm dextran. Panels show brightfield images overlaid with target nuclear staining (*upper row*) and the corresponding fluorescence image. Scale bars; 10 µm. **(B)** Dextran fluorescence intensity within the synapse was measured relative to the intensity of the extracellular solution for each dextran. Bars show the mean ± SD. Data were analysed using a Student's t-test with Welch's corrections. (n = 32 for 4 nm dextran and 39 for 32 nm dextran). Data are from3 independent experiments. P<0.0001.

To test whether or not dextran concentration had any effect on access to the IS, YTS and 221 conjugates were co-incubated with a fluorescein-labelled 4 nm dextran at a range of concentrations from 2 – 50 µM (Figure 3.7A). Whilst raw intensity values within the synapse were lower at reduced dextran concentrations, the relative intensities to the extracellular solution were not significantly different and did not reflect the change in concentration (Figure 3.7B). Therefore, whilst dextran access to

the synapse is shown to be size dependent, the actual amount that enters the synapse is dependent on the extracellular concentration, resulting in equilibrium between the synapse and extracellular solution. Importantly, even at concentrations below that used for the 54 nm dextran, the relative intensity of the 4 nm dextran remained significantly higher.

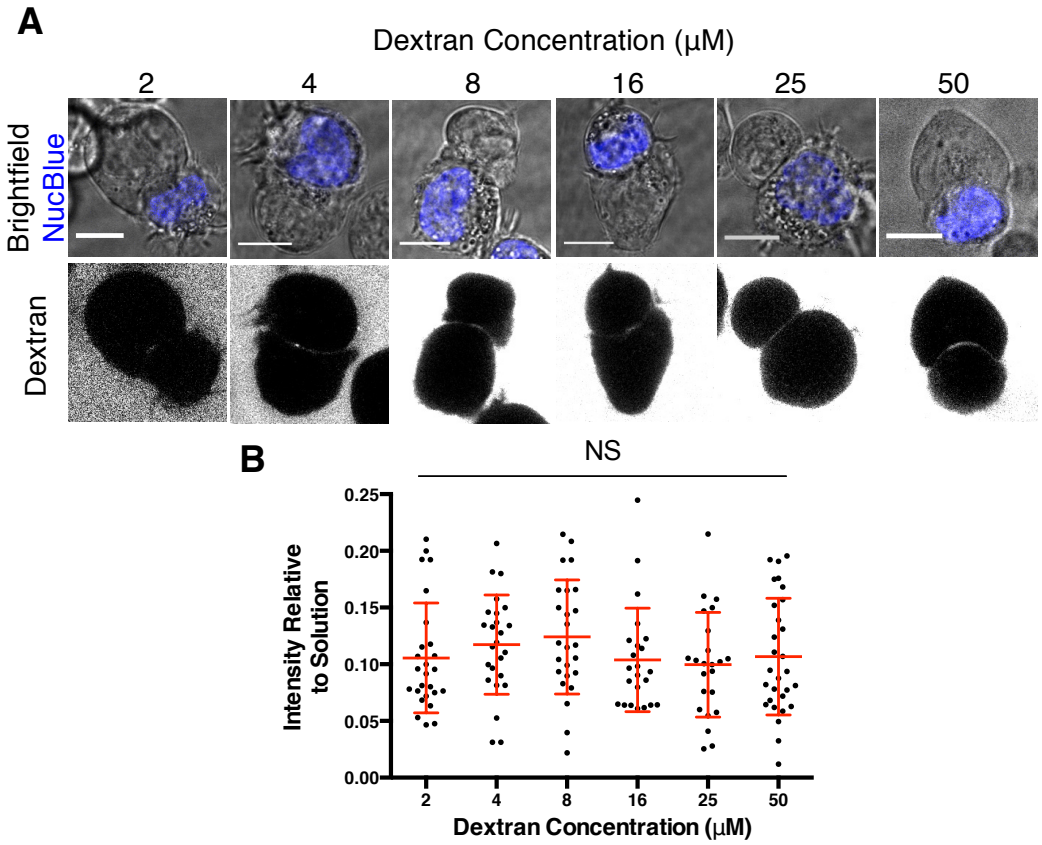


Figure 3.7. Dextran concentration does not affect the analysis of entry into the immune synapse. (A) Representative images of YTS and 221 conjugates co-incubated with fluorescein-labelled 4 nm dextran at the concentrations indicated. Panes show brightfield overlaid with target nuclear staining (*upper row*) and the corresponding fluorescence image (*lower row*). Scale bars; 10 µm. **(B)** Dextran fluorescence intensity within the synapse was measured relative to the intensity of the extracellular solution for each concentration. Bars show the mean ± SD. Data were analysed using a one-way ANOVA with Tukey corrections (n = 26, 25, 25, 23, 23 and 29 for 2, 4, 8, 16, 25 and 50 µM concentrations respectively). Data are from 3 independent experiments. NS = no significance.

The net charge of a dextran molecule depends on the fluorophore and the method of preparation. Dextrans commercially available were prepared by the manufacturer using a reaction between water-soluble amino dextrans with the succinimidyl ester derivatives of the appropriate dye, due to their selectivity towards aliphatic amines. To prevent any cross-contamination with other molecules, unreacted amines are then capped with acetic anhydride, yielding a neutral or anionic dextran. Data from Figures 3.2C and 3.4C showed that when 4 nm and 54 nm dextrans were incubated with YTS or pNK cell conjugates simultaneously, the 4 nm dextran could access the IS, whilst the 54 nm dextran was excluded. However, the 4 nm Texas Red-labelled dextran has an overall neutral charge and the 54 nm fluorescein-labelled dextran is anionic. To rule out any effect of charge on the ability of dextran to enter the synapse, 4 nm dextrans labelled with either Texas Red or Alexa Fluor 647 were used. Dextran labelled with Alexa Fluor 647, like fluorescein, yields an anionic molecule. These dextrans were simultaneously co-incubated with YTS and 221 target cells and imaged by confocal microscopy (Figure 3.8A). There was no significant difference between the access of IS of these differently labeled dextrans (relative intensity within the synapse compared to the extracellular solution of the corresponding dextran was 0.17 ± 0.05 for both Texas Red and Alexa Fluor 647 labelled dextrans) (Figure 3.8B). This was repeated using pNK cells co-incubated with 221 target cells and both 4 nm dextrans (Figure 3.9A). Again, both dextrans were able to access the IS without any significant difference (0.15 ± 0.05 and 0.14 ± 0.03 for Texas Red or Alexa Flour 647 labelled dextrans respectively) (Figure 3.9B). These assays demonstrate that charge does not affect the ability of dextran to access the IS, rather access is determined by physical size. This is consistent with previous data demonstrating size-dependent exclusion of dextran (Figure 3.1 and 3.3).

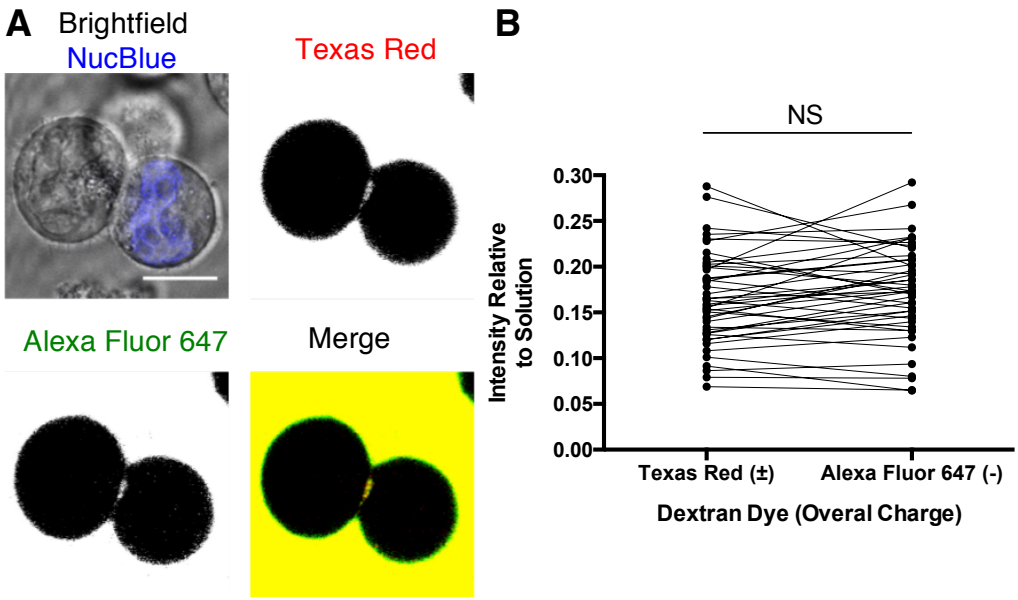


Figure 3.8. Entry into the immune synapse formed by YTS cells is not affected by dextran charge. (A) Representative images of YTS and 221 conjugates were co-incubated with 4 nm dextran labelled with Texas Red or Alexa Fluor 647. Panels show brightfield overlaid with target cell nuclear staining (*upper left panel*), corresponding fluorescence images of Texas Red- and Alexa Fluor 647-labelled dextran (*upper right and lower left respectively*) and a marge of the fluorescence images (*lower right*). Scale bar; 10 µm. **(B)** Dextran fluorescence intensity was measured relative to the extracellular solution of the corresponding dextran. Graph shows the relative intensity of each dextran in the same synapse (*connecting lines*). Data were analysed using a Student's t-test with Welch's corrections. (n = 45). Data are from 3 independent experiments. NS = no significance.

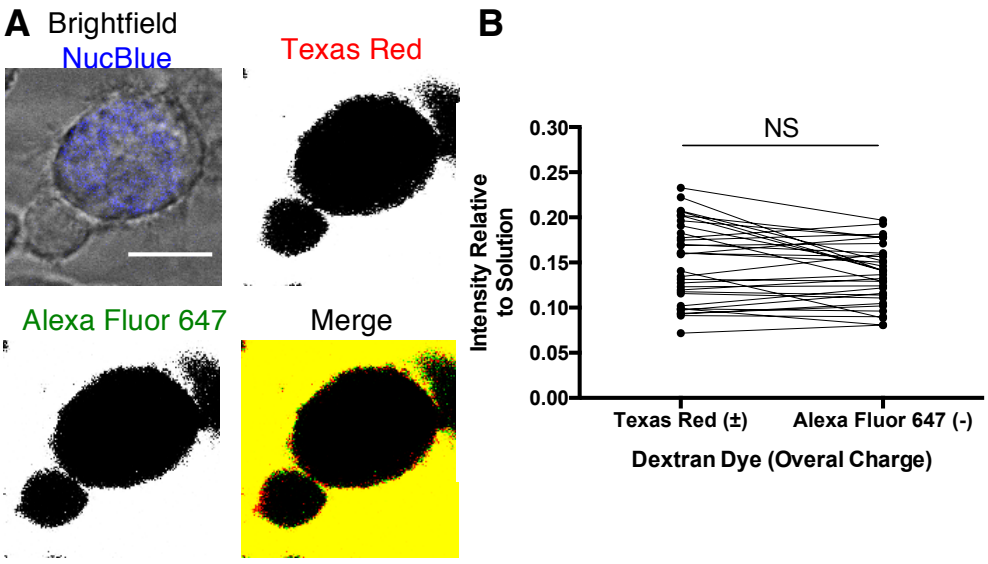


Figure 3.9. Entry into the immune synapse formed by primary human NK is not affected by dextran charge. (A) Representative images of primary human NK cells and 221 conjugates were co-incubated with 4 nm dextran labelled with Texas Red or Alexa Fluor 647. Panels show brightfield overlaid with target cell nuclear staining (*upper left panel*), corresponding fluorescence images of Texas Red- and Alexa Fluor 647-labelled dextran (*upper right and lower left respectively*) and a marge of the fluorescence images (*lower right*). Scale bar; 10 µm. **(B)** Dextran fluorescence intensity was measured relative to the extracellular solution of the corresponding dextran. Graph shows the relative intensity of each dextran in the same synapse (*connecting lines*). Data were analysed using a Student's t-test with Welch's corrections. (n = 32). Data are from 3 independent experiments. NS = no significance.

In summary, the IS formed by YTS or pNK cells with 221 target cells excludes extracellular dextran in a size-dependent manner (Figure 3.1 and 3.3). Specifically, dextrans of diameters 3 – 4 nm are able to access the IS most effectively, with an increase in dextran size leading to a reduced ability of dextran molecules to access the IS. Dextrans sized 32 and/or 54 nm (using primary and cell line effector cells respectively) are unable to access the synapse, consistent with previous estimations of the IS cleft spacing (65, 189). Moreover, access to the synaptic cleft was shown to be exclusively dependent on dextran size. Dextran concentration and charge did not affect dextran intensities, and microscope settings had no impact on measurements (Figure 3.7 – 3.9). Therefore, the IS excludes extracellular molecules in a size-dependent manner. Size is the only physical property that is a factor determining entry of extracellular proteins – and to what extent – into the synaptic cleft.

The activating immune synapse excludes extracellular molecules in a size-dependent manner with a variety of target cells

The target cell line 221 had been used in the experiments discussed above, as they are sensitive targets for both YTS and pNK cells. In order to test whether or not the IS formed with other target cells also exclude dextran in a similar size-dependent manner, pNK cells were co-incubated with either a B cell lymphoblast cell line, Daudi, or a myeloid leukaemia cell line, K562, with a range of differently sized fluorescein-labelled dextrans (4 – 54 nm) and imaged by confocal microscopy.

The synapse formed by pNK cells co-incubated with Daudi cells (Figure 3.10A) was accessible by dextrans sized 4 or 13 nm (0.11 ± 0.05 and 0.06 ± 0.04 respectively). Dextrans sized 32 nm and 54 nm were significantly restricted or excluded (0.02 ± 0.01 and 0.01 ± 0.01) (Figure 3.10B). Similarly, synapses formed with K562 target cells excluded dextrans in a size-dependent manner (Figure 3.11A). The relative intensities within the synapse for each dextran sized 4, 13, 32 and 54 nm (0.11 ± 0.05, 0.06 ± 0.04, 0.02 ± 0.01 and 0.01 ± 0.01 respectively) (Figure 3.11B) were comparable to synapses formed with 221 (Figure 3.3C) and Daudi (Figure 3.10B) target cells. Therefore, irrespective of the target cell, the NK cell IS excludes extracellular molecules in a size-dependent manner.

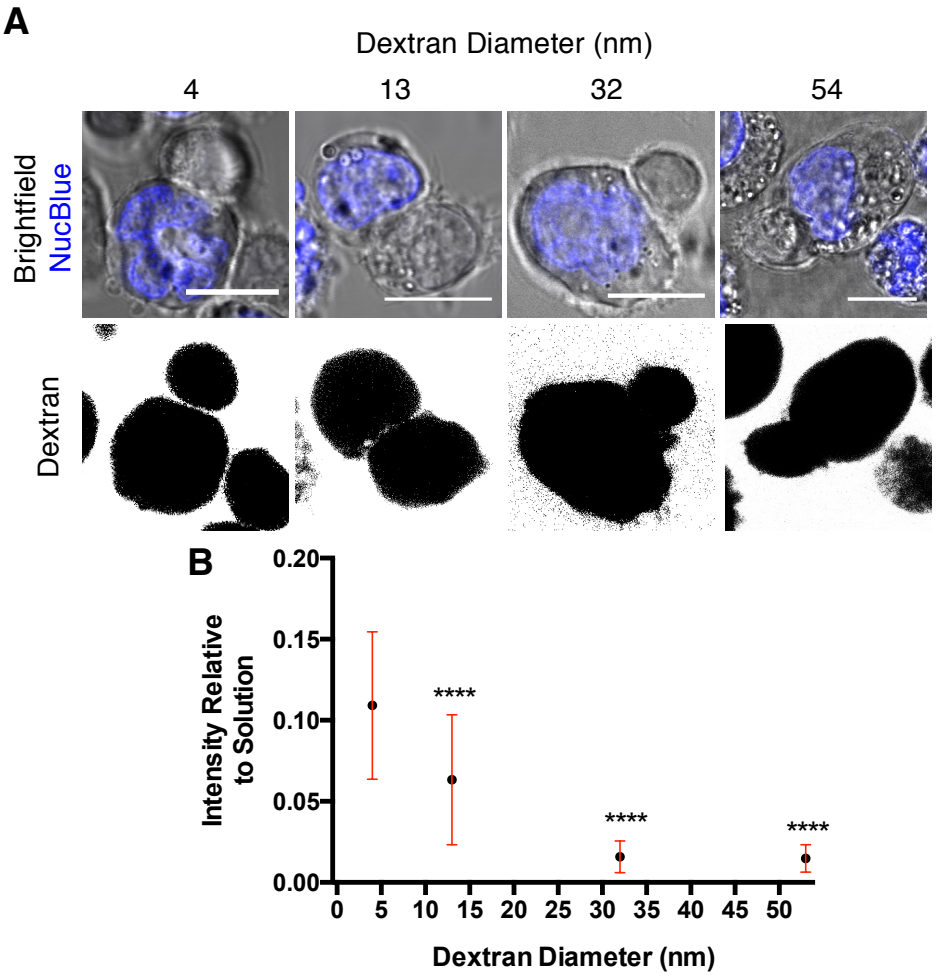


Figure 3.10. Dextran entry into the immune synapse formed by primary human NK cells and Daudi target cells is size-dependent. (A) Representative images of primary human NK cells and Daudi conjugates co-incubated with fluorescein-labelled dextrans of various sizes. Panels show brightfield images overlaid with target cell nuclear staining (*upper row*) and the corresponding fluorescence images of dextran (*lower row*). Scale bars; 10 µm. **(B)** Dextran fluorescence intensity within the synapse was measured relative to the intensity of the extracellular solution for each dextran. Graph shows the mean ± SD. Data were analysed by one-way ANOVA with Tukey corrections (n = 40, 39, 35 and 35 for 4, 13, 32 and 54 nm dextrans respectively) Data are from 3 independent experiments. ****p<0.0001.

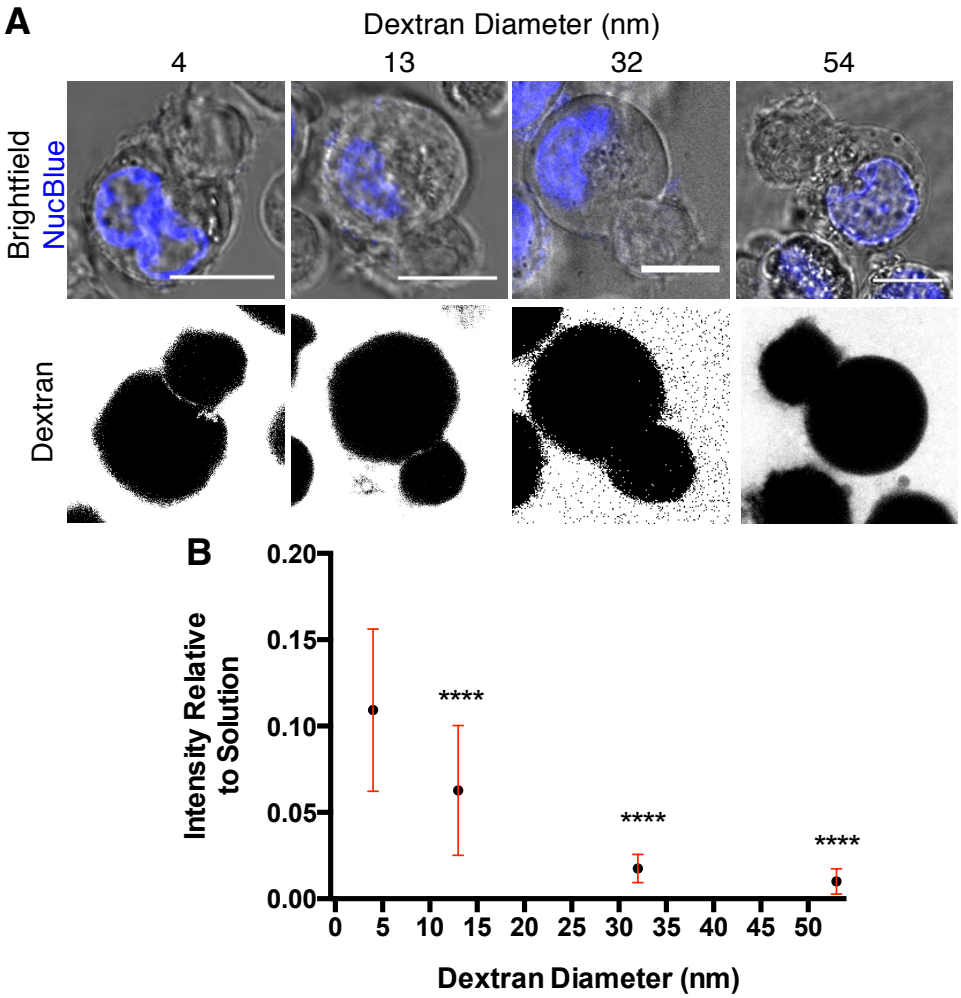


Figure 3.11. Dextran entry into the immune synapse formed by primary human NK cells and K562 target cells is size-dependent. (A) Representative images of primary human NK cells and K562 conjugates co-incubated with fluorescein-labelled dextrans of various sizes. Panels show brightfield images overlaid with target cell nuclear staining (*upper row*) and the corresponding fluorescence images of dextran (*lower row*). Scale bars; 10 µm. **(B)** Dextran fluorescence intensity within the synapse was measured relative to the intensity of the extracellular solution for each dextran. Graph shows the mean ± SD. Data were analysed by one-way ANOVA with Tukey corrections (n = 40, 38, 38 and 42 for 4, 13, 32 and 54 nm dextrans respectively) Data are from 3 independent experiments. ****p<0.0001.

3.2.2 Dextran access to the T cell immune synapse is size-dependent

The structured IS was first discovered between T cells and APCs (10). Whilst cytotoxic proteins are not secreted across this interface, various cytokines, essential to the regulation of immunity and mounting an immune response, are directionally secreted onto the target cell (194, 402-404). Many of the activating receptor-ligand complexes at the T cell IS are of a comparable size to those at the NK cell IS (209, 405, 406).

Therefore, in order to test whether or not the T cell IS also excludes extracellular dextran in a size-dependent manner, the leukaemic T cell line Jurkat was co-incubated with superantigen Enterotoxin E (SEE)-loaded Raji cells. Conjugates were formed in the presence of fluorescein-labelled dextrans sized 4, 13, 32 and 54 nm and imaged by confocal microscopy. Analysis of fluorescence intensity of dextran within the synapse relative to the extracellular solution revealed that dextran was able to access the T cell synapse in a size-dependent manner (Figure 3.12A), comparable to synapses formed by NK cells. Specifically, dextrans sized 4 nm and 13 nm dextrans were able to access the T cell IS (0.1 ± 0.05 and 0.09 ± 0.04 respectively) whereas larger 32 nm and 54 nm dextrans were both significantly restricted or excluded from T cell synapses (0.04 ± 0.02 and 0.02 ± 0.02 respectively) (Figure 3.12B).

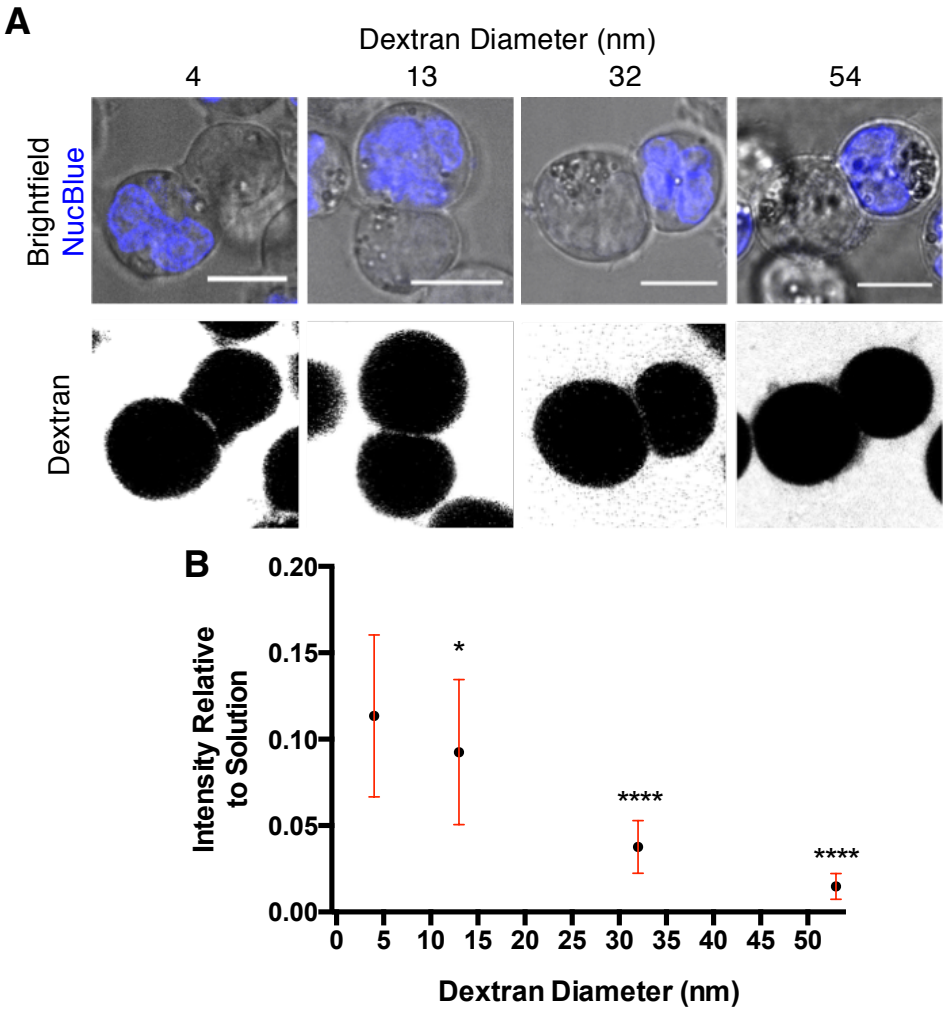


Figure 3.12. Dextran entry into the immune synapse formed by Jurkat cells and Raji target cells is size-dependent. (A) Representative images of Jurkat cells and superantigen Enterotoxin E-loaded Raji conjugates co-incubated with fluorescein-labelled dextrans of various sizes. Panels show brightfield images overlaid with target cell nuclear staining (*upper row*) and the corresponding fluorescence images of dextran (*lower row*). Scale bars; 10 µm. **(B)** Dextran fluorescence intensity within the synapse was measured relative to the intensity of the extracellular solution for each dextran. Graph shows the mean ± SD. Data were analysed by one-way ANOVA with Tukey corrections (n = 34, 36, 33 and 37 for 4, 13, 32 and 54 nm dextrans respectively) Data are from 3 independent experiments. *p<0.1 ,****p<0.0001.

These data show that the T cell IS, which comprises receptor-ligand complexes of comparable size to those in the NK cell IS, restricts the access of dextran in a size-dependent manner (Figure 3.1, 3.2, 3.10 and 3.11). This reflects the findings with NK cells. Therefore, the intermembrane span at the IS, determined by the extracellular domains of receptor-ligand complexes at the interface, may cause the size-dependent exclusion of extracellular molecules.

3.2.3 The inhibitory synapse does not exclude extracellular molecules

The inhibitory NK cell immune synapse is a short-lived, yet structured, interface that occurs when NK cells encounter a healthy cell or those expressing cognate ligands for their inhibitory receptors (9). To test whether or not inhibitory immune synapses exclude dextran in a similar manner to activating synapses, YTS cells transfected with the inhibitory receptor KIR2DL1 (YTS/KIR) were co-incubated with 221 cells expressing the cognate ligand for KIR2DL1, the class I MHC protein HLA-Cw6 (221/Cw6) (Figure 3.13).

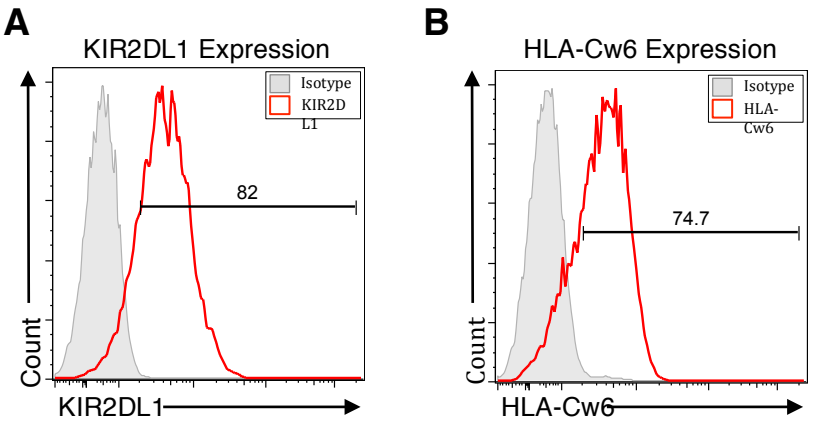


Figure 3.13. Flow cytometric analysis of YTS cells and 221 cells previously transfected with KIR2DL1 and HLA-Cw6 respectively. Surface expression of **(A)** KIR2DL1 on YTS cells or **(B)** HLA-Cw6 on 221 cells was analysed by flow cytometry following transfection. Gates represent the percentage of intact singlet cells that stained positive for KIR2DL1 or HA-Cw6 (red line), when compared to the isotype control (grey shaded), respectively.

Cells were co-incubated with fluorescein-labelled dextrans of various sizes and imaged by confocal microscopy. In contrast to the activating synapses, all dextran sizes tested were detected within the inhibitory synapse (Figure 3.14A). The raw fluorescence intensity of dextran was measured across the solution, cell bodies and synapse (Figure 3.15). Within inhibitory synapses, the peak in raw dextran fluorescence intensity within the synapse was similar for all dextran sizes tested (Figure 3.14B and 3.15). This shows that the inhibitory synapse does not restrict the access of dextran into the cleft. Strikingly, the peak of intensity within the synapse of the 54 nm dextran was similar to the smallest dextrans (3 and 4 nm), this demonstrates that none of the dextrans, diameters 3 – 54 nm, were excluded. Moreover, relative fluorescence intensities of the differently sized dextrans within the

inhibitory IS (relative to the extracellular solution) were not significantly different (between 0.11 ± 0.06 – 0.14 ± 0.05). For example, the relative intensities of the 4 nm and 54 nm dextran within the inhibitory synapse were comparable (0.13 ± 0.06 and 0.11 ± 0.04 respectively) (Figure 3.14C). These data show that the inhibitory synapse is unable to exclude extracellular molecules in a size-dependent manner.

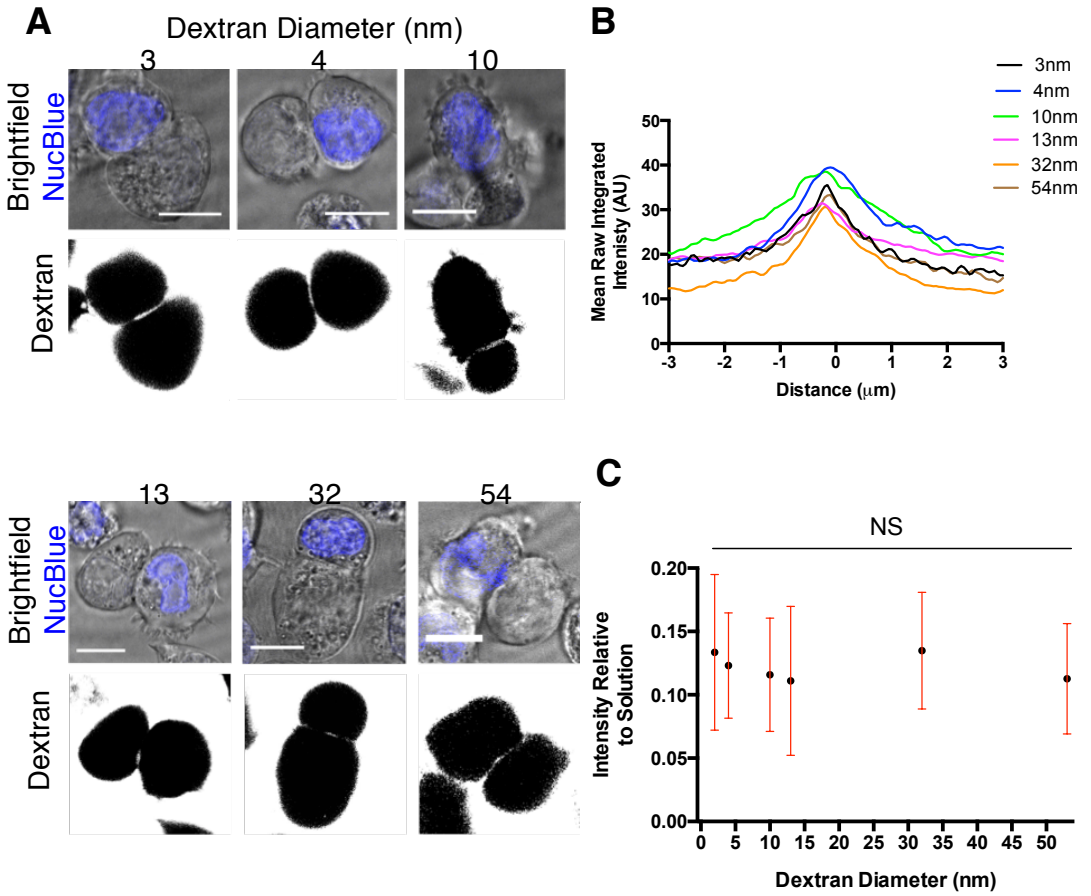


Figure 3.14. Dextran entry into the inhibitory immune synapse formed by YTS/KIR2DL1 and 221/Cw6 target cells is not size-dependent. (A) Representative images of YTS cells expressing KIR2DL1 (YTS/KIR2DL1) and 221 cells expressing HLA-Cw6 (221/Cw6) conjugates co-incubated with fluorescein-labelled dextrans of various sizes. Images show brightfield overlaid with target cell nuclear staining (*upper*) and the corresponding fluorescence images of dextran (*lower*). Scale bars; 10 μm. **(B)** Graph shows the mean raw intensities of differently sized dextrans, as indicated, across the synapse. **(C)** Dextran fluorescence intensity within the synapse was measured relative to the intensity of the extracellular solution for each dextran. Graph shows the mean ± SD. Data were analysed by one-way ANOVA with Tukey corrections (n = 42, 45, 41, 45, 35 and 35 for 2, 4, 10, 13, 32 and 54 nm dextran respectively). Data are from 3 independent experiments.

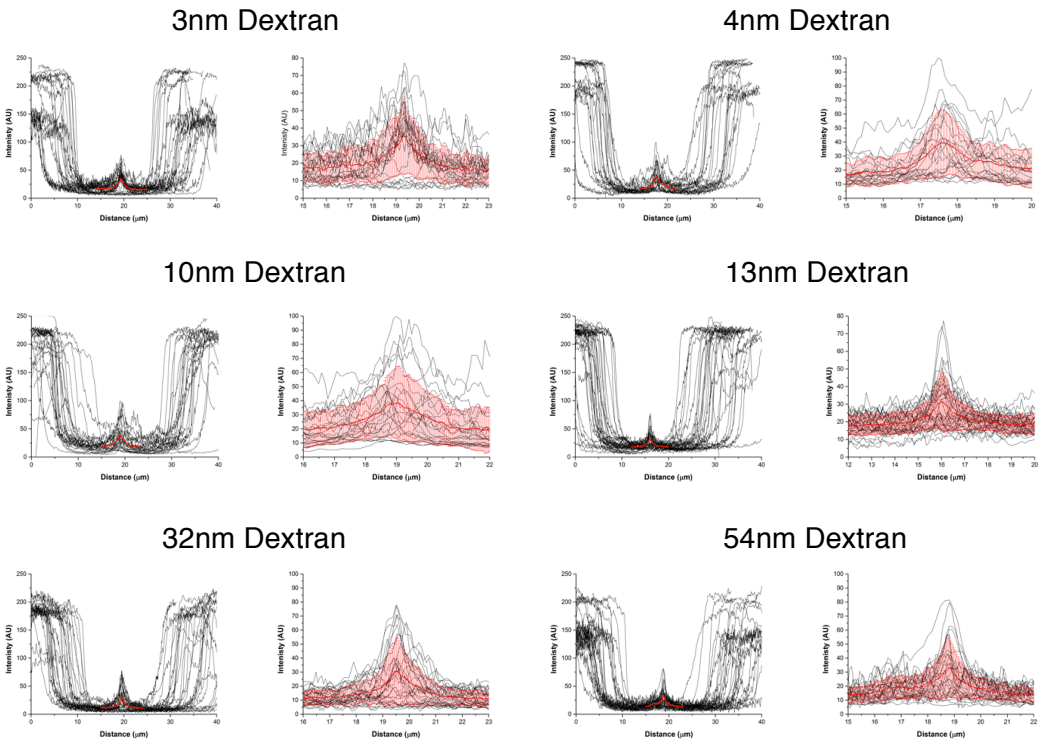


Figure 3.15. Raw intensity profiles of various sized dextrans across inhibitory synapses formed by YTS/KIR cells. Dextran raw integrated intensity was measured using a 50-pixel-wide line across the solution, cell body (*e.g.* YTS/KIR cell), synapse, cell body (*e.g.* 221/Cw6 cell) and solution. Graphs show either the raw intensity across the conjugate (*left graph*) or zoomed in across the synapse (*right graph*) for each dextran size as indicated. Red lines show the mean intensity ± SD (n = 42, 45, 41, 45, 35 and 35 for 2, 4, 10, 13, 32 and 54 nm dextran respectively).

In conclusion, these data show that dextrans of a range of sizes can access the inhibitory synapse, whereas they are excluded in a size-dependent manner from the activating IS. This suggests that the ability to exclude extracellular molecules relates to the properties of an activating synapse.

3.2.4 Dextran below the size exclusion threshold moves freely into and out of the immune synapse

Activating NK and T cell synapses have been shown to restrict the access of dextrans present in the extracellular solution in a size-dependent manner (Figures 3.1 – 3.12). However, dextran was present from the point of initial cell-cell contact and synapse assembly. Therefore, these experiments did not address whether dextran below the size exclusion threshold is able to enter a pre-formed synapse, or if dextran detected within the synaptic cleft is merely trapped during synapse assembly.

To investigate this, YTS and 221 cells were mixed to form synapses and then plated on 0.01% PLL-coated chambered coverglasses to immobilise the conjugates. Cells were then imaged by time-lapse confocal microscopy. During imaging, 4nm (Figure 3.16A) or 54 nm (Figure 3.16B) fluorescein-labelled dextrans were added to the solution (first image stack following dextran addition at *time = 0*). Fluorescence intensity of the 4 nm or 54 nm dextran was then measured at the synapse, relative to the extracellular solution, at each time point (Figure 3.16C). The data shows that 4 nm dextran (Figure 3.16C, *circles*) could be detected within the synapse almost immediately after addition to the extracellular solution. The relative intensity increased over the first 2 – 4 minutes, before reaching a plateau. In contrast, the 54 nm dextran (Figure 3.16C, *squares*) was unable to penetrate the IS throughout the course of imaging (up to ~15 minutes following dextran addition). These data are consistent with previous results showing that larger dextran (54 nm) is excluded from the IS and smaller dextran (4 nm) is able to enter the IS. Furthermore, the addition of dextran to the extracellular solution and its subsequent access or exclusion further demonstrates that the IS forms a physical barrier that can prevent the access of molecules above a size threshold, whereas those below this limit can freely pass into the synaptic cleft.

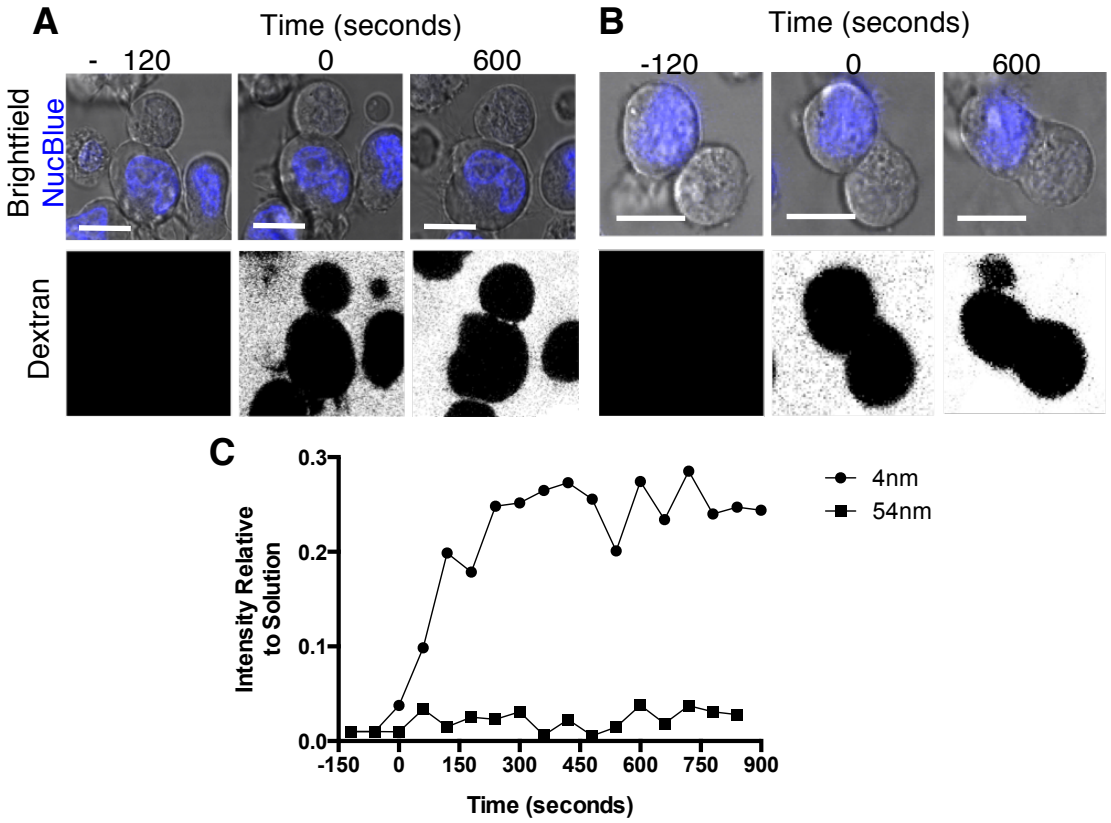


Figure 3.16. Dextran is excluded from formed immune synapses in a size-dependent manner. (A) Representative time-lapse confocal images of YTS and 221 conjugates as a fluorescein-labelled 4 nm dextran was added to the solution (*time = 0*). Panels show brightfield images overlaid with target nuclear staining (*upper row*) and the corresponding fluorescence image (*lower row*). **(B)** Representative time-lapse confocal images of YTS and 221 conjugates as a fluorescein-labelled 54 nm dextran was added to the solution (*time = 0*). Panels show brightfield images overlaid with target nuclear staining (*upper row*) and the corresponding fluorescence image (*lower row*). Scale bars; 10 µm. **(C)** Dextran fluorescence intensity within the synapse was measured relative to the intensity of the extracellular solution at each time point following addition of dextran. Graph shows representative data of the 4 nm (*circles*) and 54 nm (*squares*) dextran from 5 independent experiments.

The 4 nm dextran can access the synapse when added either prior to or following synapse formation. However, whether dextran could move freely out of the synapse, had not yet been addressed. To test whether dextran was trapped or could move out of a formed synapse, YTS cells and 221 cells were plated on 0.01% PLL-coated chambered slides in the presence of a fluorescein-labelled 4 nm dextran at a final concentration of 50 µM. Immobilisation of conjugates on PLL allowed the same conjugate to be imaged by confocal microscopy whilst serially diluting the extracellular dextran concentration (Figure 3.17A). Dextran fluorescence intensity within the synapse relative to the extracellular solution intensity was then measured after each dilution (Figure 3.17B). Analysis showed that the relative dextran

fluorescence intensity within the synapse remained similar, with no significant change following dextran dilution – establishing that dextran within the synapse equilibrates with the extracellular solution. This data shows that 4 nm-sized dextrans are not trapped within the synapse when present during its formation and are indeed able to freely move out of the synapse, in agreement with previous findings that show dextran equilibrates between the synapse and extracellular solution (Figure 3.7).

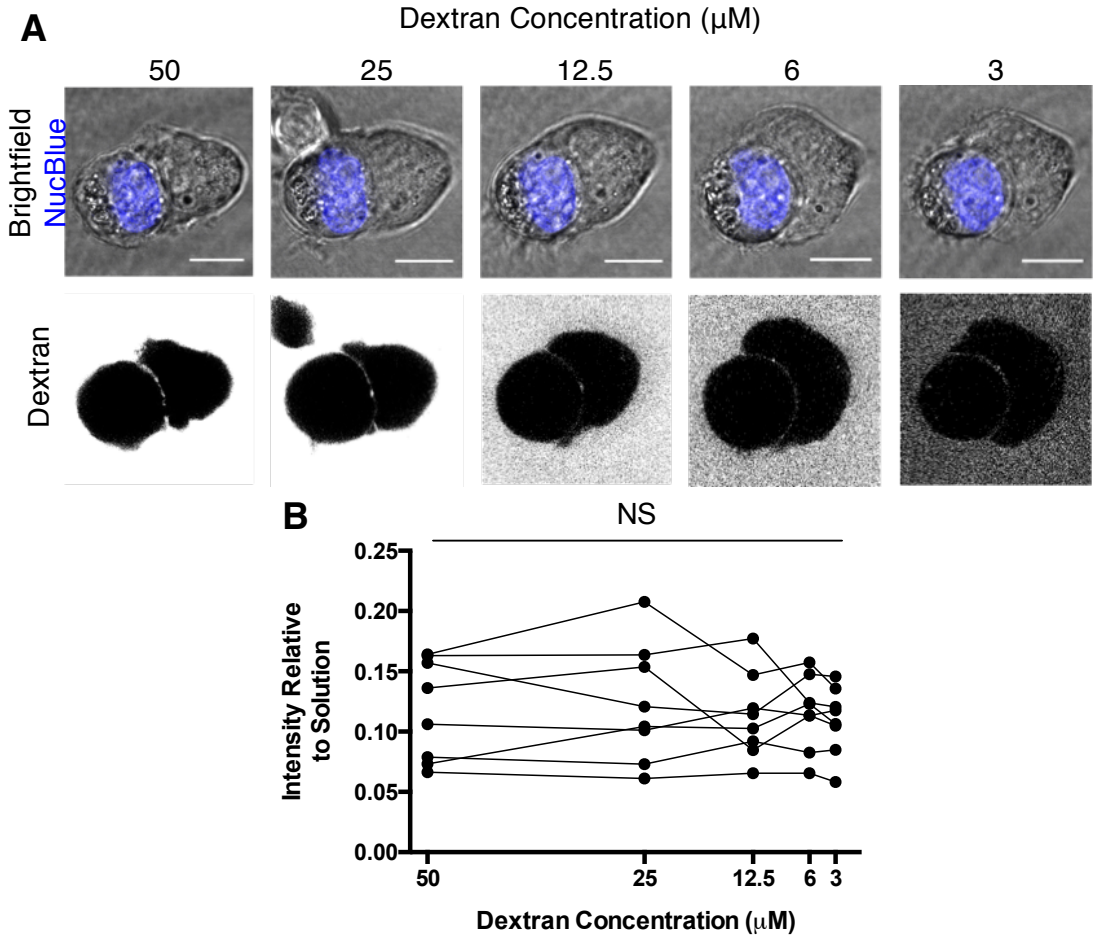


Figure 3.17. Dextran within the immune synapse equilibrates with the concentration in the extracellular solution. (A) Representative confocal images of a YTS and 221 conjugate as the extracellular solution was diluted. Panels show brightfield images overlaid with target cell nuclear staining (*upper row*) and the corresponding fluorescence image (*lower row*). Scale bars; 10 µm. **(B)** Dextran fluorescence intensity within the synapse was measured relative to the extracellular solution at each concentration. Graph shows the relative intensities of dextran at each concentration of the same conjugate (*connecting lines*) (n = 8). Data are from 8 independent experiments (each *coloured line*). The mean intensities at each concentration were analysed using one-way ANOVA with Tukey corrections. NS = no significance.

In a separate experiment, the impact of complete removal of dextran from the extracellular solution was investigated. YTS or pNK cells were co-incubated with 221 cells and fluorescein-labelled 4 nm dextran on 0.01% PLL-coated slides and imaged by confocal microscopy. The medium containing dextran was then removed and replaced with dextran-free medium and conjugates were imaged for a second time. Dextran within the synapses prior to and following removal of dextran was assessed. This was then compared to the levels of extracellular dextran that was present prior to washing. Dextran was detected initially in the synapses formed by YTS cells (pre-wash) but could not be detected following removal of the dextran (post-wash) (Figure 3.18A). Relative intensities within the synapses fell from 0.12 ± 0.05 to 0.006 ± 0.003 (Figure 3.18B). Dextran present in synapses formed by pNK cells could also be washed out of the synapse (Figure 3.19A). The relative dextran intensity fell significantly from 0.16 ± 0.04 to 0.006 ± 0.003 (Figure 3.19B). These data demonstrate that 4 nm dextran is not trapped within the IS and can be washed out.

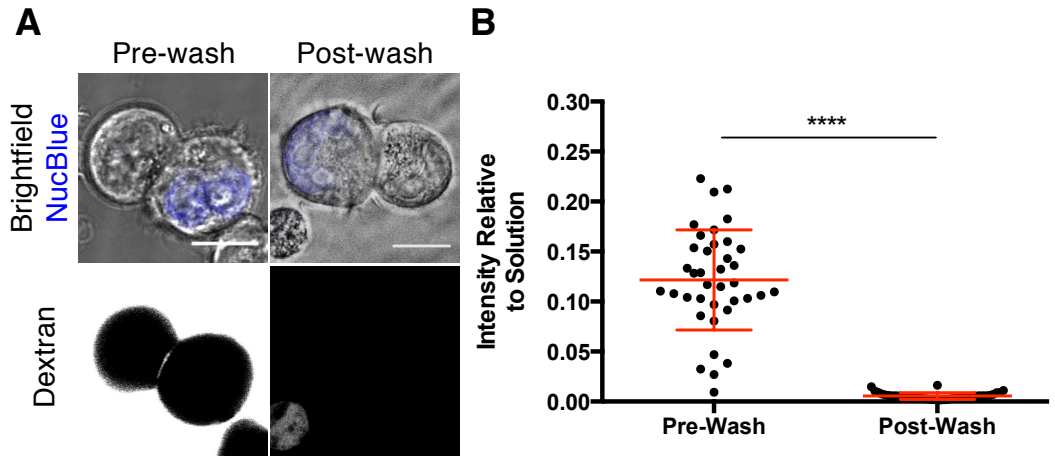


Figure 3.18. Dextran can be washed out of the immune synapse formed by YTS cells. (A) Representative images of YTS and 221 target cells prior to (*Pre-wash*) and following (*Post-wash*) the removal of extracellular fluorescein-labelled 4 nm dextran. Panels show brightfield images overlaid with target nuclear staining (*upper row*) and the corresponding fluorescence images (*lower row*). Scale bars; 10 µm. **(B)** Dextran fluorescence intensity within the synapse was measured relative to the extracellular solution intensity prior to (*Pre-wash*) and following (*Pre-wash*) the removal of dextran. Bars show the mean ± SD. (n = 38 for Pre-Wash and 40 for Post-Wash). Data was analysed using a Student's t-test with Welch's corrections. Data from 3 independent experiments. ****p<0.0001

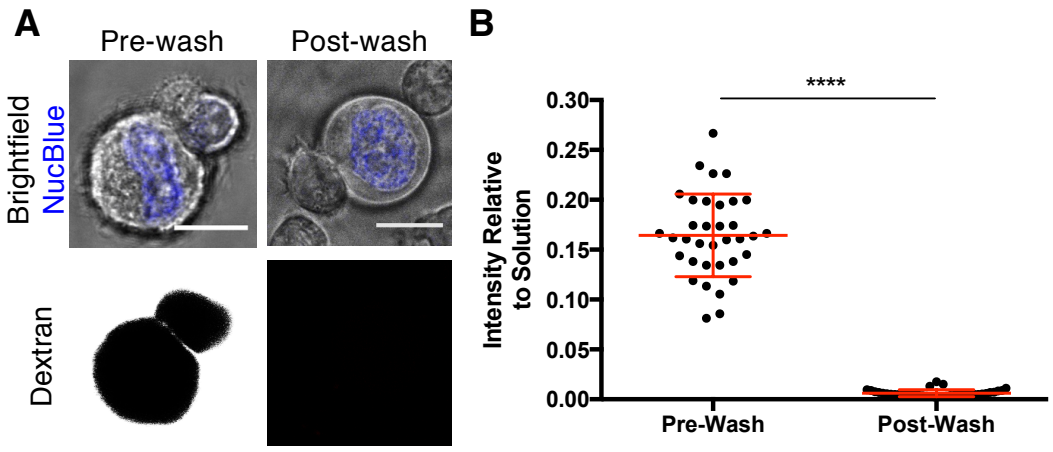


Figure 3.19. Dextran can be washed out of the immune synapse formed by primary human NK cells . (A) Representative images of primary human NK cells and 221 target cells prior to (*Pre-wash*) and following (*Post-wash*) the removal of extracellular fluorescein-labelled 4 nm dextran. Panels show brightfield images overlaid with target nuclear staining (*upper row*) and the corresponding fluorescence images (*lower row*). Scale bars; 10 µm. **(B)** Dextran fluorescence intensity within the synapse was measured relative to the extracellular solution intensity prior to (*Pre-wash*) and following (*Pre-wash*) the removal of dextran. Bars show the mean ± SD. (n = 35 for Pre-Wash and 39 for Post-Wash). Data was analysed using a Student's t-test with Welch's corrections. Data from 3 independent experiments. ****p<0.0001

Taken together, the data in this study demonstrate that not only are larger 54 nm dextrans excluded from the synapse but that smaller 4 nm dextrans are able to move both in and out of the synapse, equilibrating with the extracellular solution. This suggests that the IS is not completely sealed but rather forms a barrier that can be penetrated by molecules below a size threshold.

3.2.5 Intact actin is required to exclude dextran from the immune synapse

Previous experiments have shown that a formed synapse is able to exclude dextrans sized ≥32 nm, and those below are able to access the synapse in a size-dependent manner. During synapse formation, F-actin is rearranged at the synapse to form rings around a hypo-dense region through which cytotoxic mediators are secreted (117, 187). The polymerisation of actin is thought to provide the pushing/pulling forces that polarise NK cells (including the MTOC and machinery for directed secretion), and may also form a rigid scaffold to support the synaptic structure (180, 181). These high tensile forces at the cell-cell interface may enable the exclusion of larger dextrans by maintaining the close proximities of the cell membranes and the organisation of the receptor-ligand complexes at the synapse. Latrunculin A (Lat A) is a drug produced by the sea sponge *Latrunculia*, and has been shown to depolymerise actin by binding monomeric G-actin in a 1:1 complex (407). Conversely, Jasplakinolide (Jasp), produced by the marine sponge *Jaspis johnstoni*, has been shown to stabilise actin, preventing the polymerisation or depolymerisation of actin monomers (408). These drugs were therefore used to test whether or not the actin structure at the synapse was required to exclude dextran.

To first verify that Lat A depolymerises actin in both pNK cells and 221 cells, 10^6 cells were incubated with 1 μM Lat A or a vehicle control, DMSO, for 5 minutes. Cells were then fixed, permeabilised and stained for actin (using Phalloidin labelled with Alexa Fluor 647) before being imaged by confocal microscopy. Actin was depolymerised within 5 minutes in both pNK cells and 221 cells (Figure 3.20A and B). Actin raw intensity was reduced significantly compared to the DMSO control in pNK cells (6216 ± 2515 AU to 1435 ± 485 AU) and 221 cells (10858 ± 5841 to 3410 ± 1302 AU) (Figure 3.20C). Therefore, the addition of Lat A for 5 minutes is sufficient to depolymerise actin in pNK cells and 221 cells.

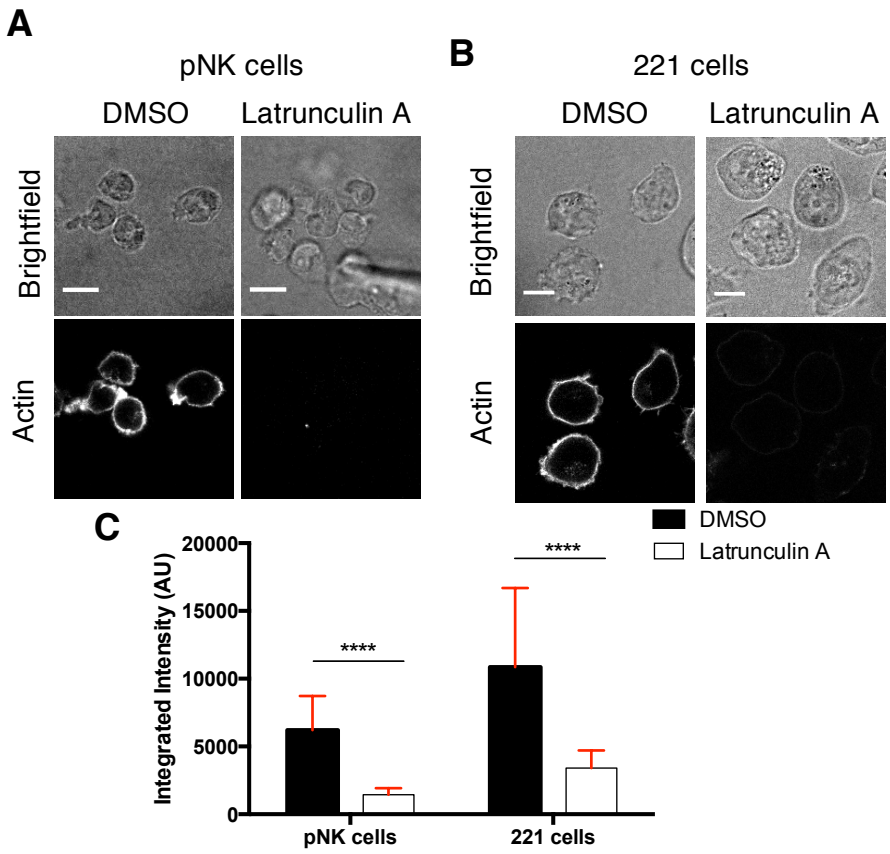


Figure 3.20. Latrunculin A depolymerises actin in primary human NK cells and 221 cells. (**A**) Primary human NK cells and (**B**) 221 cells were incubated with DMSO (*left* columns) or 1 µM Latrunculin A (*right columns*) for 5 minutes then stained for actin using Phalloidin labelled with Alexa-647. Panels show brightfield images (*upper rows*) and the corresponding fluorescence image of actin (*lower rows*). Scale bars; 10 µm. (**C**) Actin fluorescence was measured to determine the presence or depletion of actin at the cell periphery. Graph shows the mean raw fluorescence intniesty of actin. Bars represent mean ± SD (n = 119 and 117 for DMSO and Latrunculin A respectively for pNK cells and 111 and 113 for DMSO and Latrunculin A respectively for 221 cells). Data were analysed using a Student's t-test with Welch's corrections. ****p<0.0001.

As Phalloidin competes with Jasp for actin binding (408), a cell migration assay was used to test the effect of actin stabilisation on NK cells, rather than by actin staining. To do this, pNK cells were plated on fibronectin-coated slides and imaged by time-lapse confocal microscopy following incubation with either a negative control, R10 medium (Figure 3.21A); a vehicle control, DMSO (Figure 3.21B); or 0.5 µM Jasp (Figure 3.21C) for 5 minutes. In R10 medium, pNK cell mean migration speed was 0.34 ± 0.08 µm/min. Following incubation with Jasp, pNK cell migration was significantly decreased (0.22 ± 0.07 µm/min). Incubation with DMSO alone did not affect cell migration (0.39 ± 0.24 µm/min) (Figure 3.21D). This shows that incubation

with Jasp decreases NK cell migration, which is mediated through the stabilisation of actin filaments.

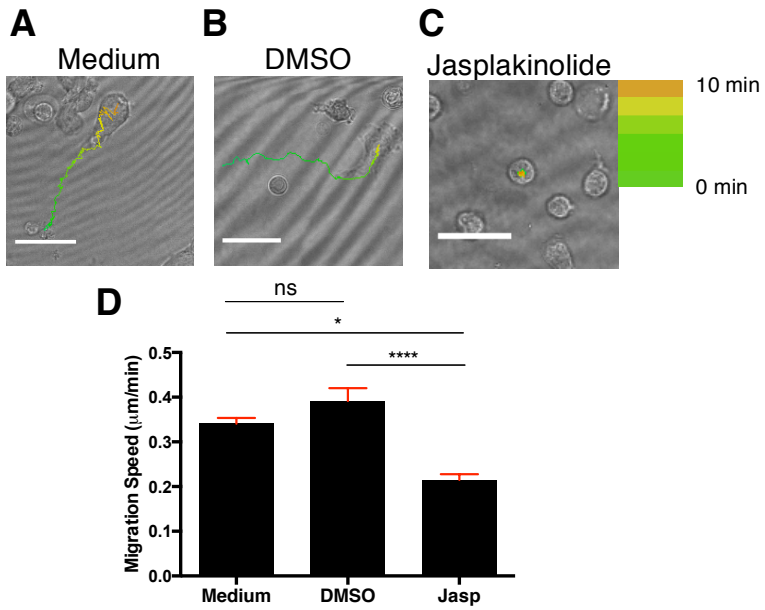


Figure 3.21. Jasplakinolide reduces NK cell migration by stabilising actin. Primary human NK (pNK) cells were incubated with (**A**) medium, (**B**) DMSO or (**C**) 0.5 µM Jasplakinolide for 5 minutes, then plated on fibronectin-coated slides. Cells were then imaged by time-lapse confocal microscopy for 10 minutes. Panels show tracked migration paths of pNK cells after incubation with the indicated additions, colour-coded by time as indicated on the scale chart. Scale bars; 10 µm. (**D**) Cell migration speed was measured. Graphs show the mean migration speeds following incubation with DMSO or Jasplakinolide, as indicated. Bars show mean ± SEM. (n = 34 for medium, 67 for DMSO and 30 for Jasplakinolide). Data are from 2 independent experiments. Data were analysed using a one-way ANOVA with Tukey corrections. p<0.1, ****p<0.0001.

Finally, it was investigated whether these concentrations of Lat A or Jasp had any significant effect on cell viability. Primary NK cells, YTS cells and 221 cells were incubated with Lat A or Jasp, at the same concentrations as previously used, then washed using R10 medium. Cells were also incubated with negative controls: DMSO or R10, and a positive control, 4% paraformaldehyde. As DAPI was used to stain for non-viable cells, fixation of cells using paraformaldehyde allowed the entry of DAPI staining, serving as a positive control (shown in blue, Figure 3.22). Once cells had been incubated with DAPI for 5 minutes, cell viability was assessed using flow cytometry. The results show that neither Lat A or Jasp had a negative effect on pNK cell, YTS cell or 221 cell viability (Figure 3.22).

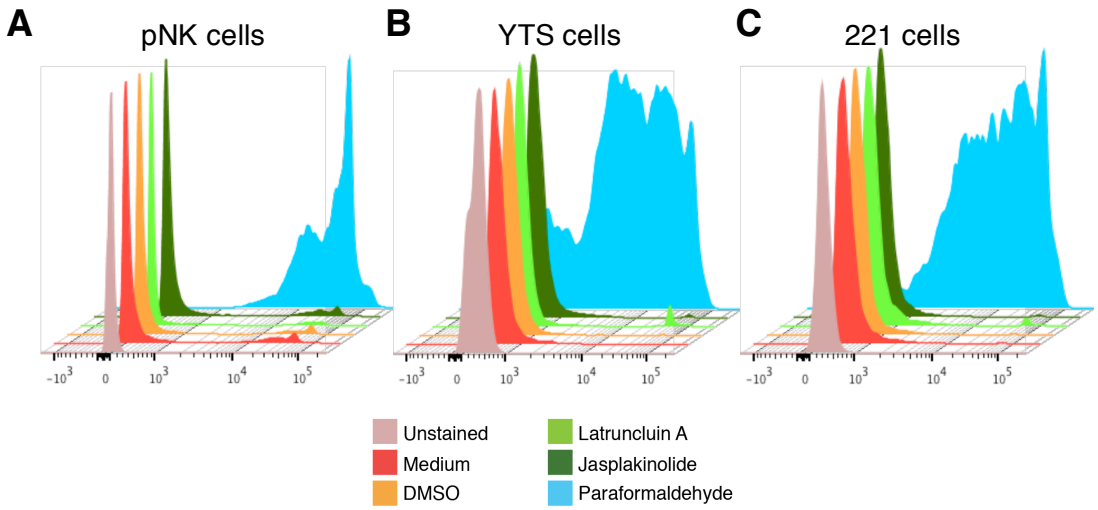


Figure 3.22. Latrunculin A or Jasplakinolide are not detrimental to cell health of primary human NK cells, YTS cells or 221 cells. (**A**) Primary human NK cells, (**B**) YTS cells and (**C**) 221 cells were incubated with medium (peach), paraformaldehyde (blue), DMSO (orange), 1 µM Latrunculin A (light green), or 0.5 µM Jasplakinolide (dark green) for 5 minutes. Cell death was then assessed by flow cytometry using a DAPI nuclear stain. DAPI staining signifies cell death. Graphs show total number of dead cells positive for DAPI normalised to the mode for each condition, as indicated. Data are representative of 2 independent experiments.

Once the function of Lat A and Jasp had been verified, the requirement for intact actin for dextran exclusion from the synapse was then tested. To do this, either pNK cells or YTS cells were co-incubated with 221 target cells and dextran sized 32 nm on PLL-coated slides. Conjugates were then imaged by confocal microscopy. A DMSO vehicle control, 1 µM Lat A or 0.5 µM Jasp were then added to the solution and the same conjugate imaged every minute for 5 minutes. The relative intensity of dextran to the extracellular solution was measured at each time point to assess if dextran access to the synapse changed following changes to actin integrity or dynamics.

The addition of DMSO to conjugates showed that this vehicle did not have any impact on the exclusion of the 32 nm dextran from synapses formed by either pNK cells or YTS cells. Analysis of the relative intensity of dextran showed that dextran within the synapse remained constant throughout the time course for synapses formed by either pNK cells (Pre-Treatment: 0.01 ± 0.01; 5 minutes post-treatment: 0.009 ± 0.004) or YTS cells (Pre-Treatment: 0.027 ± 0.012; 5 minutes Post-Treatment: 0.02 ± 0.01) (Figure 3.23 for pNK cells Figure 3.24 for YTS cells).

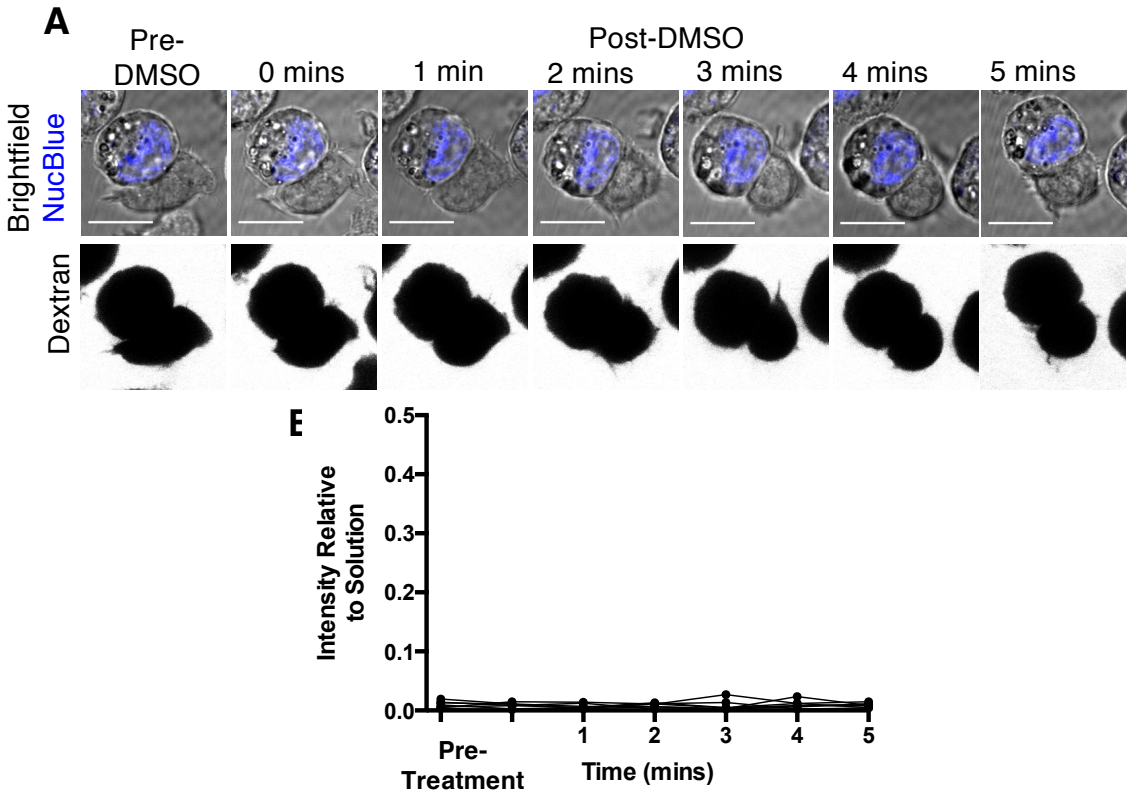


Figure 3.23. Dextran is excluded from the primary human NK immune synapse when actin remains intact. (**A**) Primary human NK cells and 221 cells were co-incubated with 32 nm dextran and imaged by confocal microscopy (*Pre-Treatment*). A vehicle control, DMSO, was then added to the cells and the same conjugate was imaged every minute for 1 minute (*time = 0 – 5*). Panels show representative brightfield images overlaid with target cell nuclear staining (*upper row*) and the corresponding fluorescence image (*lower row*) at each time point, as indicated. Scale bars; 10 µm. (**B**) Dextran fluorescence intensity within the synapse was measured relative to the intensity of the extracellular solution at each time point Graph shows the relative intniesty for the same conjugate at each time point, shown by connecting lines. The mean relative intensities at each time point were analysed by one-way ANOVA with Tukey corrections (n = 7). Data are from 7 independent experiments for each dextran size.

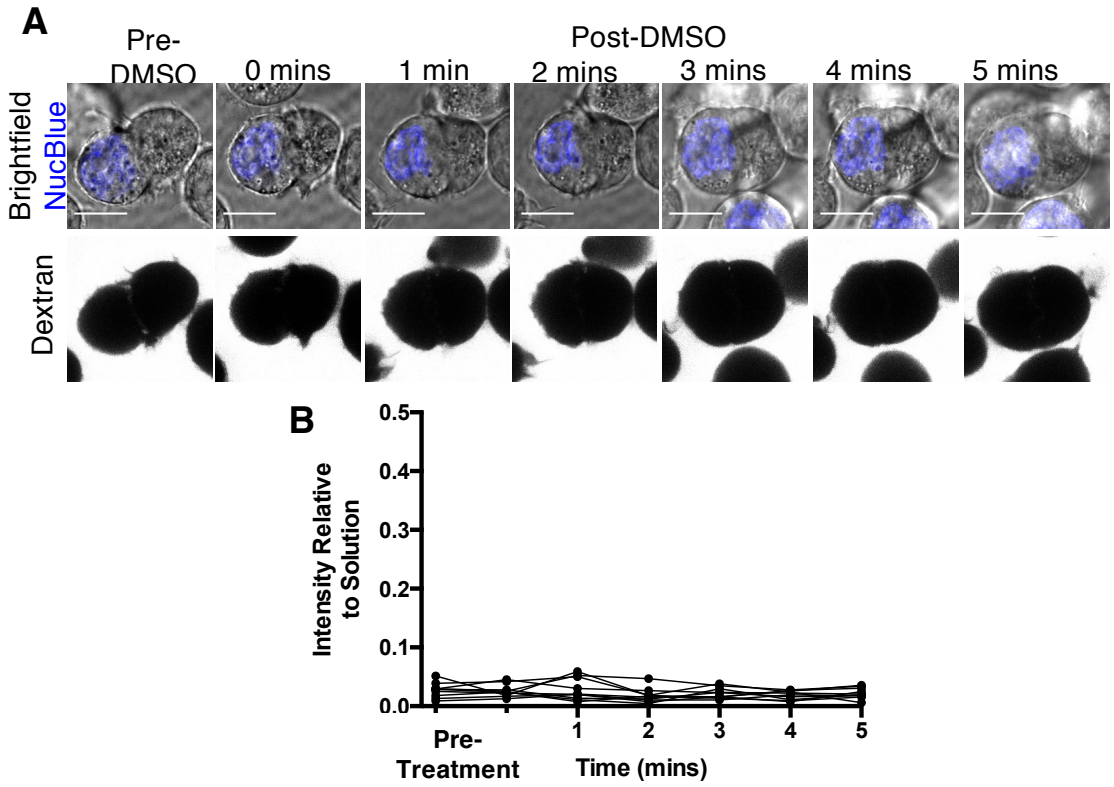


Figure 3.24. Dextran is excluded from the YTS cell immune synapse when actin remains intact. (**A**) YTS cells and 221 cells were co-incubated with 32 nm dextran and imaged by confocal microscopy (*Pre-Treatment*). A vehicle control, DMSO, was then added to the cells and the same conjugate was imaged every minute for 1 minute (*time = 0 – 5*). Panels show representative brightfield images overlaid with target cell nuclear staining (*upper row*) and the corresponding fluorescence image (*lower row*) at each time point, as indicated. Scale bars; 10 µm. (**B**) Dextran fluorescence intensity within the synapse was measured relative to the intensity of the extracellular solution at each time point Graph shows the relative intniesty for the same conjugate at each time point, shown by connecting lines. The mean relative intensities at each time point were analysed by one-way ANOVA with Tukey corrections (n = 10). Data are from 6 independent experiments for each dextran size.

Incubation of conjugates with 1 µM Lat A, shown previously to depolymerise actin, had a profound effect on the ability of the synapse to exclude dextran. Within minutes of Lat A addition, the 32 nm dextran was able to enter the synapse formed by pNK cells (Figure 3.25A). Prior to the addition of Lat A, the relative intensity of dextran within the pNK cell synapse was similar to previous experiments (0.01 ± 0.01). Immediately after the addition of Lat A, the exclusion of dextran was not affected (0.009 ± 0.005). However, after 5 minutes incubation with Lat A, the 32 nm dextran had penetrated the synapse (0.19 ± 0.05) (Figure 3.25B). These experiments were repeated with YTS cells co-incubated with 221 target cells and a fluorescein-labelled 32nm dextran. The addition of Lat A also abrogated the exclusion of 32 nm dextran from the YTS cell synapse (Figure 3.26A). Dextran relative intensity increased from

0.02 ± 0.01 immediately after the addition of Lat A to 0.26 ± 0.11 after 5 minutes incubation (Figure 3.26B). This suggests that the integrity of actin at the IS enables the size-dependent exclusion of extracellular dextran. When actin integrity is compromised, here by addition of a depolymerizing agent, the reduction in membrane rigidity most likely enables entry of dextran into the synapse.

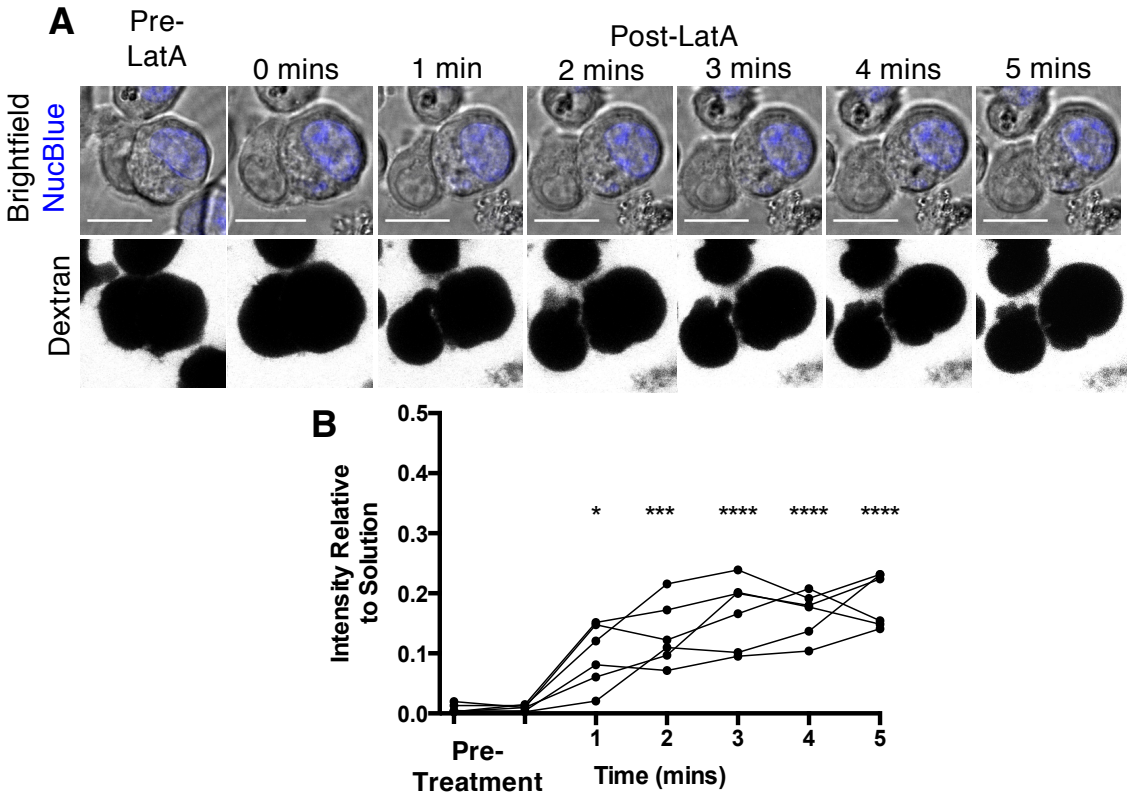


Figure 3.25. Depolymerisation of actin abolishes the exclusion of dextran from the primary human NK cell immune synapse. (**A**) Primary human NK cells and 221 cells were co-incubated with 32 nm dextran and imaged by confocal microscopy (*Pre-Treatment*). Latrunculin A at a final concentration of 1 µM was then added to the cells and the same conjugate was imaged every minute for 1 minute (*time = 0 – 5*). Panels show representative brightfield images overlaid with target cell nuclear staining (*upper row*) and the corresponding fluorescence image (*lower row*) at each time point, as indicated. Scale bars; 10 µm. (**B**) Dextran fluorescence intensity within the synapse was measured relative to the intensity of the extracellular solution at each time point. Graph shows the relative intniesty for the same conjugate at each time point, shown by connecting lines. The mean relative intensities at each time point were analysed by one-way ANOVA with Tukey corrections (n = 6). Data are from 6 independent experiments for each dextran size. *p<0.1, ***p<0.001, ****p<0.0001.

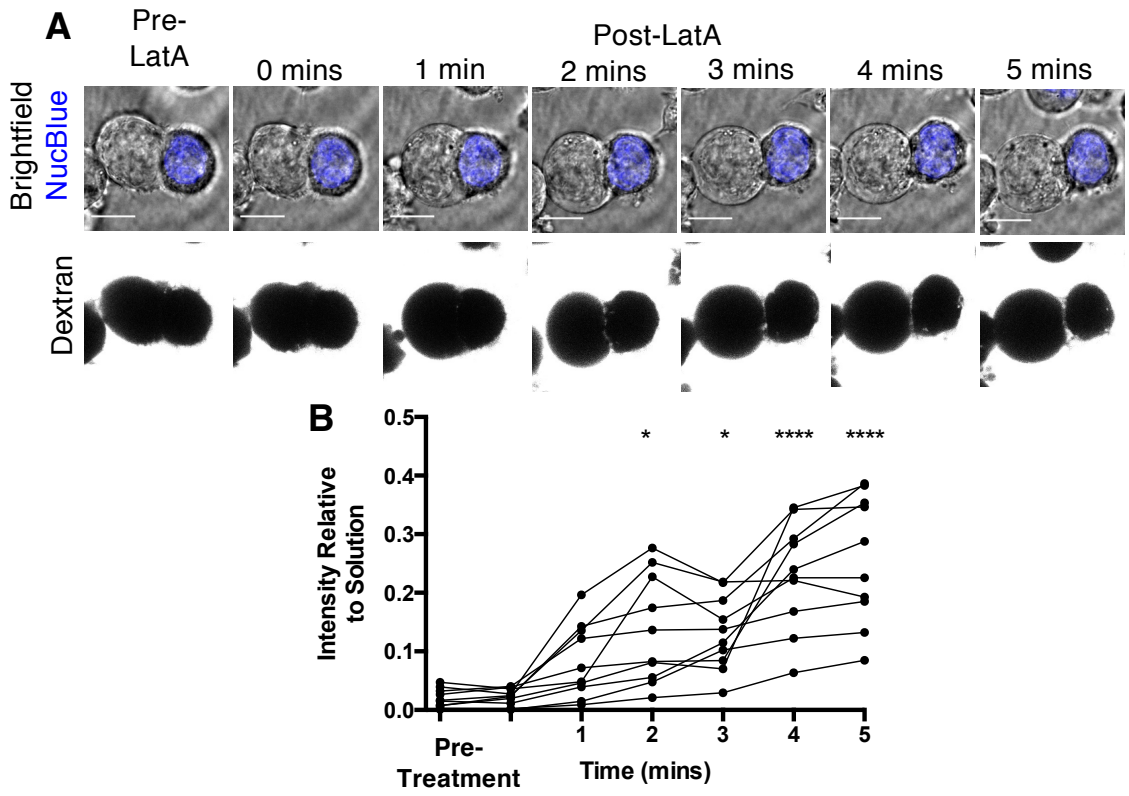


Figure 3.26. Depolymerisation of actin abolishes exclusion of dextran from the YTS cell immune synapse. (**A**) YTS and 221 cells were co-incubated with 32 nm dextran and imaged by confocal microscopy (*Pre-Treatment*). Latrunculin A at a final concentration of 1 µM was then added to the cells and the same conjugate was imaged every minute for 1 minute (*time = 0 – 5*). Panels show representative brightfield images overlaid with target cell nuclear staining (*upper row*) and the corresponding fluorescence image (*lower row*) at each time point, as indicated. Scale bars; 10 µm. (**B**) Dextran fluorescence intensity within the synapse was measured relative to the intensity of the extracellular solution at each time point. Graph shows the relative intniesty for the same conjugate at each time point, shown by connecting lines. The mean relative intensities at each time point were analysed by one-way ANOVA with Tukey corrections (n = 10). Data are from 7 independent experiments for each dextran size. *p<0.1, ****p<0.0001.

Then, to test whether actin turnover was required to maintain size exclusion, Jasp was added to pNK cells or YTS cells in conjugates with 221 target cells in the presence of 32 nm dextran and imaged by confocal microscopy. Conjugates were imaged prior to the addition of 0.5 µM Jasp, then immediately after (*time = 0*) and again every minute for 5 minutes. The addition of Jasp to pNK-221 cell conjugates did not affect the exclusion of dextran (Figure 3.27A). Dextran relative intensity within the synapse remained constant prior to the addition of Jasp (0.01 ± 0.01) to 5 minutes after addition of the drug (0.011 ± 0.004) (Figure 3.27B). Similar findings were seen with YTS-221 cell conjugates (Figure 3.28A), where the relative intensity of dextran at the synapse was not significantly altered (0.03 ± 0.01 prior to treatment; 0.04 ± 0.02 after 5 minutes treatment) (Figure 3.28B). This suggests that following

synapse formation, further rearrangement of actin is not required and dextran above the size-exclusion threshold remains unable to penetrate the synaptic cleft.

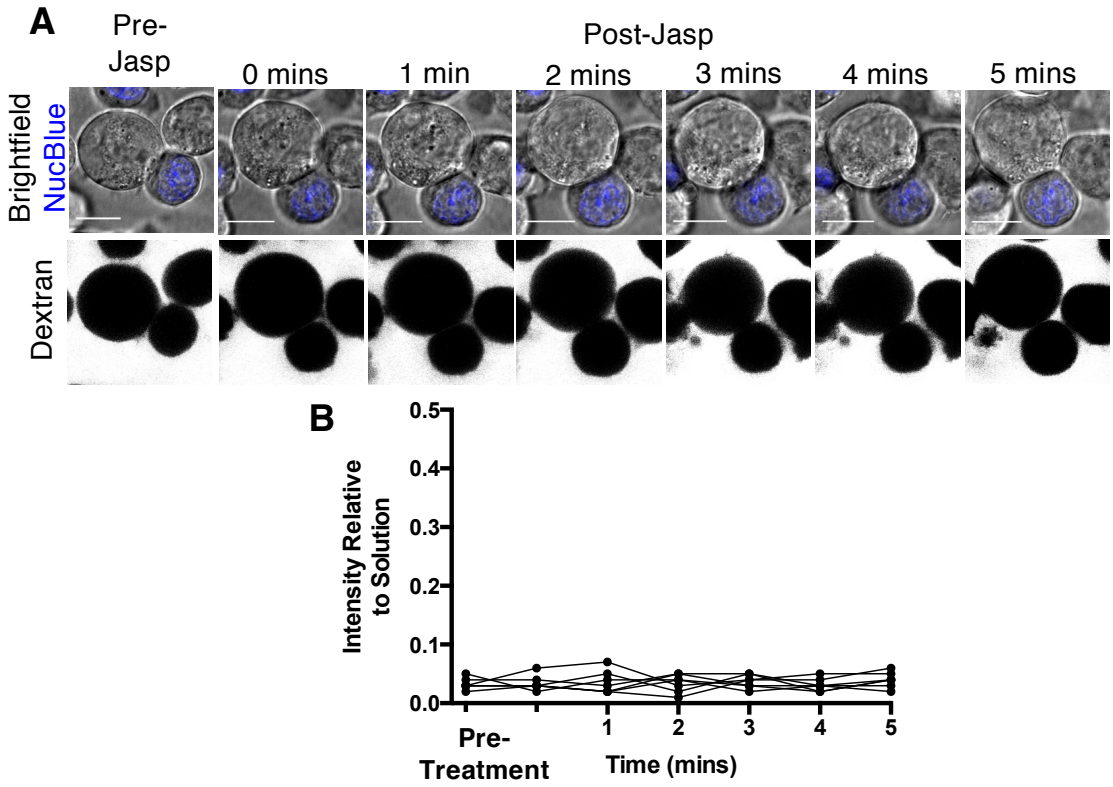


Figure 3.27. Stabilisation of actin maintains the exclusion of dextran from the YTS cell immune synapse (**A**) YTS and 221 cells were co-incubated with 32 nm dextran and imaged by confocal microscopy (*Pre-Treatment*). Jasplakinolide at a final concentration of 0.5 µM was then added to the cells and the same conjugate was imaged every minute for 1 minute (*time = 0 – 5*). Panels show representative brightfield images overlaid with target cell nuclear staining (*upper row*) and the corresponding fluorescence image (*lower row*) at each time point, as indicated. Scale bars; 10 µm. (**B**) Dextran fluorescence intensity within the synapse was measured relative to the intensity of the extracellular solution at each time point. Graph shows the relative intniesty for the same conjugate at each time point, shown by connecting lines. The mean relative intensities at each time point were analysed by one-way ANOVA with Tukey corrections (n = 7). Data are from 7 independent experiments for each dextran size.

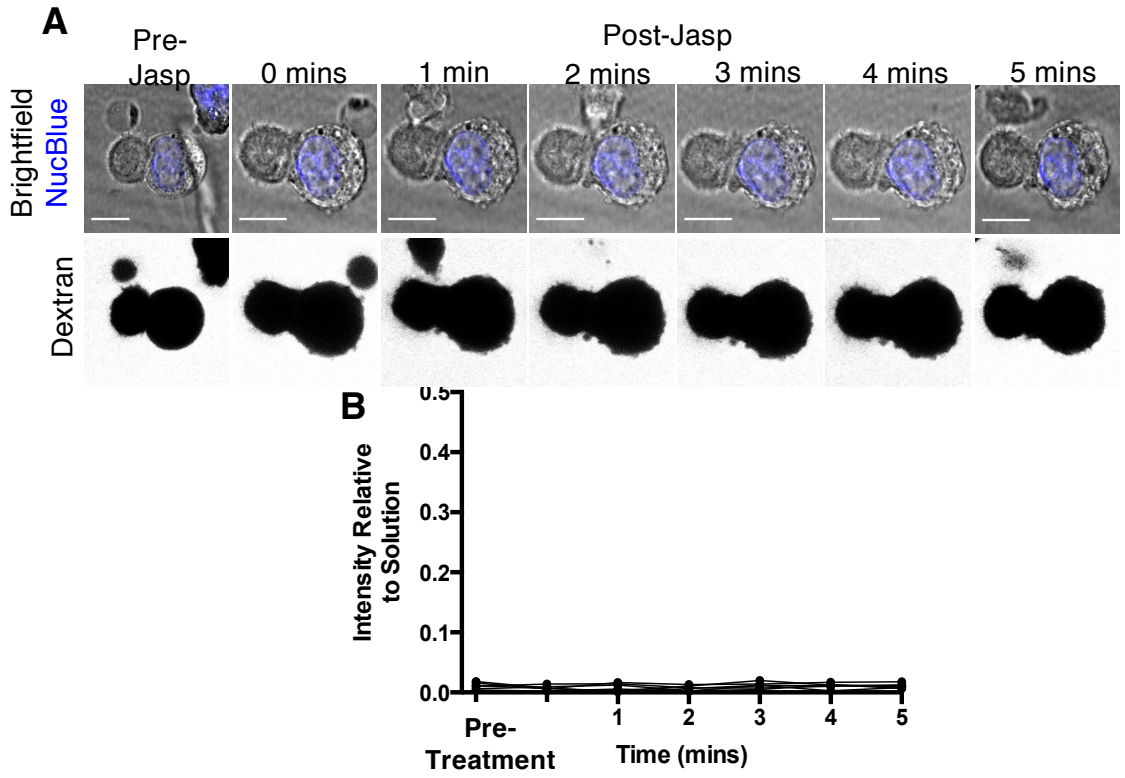


Figure 3.28. Stabilisation of actin maintains the exclusion of dextran from the primary human NK cell immune synapse (**A**) Primary human NK cells and 221 cells were co-incubated with 32 nm dextran and imaged by confocal microscopy (*Pre-Treatment*). Jasplakinolide at a final concentration of 0.5 µM was then added to the cells and the same conjugate was imaged every minute for 1 minute (*time = 0 – 5*). Panels show representative brightfield images overlaid with target cell nuclear staining (*upper row*) and the corresponding fluorescence image (*lower row*) at each time point, as indicated. Scale bars; 10 µm. (**B**) Dextran fluorescence intensity within the synapse was measured relative to the intensity of the extracellular solution at each time point. Graph shows the relative intniesty for the same conjugate at each time point, shown by connecting lines. The mean relative intensities at each time point were analysed by one-way ANOVA with Tukey corrections (n = 7). Data are from 7 independent experiments for each dextran size.

These data demonstrate that it is only the integrity of the F-actin structure at the IS that is important for maintaining exclusion of larger molecules. Within 5 minutes after the addition of Lat A, the loss of F-actin at the cell-cell interface allowed entry of dextrans that are otherwise excluded from the synapse. In contrast, when actin is stabilised at the synapse, this most likely maintains the structure and rigidity at the intercellular contact, thus there is no detectable change in exclusion of larger dextran. Therefore, whilst further rearrangement of F-actin at the synapse is not required, the integrity of the cytoskeleton is indeed critical to exclude larger dextran.

3.2.6 Dextran is cleared from the immune synapse during assembly

Whilst larger dextrans present from the initial moment of cell-cell contact (Figures 3.1, 3.3, and 3.10 – 3.12), or added to formed synapses (Figure 3.16), are excluded from the IS, the processes involved in the initial exclusion of dextran have not been identified.

To address this, YTS and 221 cells were co-incubated with fluorescein-labelled 4 nm or 54 nm dextran and plated on chambered coverglasses coated with 1 µg/mL fibronectin. This enabled migration of cells, facilitating imaging of the initial contact and synapse formation by time-lapse confocal microscopy. Dextran fluorescence intensity within the synapse was measured relative to the extracellular solution at each time point prior to and following the initial moment of cell-cell contact, and during synapse assembly (Figure 3.29A for the 4 nm dextran and 3.29B for the 54 nm dextran). At the point of cell-cell contact, both the 4 nm and 54 nm dextrans were detected in the synapse prior to conjugation. There was then an initial decrease of signal for both dextran sizes. This was due to the reduction of the imaging volume below the PSF of the microscope relative to volume imaged within the extracellular solution. The relative fluorescence intensity of the 4 nm dextran decreased over the first 2 minutes following cell-cell contact, it then reached a plateau where it remained at a similar level for the duration of imaging (Figure 3.29C, *solid line*). Conversely, the relative intensity of the 54 nm dextran continued to decrease – until it was barely detectable (Figure 3.29C, *dashed line*). The decrease in relative fluorescence intensity of the 54 nm dextran occurred at a much greater rate than the 4 nm dextran. However, the point at which the 4 nm dextran reached a plateau and the 54 nm dextran was undetectable occurred at a similar time of around 3 – 4 minutes after cell-cell contact. These data suggest that the formation of the synapse causes a size-dependent clearance of dextran during assembly, leading to the removal of 54 nm dextran from the cell-cell interface.

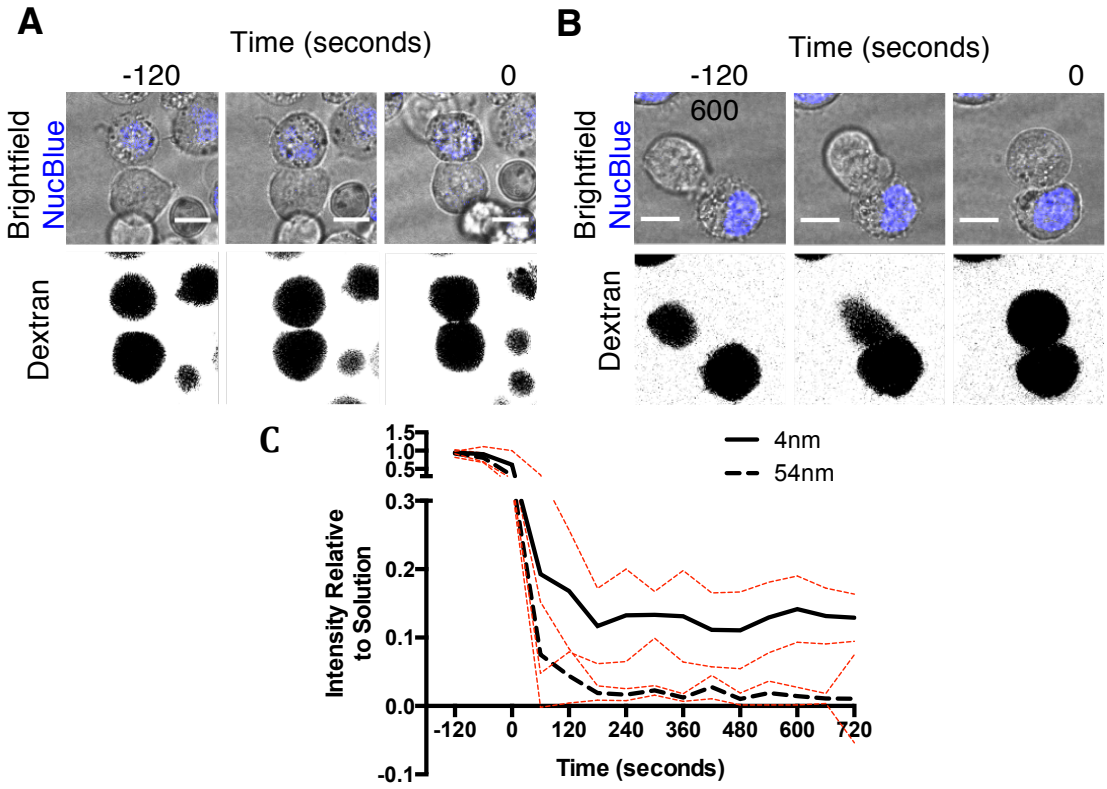


Figure 3.29. Larger dextran is cleared from the YTS cell immune synapse during assembly. **(A)** Representative time-lapse confocal images of YTS and 221 initial contact (*time* = 0) and conjugate formation in the presence of a fluorescein-labelled 4 nm dextran. Panels show brightfield images overlaid with target nuclear staining (*upper row*) and the corresponding fluorescence image (*lower row*). Scale bars; 10 µm. **(B)** Representative time-lapse confocal images of YTS and 221 initial contact (*time* = 0) and conjugate formation in the presence of a fluorescein-labelled 54 nm dextran. Panels show brightfield images overlaid with target nuclear staining (*upper row*) and the corresponding fluorescence image (*lower row*) at the indicated times. Scale bars; 10 µm. **(C)** Dextran fluorescence intensity within the synapse was measured relative to the intensity of the extracellular solution at each time point. Graph shows mean ± 95% confidence interval of the 4 nm (*solid line*) and 54 nm (*dashed line*) dextran from 8 independent experiments of each dextran size.

To further investigate the clearance of dextran from the IS, pNK cells were plated on activating surfaces coated with MICA-Fc and ICAM1-Fc, as previously described (117), in the presence of 4 nm or 32 nm dextrans. Initial contact and subsequent synapse formation with the activating surface was imaged by interference reflection microscopy (IRM) together with confocal microscopy (Figure 3.30A for 4 nm dextran and 3.30B for 32 nm dextran). Darker regions of the cell-slide contact in IRM images indicate areas of close slide-membrane proximity following cell spreading, and thus, this can be used to identify synapse formation. These images demonstrate that whilst regions of the synapse in close proximity to the slide (dark regions) are able to exclude the larger 32 nm dextran, the 4 nm dextran is able to access these regions. Furthermore, the smaller 4 nm dextran appears to collect within regions inside the

synapse where the membrane is inflected away from the slide (brighter regions of the IRM images). Importantly, whilst these regions can be identified with pNK cells in the presence of the 32 nm dextran, these areas remain devoid of dextran, as it is unable to penetrate into the synaptic cleft.

Dextran fluorescence intensity was measured in the synapse at the cell-slide interface and the extracellular solution to give relative fluorescence intensities during the course of synapse formation. Profile plots of the cell-slide interface demonstrate the differences in intensity across the synapse of the differently sized dextran (Figure 3.30C for the 4 nm dextran and 3.30D for the 32 nm dextran). The relative fluorescence intensity of the dextran at the cell-slide interface compared to the extracellular solution was measured at each time point following synapse formation. This showed a decrease in fluorescence intensity of the 4nm dextran over the first 2 – 3 minutes, then a plateau for the remainder of the imaging (Figure 3.30E, *red line*). The plateaued value is lower than 1 due to the PSF volume of the microscope imaging a greater volume in the extracellular solution compared to the narrow synaptic cleft, discussed previously. However, after 2 – 3 minutes contact with the slide, during synapse formation, the 32 nm dextran was completely undetectable (Figure 3.30E, *blue line*). These data indicate that as the pNK cell synapse assembles, dextrans above the size exclusion threshold are cleared from the synapse, concurrent with the NK cell spreading response.

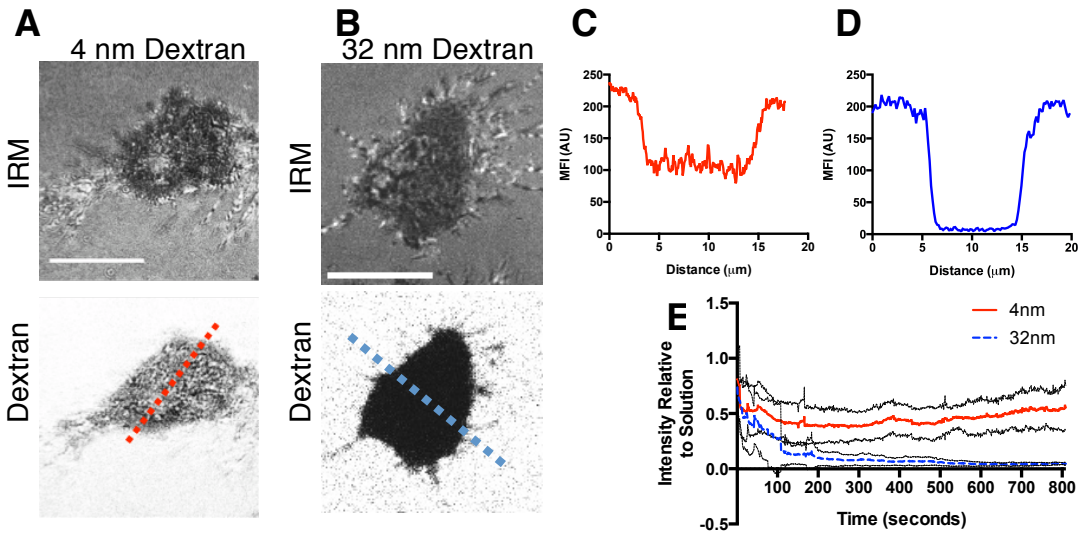


Figure 3.30. Larger dextran is cleared from the primary human NK cell immune synapse during assembly. (A and B) Primary human NK cell synapse formation with a MICA-Fc/ICAM1-Fc-coated activating slide in the presence of fluorescein-labelled 4 nm (A) or 32 nm (B) dextran imaged by time-lapse interference reflection microscopy (IRM) and confocal microscopy. Panels show IRM (*upper panel*) and the corresponding fluorescence image (*lower panel*) at 500 seconds following contact with the slide. Scale bars; 10 μm. **(C and D)** Graphs show a profile plot of the mean fluorescence intensity (MFI) of 4 nm (C; *red line*) and 32 nm (D, *blue line*) measured across the cell-slide interface along the dashed line indicated in fluorescence microscopy image panels A and B respectively. **(C)** Mean dextran fluorescence intensity over the time-lapse imaging was measured relative to the extracellular solution at each time point. Graph shows the mean (4 nm = red; 32 nm = blue) ± 95% confidence interval (grey) of 8 independent experiments (n = 8) of each dextran size.

To investigate the mechanism of clearance, pNK cell synapse formation with MICA-Fc/ICAM-Fc-coated slides was then imaged by TIRF microscopy in the presence of both Texas Red-labelled 4 nm dextran and fluorescein-labelled 32 nm dextran. Synapse formation was imaged every 20 seconds, from the initial moment of cell-slide contact, for a total of 5 minutes. To further highlight the intensities of dextran within the synapse, a look-up table, HiLo, was applied to identify pixels above (red) and below (blue) intensity thresholds of 223 and 32 AU respectively (Figure 3.31A).

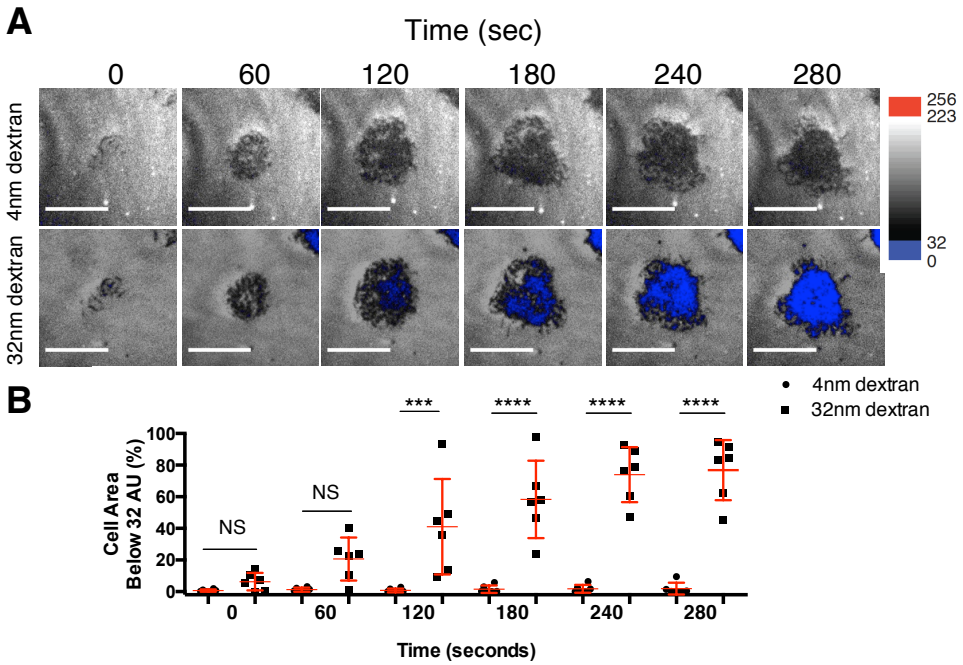


Figure 3.31: The primary NK cell clears larger dextran from the immune synapse as it assembles in a 'zipper-like' fashion. (A) Primary human NK cells were plated on MICA-Fc/ICAM1-Fc-coated slides with Texas Red-labelled 4 nm dextran and fluorescein-labelled 32 nm dextran and imaged by total internal reflection fluorescence (TIRF) microscopy. Time-lapse images were taken every 20 seconds from the point of cell-slide contact (*time = 0*). Panels show TIRF images of 4 nm (*upper rows*) and 32 nm (*lower rows*) dextran at the time points indicated. Image look-up tables (LUT) shown in HiLo, where greyscale pixels below 32 AU are highlighted as blue and those above 223 AU are highlighted as red, as indicated on the colour scale. Scale bars; 10 µm. Images are representative of 6 cells from three experiments. **(B)** Graph shows the ratio of the area of pixels below 32 AU to the area of the cell-slide interface expressed as a percentage of pixels below 32 AU. Data were analysed by one-way ANOVA with Tukey corrections (n = 6). Data are from 5 independent experiments. NS = no significance, ***p<0.001, ****p<0.0001.

The pNK cell synapse appears to form in a zipper-like manner, as dextran is cleared from the central region of the synapse towards the periphery. To quantify this, the percentage of cell-slide interface occupied by pixels below the threshold was measured (Figure 3.31B). There was no significant difference between the percentages of blue pixels (below the 32 AU threshold) in TIRF images of the 4 nm dextran compared to the 32 nm dextran after initial spreading (0.6 ± 0.8% for the 4 nm dextran and 6.3 ± 5.5% for the 32nm dextran) and during the first 60 seconds of synapse formation (1.2 ± 1.3% for the 4 nm dextran and 20.6 ± 13.6% for the 32nm dextran). Following 120 seconds after initial cell-slide contact, the percentage of area occupied by blue pixels was significantly greater in images of 32 nm dextran (41.0 ± 30.2%) than 4 nm dextran (0.8 ± 1.2%). There appeared to be a collection of dextran within the central region of the synapse (both 4 nm and 32 nm dextran) prior to 120

seconds after initial contact. This was then pushed towards the periphery of the synapse. Following this clearance, the intensity of the 32 nm dextran continued to decrease, until the synapse was almost completely cleared of 32 nm dextran at 280 seconds (76.9 ± 19% blue pixels). Conversely, the spreading and synapse formation of the same cell does not affect the 4 nm dextran to the extent of the 32 nm dextran, demonstrated by few or no blue pixels within the synapse interface (1.9 ± 3.8%). During the first 120 seconds of synapse formation, there was high variability in the percentage of area containing blue pixels. However, during 180 – 240 seconds following synapse formation, there is a decrease in the variability and no significant difference between the area of blue pixels in the 32 nm dextran images at 240 and 280seconds. This suggests that within 240 seconds (or 4 minutes), the synapse has been cleared of dextran. This suggests that a zipper-like closing of the synapse, following effector cell spreading, facilitates the NK cell to clear larger dextrans from the interface, whilst smaller dextrans remain.

Taken together, these data demonstrate that the IS is able to clear molecules larger than the receptor-ligand complexes formed at the synapse, whereas smaller dextrans remain within the synaptic cleft. Importantly, during both YTS and pNK cell synapse formation, at the point where relative intensities of either dextran plateaued, the presence of smaller dextran correlated with a complete absence of detectable larger dextran, suggesting that it is most likely cell spreading and synapse assembly that enables NK cells to clear these larger molecules from the IS.

3.3 Discussion

3.3.1 Summary

The main objective of this study was to determine whether or not the IS functions as a gasket. The results have demonstrated that the synapse does not seal the cleft, as the term gasket would suggest. Rather, extracellular molecules, here using dextran, can access the synaptic cleft in a size-dependent manner. Unexpectedly, the assembly and formation of a synapse actively cleared molecules above the size threshold. The main findings of this study are summarised below:

- The activating IS formed by both NK and T cell lines and primary NK cells restricts the access of dextran (3 – 54 nm diameter) into the synaptic cleft in a size-dependent manner

- Dextrans above a size threshold (32 – 54 nm diameter) are excluded from a formed IS

- The inhibitory IS is unable to exclude extracellular molecules (3 – 54 nm diameter)

- Dextrans of 4 nm are able to freely move into and out of the IS – resulting in an equilibrium of dextran concentration within the synapse and in the extracellular solution

- Larger dextrans (32 or 54 nm diameter) are actively cleared from the IS during cell spreading and synapse assembly, whereas smaller dextran (4 nm) are not cleared.

3.3.2 Implications of findings

The results demonstrate that, whilst not forming a complete seal, the IS forms a physical barrier that restricts the entry of extracellular dextran in a size dependent manner. Smaller dextrans (4 – 13 nm and in some cases 32 nm) were able to access synapses formed by both NK and T cell lines and primary NK cells. In contrast, the 54 nm-sized dextran, and 32 nm dextran for pNK cell synapses, was excluded from all synapses tested (Figure 3.1 – 3.4 and 3.10 – 3.12). These provide new insights into the nature of extracellular molecules that are able to access the IS. Moreover, larger dextrans were actively cleared from the synapse, suggesting a novel role of the effector cell spreading response and synapse assembly for the clearance of large molecules.

These data are consistent with previous studies that characterised the dimensions of the IS. Specifically, crystal structures of receptor-ligand complexes, in addition to electron microscopy of the IS, have shown the intermembrane span to vary between 15 and 50 nm (65, 208, 211). In addition, molecular ruling using quantum dots (QD) anchored to the NK cell membrane have demonstrated that larger QD are excluded from the cell-cell interface (189). These findings demonstrated the importance of membrane-anchored molecule size, in agreement with the kinetic segregation model, at the NK cell IS (213). The data shown here demonstrate directly for the first time that the sizes of receptor-ligand complexes govern the penetration of extracellular molecules into the cell-cell interface and IS (Figure 3.32).

Not only do dextran have decreasing maximum solubility with increasing molecular weight, but the labelling densities of each dextran increase with their larger sizes. This leads to an increase in the number of dyes per dextran, with increasing molecule size. Consequently, dextrans of higher molecular weights are brighter than smaller molecules. Initial studies shown here (Figures 3.1A and B and 3.3A and B) used dextrans at a range of concentrations based on their maximum solubility and microscope settings were adjusted accordingly in each case to maximise the visualisation of each dextran. As a result, there was the potential that artefacts were introduced due to variance in concentrations and/or overall charges of dextran, and

the labelling densities, as well as the variations in microscope settings. These caveats were addressed by matching dextran concentrations (Figure 3.1D and 3.3D), limiting the fluorescence intensities of dextran (Figure 3.5 and 3.6) and co-incubating identically sized dextrans of different charges (Figure 3.8 and 3.9).

The 32 nm dextran, measured by spectrometry, had as much as 10-fold greater labelling density than the 4 nm dextran. The use of the labelled:unlabelled mixes of the 4 nm and 32 nm dextrans showed that, irrespective of the size of dextran used, labelling densities did not affect their access to the synapse. Finally, having shown that labelled 32 nm dextran could be mixed with unlabelled dextran and yield the same results, the 4 nm and 32 nm dextran (at a labelled:unlabelled ratio of 1:10) were imaged with conjugates using the same microscope settings optimised to the 4 nm dextran. The results confirm that dextran access to the synapse is size dependent and that artefacts are not introduced by the imaging techniques used.

The results of these studies show that dextrans sized 3 – 13 nm are able to enter the activating IS, whereas those ≥32 nm were unable to penetrate into the synaptic cleft. In contrast, dextrans of all sizes were able to enter the inhibitory synapse. This suggests a mechanism unique to activating synapse formation provides the clearance of larger dextran from the synaptic cleft. Confocal and TIRF imaging have shown that this is a consequence of effector cell spreading and synapse assembly. This process occurs in a zipper-like manner and is able to drive out larger molecules from the synapse.

The activating IS excludes dextran in a size-dependent manner

To investigate the gasket function of the IS, effector and target cells were mixed with dextrans of increasing sizes and imaged by confocal microscopy. Establishing a synapse requires a tight synaptic cleft formed by nanometer spans of receptor-ligand complexes, and inclusion of molecules larger than this would require membrane bending at significant energetic penalties. The IS was able to accommodate dextrans 3 – 13 nm in all instances, whereas those 32 – 54 nm are almost or completely excluded, depending on cell type and synapse – activating or inhibitory – that was

formed. This is in agreement with the KS model of the IS (213). The KS model has established that signalling at both T cell and NK cell synapses (124, 409) requires the clustering of similarly sized receptors to facilitate balanced signalling. Specifically, longer receptor-ligand pairs are physically segregated from shorter protein-protein interactions.(124) However, the physical exclusion of extracellular molecules by the IS has never been directly tested. These findings have shown that the NK cell IS restricts the entry or excludes extracellular molecules in a size-dependent manner.

The data presented in Figures 3.1 – 3.4 establish that the IS, formed by both primary NK cells and a cell line, forms a physical barrier to extracellular dextran, restricting its entry in a size-dependent manner. Both raw and relative intensity data show that as dextran size increases, the ability of dextran molecules to penetrate and fill the synapse decreases. Dextrans sized 54 nm were excluded from all synapses tested, demonstrated by mean relative intensity values of 0.01, and raw intensity values that were constant across the cell bodies and synapse. These findings are in agreement with previous data that identified adhesive receptor-ligand complexes as the largest interactions within the synapse, spanning up to 50 – 55 nm (65). Intriguingly, the 32 nm dextran was almost entirely excluded from the pNK cells whereas it was able to access the IS formed by YTS cells. This could be attributed to the nature of the synapse formed by YTS cells (CD28 being their only major activating receptor (20)). Primary NK cells possess a wide range of activating receptors that may provide a tighter interface with the target cell. Indeed, synapses formed by pNK cells with a range of targets cells, which likely use a range of activating receptors, were able to exclude 32 nm dextrans. This suggests that it is not the specific activating receptors bound at the synapse, but rather the formation of the activating synapse itself that dictates dextran exclusion in a size-dependent manner. Whilst the mean relative intensity within the synapse decreased with increasing dextran size, the large range of relative intensity measured for the smaller dextrans (≤13 nm) demonstrates a level of variability at each synapse.

The variation in relative fluorescence intensity of small dextrans may occur for a number of reasons. Importantly, the IS is a dynamic interface with constant movement and recruitment of receptors and cytoskeletal proteins during signalling (13, 68, 173, 410). The difference in the size of receptors may influence the overall

structure of the synapse at different points in time, resulting in more or less dextran within the cleft at one point in time. Furthermore, the movement of receptors at the synapse will alter the dynamics of the cell membranes at the interface. This movement could cause fluctuations within the synapse, with downstream effects on the amount of dextran within the synaptic cleft. Whilst there is variability in the ability of smaller dextrans to access the synapse, the variation in excluded dextrans was significantly smaller. Similarly, the fluorescence intensities of dextran within inhibitory synapses, which were accessible to all sizes of dextran, have similar degrees of error. Therefore, the access of dextran and fluctuations of fluorescence intensity within the synapse may be causing variations in measurements. Thus, whilst dynamics at the synapse may influence measurements of smaller dextran at specific points in time, those excluded are unaffected by such fluctuations, indicated by minimal error bars.

Secondly, data demonstrating the reduction of dextran fluorescence intensity within the forming synapse (Figure 3.29 – 3.31) show that dextran intensity is decreased at the developing interface. It is impossible to know at what stage of development each synapse is at when imaged. Thus, this variation in fluorescence intensity could be due to differences in the development stage of the synapses measured. This variability will then be reflected in the data, for example, in Figures 3.1C and 3.3C, and in the raw data (Figure 3.2 and 3.4).

Finally, the dextran sizes given are nominal values, and therefore, each sample is likely to contain a range of sizes (molecular weight ± 15% the given nominal value; personal communication, Life Technologies). This variation could be reflected in the smaller and median sized dextrans (3 – 13 nm), where smaller dextrans within each sample could access the synapse better than the larger dextran present in the sample.

The IS formed by Jurkat T cells with Raji target cells showed similar size exclusion of extracellular dextran (Figure 3.11). T cell receptor-ligand complex dimensions have are of similar sizes to those of NK cells (208, 209). Therefore, exclusion of dextran form the T cell synapse in a size dependent manner is not only in agreement with our findings from studies of NK cells but also reflects known size of the T cell synapse.

These data suggest that the extracellular spans of receptor-ligand complexes and the resultant accumulation of protein pairs that facilitate close proximity between the cell membranes, allow access of dextrans sized ≤13 nm to the IS. Those dextrans ≥32 nm are almost, or completely, excluded, suggesting that their size exceeds that of the IS. As discussed above, dynamic membrane interactions likely cause some variability in the access of smaller dextrans to the IS. This variation is also seen in the data collected at the T cell synapse. Similarly, there was clear exclusion of dextrans with dimensions above the size threshold.

The initial experimental methods to test the access of extracellular molecules into the synaptic cleft involved co-incubation of effector cells, target cells and dextran prior to imaging. In this setting, dextran was present during the initial contact and throughout synapse formation. Therefore, to test if dextran could penetrate formed synapses, conjugates were imaged by time-lapse confocal microscopy whilst dextrans of 4 nm or 54 nm were added to the extracellular solution. The synaptic penetration of only the 4nm dextran further demonstrated size exclusion at the synapse, with larger molecules physically excluded from the cell-cell interface.

Whilst the IS does not form a complete seal around its secretory domains, the synapse acts as a size-restrictive barrier, most likely determined by both the dense accumulation and inter-membrane span of receptor-ligand pairs. The penetration of this barrier by smaller molecules was further demonstrated by the sequential dilution of 4 nm dextran during imaging of the same cell conjugate. The relative intensity of dextran within the synapse to the extracellular solution remained constant. This suggests that the dextran within the synapse equilibrates with the extracellular dextran, which could only occur if the molecules were able to move freely out of the synapse. Furthermore, the complete removal of dextran from the extracellular solution also resulted in loss of dextran from the synapse – demonstrating that dextran is not trapped within the synapse (Figure 3.16 and 3.17). Together these data show that dextrans below the size exclusion threshold are able to freely move into and out of the synapse. This establishes that the synapse is not a completely sealed structure, and can be accessed by molecules of specific physical dimensions.

Size, primarily of receptor-ligand pairs, has a direct impact on IS function – particularly on signalling (124). Here it has been demonstrated that the dimensions of the IS are not only crucial for signalling, but also determine the size of molecules that can access the synaptic cleft. The size-restrictions detailed in this study are in agreement with previous measurements of the synapse, specifically the receptor-ligand complexes found at the interface (65, 84, 209-211, 356, 411). However, the consequence that the dimensions of these complexes have on extracellular molecules has not been investigated previously. Molecular ruling using QD anchored to NK cell membranes has shown that those of diameter greater than ~25 nm were unable to access the IS (189). These studies were similar to those that used elongated extracellular proteins protruding from the membrane to extend the size of the IS (124). The data presented here demonstrate that simply solving protein structures is insufficient to accurately predict the sizes of molecules that could enter the IS. Whilst the activating and inhibitory synapses possess membrane spans of similar dimensions, the data show here that the extent to which molecules can penetrate the synapse is also dependent on the nature of synapse formed.

The inhibitory IS does not exclude extracellular dextran

The lack of size exclusion from the inhibitory IS was unexpected. Whilst inhibitory synapses are short-lived interactions (412), membranes must come into close contact to allow the ligation of receptors and their cognate ligands. Previous crystal structure analyses of NK cell inhibitory receptor-ligand pairs have shown them to span ~15 nm (84), similar to activating receptor-ligand complexes. However, all dextrans tested (3 – 54 nm) were able to access the inhibitory synapse to similar degrees. In contrast with activating synapses, where the peak of intensity within the synapse reduces as dextran size increases, inhibitory synapses show similar peaks for all dextran sizes.

Ligation of KIR2DL1 fails to induce a spreading response, shown by a lack of F-actin accumulation or the formation of rings at the synapse. This is in contrast with activation, which induces symmetrical F-actin rings that are formed by concurrent waves of actin moving away from the centroid of the synapse (123, 413). The absence of spreading and rearrangement of F-actin at the inter-cellular contact may

prevent the inhibitory synapse from excluding larger molecules. In agreement with this, drug-induced actin depolymerisation at the activating synapse allowed larger dextrans to access the synaptic cleft. This further demonstrated an important role for actin in establishing size-dependent exclusion at the cell-cell interface. Furthermore, without the effector spreading response, the larger dextran may not be cleared, as seen with the activating synapses (Figure 3.29 – 3.31). Therefore, the inhibitory synapse may not have the same ability to exclude dextran in solution, due to the absence of cell spreading and cytoskeletal structures following inhibitory signalling. In the absence of the organised structure as seen at the activating synapse, NK cells are able to make rapid and transient contacts with healthy cells, discerning their condition quickly. This means that diseased cells can be sought after and killed more efficiently. This more transient interaction occurs without the formation of a size-dependent barrier to extracellular molecules. However, the exclusion of molecules from the inhibitory IS may not be essential, as no cytotoxic proteins or cytokines are secreted (9, 166).

An intact actin structure at the immune synapse is required to exclude extracellular dextran in a size-dependent manner

The involvement of F-actin and other proteins associated with its reorganisation (such as WASp) are known to be critical to synapse function. Previous studies have investigated the role of actin in the formation of the synapse and subsequent cytotoxicity (165, 414, 415), as well as the movement of receptors within the cell-cell interface (91). These data have shown that without F-actin turnover, the synapse cannot assemble and NK cell-mediated cytotoxicity is abrogated. Furthermore, signalling proteins required for actin reorganisation are cycled throughout the synapse lifetime, leading to repeated waves of actin polymerisation at the cell-cell interface (171). Due to the essential requirement for actin at the IS for its formation and for cytolysis, the role of actin in extracellular molecule exclusion was tested.

The data demonstrate that further reorganisation of F-actin at the fully formed synapse is not required to exclude dextran, but actin is required for structural integrity, which is essential for exclusion to occur. Depolymerisation of F-actin abrogated the ability of the synapse to exclude dextran (Figure 3.25 and 3.26),

whereas its stabilisation had no aberrant effect (Figure 3.27 and 3.28). F-actin is important for maintaining the structure of the activating synapse, and its reorganisation is a crucial factor following the decision to initiate effector functions (108). Furthermore, actin is required to provide an anchor for integrins through such proteins as Talin (414, 416). It may be the combination of these interactions that provide rigidity at the membrane, which facilitates exclusion of larger molecules. This role may have important physiological consequences for the successful function of the synapse, providing a barrier to extracellular molecules that would otherwise be able to penetrate and interfere with the action of proteins secreted at the synapse.

Clearance of dextran above the size exclusion threshold during IS assembly

Dextran above the size exclusion threshold was excluded from, or unable to enter, the IS (Figures 3.2, 3.3 and 3.14). However, these initial experiments did not address the mechanism involved in exclusion of larger dextrans from the immune synapse. To investigate this, time-lapse confocal microscopy was used to image synapse formation in the presence of differently sized dextrans. This enabled the visualisation of dynamics at the synapse and the effect this had on dextran at the point of cell-cell contact and during synapse assembly. The data shows that following initial contact, both larger and smaller dextrans are present within the IS, but after 3 – 4 minutes, larger dextran are barely detectable within the cleft. This suggests that dextran is cleared from the synapse during assembly. Indeed, it has been well established that NK cells, when in contact with a target cell or activating surface, initiate a spreading response, mediated by the movement of F-actin waves, specifically following ligation of activating receptors (117, 123, 187). Whilst the decrease in fluorescence of the 54 nm dextran at the synapse was much more rapid, the point at which the fluorescence intensity of the 4 nm dextran reached a plateau and the 54 nm dextran was undetectable both occurred around 3 minutes after initial cell-cell contact. This suggests that within the first 3 minutes of synapse assembly, processes such as spreading and ligand ligation may facilitate larger dextran clearance.

IRM images can be used to discriminate the distance between the NK cell membrane and the plane of the slide. Darker regions indicate a tighter interaction between the cell membrane and the slide and lighter areas demonstrate greater distances. Both lighter and darker regions can be seen in the NK cell interface when plated with 4 nm or 32 nm dextrans (Figure 3.30A and B). Moreover, the lighter regions of the IS (where the membrane curves away from the slide) correlate with brighter areas of fluorescence intensity of the 4 nm dextran. This suggests that the dextran is able to fill the spaces in between the cell membrane and slide, moving across the regions of tighter contact. In contrast, whilst these curvatures of the membrane can be seen at IS formed in the presence of the 32 nm dextran, there is no fluorescent signal within darker regions of the membrane, showing that the larger dextran has been cleared and cannot move across regions of tighter contact. This implies that following the clearance of dextran from the synapse, the structure of the IS acts as a barrier that prevents the movement of larger molecules into the synaptic cleft.

Finally, the use of TIRF microscopy enabled high resolution imaging of both 4 nm and 32 nm dextrans at the cell-slide interface within an imaging depth of ~100 nm. These data show that the effector cell spreading response results in a zipper-like closure of the synaptic cleft (Figure 3.31A). It is this mechanism that appears to drive the clearance of molecules from the synapse. The images show that both the larger and smaller dextrans collect within the synapse during the initial stages of synapse formation. The subsequent spreading of the cell pushes dextran from the central region of the synapse towards the periphery. At this point, the 32 nm dextran is further excluded from the synapse until the synapse contains only 4 nm dextran. The timing of this clearance (within 180 – 240 seconds) is consistent across all time-lapse experiments. The quantification of the percentage area of the cell-slide interface with pixels below the 32 AU threshold shows that there appears to be a slight delay in dextran clearance, following effector cell spreading (Figure 3.31B). The approach to ‘black’ pixels within the synapse indicates a close proximity between the cell membrane and the coverglass. This is initially seen in images of both the 4 nm and 32 nm dextrans. It is not until the cell has spread that a significant proportion of the cell-slide interface is below the 32 AU threshold. This may be caused by a complete clearance of larger dextrans from the synapse initiated by a later stage of activating receptor binding. It may be this receptor ligation that initiates the mechanisms to

clear larger dextran from the synapse. These studies further demonstrate how effector cell spreading of an NK cell and its ligation of activating ligands provide the mechanism to clear dextran from the synapse.

Consistent with the clearance of larger dextran from the synapse, Culley *et al.* showed that the NK cell spreading response reaches a maximum diameter at 3 – 4 minutes following initial cell-cell contact (123) and Stinchcombe *et al.* demonstrated that CTL polarised their lytic granules to the synapse within 3 minutes (365). Within this time frame, the synapse may need to be cleared of extracellular molecules, perhaps in order to maximise concentrations of cytotoxic mediators within the synaptic cleft. The initial gradual decrease of fluorescence intensity of the dextran can be attributed to the PSF volume of the microscope imaging an increasingly smaller volume, to the order of nanometers compared to a PSF of up to 3 µm, at the cell-cell interface. However, once the IS had been assembled, the decrease in fluorescence intensity of the 4 nm dextran arrested and was maintained at a constant level for the remaining duration of imaging. Conversely, at the point of the 4 nm reaching a plateau, the 54 nm dextran had been completely excluded from the synapse. Therefore, the NK cell spreading response may provide a pushing force to clear larger dextran. More specifically, during the polarisation of the MTOC towards the synapse, proteins (such as WASp) facilitate F-actin rearrangement at the synapse. Moreover, Arp2/3 mediates the reorganisation of F-actin, through constant polymerisation and depolymerisation, in waves from the centroid of the synapse towards the periphery (169-171). It may be this dynamic reorganisation that drives the clearance of molecules from the synapse.

These data collectively show that exclusion of larger dextrans from the IS may not only be a result of the formation of a dense mesh of protein-protein complexes, but that the NK cell spreading response and synapse assembly can physically clear molecules from the cell-cell interface. Once a synapse has been formed, this tight interface restricts further access of molecules greater in size than those of the receptor-ligand complexes that make up the synapse. The clearance of dextran from the interface demonstrates a novel role of the IS and its assembly that has not been shown previously. In conclusion, the immune synapse clears and excludes dextran above a size threshold.

Chapter 4 – Size-Dependent Exclusion of Functional Proteins from the Immune Synapse

4.1 Introduction

In Chapter 3, it demonstrated for the first time that the IS was able to exclude or restrict the entry of extracellular molecules below a size threshold. This was dependent on the assembly of the synapse and an intact F-actin scaffold. In addition, the formation of the synapse cleared larger dextran molecules from the synapse as it formed in a zipper-like manner. This size-dependent exclusion would likely also restrict the entry of functional extracellular molecules, for instance, monoclonal antibody therapies. Studies detailed in this chapter investigate the ability of antibodies of varying size to access the IS.

4.1.1 Antibodies and fragments

Monoclonal antibodies (mAb) are monospecific proteins, termed immunoglobulins (Ig). They are produced as clones from one parent plasma cell. Antibodies are 'Y-shaped' glycoproteins that can form a variety of structures (multiple antibodies creating a polymer) that identify and/or neutralise foreign microbes such as viruses or bacteria (417). IgG antibodies are 150 kDa proteins, measuring 16 nm in their longest dimension, that consist of 2 light and 2 heavy chains comprising 2 or 4 domains, respectively (418, 419) (Figure 4.1A). Each chain contains both constant and variable domains. The structures of constant domains are consistent for all antibodies, whereas the variable domains determine the specificity towards a specific epitope (420, 421).

MAb can be enzymatically processed *in vitro* to create smaller antigen-binding proteins, Fab' and $F(ab')_2$ fragments. These can be generated from papain or pepsin digestion respectively (388). These enzymes cleave mAb at either the hinge region above the Fc fragment to generate a $F(ab')_2$ fragment or the entire hinge region generating two separate Fab' fragments and an Fc fragment. $F(ab')_2$ fragments are 9 nm in their longest dimension (386) (Figure 4.1B).

Single variable domains were first discovered in camelids (even-toed ungulate mammal, *e.g.* camels) and have been shown to be able to bind a wide variety of epitopes (422). These single-domain antibodies have led to the development of nanobodies, exhibiting high stability and solubility (389). More recently, the production of human domain antibodies (dAb) has been developed (423, 424) Dab are antibody fragments that consist of the variable domain of an antibody heavy chain (V_H) or light chain (V_L) (389). The smallest known antigen-binding dAb are 11 – 15 kDa in molecular weight and ~4 nm in their longest dimension (425) (Figure 4.1C). In comparison to mAb (150 kDa, 16 nm) and $F(ab')_2$ fragments (57 kDa, 9 nm), these single-domain fragments are significantly smaller. Human dAb are modified at the reside positions 44, 45 and 47 to those found in camel single-domain antibodies, leading to a more hydrophilic molecule. Such modifications can eliminate dAb aggregation and increase solubility (423). A major advantage of dAbs is that they can be expressed in phage display libraries, generating antibodies with affinities up to 303×10^9 M^{-1} (426). Other modifications of dAb include the fusion of two dAbs together or fusion with an Fc portion of a monoclonal antibody. These properties make dAbs a diverse and useful technology that could have many advantages in future medical therapies (426).

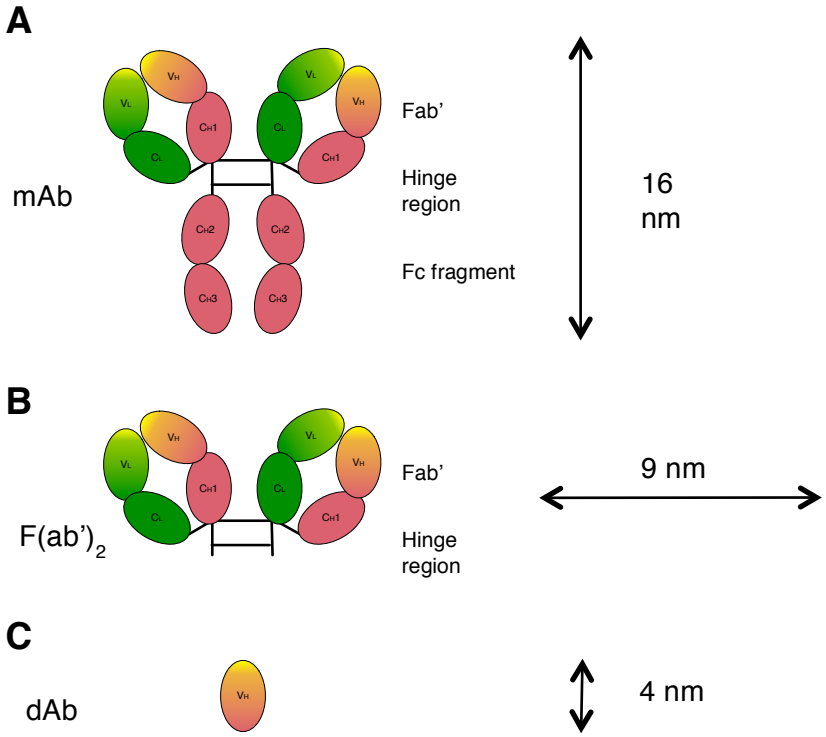


Figure 4.1. Schematic diagrams of the structures of a monoclonal antibody (mAb), a F(ab')$_2$ fragment and a domain antibody (dAb). Antibodies can exist in whole or various fragmented forms and consist of light (*green*) and heavy (*pink*) chains that bind targets at the binding site located at the tip of the variable domains (*yellow*). **(A)** Human mAb (e.g. IgG) are 150 kDa proteins comprising light and heavy chains consisting of 2 or 4 domains respectively. A mAb contains two Fab' fragments (2 variable domains and 2 constant domains) and an Fc fragment (4 constant domains), linked at a hinge region (*black lines*). A monoclonal antibody is 16 nm in its longest dimension. **(B)** F(ab')$_2$ fragments are 100 kDa proteins comprising the 2 Fab' fragments of a mAb connected by the hinge region. A F(ab')$_2$ fragment is 9 nm in its longest dimension. **(C)** Domain antibodies are 15 kDa proteins comprising the variable domain of the heavy chain. A dAb is 4 nm in its longest dimension. Diagrams not to scale.

4.1.2 Current immunotherapies and their limitations

Paul Ehrlich first conceived the idea of a 'magic bullet', a compound capable of being selectively targeted against a disease-causing organism in the early 1900s. However, it was not until 1973, following the identification of paraproteins (an abnormal immunoglobulin produced in excess by multiple myeloma B cells) that the successful production of monoclonal antibodies was described (427) and in 1988, Greg Winter and his team pioneered the techniques by which humanized mAb could be successfully produced (428, 429). Since then, increasing numbers of monoclonal

antibodies have been used widely as immunotherapies to treat a variety of diseases (430).

The treatment of autoimmune diseases (431-435) and cancer (326, 436, 437) using mAb has been extremely successful. A notable example is the development of a mAb against TNFα (438-440). To date, there are over 23 commercial mAb products approved for use on the US market (441). Recently, Fab' fragments (442, 443), $F(ab')_2$ fragments (444, 445) and various forms of single domain antibodies (446-448) have been investigated as novel therapeutics and their development is currently underway. Targets include viral proteins (*e.g.* H5N1 surface protein), tumour cell-expressed proteins (*e.g.* Folate-binding proteins of ovarian cancers) and NK cell activation (binding CD16). However, most of these trials or experiments have only been conducted in animal or *in vitro* studies.

Despite the vast repertoire of specific antibody therapies available, they are targeted towards cell surface or soluble, non-directionally secreted proteins – primarily cytokines. This may be because current mAb therapies are unable to access structures through which proteins are directionally secreted, or presented, to other cells. It may also be the case that these targets have never been considered. Indeed, there is anecdotal evidence that the NK cell IS may restrict the entry of mAbs (366, 367) and therefore, mAb therapies cannot be used in this setting. It is likely that this restriction is due to the large size of antibodies, which prevents them from accessing the synapse. Thus, it may be possible for smaller antibody fragments to access the IS, which would facilitate the potential use of target-specific therapies against proteins secreted across the IS, such as PFN.

4.1.3 Aims

The data in Chapter 3 show that the IS does not form a gasket but rather a size-restrictive barrier that can be penetrated by molecules of sufficiently small dimensions. The inability of therapeutic mAb to target proteins secreted across the IS could be due to the clearance and exclusion of mAb from the synapse by effector cell spreading. The extracellular domains of receptor-ligand complexes that govern the size of the synapse will likely also restrict access to mAb. However, antibodies engineered to be smaller than current therapeutic antibodies may be able to access the synaptic cleft.

The main objective of this investigation was to use functional proteins, including antibodies of various sizes and low-density lipoproteins (LDL), to investigate if there is size-dependent access to the immune synapse. Specifically, the aims of this study are:

i. To generate a domain antibody against an irrelevant target (not expressed by NK cells)

ii. To determine whether antibodies and/or antibody fragments of various sizes are able to penetrate the IS

iii. To investigate if the clearance and exclusion of extracellular molecules can restrict the access of serum proteins, such as LDL

4.2 Results

4.2.1 Production of a domain antibody

A dAb against GPVI was generated as previously described (390) and transferred to PBS buffer to maintain physiological salt concentrations during incubation with cells, and for consistency with dextrans tested in previous experiments. To confirm the monomeric structure of the dAb, the protein was run on an SDS-PAGE gel under reducing and non-reducing conditions (Figure 4.2). The bands at 15 kDa showed that the dAb is a monomeric protein, as expected. The dAb was then labelled with Texas Red fluorophore for visualisation using confocal fluorescence microscopy. To assess the ability of various sized antibodies to enter the synapse, fluorescently labelled murine mAb and a $F(ab')_2$ antibodies against murine IgG were also used. All antibody types were run on an SDS-PAGE gel under non-reducing conditions to confirm their relative molecular weights (Figure 4.3). The bands at 150 kDa, 100 kDa and 15 kDa indicate that the mAb, $F(ab')_2$ fragment and dAb are of the correct molecular weights and physical dimensions reported in the literature (386, 418, 425).

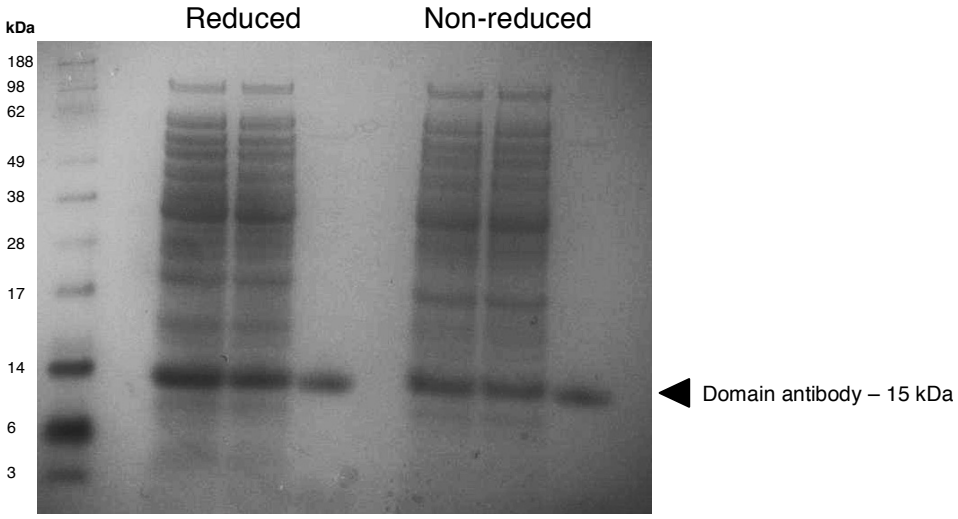


Figure 4.2. SDS-PAGE of bacterially expressed anti-glycoprotein VI domain antibodies. Domain antibodies against glycoprotein VI were expressed in HB2151 *E. coli*. Samples were prepared either under reducing (*left group*) or non-reducing (*right group*) conditions as indicated. Bacterial cell exudates (*left and central columns*) or purified dAb (*right column*) were run on an SDS-PAGE gel.

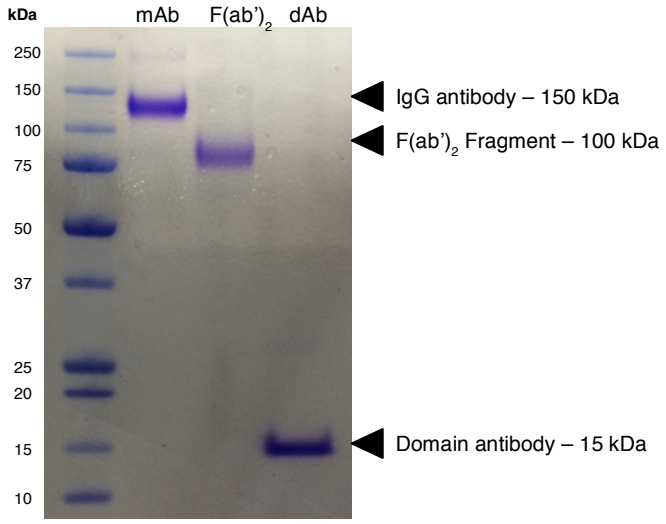


Figure 4.3. SDS-PAGE of a goat anti-murine IgG monoclonal antibody (mAb), a goat anti-murine IgG F(ab')$_2$ fragment and an anti-glycoprotein VI domain antibody (dAb). Antibodies, F(ab')$_2$ fragments and domain antibodies were run on an SDS-PAGE, as indicated, and then stained with Coomassie Blue.

4.2.2 The NK cell immune synapse restricts the access of antibodies in a size-dependent manner

To test whether or not antibodies of various sizes were able to access the IS, YTS and 221 conjugates were co-incubated with fluorescently labelled antibodies (mAb), antibody fragments (F(ab')$_2$) or single domain antibodies (dAb) and imaged by confocal microscopy. Previous measurements of mAb, F(ab')$_2$ and dAb have shown them to be 16 nm (418), 9 nm (386) and 4 nm (425) in their longest dimensions. Confocal microscopy revealed that antibodies could access the YTS IS in a size dependent manner (Figure 4.4A), as described in chapter 3 using dextran. Access to the IS was quantified using the same method as was used previously to assess the entry of dextran. Fluorescence intensity of the antibody within the immune synapse was measured relative to the extracellular solution. Access to the IS of the largest antibody, mAb, was the least efficient (0.05 ± 0.02). Smaller F(ab')$_2$ fragments were able to access the synapse to a greater extent (0.08 ± 0.04) and the dAb, the smallest antibody tested, entered the IS most successfully (0.11 ± 0.04) (Figure 4.4B). These data confirm that access of antibodies to the synapse is size-dependent.

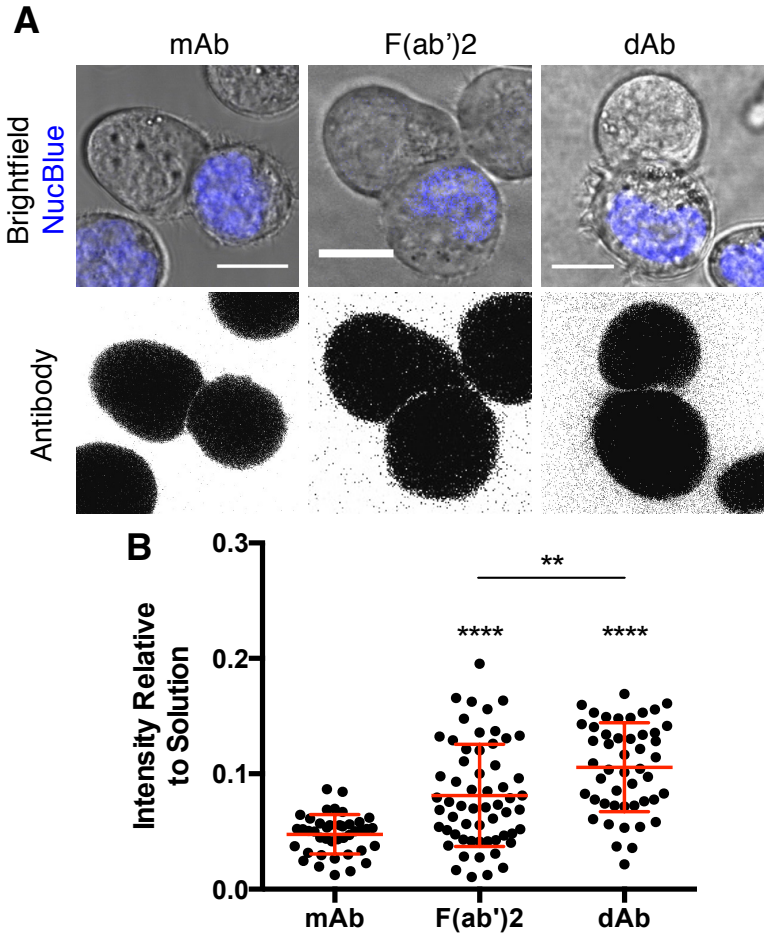


Figure 4.4. Antibody entry into the YTS cell immune synapse is size-dependent. (A) Representative images of YTS and 221 conjugates co-incubated with fluorescently labelled monoclonal antibodies (mAb), F(ab')$_2$ fragments or domain antibodies (dAb). Panels show brightfield images overlaid with target cell nuclear staining (*upper row*) and the corresponding fluorescence images (*lower row*). Scale bars; 10 µm. **(B)** Antibody fluorescence intensity in the synapse was measured relative to the extracellular solution intensity. Bars show mean ± SD. (n = 41, 59 and 48 for mAb, F(ab')$_2$ and dAb respectively). Data were analysed using a one-way ANOVA with Tukey corrections. Data from 3 independent experiments, **p<0.01, ****p<0.0001.

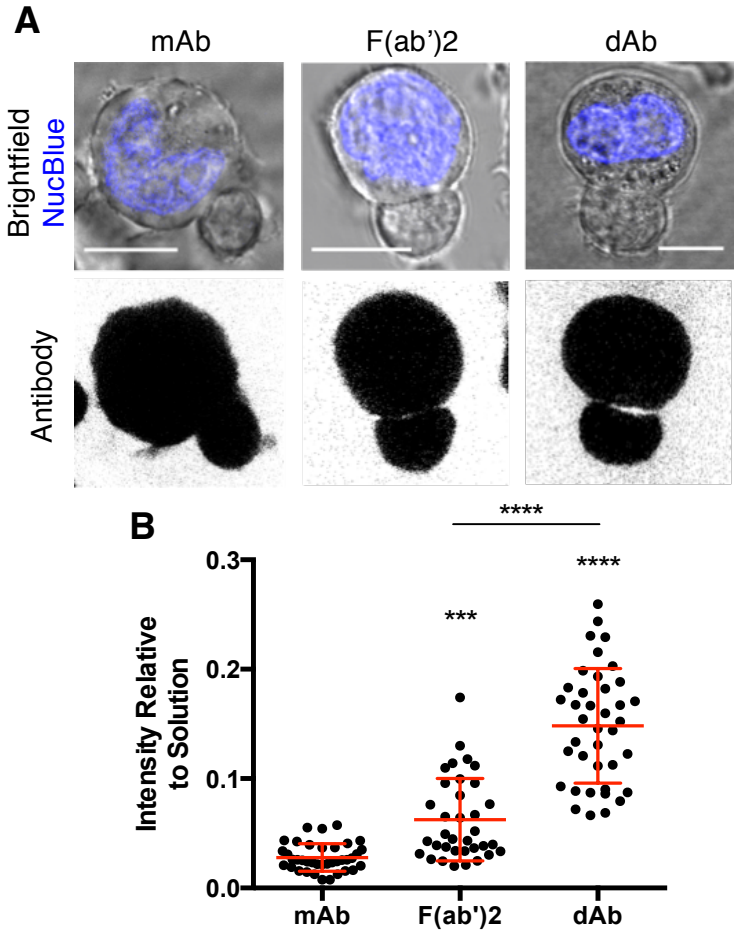


Figure 4.5. Antibody entry into the primary human NK cell immune synapse is size-dependent. . (A) Representative images of primary human NK cells and 221 conjugates co-incubated with fluorescently labelled monoclonal antibodies (mAb), F(ab')$_2$ fragments or domain antibodies (dAb). Panels show brightfield images overlaid with target cell nuclear staining (*upper row*) and the corresponding fluorescence images (*lower row*). Scale bars; 10 µm. **(B)** Antibody fluorescence intensity in the synapse was measured relative to the extracellular solution intensity. Bars show mean ± SD. (n = 38, 35 and 39 for mAb, F(ab')$_2$ and dAb respectively) Data were analysed using a one-way ANOVA with Tukey corrections. Data from 3 independent experiments. ***p<0.001, ****p<0.0001.

Whether these antibodies could penetrate a synapse formed by pNK cells was then tested. Co-incubation of pNK and 221 cells with fluorescently labelled mAb, F(ab')$_2$ and dAb was imaged by confocal microscopy. Antibody access to the pNK synapse was size dependent (Figure 4.5A), consistent with synapses formed by YTS. Again, the mAb was least able to enter the synaptic cleft and was almost entirely excluded from the synapse (0.03 ± 0.01). The F(ab')$_2$ fragments accessed the synapse to some extent (0.06 ± 0.04), but crucially, the dAb were able to access the IS to the most efficiently (0.15 ± 0.01) (Figure 4.5B). The results demonstrate that the synapses of both YTS and pNK cells impose a size-dependent restriction on protein

access to the synaptic cleft. These data were consistent with the size-dependent exclusion of dextran from the NK cell IS (Figure 3.1 and 3.3). This indicates that the use of mAb, such as IgG, to block proteins secreted across the IS is likely to fail due to the size restriction identified here.

4.2.3 Monoclonal IgG antibodies against perforin are unable to access the immune synapse

The restriction of a mAb demonstrates that the synapse can exclude antibodies from the synapse. This may explain why the IgG antibodies against proteins secreted across the synapse are unable to bind their targets. However, the anti-murine IgG antibodies used above are not specific to synapse-associated proteins. To test whether a mAb against PFN was able to bind its target when secreted across the synapse, a protein capture assay was used. Here, slides were coated with MICA-Fc and ICAM1-Fc in order to activate NK cells and induce degranulation. Following activation, cells were then incubated with fluorescently labelled anti-PFN antibodies, and their ability to bind PFN within the synapse was assessed by confocal microscopy.

To show that the capture assay effectively induces degranulation of NK cells and captures PFN protein, pNK cells were incubated on coated slides for 30 minutes, and then incubated with a non-enzymatic cell dissociation solution to remove bound NK cells. Captured PFN was then immunostained with an anti-PFN antibody labelled with Alexa Fluor 488 (anti-PFN-488) and imaged by confocal fluorescence microscopy (Figure 4.6). The images show that the activating slides are sufficient to induce degranulation by NK cells and that secreted PFN can be captured and stained.

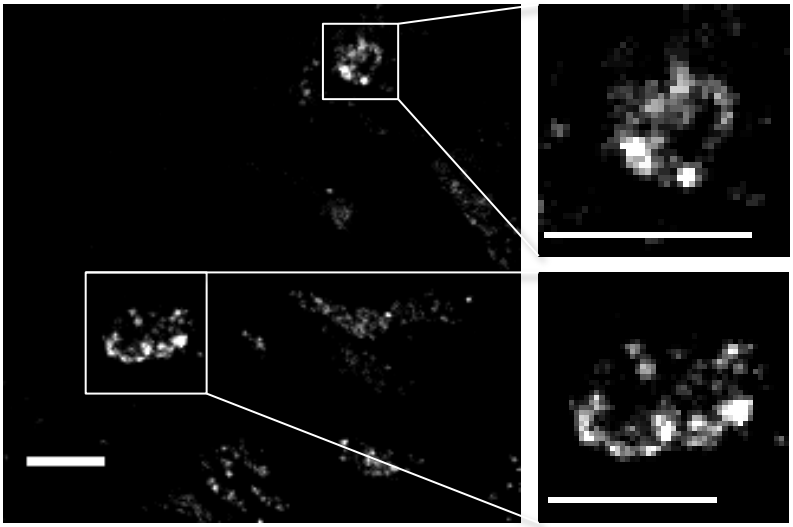


Figure 4.6. Perforin secreted by primary human NK cells can be captured on an activating surface. Primary human NK cells plated on slides coated with MICA-Fc, ICAM1-Fc and anti-perforin were incubated for 30 minutes. Cells were removed and captured perforin stained with an anti-perforin antibody labelled with Alexa Fluor 488 antibody. Panels show zoomed out (*left panel*) and zoomed in regions (*right panels*) of captured and stained perforin.

The capture of PFN at the cell-slide interface meant that the NK cell IS could next be tested for its ability to exclude IgG antibodies against PFN. To test this, pNK cells were plated on activating slides, as described above. To test whether cells were activated (identified by effector cell spreading and actin accumulation at the interface) and that PFN could be stained, NK cells were fixed, permeabilised and stained for actin (using Phalloidin conjugated to Alexa Fluor 647) and PFN. To then both test whether anti-PFN antibodies could penetrate the synapse, and whether cell fixation could affect exclusion, cells were incubated with anti-PFN-488 antibodies prior to or following fixation.

Cells in contact with the slide were imaged by confocal fluorescence microscopy (Figure 4.7A). The results show that when NK cells were fixed and permeabilised, anti-PFN-488 antibodies were able to access PFN at the cell-slide interface (identified using the IRM images) and within the NK cell body. However, if cells were not permeabilised, the antibodies were significantly hindered in their ability to stain PFN at the IS, either following fixation or prior to fixation. In order to quantify this, cells were scored on the presence of fluorescent signal at the cell-slide interface. PFN staining was determined by the presence of fluorescence signal at the cell-slide interface. When cells were permeabilised, PFN was stained in 78% of cells. However, the percentages of cells positive for PFN staining at the cell-slide interface

following either fixation then staining or staining then fixation were 30% and 7% respectively (Figure 4.7B). This demonstrates that the formation of the IS restricts the access of mAb into the synapse.

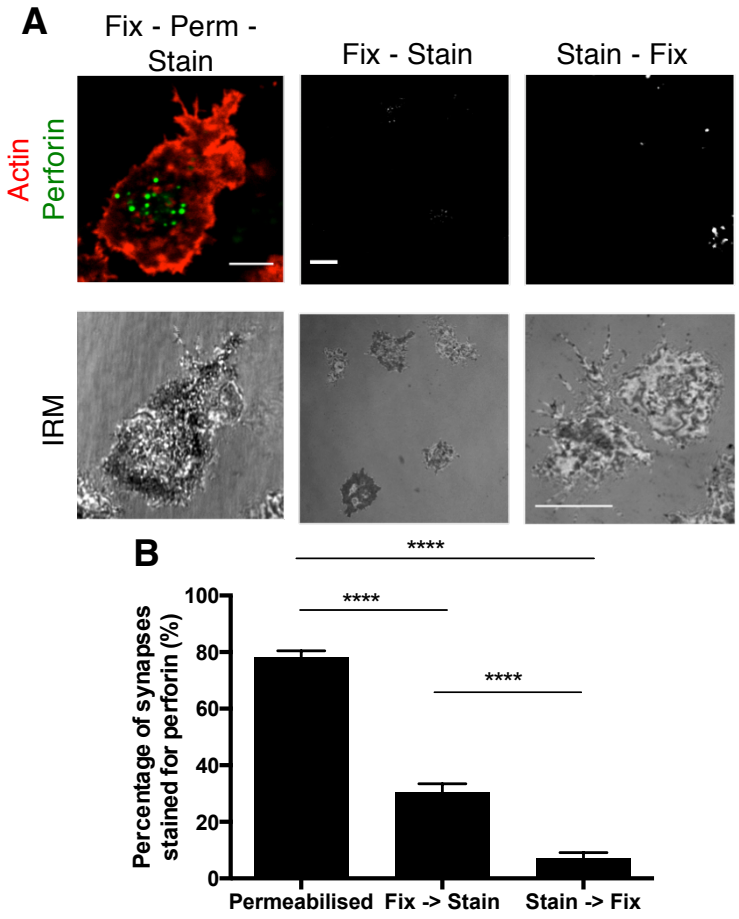


Figure 4.7. The primary human NK cell immune synapse excludes anti-perforin antibodies. Primary human NK cells were plated on slides coated with MICA-Fc, ICAM1-Fc and anti-perforin antibodies and incubated for 30 minutes. Panels show fluorescence images and the corresponding interference reflection microscopy (dark areas indicate contact with the slide). **(A)** Cells were fixed, permeabilised and stained for actin and perforin by Phalloidin Alexa Fluor 674 and an anti-perforin antibody labelled with Alexa Fluor 488 respectively (Fix – Perm – Stain). Cells were fixed then stained for perforin using an anti-perforin antibody labelled with Alexa Fluor 488 antibody (Fix – Stain). Cells were stained for perforin using an anti-perforin antibody labelled with Alexa Fluor 488 antibody then fixed (Stain – Fix). Scale bars; 10 µm. **(B)** Cells with positive staining for perforin were then counted. Graph shows the percentage of cells stained positive or negative for perforin in each condition as indicated. Data were analysed by one-way ANOVA with Tukey corrections. (n = 54, 49 and 51 for permeabilised, fix – stain, and stain – fix, respectively). Data are from 2 independent experiments. ****p<0.0001.

The exclusion of anti- antibodies from the IS in up to 93% of synapses formed with an activating surface is in agreement with previous data demonstrating that mAb are excluded from the IS formed by pNK and 221 cells (Figure 4.5). Most likely their size prevents access into the synaptic cleft. Therefore, the structure of the synapse, specifically the binding of receptor-ligand complexes, forms a physical barrier that is able to prevent larger proteins from accessing the synapse, illustrating why directly secreted proteins cannot be targeted by conventional antibodies.

4.2.4 Low-density lipoproteins are excluded from the primary NK cell immune synapse but not from the activating or inhibitory YTS cell immune synapse

Low-density lipoproteins (LDL) are able to inhibit the cytolytic action of PFN by binding to its nascent hydrophobic domains; this prevents oligomerisation and pore-formation (449, 450). Experimentally, this was first implicated by the inhibition of granule-mediated haemolysis by whole human serum, suggesting that one or more components prevented the action of the cytolytic proteins. Immunoblotting of incubations revealed that LDL were bound to PFN, confirming the cause of reduced granule-mediated lysis. Furthermore, incubation of granules with other serum proteins, such as albumin, has no impact on haemolysis. This demonstrated that the interaction between lipoproteins and PFN inhibits lytic action. For this reason, the presence of LDL within the IS would have a negative effect on NK cell lysis of targets.

LDL have previously been shown to have a mean diameter 21.4 ± 1.3 nm (451-453). To test whether LDL are excluded from the IS, YTS or pNK cells were co-incubated with 221 target cells and fluorescently labelled LDL. Conjugates were then imaged by confocal microscopy. In addition, the YTS/KIR and 221/Cw6 inhibitory synapse system was used to investigate whether LDL was excluded in this setting, as suggested by previous data (Figure 3.14). All conjugates were imaged by confocal microscopy and access to the synapse was measured relative to the extracellular solution (Figure 4.8A).

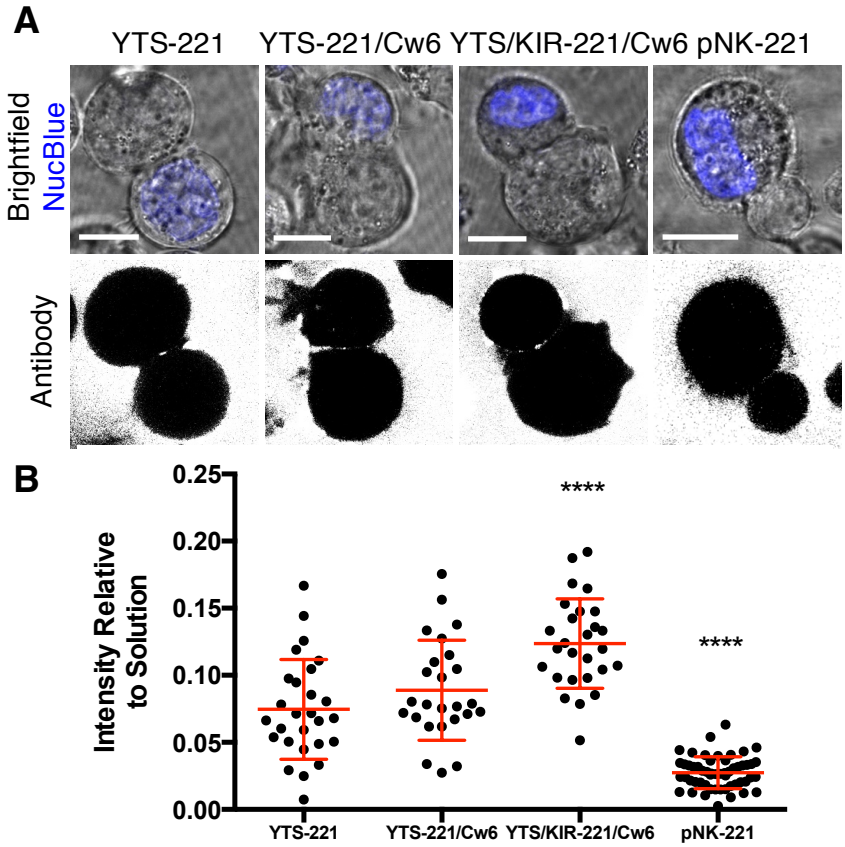


Figure 4.8.Low-density lipoproteins (LDL) are excluded from the activating immune synapse but not the inhibitory immune synapse. (A) NK cell lines forming activating (*first and second columns*) or inhibitory synapses (*third column*) and primary NK cells in conjugate with 221 target cells were co-incubated with fluorescently-labelled LDL and imaged by confocal microscopy. Panels show brightfield images overlaid with target cell nuclear staining (*upper row*) and the corresponding fluorescence images (*lower row*). Scale bars; 10µm. **(B)** LDL fluorescence intensity within the synapse was measured relative to the extracellular solution intensity. Graph shows each data point and mean ± SD from 3 independent experiments. (n = 27, 25, 27 and 54 for YTS/221, YTS-221/Cw6, KIR/KIR-221/Cw6 and pNK-221 respectively). Data were analysed using a one-way ANOV with Tukey comparisons. ****p<0.0001

Confocal imaging revealed that the synapse formed by YTS cells and 221 target cells allowed the access of LDL from the synaptic cleft (relative intensity in the synapse compared to the solution 0.08 ± 0.04). Similarly, the incubation of YTS/KIR cells with 221 target cells and LDL resulted in a non-significantly different access of LDL (0.9 ± 0.04). However, the inhibitory synapses by YTS/KIR and 221/Cw6 cells were unable to exclude LDL (0.12 ± 0.03). This shows that the presence of inhibitory receptors does not affect the extent to which LDL enters the synapse– it is the formation of an inhibitory synapse that prevents molecule exclusion. The pNK cell activating synapse was also able to exclude LDL from the synapse (0.03 ± 0.01) (Figure 4.8B). These data demonstrate the inability of inhibitory synapses to exclude extracellular

molecules, and that the pNK cell synapse excludes larger extracellular molecules more efficiently than the activating YTS cell synapse, consistent with previous findings in Chapter 3.

These results demonstrate that the pNK cell cytolytic synapse restricts access of LDL to the synaptic cleft, to a much greater extent than YTS synapses. This may provide a mechanism by which NK cell secretions are protected at the synapse, preventing inhibition of PFN, which may have a detrimental effect on target cell cytolysis.

4.3 Discussion

4.3.1 Summary

Previous data (Chapter 3) have shown that the size of a molecule dictates its ability to access the immune synapse. The main objective of this study was to determine whether functional proteins are excluded from the IS in a similar manner. Here we show that the IS restricts access of proteins based on their physical dimensions. The main results from this study are as follows:

- The IS formed by both YTS and pNK cells excludes antibodies in a size dependent manner

- MAb against PFN are unable to stain captured PFN secreted at the IS, due to exclusion of these molecules from the synapse by the size threshold

- LDL are almost completely excluded from the synapse formed by pNK cells

- Inhibitory synapses are unable to clear and exclude LDL

4.3.2 Implications of findings

The experiments detailed in this chapter investigated whether the IS excluded functional proteins. The results demonstrate that extracellular proteins are subject to size-dependent exclusion from the synapse, consistent with the size-dependent exclusion of dextran molecules used in earlier studies. MAb were almost completely excluded from the pNK cell synapse, as were LDL, whereas the inhibitory synapse was unable to exclude LDL. However, smaller $F(ab')_2$ fragments and dAbs were able to access the synapse. Therefore, the activating IS is able to exclude all manner of extracellular molecules, which is dictated by their physical dimensions.

Size-dependent exclusion of extracellular antibodies from the IS

Synapses formed by both YTS and pNK cells restrict protein access to the synapse in a size-dependent manner. This is consistent with previous data demonstrating a size-dependent exclusion of dextran from the synapse (Chapter 3). MAb were largely excluded from the synapses of both YTS cells and pNK cells, whereas smaller $F(ab')_2$ and dAb penetrated the synapse. The enhanced penetration of dAb compared to $F(ab')_2$ further demonstrates the importance of molecule size in determining whether it is able to penetrate the IS. The restriction of mAb is in agreement with previous studies that have suggested that mAb are unable to block proteins and cytokines secreted across the synapse (366, 367). For this reason, such mAb are prevented from blocking the action of cytotoxic mediators directly secreted across the IS.

In addition to testing the ability of irrelevant antibodies to enter the synapse, a fluorescently labelled mAb against PFN was also tested. These antibodies were added to pNK cells engaged to MICA-Fc/ICAM1-Fc/anti-PFN-coated slides, prior to or following fixation to test the exclusion of antibody from the synapse, and whether fixation affected exclusion. PFN was stained in less than 10% of synapses. The greater incidence of PFN staining within the synapse of cells that were fixed prior to the addition of the anti-PFN-488 antibody may be due to breakdown of the IS following fixation. It has been demonstrated that fixation can cause shrinkage and expansion of cells (454). This will have a negative impact on the synapse, potentially

causing ruptures in the barrier between some of cells, allowing access of the mAb. The exclusion of anti-PFN antibodies from up to 97% of conjugates demonstrates that exclusion of these proteins from the synapse is almost total. Therefore, the pNK cell synapse consistently prevents the access of larger molecules into the IS.

Taken together, these data demonstrate that the IS is able to exclude antibodies in a size-dependent manner. Domain antibodies have been shown to effectively access the IS, akin to dextrans of comparable sizes (Figure 3.2 and 3.3). Therefore, antibodies targeted against proteins secreted within the synapse should be engineered to the dimensions identified here. Specifically, a dAb, 4 nm in its longest dimension, is able to effectively access the IS, and could provide a therapeutic tool to target cytotoxic mediators within the IS.

Cell-dependent exclusion of LDL from the IS formed by YTS or pNK cells

LDL are micellar (a particle of colloidal dimensions that exists in equilibrium with the molecules or ions in solution from which it is formed) complexes constructed from proteins and lipids consisting of an amphipathic surface monolayer and a hydrophobic core (455-458). Formed in the circulation through a metabolic cascade of apolipoprotein B-100 (459), LDL particles are a heterogeneous group that vary in diameter (18 – 25 nm, mean 22 nm) and density (±1.019 – 1.063 g/mL) (452, 453). LDL inhibit the action of PFN, inhibiting oligomerisation and pore formation in the cell membrane (449). Co-incubation of lipoproteins with CTL-derived granules inhibited haemolysis by up to 70%. Further, HDL and LDL were shown to inhibit haemolysis by up to 60% and 100% respectively (450). Therefore, if LDL were present within the cytolytic synapse during degranulation, target cell lysis could be inhibited.

Synapses formed by pNK cells almost completely excluded LDL from the interface. This suggests that clearance and exclusion of LDL from the synapse would protect PFN. The ability of LDL to inhibit PFN may have a protective role, preventing damage to bystander cells, should PFN be released into the serum. This may occur following cytosol leakage during necrosis of PFN-containing cells (460). Bacteria that secrete pore-forming proteins, known to be structurally similar to PFN (461), may also induce release from PFN-expressing cells (462).

The activating synapses formed by YTS and YTS/KIR cells excluded LDL to a similar degree, and the fluorescence intensities of LDL within these synapses, relative to the extracellular solution, were not significantly different. This suggests that the formation of an activating synapse by YTS cells, whether the inhibitory receptor KIR2DL1 is expressed or not, is able to exclude LDL to a similar degree. In contrast, the inhibitory synapse formed by YTS/KIR cells with 221/Cw6 cells was completely unable to restrict the access of LDL, with the relative intensities within the synapse comparable to those of all dextrans tested previously (Figure 3.14). This provides further evidence that the inhibitory synapse is unable to clear or exclude molecules from the cell-cell interface as efficiently as activating synapses. As discussed previously in Chapter 3, the transient nature of the inhibitory synapse means that exclusion of extracellular molecules does not occur. The expression of inhibitory receptors alone does not affect exclusion from the synapse, compared to the formation of an inhibitory synapse. This suggests that the process of activating synapse formation is essential for exclusion of extracellular molecules from the IS.

The synapse formed by pNK and 221 cells almost completely excluded LDL from the cell-cell interface, compared to activating synapses formed by the NK cell line YTS. This could explain why YTS cells are less efficient killers than pNK cells (20, 463). Consistent with this, previous studies have demonstrated that the addition of high amounts of H/LDL to some CTL-target cell conjugates was unable to significantly affect cell-mediated lysis (449). However, CTL clones that were less efficient killers were more susceptible to the effect of LDL than their more effective counterparts. This suggests that there may be a link between the ability of a lymphocyte to kill and the extent to which it can exclude extracellular proteins. Therefore, the inclusion of LDL within the synaptic cleft may have a negative impact on YTS-mediated cytolysis. The exclusion of LDL from the pNK cell synapse may provide insight into why these cells are more efficient killers. It may also demonstrate the important role of the IS for protecting cytolytic proteins from such inhibitors present in the extracellular environment.

In conclusion, the clearance and exclusion of LDL from the pNK cell synapse may protect secretions at the IS. Both mAb and LDL are similarly excluded from the synapse, and both of these molecules could negatively affect NK cell-mediated lysis of target cells. The data presented here demonstrate that the IS excludes molecules above a size threshold, potentially to protect proteins secreted across the IS cleft – a novel role of the NK cell synapse.

Chapter 5 – NK Cell Perforin Secretion Varies with Ligand Density and Serial Stimulation

5.1 Introduction

5.1.1 NK cell serial killing and redirected lysis

NK cells require a skewed balance of signals in favour of activation to prevent the dephosphorylation of adapter protein ITAM motifs, which inhibit the intracellular signaling events that initiate cytolysis of a target cell (464). This can occur sequentially with a number of targets, termed serial killing. Serial killing is the sequential lysis of target cells by the same effector cell, previously demonstrated by a number of groups (465-467). Recently, Vanherberghen *et al* used microwells (silicon chips engineered to contain wells of area 650 μm^2) to image NK cells and to characterise serial killers (467). These wells contained only a few cells (in the order of tens), which allowed individual NK cell interactions to be imaged over time. Single NK cells were reported to kill more than one target, and in some cases, a single NK cell could lyse up to 7 targets. Whilst there was a vast heterogeneity in the ability of NK cells to serially kill targets, the specific phenotype of these cells was not reported. This study suggests that subsets of NK cells possess the capacity for serial lysis of target cells, but how this is determined by the specific phenotype of individual NK cells remains to be determined.

Serial killing has also been demonstrated using cytotoxic release assays with an excess of target cells. These studies illustrated that a percentage of target cell specific lysis could only have been achieved if NK cells were able to kill more than one target cell (466). NK cells are also able to serially kill tumour cells, particularly solid tumours, where there is a mass of transformed cells in a single location (465). In this setting, serial killing is required to enable the elimination of the tumour. Whilst not all NK cells are ‘serial killers’ (467), the mechanisms and prerequisites for this

phenotype are not yet known. However, the ability to induce serial lysis of target cells by individual NK cells would vastly improve immune responses, especially in the fight against cancerous tumours.

Serial killing mediated by NK cells and $CD8^+$ T cells has been exploited in both redirected lysis and the opsonisation of virally infected or transformed cells. Redirected lysis exploits both the Fc receptors expressed by some target cells and antibody ligation of activating receptors to induce effector cell activation (468). Antibodies can also be used to bind specific epitopes expressed by tumour cells (466) or presented by MHC proteins on virally infected cells (469). Once a target has been specifically opsonised by antibodies, the exposed Fc portions are ligated by the NK cell Fc receptor, CD16, triggering ADCC of the target cell (320). These techniques have been shown to not only promote the lysis of targets resistant to NK cell natural cytotoxicity (468), but to also direct and increase the efficacy of tumour cell lysis (151, 470-473). For efficient target cell clearance, these techniques require NK cells to be serially activated and degranulate sufficient amounts of PFN to lyse the target cell. Unfortunately, NK cells are only able to lyse a finite amount of targets. This may be due to receptor internalisation following ligation (474), or the finite stores of PFN immediately available within NK cells (466), possibly acting as a safety mechanism to limit NK cell killing should autolysis occur. However, NK cell serial killing is a focus for research into potential mechanisms of tumour control. Specifically, particular areas of interest include how this phenotype is maintained and ways to redirect NK cell-mediated cytolysis towards specific targets. Further work determining how and why serial killing occurs, and how it may be manipulated for therapeutic purposes, is an important focus for future research.

5.1.3 Aims

Neural synapses can be activated in an analogue fashion, where the response is metered to the amount of stimulation received by the cell (475) NK cell activation is reported to function in a binary fashion, where a threshold of activation must be reached to initiate target cell lysis (476). An analogue response to the number of activating signals facilitating metered cytokine secretion by T cells has recently been reported (477). In addition, macrophages utilise the paracrine secretion of cytokines during innate and adaptive inter-system communication (478). Paracrine signalling delivers a dose-dependent response to cells, where those closer to the source are stimulated to a greater degree than those more distal. The report of analogue signalling within the immune - as well as neuronal - system, leads to the question of whether the PFN-mediated response of NK cells may also be dependent on the amount of activating signals received, and the nature of the ligand ligated. Whilst it is known that serial NK cell-mediated cytolysis can occur (467), the effect of repeated NK cell stimulation, on the actual amounts of PFN secreted has not been investigated. As secretion of PFN is paramount for NK cell-mediated cytolysis, the effect that receptor ligation has on PFN secretion is an important consideration when developing strategies to increase killing efficacy. Therefore, the specific aims of this study were as follows:

i. To investigate the effect of ligand density on PFN secretion

ii. To investigate the effect of different ligands on PFN secretion

iii. To quantify the effect of serial activation through one or more ligands on PFN secretion

iv. To estimate the amount of PFN, by number of molecules and concentration within the synapse, secreted by NK cells

5.2 Results

NK cells elicit cytotoxicity to diseased target cells following the ligation of activating receptors by a range of stress signals. Cytolysis is initiated by a balance of signalling in favour of activation followed by polarisation and direct secretion of cytotoxic mediators onto the target cell (479). It is well established that secretion of PFN is paramount to successful lysis of target cells (258, 259).

NK cells are activated and polarise upon contact with activating slides (117). To determine the relative amounts of PFN secreted by NK cells in response to ligand ligation, a protein capture assay was used (Chapter 2, Section 2.7.1). To do this, chambered microscope slides were coated with activating proteins along with the ICAM-Fc and anti-PFN antibodies. Cells were incubated on activating slides then removed with non-enzymatic cell dissociation solution. Captured PFN was then stained using fluorescently labelled anti-PFN antibodies. Stained PFN was imaged by confocal microscopy. Activation of NK cells on these slides induced the polarisation and secretion of PFN towards the coverglass, as shown previously (Chapter 4, Figure 4.7A). Following cell removal from the slide, PFN appeared as clusters within circular regions, covering a similar area to an activated NK cell. For this reason, each isolated cluster was assumed to be from one cell, and was used to determine the mean secretion of PFN per cell (Chapter 2, Section 2.8.2).

Using a reconstituted S2 cell system, studies by Bryceson *et al.* have shown that NK cells are unable to degranulate in response to NKG2D or LFA1 signalling alone. Conversely, ligation of CD16 was sufficient to induce degranulation and lysis of target cells (8, 154). To verify these findings using the protein capture assay, NK cells were first incubated for one hour on control slides. All slides were first coated with PLL (to adhere proteins to the glass surface), then anti-PFN antibodies (to capture secreted PFN) in addition to other proteins/antibodies, as summarised in Table 5.1 (Figure 5.1A).

Slide Surface	Justification
PLL + anti-PFN antibodies	To test whether PLL and/or anti-PFN antibodies can induce degranulation
Noggin-Fc	To test whether Fc ligation can induce degranulation, as noggin does not ligate NK cell expressed receptors
ICAM1-Fc	To test whether ICAM1 alone can induce degranulation
MICA-Fc	To test whether MICA alone can induce degranulation
Anti-CD16 antibodies	To test whether anti-CD16 alone can induce degranulation
MICA-Fc + ICAM1-Fc	To test whether MICA and ICAM1 co-ligation can induce degranulation
Anti-CD16 antibodies + ICAM1-Fc	To test whether anti-CD16 and ICAM1 co-ligation can induce degranulation

Table 5.1. Control surface coatings used for protein capture assay (Figure 5.1)

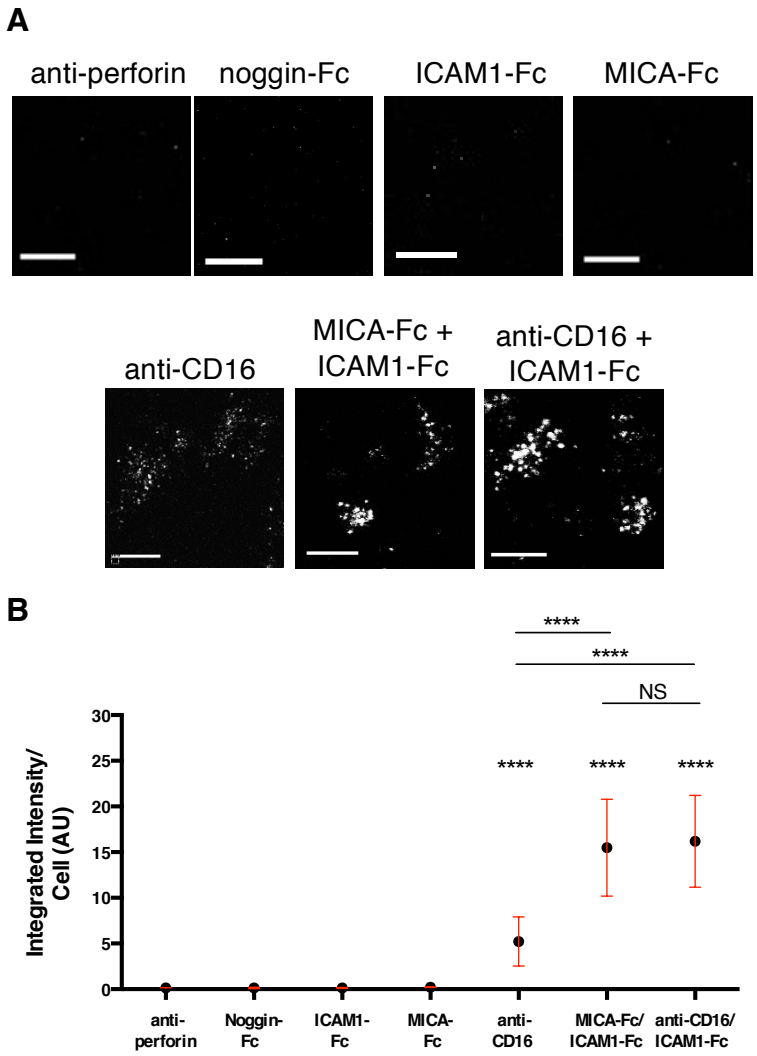


Figure 5.1. NK cell degranulation is induced through CD16 alone whereas NKG2D requires LFA1 co-ligation. (A) Primary human NK cells were plated on slides coated with anti-perforin only or in combination with Noggin-Fc, ICAM1-Fc, MICA-Fc, anti-CD16, MICA-Fc and ICAM1-Fc, or anti-CD16 and ICAM1-Fc. After 1 hour incubation, cells were removed and captured perforin was stained with an anti-perforin antibody labelled with Alexa Fluor 488 and imaged by confocal microscopy. Panels show representative confocal images of perforin captured and stained on slides. Scale bars; 10µm. **(B)** The integrated intensity of perforin spots in a defined area (one cell) were measured. Bars show the mean ± SD. Data were analysed using a one-way ANOVA with Tukey. (n = 102, 144, 101, 106, 141, 102, and 107 respectively). Data from 3 independent experiments. NS = no significance, ****p<0.0001.

The data show that anti-PFN murine IgG antibodies, noggin-Fc, ICAM1-Fc or MICA-Fc did not induce NK cell PFN secretion (0.14 ± 0.02, 0.13 ± 0.07, 0.14 ± 0.05 and 0.22 ± 0.03 AU respectively). In agreement with Bryceson *et al*., NK cells required CD16 signalling (5.2 ± 2.7 AU) or co-ligation of NKG2D or CD16 with LFA1 (15.5 ± 5.3 and 16.2 ± 5 AU respectively) to induce PFN secretion (Figure 5.1B). PFN secretion induced by anti-CD16 alone was significantly less than when anti-CD16 or MICA-Fc was added in the presence of ICAM1. Secretion on either activating ligand with ICAM1-Fc was similar. These initial findings show that NK cells can secrete PFN following stimulation through CD16 alone, but that the co-ligation of CD16 and LFA-1 increased the amount of PFN secreted by NK cells. NKG2D signalling also required LFA-1 to initiate PFN secretion. Finally, the ligation of the Fc control, noggin-Fc showed that the Fc portion of the chimera proteins was insufficient to induce PFN secretion.

5.2.1 NK cells perforin secretion begins within three minutes of activation

CTL polarise and/or trigger apoptosis in transformed target cells within minutes (177, 365). Therefore, the time scale of PFN secretion following activation was assessed. NK cells were plated on activating slides coated with either MICA-Fc or anti-CD16 with ICAM1-Fc and incubated for various times between 3 – 120 minutes (3-minute intervals for 15 minutes and 15-minute intervals for 120 minutes). Following which, NK cells were removed and captured PFN stained and imaged by confocal microscopy.

The detection of fluorescence signal showed that NK cells activated on MICA-Fc coated slides began to secrete PFN within 3 minutes. The size and intensity of these spots increased with increasing lengths of incubation on activating slides (Figure 5.2A). PFN secretion after 3 minutes activation (mean integrated intensity/cell of 3.2 ± 1.2 AU) continued to increase for around 30 – 45 minutes, until there was no further significant change in PFN (18.3 ± 7.4 AU at 45 minutes and 23.3 ± 8.43 AU at 120 minutes) (Figure 5.2B). Similarly, activation on anti-CD16 induced NK cell degranulation within 3 minutes (1.9 ± 1.0 AU). Secretion of PFN increased with longer incubation times (Figure 5.3A), similarly to cells activated through NKG2D. NK

cells continued to secrete PFN for ~60 minutes on anti-CD16/ICAM1-Fc-coated slides, following which no further increase of integrated intensity was detected (16.4 ± 5.6 AU at 60 minutes and 20.1 ± 6.4 AU at 120 minutes) (Figure 5.3B).

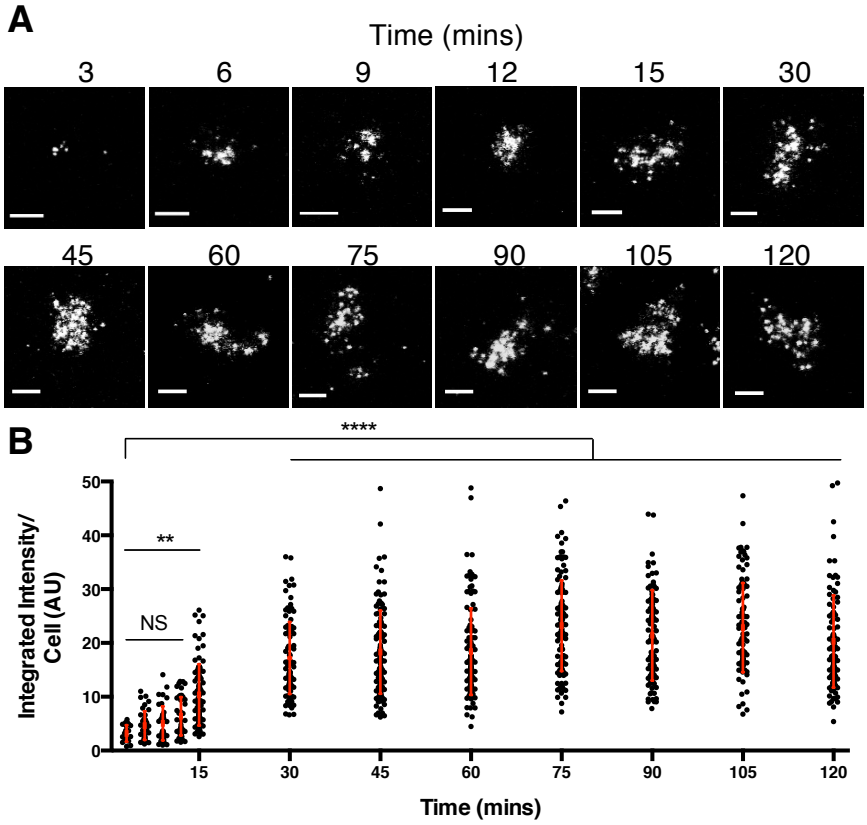


Figure 5.2. NK cells activated through NKG2D/LFA1 secrete perforin within three minutes of activation. (A) Primary human NK cells were plated on slides coated with MICA-Fc, ICAM1-Fc and anti-perforin for the times indicated. Cells were removed and captured perforin was stained with an anti-perforin Alexa Fluor 488 antibody. Slides were then imaged by confocal microscopy. Panels show representative images of secreted perforin captured and stained at each time point. Scale bars; 5 µm. **(B)** The integrated intensity of perforin spots in a defined area (one cell) were measured. Bars show the mean ± SD. Data were analysed using a one-way ANOV with Tukey corrections. (n = 88, 103, 122, 119, 122, 105, and 100, respectively). Data from 3 independent experiments. NS = no significance, **p<0.01, ****p<0.0001

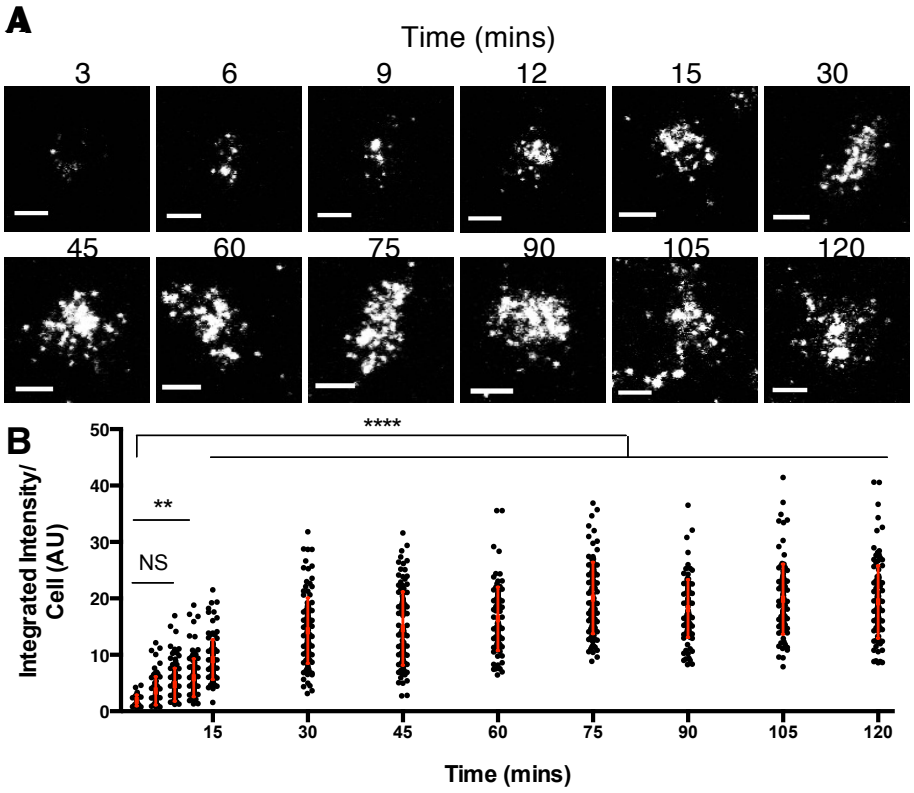


Figure 5.3. NK cells activated through CD16/LFA1 secrete perforin within three minutes of activation. (A) Primary human NK cells were plated on slides coated with MICA-Fc, ICAM1-Fc and anti-CD16 for the times indicated. Cells were removed and captured perforin was stained with an anti-perforin Alexa Fluor 488 antibody. Slides were then imaged by confocal microscopy. Panels show representative images of secreted perforin captured and stained at each time point. Scale bars; 10 µm. **(B)** The integrated intensity of perforin spots in a defined area (one cell) were measured. Bars show the mean ± SD. Data were analysed using a one-way ANOV with Tukey corrections. (n = 113, 102, 102, 101, 95, and 111, respectively). Data from 3 independent experiments. **p<0.01, ****p<0.0001

These data show that NK cells, upon co-ligation of NKG2D or CD16 with LFA1, secrete PFN within 3 minutes. On both ligands, NK cells continue to secrete PFN for 45 – 60 minutes. Whilst ligation by MICA-Fc induced a greater amount of PFN in a shorter time frame, the maximum amounts of PFN measured on both ligands were not significantly different.

5.2.3 The amount of perforin secreted by NK cells varies with ligand density

Ligand distribution and density on the target cell has been shown to control cytotoxicity. Regunathan *et al.* demonstrated that murine NK cell-mediated lysis of target cells *in vitro* was directly proportional to the expression level of cognate activating ligands on the target cell surface (480). Further to this, Martinez *et al.* demonstrated that when ULBP1 (a cognate ligand for NKG2D) was fused to the extracellular domain of CD45, the reduced number of receptor-ligand micro-clusters caused a decrease in NK cell-mediated cytotoxicity (481). This suggests that the clustering of ULBP1 on the target cell membrane is crucial for efficient lysis. Consistent with these data, downregulation or shedding of stress-induced ligands decreases tumour cell susceptibility to NK cell-mediated lysis (482, 483). These data together suggest that the extent of activating receptor ligation can control NK cell cytotoxicity.

To test the effect of ligand density on NK cell PFN secretion, NK cells were plated and incubated for one hour on slides coated with ICAM1-Fc, anti-perforin and increasing amounts (25, 50, 100, 200 or 400 ng) of either MICA-Fc or anti-CD16. One-hour incubation was chosen as previous data indicated that maximum PFN secretion occurred by this time point on both MICA-Fc- and anti-CD16-coated slides (Figure 5.4A). Images show that PFN secreted by NK cells increased with greater densities of activating ligand. NK cell activation on 25 ng MICA-Fc resulted in the lowest PFN secretion (3.1 ± 2.0 AU) and activation on 400 ng MICA-Fc induced the greatest PFN secretion (15.7 ± 5.6 AU), a 5-fold increase. NK cells plated on ICAM1-Fc alone did not degranulate (0.10 ± 0.01 AU) (Figure 5.4B), as shown previously (Figure 5.1). Whilst PFN secretion was not directly proportionate to ligand density (*i.e.* a 2-fold increase of ligand did not result in a 2-fold increase of PFN), increased PFN secretion is consistent with previous work demonstrating that NK cell-mediated lysis was proportional to the expression of target cell ligands (480).

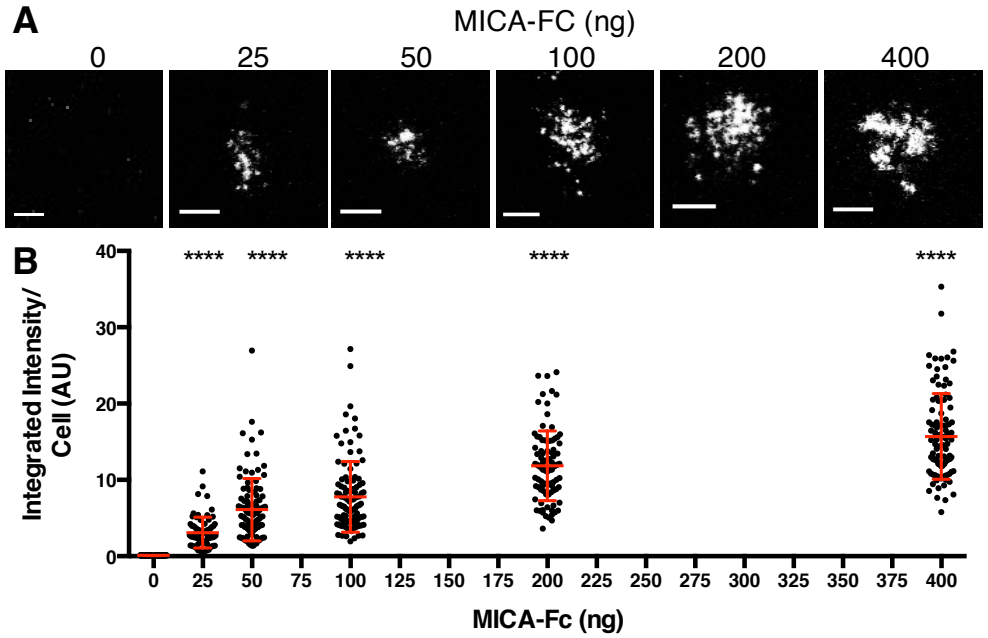


Figure 5.4. The amount of perforin secreted by NK cells varies with the density of activating ligand MICA-Fc. (A) Primary human NK cells were plated on slides coated with MICA-Fc (at amounts indicated), ICAM1-Fc and anti-perforin for 1 hour. Cells were removed and captured perforin was stained with an anti-perforin Alexa Fluor 488 antibody. Slides were then imaged by confocal microscopy. Panels show representative images of secreted perforin captured and stained at each ligand density. Scale bars; 10 μm. **(B)** The integrated intensity of perforin spots in a defined area (one cell) were measured. Bars show the mean ± SD of integrated intensities of perforin secreted from each cell. Data were analysed using a one-way ANOV with Tukey corrections. (n = 102, 74, 103, 107, 92, and 103, respectively). Data from 3 independent experiments. ****p<0.0001

Similarly, increasing amounts of anti-CD16 resulted in increased PFN secretion (Figure 5.5A). NK cell degranulation increased over 3-fold when activated on 400 ng of anti-CD16 (16.4 ± 5.1 AU) compared to 25 ng (5.2.1 ± 3.37 AU) (Figure 5.5B). Activation on ICAM1-Fc alone did not induce PFN secretion (0.10 ± 0.01 AU), as shown in the control experiments (Figure 5.1). Activation on increasing densities of anti-CD16 did not induce directly proportional increases of PFN. The amounts of PFN secreted on the lowest density of either ligand (25 ng) were statistically different ($p = 0.0004$, two-tailed Student's t-test with Welch's corrections), whereas no difference was measured between the amounts secreted on the greatest density (400 ng) ($p = 0.3592$, two-tailed Student's t-test with Welch's corrections).

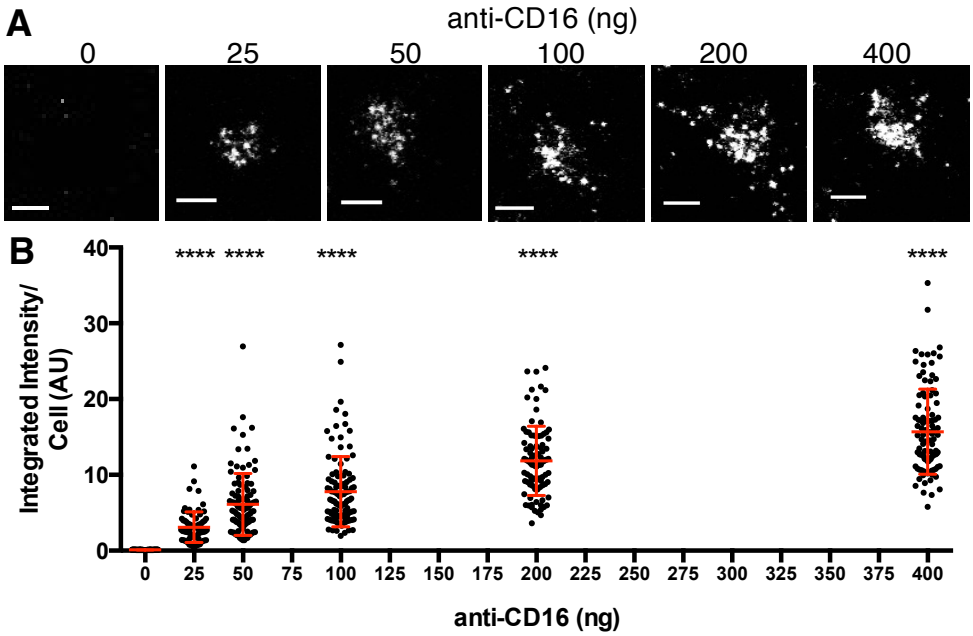


Figure 5.5. The amount of perforin secreted by NK cells varies with the density of activating ligand anti-CD16 antibody. (A) Primary human NK cells were plated on slides coated with anti-CD16 (at amounts indicated), ICAM1-Fc and anti-perforin for 1 hour. Cells were removed and captured perforin was stained with an anti-perforin Alexa Fluor 488 antibody. Slides were then imaged by confocal microscopy. Panels show representative images of secreted perforin captured and stained at each ligand density. Scale bars; 10 µm. **(B)** The integrated intensity of perforin spots in a defined area (one cell) were measured. Bars shows the mean ± SD. Data were analysed using a one-way ANOV with Tukey corrections com. (n = 102, 44, 60, 100, 98, and 109, respectively). Data from 3 independent experiments. ****p<0.0001

Increased densities of activating ligand are shown here to modulate the amount of PFN secreted by NK cells. Whilst a variation in the density of either ligand was able to induce a metered response, this was not directly proportionate to the amount of protein plated. This suggests that NK cells are sensitive to ligand density at the IS and that this signalling is not digital (an all-or-nothing response) but analogue (metered), where an increase of ligand ligation can trigger an increased response, consistent with previous studies.

5.2.3 The amount of perforin secreted by NK cells decreases with subsequent serial stimulations

The number of targets that can be serially killed by individual NK cells varies significantly, where 25% of NK cells can lyse up to 2 targets compared with only 6% or less capable of serially lysing 3 or more (467). However, it is not currently known what the effect of serial killing is on the amounts of PFN secreted by NK cells. To investigate the effects of serial killing on the amounts of PFN secreted by NK cells, a serial activation assay was used (Chapter 2, Section 2.7.2).

Serial activation through NKG2D resulted in a decrease of PFN secretion with every subsequent stimulation (Figure 5.6A). Following the initial amount of PFN secreted after the first activation (15.3 ± 6.8 AU), PFN release decreased to 10.7 ± 4.7 AU, 5.4 ± 3.3 AU and finally, 2.8 ± 2.2 AU. By the fourth stimulation, the amount of PFN secreted had decreased by 81.5% (Figure 5.6B). This suggests that NK cells either secrete a specific proportion of their total PFN stores, decreasing with each degranulation, or they lose ability to release as much PFN following serial stimulation. Similarly, serial stimulations on anti-CD16 decreased the amount PFN secreted by NK cells (Figure 5.7A). The initial stimulation induced PFN secretion (16.9 ± 6.5 AU) similar to previous experiments. Subsequent stimulations decreased PFN secretion to 9.81 ± 3.0 AU, 4.9 ± 1.8 AU and finally, 2.3 ± 1.3 (Figure 5.7B). After four stimulations on anti-CD16, the PFN secreted by NK cells was only 13% of that induced by the first stimulation.

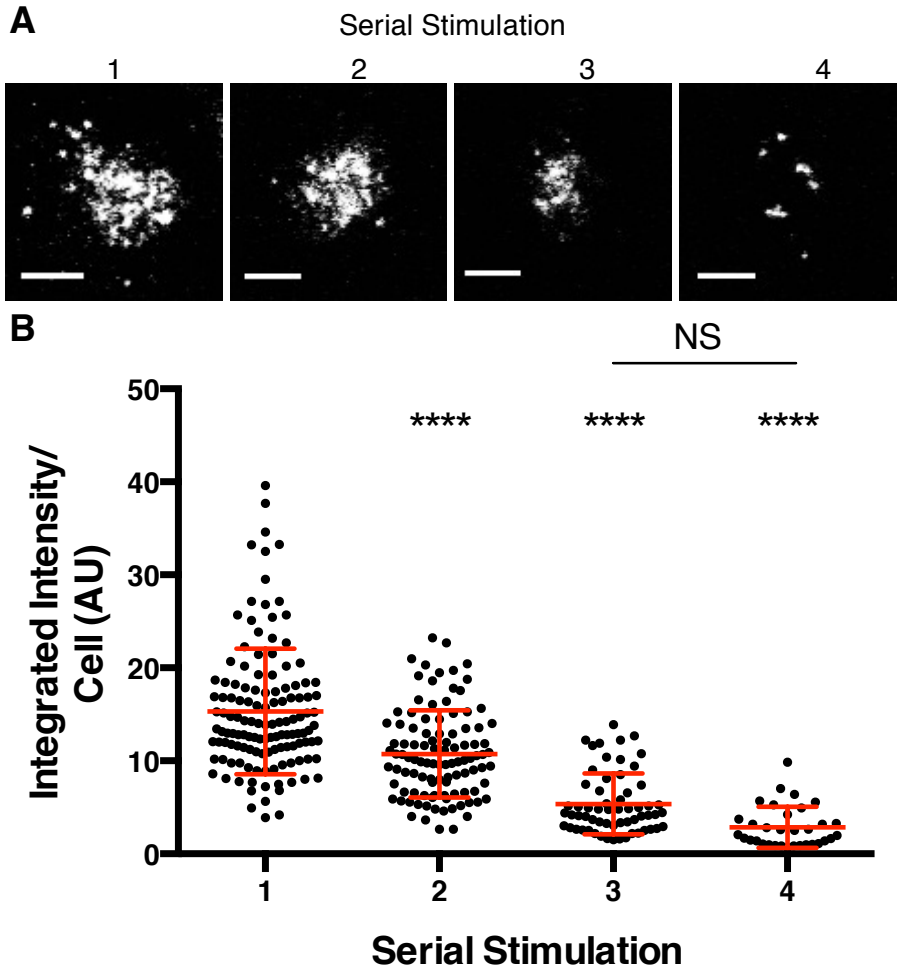


Figure 5.6. NK cells secrete reducing amounts of perforin following serial stimulation through NKG2D/LFA1. (A) Primary human NK cells were plated on slides coated with MICA-Fc, ICAM1-Fc and anti-perforin for 1 hour. Cells were removed, washed and plated again. Activation was repeated until NK cells had been activated 4 times. Captured perforin was stained with an anti-perforin Alexa Fluor 488 antibody. Slides were then imaged by confocal microscopy. Panels show representative images of secreted perforin captured and stained at each ligand density. Scale bars; 10 µm. **(B)** The integrated intensity of perforin spots in a defined area (one cell) were measured. Bars show the mean ± SD. Data were analysed using a one-way ANOV with Tukey corrections. (n = 130, 104, 61, and 33, respectively). Data from 3 independent experiments. NS = not significant.****p<0.0001.

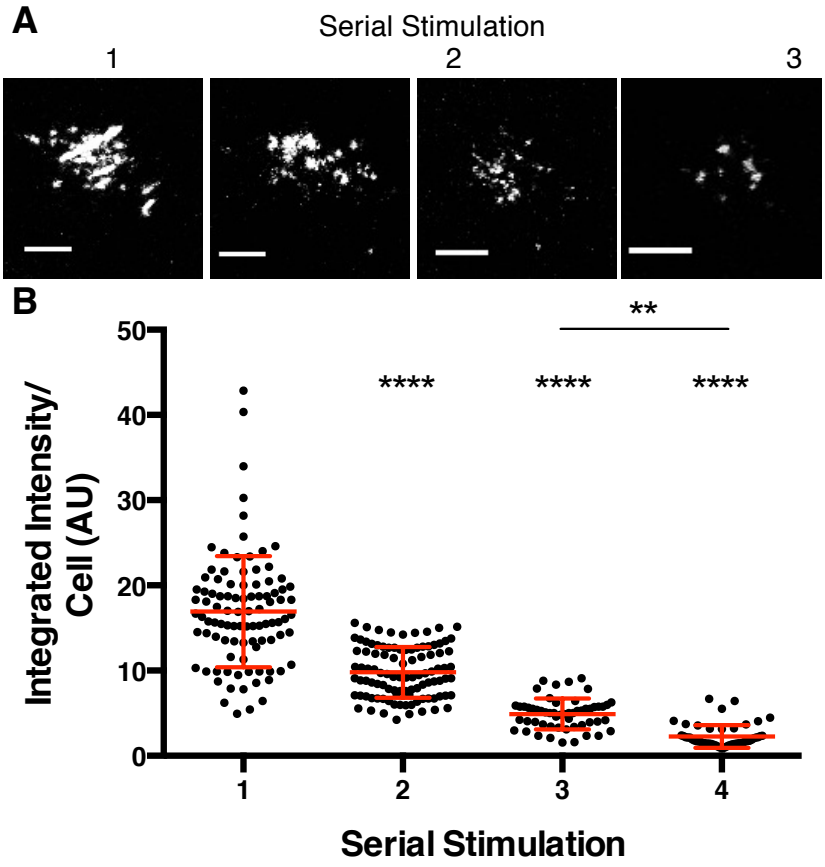


Figure 5.7. NK cells secrete reducing amounts of perforin following serial hits of activation through CD16/LFA1. (A) Primary human NK cells were plated on slides coated with anti-CD16, ICAM1-Fc and anti-perforin for 1 hour. Cells were removed, washed and plated again. Activation was repeated until NK cells had been activated 4 times. Captured perforin was stained with an anti-perforin Alexa Fluor 488 antibody. Slides were then imaged by confocal microscopy. Panels show representative images of secreted perforin captured and stained at each ligand density. Scale bars; 10 µm. **(B)** The integrated intensity of perforin spots in a defined area (one cell) were measured. Bars show the mean ± SD. Data were analysed using a one-way ANOV with Tukey corrections. (n = 96, 100, 55, and 51, respectively). Data from 3 independent experiments. **p<0.01, ****p<0.0001

Serial activation of NK cells results in a reduced capacity to secrete PFN. The decrease in PFN secreted correlated with previous experiments showing a decrease of ligand density induced less PFN secretion (Figure 3.4 and 3.5). This suggests that the reduction in the ability of NK cells to secrete PFN may be due to a loss of surface receptors, diminishing their ability to bind ligands, resulting in a reduction in PFN secretion.

5.2.4 Effective restimulation of NK cells is receptor-dependent

The binding of cognate ligands has been shown to cause the internalisation of NK cell activating surface receptors (484), in addition, serial killing is associated with a loss of NK cell PFN and GzmB stores (466). To test whether NK cell activation induced the secretion of a pre-determined percentage of total PFN stores or whether NK cells became desensitised to a specific ligand, cells were serially activated on alternating ligands (Figure 5.8A), as summarised in Table 5.2.

Stimulation	Surface Coating
1	MICA-Fc + ICAM1-Fc
2	MICA-Fc + ICAM1-Fc
3	Anti-CD16 + ICAM1-Fc
4	Anti-CD16 + ICAM1-Fc

Table 5.2. Pattern of activating surface coating used to test restimulation of NK cells (Figure 5.8)

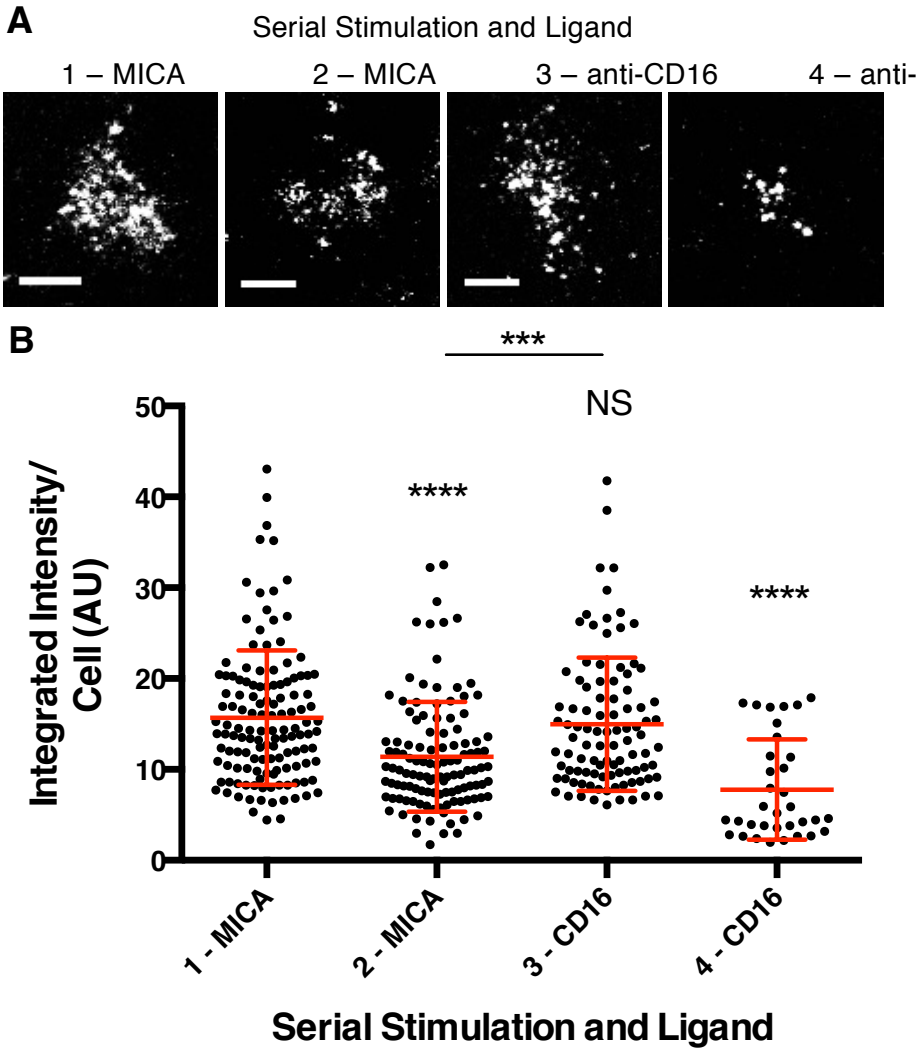


Figure 5.8. Serial stimulation through NKG2D/LFA1 does not affect subsequent stimulation through CD16/LFA1. (A) Primary human NK cells were plated on slides coated with MICA-Fc or anti-CD16 (as indicated), ICAM1-Fc and anti-perforin for 1 hour. Cells were removed, washed and plated again. Activation was repeated until NK cells had been activated 4 times. Captured perforin was stained with an anti-perforin Alexa Fluor 488 antibody. Slides were then imaged by confocal microscopy. Panels show representative images of secreted perforin captured and stained at each ligand density. Scale bars; 10 µm. **(B)** The integrated intensity of perforin spots in a defined area (one cell) were measured using a threshold mask. Bars show the mean ± SD. Data were analysed using a one-way ANOV with Tukey corrections. (n = 132, 118, 97, and 34, respectively). Data from 3 independent experiments. NS = no significance, ****p<0.0001

Consistent with previous experiments, a second stimulation through NKG2D reduced PFN secretion (15.7 ± 7.4 AU to 11.4 ± 6.1 AU). The third stimulation, on anti-CD16, triggered an increase in PFN secretion (15.0 ± 7.3). The fourth stimulation continued to decrease the amount of PFN secreted (7.8 ± 5.5 AU) (Figure 5.8B). However, the amount of PFN secreted at this point was greater than after 4 stimulations on either MICA-Fc (Figure 5.6) or anti-CD16 (Figure 5.7). These data suggest that, whilst

serial stimulation by MICA-Fc results in a decrease of PFN secreted, PFN secretion through CD16 is not affected. Next, NK cells were activated twice on anti-CD16, followed by twice on MICA-Fc, as summarised in Table 5.3.

Stimulation	Surface Coating
1	MICA-Fc + ICAM1-Fc
2	MICA-Fc + ICAM1-Fc
3	Anti-CD16 + ICAM1-Fc
4	Anti-CD16 + ICAM1-Fc

Table 5.3. Pattern of activating surface coating used to test restimulation of NK cells (Figure 5.9)

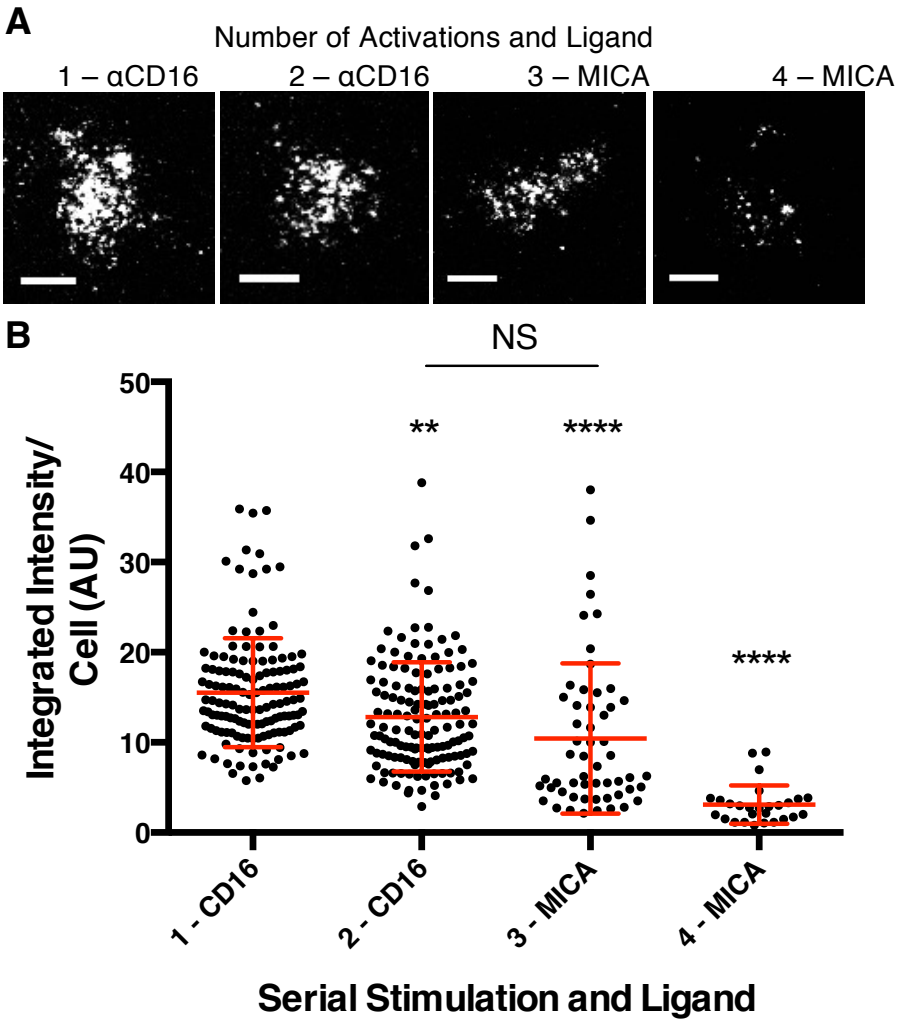


Figure 5.9. Serial stimulation through CD16 affects subsequent stimulation through NKG2D. **(A)** Primary human NK cells were plated on slides coated with anti-CD16 or MICA-Fc (as indicated), ICAM1-Fc and αPerforin for 1 hour. Cells were removed, washed and plated again. Activation was repeated until NK cells had been activated 4 times. Captured perforin was stained with an anti-perforin Alexa Fluor 488 antibody. Slides were then imaged by confocal microscopy. Panels show representative images of secreted perforin captured and stained at each ligand density. Scale bars; 10 µm. **(B)** The integrated intensity of perforin spots in a defined area (one cell) were measured using a threshold mask. Bars show the mean ± SD. Data were analysed using a one-way ANOV with Tukey corrections. (n = 136, 141, 55, and 27, respectively). Data from 3 independent experiments. NS = no significance, ****p<0.0001.

The amounts of secreted by NK cells continued to decrease, irrespective of the ligand variation (Figure 5.9A). The first two stimulations on anti-CD16 induced decreasing amounts of PFN secretion (15.5 ± 6.0 AU to 12.8 ± 6.1 AU). The third stimulation, on MICA-Fc, did not increase PFN secretion, but rather resulted in a non-significant decrease (10.4 ± 8.3 AU). The fourth stimulation resulted in a substantial, significant decrease in the amount of PFN secreted (3.1 ± 2.1 AU) (Figure 5.9B). These data imply that ligation of MICA-Fc following anti-CD16 ligation cannot trigger

increased PFN secretion by NK cells, suggesting that CD16 ligation has an effect on NKG2D-mediated PFN secretion.

To further test whether this response was a direct effect of stimulation on anti-CD16 following MICA-Fc stimulation, NK cells were serially stimulated on MICA-Fc twice, and then the same population of NK cells was split and plated 50/50 on either MICA-Fc/ICAM1-Fc-coated slide or anti-CD16/ICAM1-Fc-coated slides (Figure 5.10A), as summarised in Table 5.4.

Stimulation	Surface Coating	NK cells plated (%)
1	MICA-Fc + ICAM1-Fc	100
2	MICA-Fc + ICAM1-Fc	100
3a	MICA-Fc + ICAM1-Fc	50
3b	Anti-CD16 + ICAM1-Fc	50

Table 5.4. Pattern of activating surface coating used and percentage of total NK cells plated to test restimulation of NK cells (Figure 5.10)

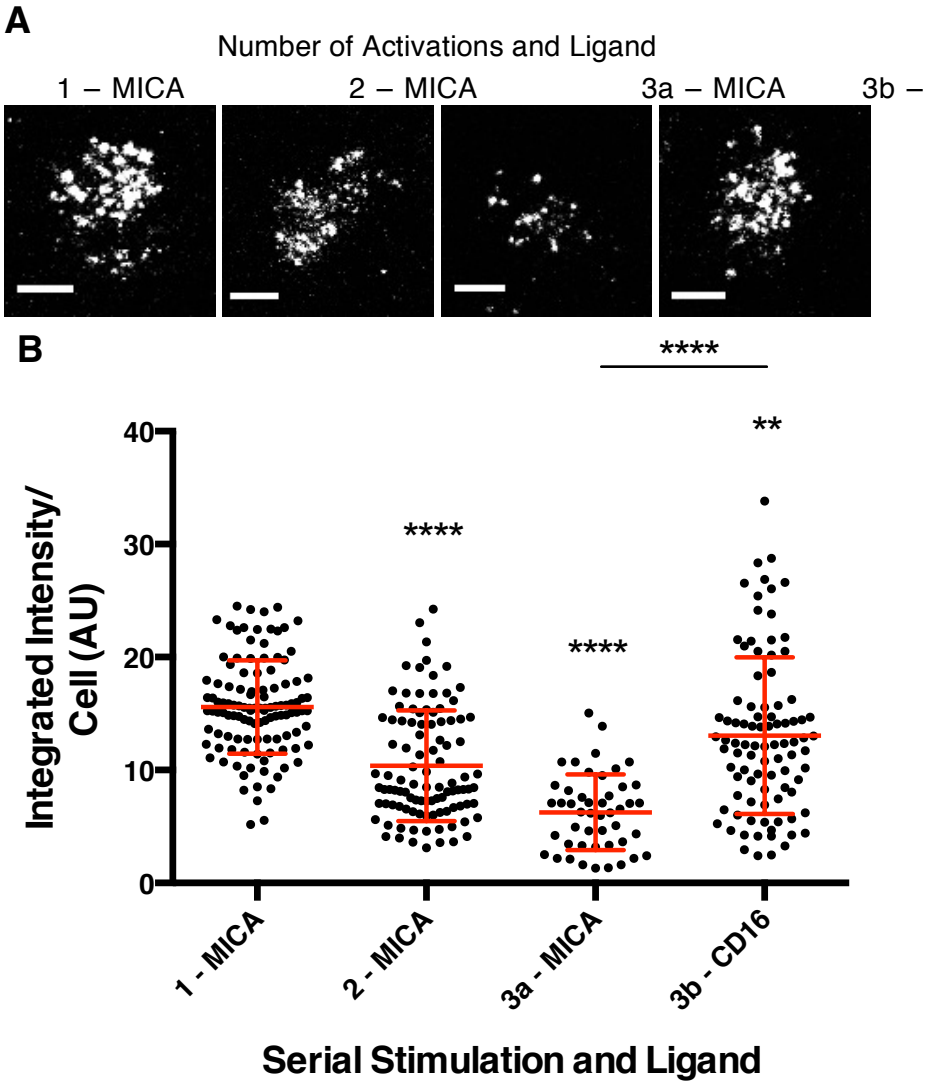


Figure 5.10. Serial stimulation through NKG2D/LFA1 affects continued stimulation through the same receptors but not CD16/LFA1 stimulation. (A) Primary human NK cells were plated on slides coated with MICA-Fc, ICAM1-Fc and anti-perforin for 1 hour. Cells were removed, washed and plated again. NK cells were then removed, and 50% plated out on slides coated with MICA-Fc or anti-CD16, ICAM1-Fc and anti-perforin. Captured perforin was stained with an anti-perforin Alexa Fluor 488 antibody. Slides were then imaged by confocal microscopy. Panels show representative images of secreted perforin captured and stained at each ligand density. Scale bars; 10 µm. **(B))** The integrated intensity of perforin spots in a defined area (one cell) were measured. Bars show the mean ± SD. Data were analysed using a one-way ANOV with Tukey corrections. (n = 116, 101, 47, and 92, respectively). Data from 3 independent experiments. **p<0.01, ****p<0.0001

The first 2 stimulations on MICA-Fc decreased the amount of PFN secreted (15.6 ± 4.2 AU to 10.4 ± 5.0 AU). When NK cells were then plated on either MICA-Fc/ICAM1-Fc or anti-CD16/ICAM1-Fc, PFN secretion decreased (6.3 ± 3.4 AU) or increased (13.1 ± 6.9 AU), respectively (Figure 5.10B). These findings further demonstrate that following serial stimulation through NKG2D, CD16 ligation can trigger an increase in PFN secretion by NK cells, whereas continued NKG2D stimulation reduces

degranulation. These findings are consistent with previous experiments (Figure 5.2 and 5.8 and 5.8)

This experiment was then repeated, activating NK cells on anti-CD16 twice, then plating NK cells 50:50 on either anti-CD16/ICAM1-Fc or MICA-Fc/ICAM1-Fc (Figure 5.11A), as summarised in Table 5.5.

Stimulation	Surface Coating	NK cells plated (%)
1	Anti-CD16 + ICAM1-Fc	100
2	Anti-CD16 + ICAM1-Fc	100
3a	Anti-CD16 + ICAM1-Fc	50
3b	MICA-Fc + ICAM1-Fc	50

Table 5.5. Pattern of activating surface coating used and percentage of total NK cells plated to test restimulation of NK cells (Figure 5.11)

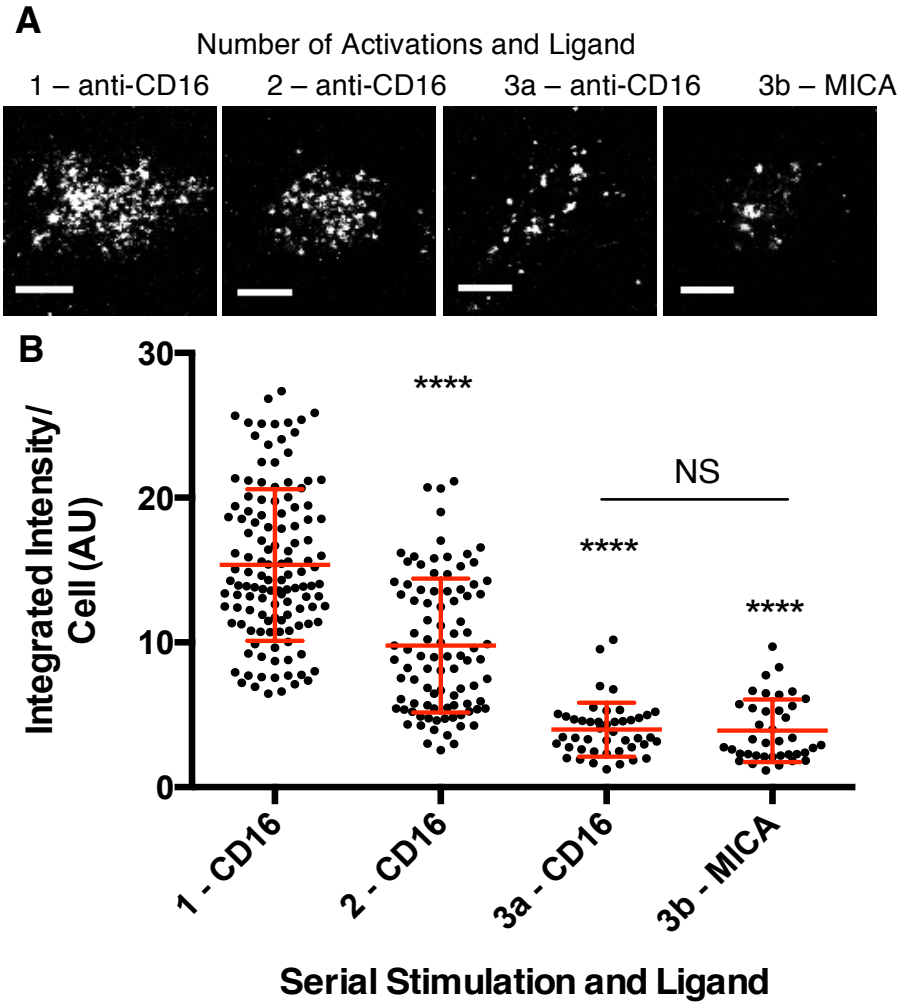


Figure 5.11. Serial stimulation through CD16/LFA1 affects further stimulation through both NKG2D/LFA1 and CD16/LFA1. **(A)** Primary human NK cells were plated on slides coated with anti-CD16, ICAM1-Fc and anti-perforin for 1 hour. Cells were removed, washed and plated again. NK cells were then removed, and 50% plated out on slides coated with anti-CD16 or MICA-Fc, ICAM1-Fc and anti-perforin. Captured perforin was stained with an anti-perforin Alexa Fluor 488 antibody. Slides were then imaged by confocal microscopy. Panels show representative images of secreted perforin captured and stained at each ligand density. Scale bars; 10 µm. **(B))** The integrated intensity of perforin spots in a defined area (one cell) were measured. Bars show the mean ± SD. Data were analysed using a one-way ANOV with Tukey corrections. (n = 128, 93, 45, and 39, respectively). Data from 3 independent experiments. NS = no significance, ****p<0.0001.

The decrease in PFN secreted when serially activated by anti-CD16 was similar to previous experiments (15.4 ± 5.2 AU, 9.8 ± 4.6 and 4.0 ± 1.8 AU). A third stimulation on either MICA-Fc or anti-CD16 resulted in a decrease in PFN secretion that were not significantly different (4.0 ± 1.9 AU on MICA-Fc/ICAM1-Fc and 3.9 ± 2.2 AU on anti-CD16/ICAM1-Fc) (Figure 5.11B). These results show that subsequent serial NK cell activation though CD16 decreases the amount of PFN secreted by NK cells and that ligation of NKG2D cannot increase PFN secretion.

Taken together, these findings suggest that stimulation through NKG2D or CD16 gradually desensitises NK cells to further stimulation through the same receptor. However, stimulation through NKG2D does not affect PFN secretion through subsequent CD16 ligation, whereas CD16 stimulation causes the desensitisation of NK cells to both anti-CD16 and MICA-Fc.

5.2.5 Serial stimulation affects the surface expression of NK cell receptors

In order to test whether the ligation of NKG2D or CD16 was inducing downregulation of receptors, NK cell surface expression of NKG2D and CD16 was measured by flow cytometry. NK cells were first incubated for one hour on control slides (PLL, Noggin-Fc, ICAM1-Fc, MICA-Fc, or anti-CD16). Cells were then assessed for surface expression of NKG2D and CD16, calculating the proportion of cells expressing the receptors and measuring the geometric mean fluorescence intensity (gMFI) of expression. To calculate the percentage of cells that were positive for receptor expression, histograms were gated on all events with stain levels above that of an isotype control. GMFI provides a measure of the amount of each receptor that was expressed on the surface of NK cells under different conditions. To compare the gMFI, data were normalised to expression levels following incubation on PLL, where no activating stimulation would have occurred.

The incubation of pNK cells on control slides demonstrated that the proportion of cells expressing NKG2D or CD16 did not alter (70 – 87% for NKG2D and 97% – 86% for CD16) (Figure 5.12A). The gMFI of NKG2D expression levels remained similar (0 – 3% decrease) (Figure 5.12B), except in the case of ICAM-Fc (19% decrease compared to incubation on PLL). Similarly, the level of CD16 expression was unchanged on negative controls (0 – 2% decrease), however stimulation with MICA-Fc or anti-CD16 resulted in a decrease in the expression of CD16 (27% and 32% respectively) (Figure 5.12C). This suggests that NKG2D expression is not affected by any of the ligands alone, whereas CD16 expression can be altered by either MICA-Fc or anti-CD16 ligation. The negative controls, particularly, Noggin-Fc, indicate that this is an effect of the MICA protein, not the Fc portion, as incubation on Noggin-Fc

did not induce a change in either NKG2D or CD16 expression. However, exposure to ICAM1-Fc decreased NKG2D expression, suggesting that ligation of LFA1 can have a direct impact on the levels of NKG2D on the surface of NK cells.

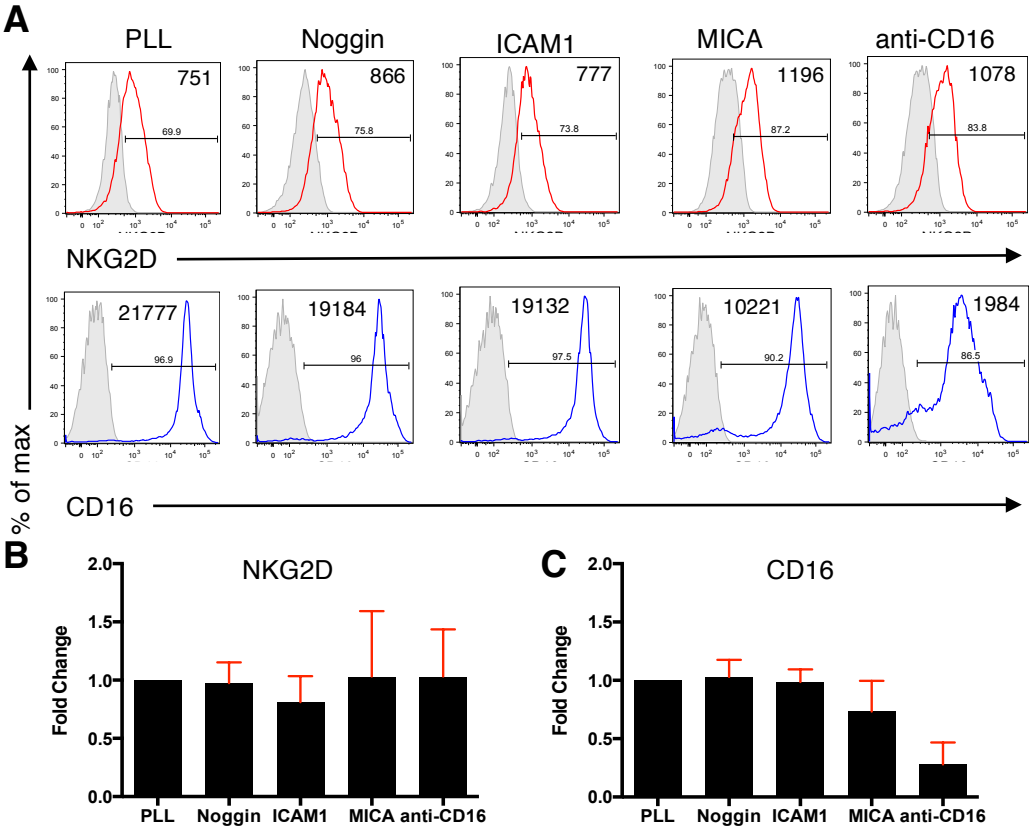


Figure 5.12. NKG2D expression is not affected by single receptor ligation whereas CD16 is affected by ligation of either MICA-Fc or anti-CD16. Primary human NK cells were plated on slides coated with poly-L-lysine (PLL), ICAM1-Fc, MICA-Fc, anti-CD16 antibodies or Noggin-Fc and incubated for 1 hour at 37ºC, then removed using an EDTA solution. **(A)** Cells were analysed by flow cytometry. Cells were first gated for $CD3^{-}$ $CD56^{+}$ populations, and then expression of NKG2D (*upper row*) and CD16 (*lower row*) was measured. Data representative of 2 independent experiments from 2 donors. **(B)** The geometric mean fluorescence intensity (gMFI) of NKG2D expression levels were normalised to expression following plating on PLL-coated slides. Bars show mean ± SEM. **(C)** The gMFI of CD16 expression levels were normalised to expression following plating on PLL-coated slides. Bars show mean ± SEM. Data from 2 independent experiments from 2 donors.

The expression of NKG2D was then measured on pNK cells after serial stimulation by MICA-Fc/ICAM1-Fc or anti-CD16/ICAM1-Fc. In contrast to stimulation on MICA-Fc alone, simultaneous exposure to MICA-Fc and ICAM1-Fc led to a reduction in the proportion of NK cells expressing NKG2D, with decreased expression between 1 and 4 stimulations (51% to 26%) (Figure 5.13A). In parallel, there was an even more marked reduction in the expression levels (40% to 67%, first and fourth stimulation

respectively). There was no effect on expression by MICA-Fc alone, and only a minor decrease in response to ICAM1-Fc (Figure. 5.13B). Stimulation through CD16/LFA1 also caused a decrease in the proportion of NK cells expressing NKG2D (compared to plating on PLL) (58% positive for NKG2D after the first stimulation, and 39% after the fourth) (Figure 5.13C). The expression level of NKG2D was unchanged after the first stimulation (1% decrease compared to PLL control). However, expression had decreased by more than 25% after the fourth stimulation through CD16 and LFA1 (Figure 5.13D). This suggests that it is only exposure to MICA-Fc and ICAM1-Fc in tandem – not anti-CD16/ICAM1-Fc – that greatly impacts the expression level of NKG2D.

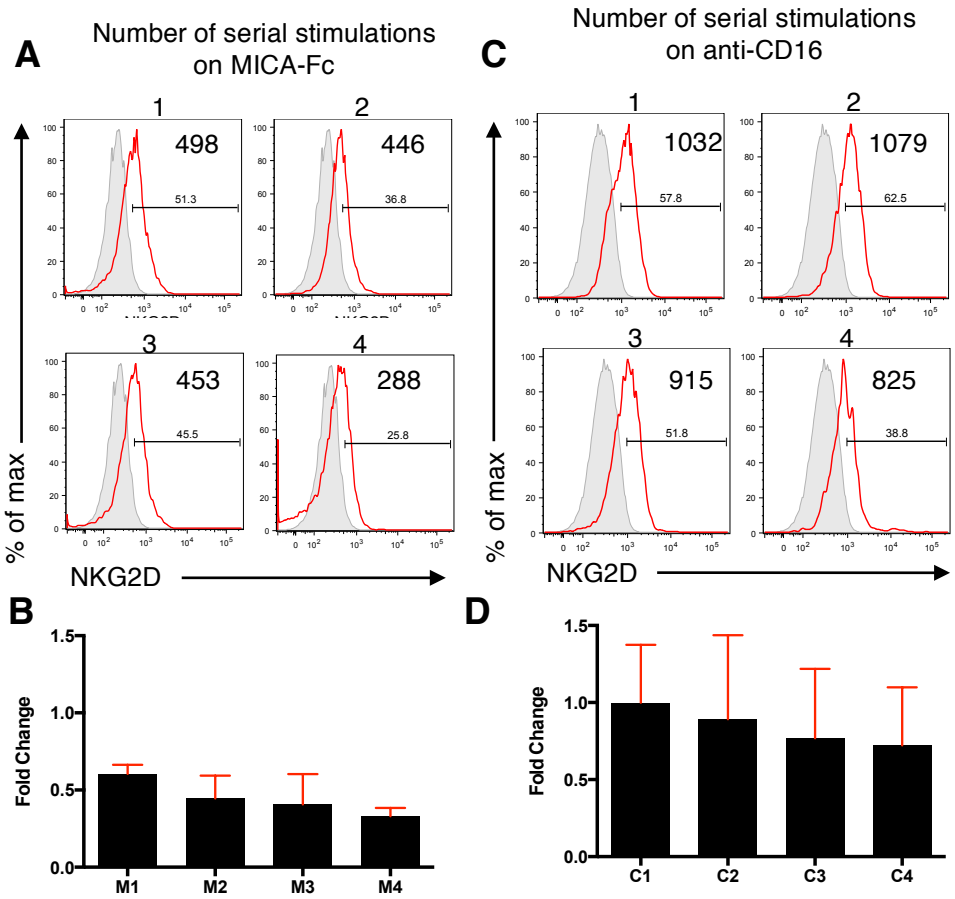


Figure 5.13. NK cell surface expression of NKG2D is down regulated following serial stimulation through either NKG2D/LFA1 or CD16/LFA1. Primary human NK cells were plated on slides coated with ICAM1-Fc and MICA-Fc or anti-CD16 and incubated for 1 hour at 37ºC, then removed using an EDTA solution. **(A)** Cells serially stimulated by ICAM1-Fc/MICA-Fc were analysed by flow cytometry. Cells were first gated for $CD3^-$ $CD56^+$ populations, then expression of NKG2D was measured after each stimulation, as indicated. Data representative of 2 independent experiments from 2 donors. **(B)** The geometric mean fluorescence intensity (gMFI) of NKG2D expression levels after each stimulation on MICA-Fc (M1–4) were normalised to expression following plating on PLL-coated control slides. Bars show mean ± SEM. Data from 2 independent experiments form 2 donors. **(C)** Cells serially stimulated by ICAM1-Fc/anti-CD16 were analysed by flow cytometry. Cells were first gated for $CD3^-$ $CD56^+$ populations, then expression of NKG2D was measured after each stimulation, as indicated. Data representative of 2 independent experiments from 2 donors. **(B)** The geometric mean fluorescence intensity (gMFI) of NKG2D expression levels after each stimulation on anti-CD16 (C1–4) were normalised to expression following plating on PLL-coated control slides. Bars show mean ± SEM. Data from 2 independent experiments from 2 donors.

Next, the expression of CD16 was examined after serial stimulation on slides coated with MICA-Fc/ICAM1-Fc or anti-CD16/ICAM1-Fc. Serial ligation of NKG2D had little impact on the expression of CD16 (96% of cells were positive for CD16 after the first stimulation and 83% after the fourth). (Figure 5.14A). The expression levels of CD16 were reduced comparatively to MICA-Fc alone when ICAM1-Fc was present (20% decrease compared to plating on PLL). Serial stimulation continued to decrease the level of CD16 expression; with a 67% decrease detectable by the fourth stimulation

(Figure 5.14B). Serial stimulations on anti-CD16/ICAM1-Fc-coated slides decreased the proportion of cells expressing CD16 to a greater extent than NKG2D ligation (89% positive after the first stimulation to 58% after the fourth stimulation) (Figure 5.14C). The co-ligation of CD16 and LFA1 had a profound effect on the expression levels of CD16, particularly when compared to anti-CD16 alone. After the first stimulation, the level of expression decreased by 70%. Following 3 or 4 stimulations, expression remained relatively constant (92% and 93% decrease, respectively, compared to PLL) (Figure 5.14D). This suggests that CD16 expression is affected to a greater extent by anti-CD16 ligation, compared to MICA-Fc. The co-ligation of anti-CD16 and ICAM1-Fc had a greater impact on both the proportion of cells expressing CD16 and the level of expression.

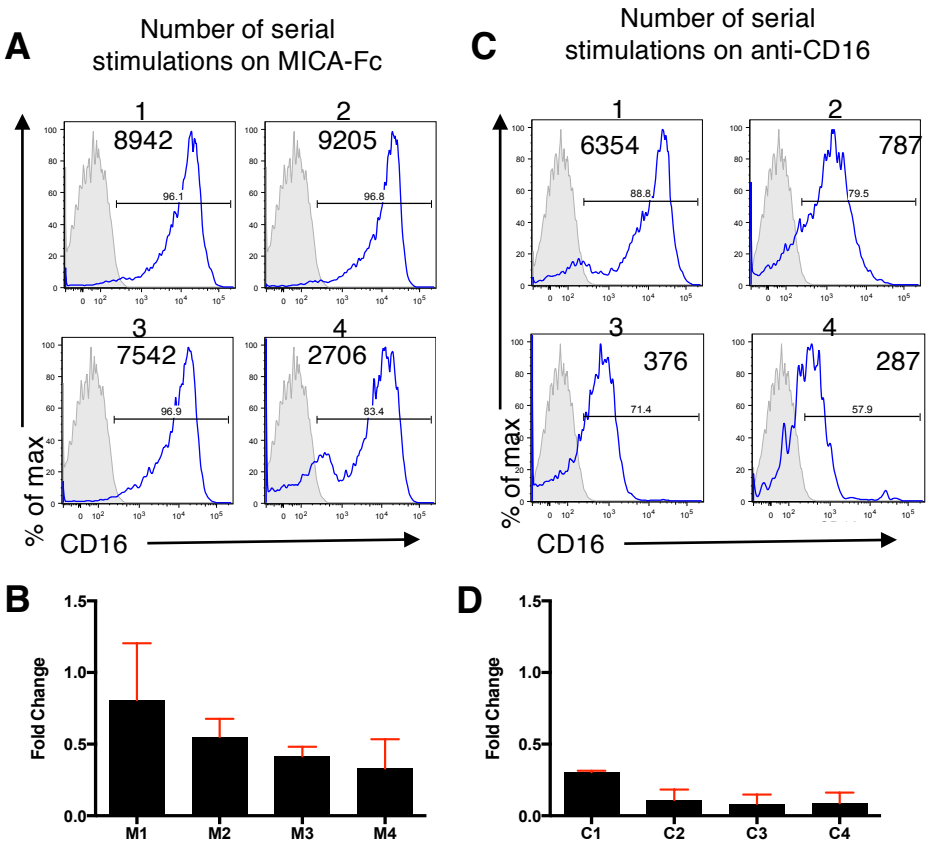


Figure 5.14. NK cell surface expression of CD16 is down regulated following serial stimulation through either NKG2D/LFA1 and CD16/LFA1. Primary human NK cells were plated on slides coated with ICAM1-Fc and MICA-Fc or anti-CD16 and incubated for 1 hour at 37ºC, then removed using an EDTA solution. **(A)** Cells serially stimulated by ICAM1-Fc/MICA-Fc were analysed by flow cytometry. Cells were first gated for $CD3^-$ $CD56^+$ populations, then expression of CD16 was measured after each stimulation, as indicated. Data representative of 2 independent experiments from 2 donors. **(B)** The geometric mean fluorescence intensity (gMFI) of CD16 expression levels after each stimulation on MICA-Fc (M1–4) were normalised to expression following plating on PLL-coated control slides. Bars show mean ± SEM. Data from 2 independent experiments form 2 donors. **(C)** Cells serially stimulated by ICAM1-Fc/anti-CD16 were analysed by flow cytometry. Cells were first gated for $CD3^-$ $CD56^+$ populations, then expression of CD16 was measured after each stimulation, as indicated. Data representative of 2 independent experiments from 2 donors. **(B)** The geometric mean fluorescence intensity (gMFI) of CD16 expression levels after each stimulation on anti-CD16 (C1–4) were normalised to expression following plating on PLL-coated control slides. Bars show mean ± SEM. Data from 2 independent experiments from 2 donors.

These data show that NKG2D/LFA1 co-ligation decreased the expression levels of both NKG2D and CD16, but only dramatically affected the proportion of cells expressing NKG2D. Whilst simultaneous exposure to anti-CD16 and ICAM1-Fc decreased both the proportion of cells expressing NKG2D and CD16 and the levels of expression, CD16 expression levels were decreased to a greater extent. This shows that CD16 ligation has a greater impact on NKG2D expression than the effect of NKG2D ligation on the CD16 expression. These findings are consistent with the

PFN secretion data, which demonstrated that CD16 ligation abrogated the ability of NKG2D to induce increased PFN secretion. However, flow cytometric analysis of pNK cells has shown that NKG2D expression is not severely affected by CD16 ligation. This suggests that a decrease in the ability of NK cells to secrete PFN may be attributable to intracellular signaling events, rather than receptor expression alone.

5.2.6 Estimation of perforin secretion by NK cells

To investigate the number of PFN proteins secreted by NK cells, bead populations with known densities of anti-murine IgG antibodies (antibody binding coefficient; ABC) were washed and incubated sequentially with an excess of murine anti-PFN antibodies, recombinant PFN and anti-PFN-488 antibodies. Beads were then imaged by confocal microscopy to determine the relationship between integrated intensity to number of molecules.

This was used to estimate the amounts of PFN secreted by NK cells. The data indicate that after 3 minutes of stimulation, NK cells had secreted 4500 ± 3000 molecules of PFN on MICA-Fc/ICAM1-Fc-coated slides and 2000 ± 1900 molecules on anti-CD16-coated slides. Upon stimulation by MICA-Fc/ICAM1-Fc or anti-CD16/ICAM1-Fc for 120 minutes, NK cells secreted a mean of 38500 ± 17100 or 36700 ± 12900 molecules of PFN respectively. Whilst these values are obtained from NK cells in contact with a slide in the absence of any inhibitory signals, they provide some indication as to the amount of PFN secreted by NK cells within the IS. As described in the methods, these numbers of molecules can be used to estimate the concentration of PFN within the synapse. Based on a volume of ~5 μm^3 containing ~5 fL of fluid, the following estimations of PFN concentration can be made. After a 3-minute stimulation, PFN concentration within the synapses was 0.6 ± 1.0 µM or 0.7 ± 0.6 µM on MICA-Fc- or anti-CD16-coated slides respectively. After 120 minutes, PFN concentration had increased to 13.0 ± 5.7 µM or 12.2 ± 4.3 µM on MICA-Fc- or anti-CD16-coated slides respectively.

However, these higher concentrations at 120 minutes would most likely not be reached within the synapse in a physiological setting, *i.e.* within a cell-cell conjugate rather than in response to contact with a slide, due to internalisation/endocytosis of PFN by the target cell. Vanherberghen *et al.* report that the majority of NK cell-mediated killing occurred within 10 minutes of conjugation (467). Therefore, it may be more physiologically relevant to determine the amounts and concentrations around this time point. The number of molecules of PFN secreted by 12 minutes on MICA-Fc or anti-CD16 was 10700 ± 7200 and 10000 ± 7000 molecules respectively. These amounts would give concentrations within the synapse of 3.6 ± 2.4 and 3.3 ± 2.2 μM respectively.

5.3 Discussion

5.3.1 Summary

The main objective of this study was to investigate the amount of PFN secreted by NK cells. Using ligand/integrin-coated slides, PFN secretion was investigated over time, in response to different activating ligands, different ligand densities and serial stimulation through the same or alternating ligands. Finally, the amount and concentration of PFN secreted into the synaptic cleft was estimated. The data indicate that NK cells are sensitive to the amount of ligand that they come into contact with and are affected by previous stimulations. Importantly, the activating receptor that is ligated can have profound effects on subsequent stimulations. The main results from this study are as follows:

- NK cells secrete PFN within 3 minutes of MICA-Fc or anti-CD16 exposure
- NK cell PFN secretion varies proportionately with ligand density
- Serial stimulation reduces the amount of PFN secreted by NK cells
- Ligation of CD16 following NKG2D-mediated PFN secretion can recover levels of PFN secretion after serial stimulation of NKG2D, whereas NKG2D ligation is unable to induce increased PFN secretion following CD16 ligation
- NK cells can secrete up to 10700 ± 7200 molecules of PFN into the synapse within 12 minutes of activation, the average time to kill, which correlates to a 3.6 ± 2.4 μM concentration within the synaptic cleft.

5.3.2 Implications of findings

The main purpose of this study was to quantify PFN secretion by NK cells, estimating the amount released following activation through either NKG2D or CD16. A protein capture assay was developed to image PFN secreted by NK cells. This comprised incubating pNK cells on slides coated with anti-PFN antibodies to capture secreted PFN. This was done in the presence of Fc-conjugated ICAM1 or MICA, or anti-CD16 bound to the surface of the well, to mimic exposure to adhesion molecules and activating ligands. PFN was then stained by fluorescently labelled anti-PFN antibodies and imaged by confocal microscopy. This assay could be used to assess the secretion of PFN in response to different ligands over time, with varying densities and following serial stimulation.

The results demonstrate that whilst MICA-Fc alone is insufficient to induce NK cell degranulation, anti-CD16 can trigger the secretion of PFN. These findings are consistent with previous studies by Bryceson *et al.*, demonstrating that ligation of NKG2D alone cannot trigger cell-mediated lysis of target cells, whereas CD16 ligation is sufficient (154). NK cells secreted PFN within 3 minutes following stimulation by either activating ligand, and secretion continued for up to 60 minutes. This suggests that the NK cell response to activation is rapid but can be sustained for a long period of time with continued signalling through either NKG2D or CD16. Furthermore, signalling through either NKG2D or CD16 was shown to be an analogue response, as opposed to an all-or-nothing binary response. The density of ligand that the cell came into contact with modulated the amount of PFN that was secreted. This was consistent with previous studies of murine NK cells showing that NK cell-mediated lysis is proportionate to expression levels of activating ligands on target cells (480).

The ability of NK cells to serially lyse targets has been shown previously (467), however, the effect that this has on PFN secretion had yet to be determined. Levels of PFN secretion decreased following serial activations with the same ligand. Unexpectedly, binding to anti-CD16 could recover PFN secretion when NK cells had been repeatedly stimulated with MICA-Fc, whereas NKG2D ligation after CD16 serial stimulation was unable to trigger an increase. Flow cytometric analysis of the

expression of NKG2D and CD16 after serial stimulations with slides coated with either MICA-Fc or anti-CD16 antibodies in the presence of ICAM1-Fc showed that co-ligation of either receptor along with LFA1 affects the expression of both NKG2D and CD16. CD16 ligation had a greater impact on NKG2D expression than NKG2D ligation had on CD16, but these changes do not account for the inability of NK cells to be sufficiently activated by MICA-Fc following anti-CD16 stimulation. This suggests that it is intracellular signalling following receptor ligation that may differ. Specifically, ligation of CD16 desensitised NK cells to further stimulation through either the same ligand or with MICA-Fc, whereas NKG2D ligation did not have this effect. Therefore, following a cytotoxic response to NKG2D ligands, NK cells remain highly sensitive to stimulation that induces ADCC, possibly through signalling pathways utilised by CD16 independently of NKG2D.

Finally, using beads of known antibody concentrations to sequentially capture anti-perforin antibodies, PFN protein and fluorescently labelled anti-PFN antibodies, the relationship between fluorescence intensity to number of molecules was determined. This was used to estimate the amount of PFN secreted by NK cells. Using the fluorescent intensities of labelled PFN at various time points, the results showed that at around 12 minutes after stimulation, the average time to kill a target cell (467), NK cells had secreted between 3.3 ± 2.2 μM and 3.6 ± 2.4 μM of PFN into the synaptic cleft.

The results of these studies show that NK cell PFN secretion is dependent not only on the ligation of receptors but, more importantly, the density and type of ligand. This indicates that NK cells are sensitive to the amount of ligand they encounter, as well as the type of cytotoxicity triggered through a specific ligand. Most importantly, these findings demonstrate that in order to modulate the NK cell response, through redirected lysis or ADCC, the consequences of NK cell receptor ligation should be considered in order to mediate the appropriate response.

NK cells require co-ligation of receptors for efficient degranulation

Secretion of PFN is a tightly regulated process. The binding to activating ligands is required in sufficient number in order to overcome inhibition. A balance in favour of phosphorylation over dephosphorylation of activating receptor-associated ITAMs, caused by inhibitory receptor ligation, is necessary to induce polarisation of LG to the synapse and the release of cytotoxic proteins (485). The assay used in this study was designed to enable the capture of PFN proteins in order to quantify the amounts secreted by NK cells in response to different conditions. The results have demonstrated the varying effects that ligands and ligand densities can have on PFN secretion.

Firstly, the Fc portions of the MICA and ICAM1 chimera proteins were shown to be unable to induce degranulation. To test this, NK cells were incubated on Noggin-Fc proteins, a negative control, as Noggin is not a ligand for NK cells. The lack of degranulation or a change in receptor expression profile indicates that the Fc proteins are insufficient, or unable, to bind CD16. Therefore, it can be assumed that these Fc portions do not have an effect on NK cell responses and that degranulation and changes in receptor profiles were due to ligation of the NK cell activating receptors CD16 and NKG2D, and/ or the adhesion molecule LFA1.

In contrast to data shown here, Bryceson *et al.* (154) demonstrated that co-ligation of CD16 and LFA1 reduced the degranulation of freshly isolated NK cells. Here, increased secretion of PFN was detected in response to CD16 and LFA-1 co-ligation (Figure 5.5). This difference may be due to the use of freshly isolated NK cells by Bryceson and colleagues, whereas the pNK cells used in the protein capture assays described here were IL-2-expanded and 6-day rested. This previous study also demonstrated that the co-ligation of NKG2D and 2B4 was sufficient to induce the degranulation of NK cells, independently of LFA-1 signalling. Therefore, the degranulation of NK cells – IL-2 activated or not – appears to require the co-ligation of at least 2 activating receptors against cell-expressed ligands, or CD16 ligation alone. The effect of LFA1 signalling increasing the amount of PFN secretion could be attributed to the activation and expansion of NK cells using IL-2. Previously, stimulation using this cytokine has been shown to upregulate a vast number of

transcriptional cytotoxic factors (486). The addition of IL-2 mimics the influence of this cytokine during an infection, where it effectively primes NK cells for attack against a pathogenic cell (virally-infected or transformed) (8). Despite the differences between this study and those performed using fresh NK cells, both suggest that NK cell cytotoxicity through 'cell surface-expressed ligands' requires signalling from more than one receptor. In addition, IL-2 activated cells appear more sensitive to activation and degranulation than freshly isolated cells. In conclusion, the initial results of this study show that activated NK cells require the co-ligation of LFA-1 and NKG2D to induce degranulation, whereas CD16 binding alone is sufficient.

Secretion of PFN occurs within 3 minutes of activation and continues for up to 60 minutes

Previous studies have shown that NK cell polarisation of the MTOC can take up to 30 minutes following cell-cell contact (173). However, NK cells have also been shown to rapidly degranulate without full MTOC polarisation, allowing for an extremely fast response to a pathogenic or transformed target cell within a matter of minutes (192). This may be a response that is accentuated during cytotoxicity to enhance the clearance of diseased cells, particularly transformed cells, where cytolysis versus proliferation is extremely important in the successful elimination of disease. The PFN secretion response of NK cells may therefore play a significant role in the early detection and elimination of viral infection or cellular transformation.

Activation and degranulation using the protein capture assay showed that NK cells were able to secrete PFN within 3 minutes, demonstrated by small spots of fluorescence signal on the capture assay slides. The size and intensity of the spots increased during the first 60 minutes, suggesting that NK cells secreted PFN up until this time point. Secretion of PFN for up to 60 minutes raises the question as to why NK cells can, or would, secrete PFN for such a long period of time. Immune cells have been shown to be extremely sensitive to surface tension (487, 488). A tension-sensitive system within NK cells may govern their continued secretion of PFN. During IS formation, the spreading and subsequent contraction of the membranes would result in a high tensile force between the cells (10, 489-491). Following secretion of cytotoxic mediators, apoptosis and breakdown of the target cell would release this

tension. NK cell sensing of this change may result in signals that initiate the detachment from the dying cell (492, 493). The high tensile forces resulting from NK cell binding to a coverglass may explain why NK cells continue to secrete PFN for up to 60 minutes. There is no release in tension, thus termination signaling does not occur, and the NK cell would not be instructed to detach. However, the reason for the cessation of secretion after 60 minutes is not known. Restimulation of NK cells, and the repeated secretion of PFN (albeit in decreasing amounts), demonstrated that arresting secretion is not due to a complete depletion of PFN stores. Therefore, there may exist a finite level of signalling, as opposed to continuous restimulation, that receptor ligation can induce, limiting the total amount of PFN that can be released by NK cells.

PFN secretion is dependent on ligand density

Exposure to higher densities of activating ligands induced increased PFN secretion by NK cells, compared to those exposed to low density of ligands. This finding suggests that the number of ligands bound by NK cells directly affects the amount of PFN secreted, possibly a result of enhanced intracellular signalling. This type of secretion is termed analogue, where the response is metered by the amount of signal, as opposed to a digital on/off system, which is all-or-nothing.

Such a metered response by a cytotoxic cell was not expected. The decision to kill a target cell, determined by a balance of signals in favour of activation, must be carefully tuned so that the correct response is initiated. The release of PFN in response to a small number of ligands could have dangerous consequences, should healthy cells express such self-ligands. However, an analogue NK cell response has been demonstrated with *ex vivo* murine NK cells. Cytotoxicity release assays have shown that the level of expression of activating ligands on a target cell is directly proportional to the amount of cytotoxicity mediated by NK cells (480). Furthermore, NK cells secrete greater amounts of IFNγ in response to higher concentrations of bacterial antigen (494, 495). Recent work also suggests that this response occurs with increasing concentrations of plate-bound MICA (personal communication; Kathryn Lagrue, unpublished data). Thus, the density-dependent secretion of NK

cells shown here, suggests that a metered response may play an important role in PFN secretion.

This analogue response could have advantages for both low and high ligand densities and/or surface expression of receptors. Whilst stress-induced ligands, such as MICA/B, are upregulated on virally infected or transformed cells (496-498), it has been shown that some types of normal, healthy cells express low levels of activating ligand mRNA transcripts or proteins (499). Reduced responses to lower ligand densities may be a mechanism used to prevent the erroneous secretion of PFN onto otherwise healthy cells, or perhaps release only a small amount of PFN that is sub-lytic, which the target cell can survive. The balance of signals on these healthy targets will also be in favour of inhibition, yet the dynamic regulation of PFN secretion may provide some further protection against collateral damage. Furthermore, the presence of inhibitory ligands can also meter the NK cell cytotoxic response (480), indicating that the effect inhibitory signals have on PFN secretion is of important consideration for future investigation.

Ligand density-dependent secretion of PFN may also have a negative impact on control of tumour growth. Tumour cells are known to upregulate activating ligands in the event of initial transformation (496). However, selective pressure from the immune system directs their ‘evolution’ to subsequently downregulate such surface proteins to evade detection (483, 500-502). The downregulation of activating ligands on tumour cell surfaces would have a negative impact on PFN secretion, resulting in the secretion of sub-lytic amounts of PFN, which fail to lyse the target cell. Evasion by this means would result in the expansion of a colony of reduced-ligand bearing cells, allowing immune escape and excessive proliferation of tumour tissue.

Evidence from studies assessing cytolysis of tumour cells that have downregulated stress-induced ligands have demonstrated a reduced susceptibility to NK cell-mediated lysis (480, 482). However, there have been no direct investigations addressing the effect of ligand density on the amount of PFN secreted by NK cells, or other CTL. Therefore, one outcome of density-dependent ligand binding by NK cells may be the modulation of PFN secretion. Whilst this study did not dissect the mechanisms of increased PFN release in response to greater ligand density, the

evidence that PFN secretion varies with the density of activating ligand illustrates that pharmacological modulation of NK cell activity should consider this phenomenon.

NK cells secrete less PFN following serial stimulations

Serial activation of NK cells, through either NKG2D or CD16, resulted in decreased ability to secrete PFN. This data may suggest that the ligation of an activating receptor initiates the release of a percentage of total PFN. However, an alternative interpretation of this finding is a loss of sensitivity to that ligand, possibly through internalisation and downregulation of its receptor (484).

A number of techniques have been used to demonstrate that NK cells are able to serially kill targets. These include single-cell imaging and chromium release assays using an excess of target cells (465-467). It has been reported that certain subsets of NK cells possess the ability to sequentially lyse more than one target. A study by Choi *et al.*, showed that NK cells are able to kill up to 14 target cells over a period of 6 hours, but that initial kills are slower – especially with 'poor' targets. Data shown in this chapter suggest that NK cells secrete less PFN with serial stimulations. The experiments performed by Choi *et al.* were run over a course of 6 hours, with time between kills up to 20 minutes, potentially allowing for the recovery of NK cells. The diminished ability to kill, shown by various groups, and the decrease in PFN secretion shown here, may be a response mechanism to re-stimulation. This response may be employed to prevent lysis of healthy host cells unnecessarily. This mechanism could be facilitated by the downregulation, or internalisation, of activating receptors, following ligation (484). Indeed, both soluble and cell-bound ligands have been shown to induce downregulation of activating receptor expression (483, 503). NKG2D on the NK cell surface is internalised and degraded in response to soluble or cell-surface MIC proteins (504), and ligation of CD16 has shown to cause degradation or shedding of the bound receptor (505).

The data presented here, along with previously published data, suggest that serial ligation of receptors negatively impact NK cell-mediated lysis. Desensitisation to a specific ligand, potentially mediated by receptor internalisation, will render NK cells unresponsive to other target cells expressing this ligand. Whilst this could represent a

protective mechanism to avoid aberrant lysis of healthy cells, the reduced secretion of PFN and resulting decrease in lytic capacity, may have the undesirable consequence of unchecked growth and development of tumour cells, or persistent viral infections *in vivo*.

NK cell desensitisation to further stimulation is ligand-dependent

Serial activation of NK cells using the same ligand reduced the amount of PFN secreted upon repeated stimulation. However, PFN secretion increased following stimulation via CD16, following serial ligation of NKG2D. However, this restimulation could not be achieved when CD16 was ligated first. This demonstrated that decreased NK cell-mediated lysis was not due to a depletion of PFN stores, contradictory to the mechanism suggested by other studies (466). Findings described here suggest that repeated activation through the same receptor leads to desensitisation to that particular ligand, rather than a depletion of PFN stores, particularly during initial serial killing. Furthermore, the response of NK cells to specific ligands differs, depending on the type of response – ligation of 'natural' cell-expressed ligands or induction of ADCC. Therefore, the specific receptor ligated by NK cells to mediate cytolysis may play a significant, and previously unappreciated, role. This is an NK cell-mediated response that should be considered if/when developing therapies to target activating receptors to enhance NK cell function.

Ligation of activating receptors on NK cells leads to a signalling cascade, ultimately causing degranulation (506). NKG2D and CD16, whilst both activating receptors, signal through different pathways, albeit converging to the same MAPK signalling events. The main differences between NKG2D and CD16 signalling are within initial stages. NKG2D associates with DAP10, whereas CD16 associates with CD3ζ and FcRγ (122). Importantly, NKG2D signalling is independent of Syk-family protein tyrosine kinases (146, 507) and is associated with signalling through Grb2/Vav1, whereas CD16 signals through Syk, ZAP70, and Vav2/3 (152, 508). Both of these signalling pathways eventually converge to Rac (509). The different signalling pathways employed by these receptors may therefore result in the overall desensitisation of NK cells by CD16 signalling, whilst downstream signalling following NKG2D ligation may not have the same impact on receptor expression. Potentially,

the lack of Syk-associated signalling may explain why NK cells can be activated through both NKG2D and then CD16 serially, whereas CD16 ligation prior to NKG2D may desensitise NK cells to both receptors. Therefore, CD16 ligation may affect NKG2D expression, possibly through inducing receptor internalisation, or by signalling through pathways independent of NKG2D signalling.

The re-stimulation of NK cells following receptor ligation is not exclusively dependent on receptor expression

The flow cytometric analysis of NK cell populations showed that upon serial stimulation, NKG2D and CD16 expression decreased. The identification and characterisation of NK cell 'serial killers' by Vanherbergen *et al.* show that a small number were responsible for a significant amount of killing (467). Whilst no phenotypic analysis was performed in that study, the serial killing phenotype may be attributed to the expression of cell surface receptors, or previous contact with other cells. In their study, Vanherbergen *et al.* showed that a very small number of cells (2%) were able to serially kill up to 7 target cells, whereas the majority of NK cells could lyse at least 1 target cell. This is in parallel with the findings presented here, demonstrating a decrease in the population of cells expressing either receptor following serial stimulation, suggesting that ligation has an effect on the ability of NK cells to lyse a subsequent target. Regardless of the ligands ligated, the results of the study investigating PFN secretion showed that by the fourth hit, PFN levels were massively reduced. This was not due to cell viability during the assays, as forward scatter/side scatter plots showed the majority of cells were viable (data not shown). In this study, both NKG2D and CD16 ligation severely affected both the proportion of cells expressing NKG2D and the level of expression on the cell surface. This is in agreement with the serial killer characterisation by Vanherberghen *et al*. Reduced function may be due to the expression profiles of the individual NK cell, as a result of previous cell-cell interactions. Those cells expressing a higher density of receptors may be able to respond more efficiently to ligation of receptors, whilst also being able to more efficiently serially lyse target cells. It would be extremely interesting, using the microwell system employed by Vanherberghen *et al*., to investigate whether the addition of antibodies to trigger ADCC part way through the time course improved serial target cell lysis. This would begin to establish the relationship between serial

killing and the ligands ligated, and more importantly, whether this has a direct physiological effect on the ability of NK cells to serially lyse targets.

The flow cytometric analysis of NK cell receptor expression does not explain the severe abrogation of PFN secretion through NKG2D stimulation following anti-CD16 exposure. As discussed above, this effect could be due to differences in the intracellular signalling pathways employed by NKG2D and CD16. In support of this theory, Syk-/- ZAP70-/- murine NK calls are able to lyse targets through NKG2D, but not ADCC (507). Conversely, PLCγ has been shown to be critical for natural cytotoxicity (510-512), but dispensable in ADCC (513). Whilst the cytolytic capacity of NK cells has been addressed through pharmacological inhibition or gene KO, the involvement of signalling pathways in serial activation is yet to be addressed. Data presented here suggest that, following activation of NK cells through natural ligands or ADCC, there may be cross talk between signalling pathways. Unfortunately, the dissection of these pathways was beyond the scope of this thesis. Further investigation will uncover the roles that both natural cytotoxicity and ADCC can play in mediating and maintaining NK cell serial lysis.

The ability of NK cells to secrete increased amounts of PFN in response to anti-CD16 after NKG2D ligation highlights the advantages of antibody-based therapies aimed at improving an NK cell lytic response to infection or transformation. This could be through either redirected lysis or the opsonisation of specific cells. The data here demonstrate that NK cell degranulation is markedly increased with CD16 ligation following serial activation through NKG2D. Therefore, as most transformed or virally infected cells would express ligands for the natural cytotoxicity receptors, these targets could be opsonised with IgG antibodies against proteins expressed specifically on their surface. Ligation of the NK cell Fc-receptor CD16 may increase degranulation, improving the clearance of transformed or virally infected cells.

Estimation of perforin secretion

Estimation of the amounts of PFN using the mean integrated intensities from the protein capture assays showed that NK cells secreted up to 38500 ± 17100 molecules of PFN. The number of molecules was then used to estimate the concentration of PFN within the synapse. The results indicate that the concentration of PFN within the synapse would be 13.0 ± 5.7 μM. More physiologically relevant, the amount of PFN secreted after 12 minutes of stimulation, the modal time for NK cells to kill (467), was 10700 ± 7200 and 10000 ± 7000 molecules on MICA-Fc- or anti-CD16-coated slides respectively, which give theoretical concentrations within the synapse of 3.6 ± 2.4 and 3.3 ± 2.2 μM.

Whilst the quantification of PFN secreted at the IS has not been investigated before, the effect of PFN in solution at various concentrations has been addressed by other groups. Keefe *et al.* and Voskoboinik *et al.* directly investigated the effects of soluble PFN on U937 cells (a lung lymphoblast cell line) and erythrocytes, respectively (248, 261). These studies show conflicting results, with 50% lysis triggered by either 5 μM (Keefe) or 0.175 μM (Voskoboinik) of PFN – a 29-fold difference. Whilst the sources of PFN differed for each study (Keefe *et al.* isolated PFN from rat NK cells whereas Voskoboinik *et al*. expressed recombinant PFN in insect cells), it was unexpected that the reported concentrations of PFN required for 50% lysis differed so greatly. The difference between isolated and recombinant PFN may have different effects on the lysis of target cells, and indeed, different target cells may require different concentrations of PFN to initiate cytolysis – possibly depending on their surface receptor expression. In addition, PFN has been shown to be extremely sensitive to the concentration of calcium ions and pH within medium (248, 255, 291, 514-516) and therefore, slight differences in experimental conditions may be the cause of the conflicting results.

In summary, these data have begun to address the physiological amounts of PFN secreted by NK cells. Whilst these data are only estimations, the reported concentrations at critical time points during NK cell effector function are in agreement with previous studies. However, these amounts will vary depending on the receptors ligated, both number and, most likely, the combination. Therefore, further development of this assay would enable a more accurate quantification of PFN secretion by NK cells.

Chapter 6 – Discussion and Conclusions

6.1 Overview

The ability of NK cells to recognise and lyse virally infected and transformed cells is integral to the body's defense against disease. These effector functions are tightly controlled through a structured cell-cell interaction, the IS. Ligation of a dense accumulation of activating and inhibitory receptors, coupled with integrins, trigger a balance of signals towards either activation or inhibition of NK cell-mediated cytolysis. A balance in favour of activation induces NK cell polarisation and secretion of cytotoxic mediators, including PFN and Gzms. A relatively unexplored function of the IS is to form a gasket, or seal, around its secretory domains. The structure of the IS, including dense protein-protein complexes, close membrane proximation and inter-digitation, may contribute to forming this barrier, which may function to prevent both the leakage of secreted proteins and the access of extracellular molecules.

Using fluorescently labelled molecules of nanometer-scale diameters, this study revealed that the IS does not function as a gasket *per se*, but rather excludes molecules above a size threshold. This barrier excludes larger functional proteins, including mAb and LDL, preventing access into the synaptic cleft. Molecules that are below the size exclusion threshold, such as dAb, are able to access the synapse. These could be engineered to target proteins directionally secreted across the synapse. Unexpectedly, time-lapse imaging revealed that molecules above the size exclusion threshold were actively cleared from the cell-cell or cell-slide interface during synapse assembly. This suggests a role of IS assembly, including the spreading response coupled with receptor ligation, to move larger extracellular proteins from the synaptic cleft. These data demonstrate that antibody-based therapies targeting directly secreted proteins within the synapse must be engineered below the size threshold identified here to avoid clearance and exclusion from the synapse.

PFN secretion by NK cells is critical for mediating cytolysis. However, the amount released by NK cells had not yet been investigated or quantified. A protein-capture assay, activating NK cells on varied ligand densities, revealed that NK cell signalling appears to be an analogue-based system. In addition, the number of times receptors had previously been stimulated directly affected NK cell PFN secretion. Estimation of the amount of PFN secreted at the synapse revealed that after 12 minutes stimulation, the typical time taken for an NK cell to lyse its target, around 10000 molecules of PFN had been released. This was estimated to be a 3.5 μM concentration of PFN within the synaptic cleft. Previous studies have demonstrated serial target lysis mediated by NK cells. Whilst the efficiency of cytolysis decreases with increased frequencies of serial lysis, the effect this has on PFN secretion is unknown. It is shown here that serial stimulation rendered NK cells refractory to further engagement with the same ligand. However, following NKG2D ligation, stimulation through CD16 was able to trigger PFN secretion similar to their initial activation. NKG2D ligation following stimulation through CD16 was, however, unable to trigger the same response.

In summary, this investigation has revealed that the NK cell IS acts as a physical barrier to extracellular molecules above a size threshold, and that PFN secretion at the IS is a result of analogue signalling, dependent on ligand densities and influenced by previous exposure to activating ligands.

6.2 The immune synapse clears and excludes extracellular molecules in a size-dependent manner

Formation of an IS and subsequent activating or inhibitory signalling is critical in regulating host defense against pathogens and transformed cells, whilst preventing the lysis of healthy cells. The ability to exclude molecules above a size threshold, coupled with the clearance of larger molecules during synapse assembly, demonstrates that the process of IS formation, and the resulting dimensions of the synaptic cleft, have a direct effect on molecules in the extracellular environment.

F-actin reorganisation at the synapse facilitates the effector cell spreading response. The accumulation of receptors, with an underlying F-actin scaffold, at the IS has been demonstrated by a number of groups (13, 18, 66, 410, 517). The data show that the structure of the F-actin scaffold at the synapse is critical in excluding dextran. In contrast, further reorganisation after synapse formation is not required. The movement of the NK cell, over a target cell or activating surface, cleared larger molecules from the interface. This is most likely due to the formation of receptor-ligand constructs that are smaller than excluded molecules. High-resolution TIRF imaging demonstrated that this occurs as the synapse forms in a zipper-like manner, excluding larger dextran following the cell spreading response, from the central region of the synapse towards the periphery.

The dense accumulation of complexes, including both activating, inhibitory and integrin receptor-ligand pairs, is required to facilitate an appropriate response from the NK cell. Prior to this work, the hypothesis that the IS functions as a gasket (366, 367, 518, 519) had not been directly tested. Studies detailed here indicate that the formation and inter-membrane span of the IS should be considered when designing therapeutics to access the IS. Any potential therapy should be engineered below the size thresholds identified here to avoid clearance and to facilitate access to directionally secreted proteins.

Initial analysis and quantification of dextran within the synapse addressed the ability of differently sized molecules to enter the IS. The most significant caveat to the investigation was the varying solubility and degrees of labelling of the dextrans –

larger dextrans had lower solubility with increased labelling densities – which could influence quantification. Varying microscope settings were used to optimise the visualisation of differently sized dextran at the IS. These differences in settings had the potential to introduce artefacts when quantifying dextran concentration. To rule out any artifactual bias, conjugates were imaged with increasing concentrations of dextran or mixtures of labelled and unlabelled dextrans to dilute their fluorescence intensities. This meant that the same settings on the microscope could be used to image dextrans of significantly different sizes (Figure 3.5 and 3.6). Neither varying dextran concentration nor reducing fluorescence intensity by addition of unlabelled dextrans affected the quantification of molecule access into the IS. Therefore, whilst the IS is able to restrict the access of dextrans into the synaptic cleft, this occurs in a size-dependent manner, irrespective of dextran concentration or labelling density.

Dextrans sized 3 – 13 nm were able to access the synapse, with the increase in size determining the extent dextran was able to enter the synapse. Dextrans sized 32 and 54 nm were completely excluded from the pNK cell synapses. Dextran fluorescence intensity was measured across the solution, cell bodies and synapse. The mean raw intensity profiles demonstrate that dextrans that access the synapse have a peak in intensity over background across the synaptic cleft. This decreased with increasing dextran size (Figure 3.1B and 3.3B). Similar findings were obtained for conjugates formed by the NK cell line YTS or pNK cells with 221 targets, suggesting that the IS excludes dextrans in a size-dependent manner (Figure 6.1). To further demonstrate that the synapse functions as a size-dependent barrier, rather than a gasket, dextran was shown to be able to either equilibrate within the synapse or be washed out completely (Figure 3.7 and 3.17 – 3.19). If a true gasket were formed, dextran would neither be able to equilibrate nor be washed out from the synapse.

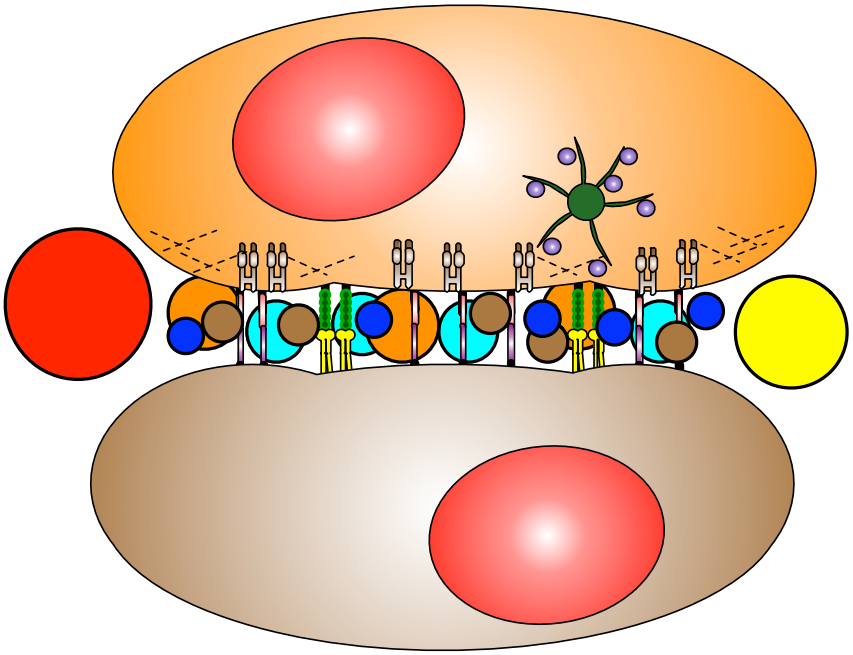


Figure 6.1. NK cell size-dependent exclusion of dextran molecules of various sizes from the activating immune synapse. The activating NK cell immune synapse forms following the ligation of integrin (yellow/green) and activating (red/purple) receptor-ligand complexes. This results in the spreading of the NK cell membrane that clears molecules above a size threshold from the synaptic cleft. The exclusion of dextran is determined by the maintenance of F-actin (dashed lines) at the synapse and the span of the various receptor-ligand complexes that accumulate at the cell-cell interface. Dextrans sized 54 nm (red) and 32nm (yellow) are largely excluded, whereas those 13 nm (orange), 10 nm (turquoise), 4 nm (brown) and 3 nm (blue) are able to access the synapse, where penetration increases with decreasing dextran size. Diagram not to scale.

The similar size of the TCR and NK cell activating receptors (208, 211) may explain a comparable size threshold for T cell and NK cell synapses. The exclusion of serum proteins such as LDL would be beneficial for $CD8^+$ cytotoxic T cells that, like NK cells, directly secrete cytotoxic proteins to lyse diseased cells (520, 521). The interaction of a $CD4^+$ T cell and APC, is the site of directed secretion of cytokines (19). Whilst the NK cell may function to prevent the leakage of cytotoxic proteins, the cytokine IFNγ (shown to be ~6 nm in their longest dimensions (522)) was shown to leak from the CD8+ T cell synapse formed with an antigenic target cell (523). This may provide a paracrine, dose-dependent response to surrounding cells following the activation of a single T cell. In addition, a study by Perona-Wright and Mohrs in murine infection with the Th2-inducing gastrointestinal helminth *Heligmosomoides polygyrus* demonstrated a polarised response throughout the entire draining lymph node (LN) (524). Whilst IFNγ production within the LN is localised primarily to the T cell-APC synapse, this study found that during *H. polygyrus* infection, the majority of T cells within the LN were activated. This was confirmed by microscopy studies,

demonstrating the directional secretion of IFNγ, but multidirectional secretion of IL-4. Whilst not considered in this study, the leakage of such cytokines from the T cell synapse, as shown by Sanderson *et al.*, may explain how the activation of a single T cell can have a paracrine, as opposed to local, effect. However, close membrane proximities, due to the dimensions of the extracellular domains of the receptor-ligand complexes, will exclude larger proteins from the T cell synapse. As a result, the T cell IS will exclude larger serum proteins. This may be to provide both a greater concentration of cytokines or cytotoxic mediators within the synapse to elicit as potent a response as possible.

Dextran was actively cleared from the cell-cell or cell-slide interface (Figure 3.29 – 3.31). The data suggest that the NK cell spreading response (123, 213), an integrin-mediated force that pushes the NK cell outwards from its contact point, physically clears molecules that are above the size exclusion threshold. The TIRF microscopy of synapse formation in the presence of both 4 nm and 32 nm dextran demonstrated this clearly. The accumulation of dextran within the cell-slide interface at early time points, only to be pushed out of the central region of the synapse, suggests that the synapse forms in a zipper-like manner. This spreading may be dependent on integrin ligation and preceded by the ligation of activating receptors, which enable the clearance of the larger dextran after an initial lag period (Figure 6.4). This suggests that it is later signalling events that initiate the clearance of larger dextran from the interface. Consistent with the kinetic segregation model (213), the clearance of larger molecules may depend on bending of the membrane, minimizing the energy required at the synapse. This idea is consistent with previous studies demonstrating that receptors (124) or large particles bound to the NK cell membrane (189) are segregated according to size. Whilst these proteins require reorganisation at the cell-cell interface, extracellular molecules can be physically cleared from the synapse to prevent expenditure of energy at the synapse. Therefore, the cell spreading response, coupled with receptor ligation on a dense F-actin scaffold, may provide a force to remove large molecules from the synaptic cleft (Figure 6.2).

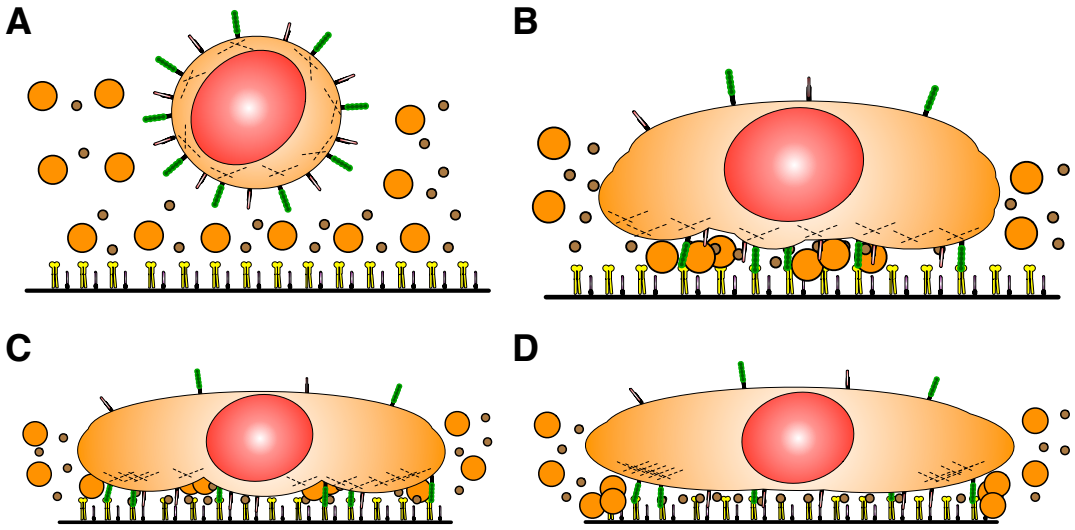


Figure 6.2. The NK cell activating immune synapse clears and excludes larger molecules during cell spreading and assembly. NK cell immune synapse formation clears larger 32 nm dextran from the synapse in a zipper-like fashion. (**A**) Prior to NK cell contact with the slide, NKG2D (purple) and LFA1 (green) are not engaged with MICA (pink) or ICAM1 (yellow) and both 4 nm dextran (brown) and 32 nm dextran (orange) are homogenous throughout the solution. (**B**) After initial contact, both 4 nm and 32 nm dextran intensities are decreased as some dextran is pushed from the cell-slide interface as initial ICAM1-LFA1 receptor-ligand complexes form. (**C**) Following initial contact, the NK cell spreads on the slide, creating more ICAM1-LFA1 complexes, collecting the larger dextrans into areas of wider span between the slide and the cell membrane. Soon after spreading, NKG2D receptors begin ligating their ligand, MICA, resulting in increased removal of 32 nm dextran from the synapse. (**D**) As further NKG2D receptors engage their ligands, this results in a wave outwards from the central region of the synapse, clearing the larger 32 nm dextran from the synapse, in a zipper-like manner, until only the 4 nm dextran remains within the cleft and the 32 nm dextran are excluded form the interface.

Functional and therapeutic implications of size-dependent exclusion at the synapse

The co-incubation of fluorescently labelled antibodies or LDL with effector-target conjugates showed that these too are subject to size discrimination regarding their access to the synapse. Importantly, mAb were almost completely excluded from the pNK synapse, whereas smaller antibodies, $F(ab')_2$ fragments and dAb, could be found in the synaptic cleft (Figure 6.3). These data show that size is important for therapeutic antibody access to the IS, in agreement with previous anecdotal evidence demonstrating their inability to block secreted proteins, such as PFN or IL-18 (366, 367). For this reason, antibody-based therapeutics designed to access the synapse must be engineered within these size constraints in order to target directionally secreted proteins. For instance, the blockade of PFN during cell-mediated destruction of pancreatic tissue in type I DM may reduce or prevent the loss of β cells within the islets of Langerhans. Additionally, previous work by Perona-

Wright and Mohrs (524), described above, demonstrated a polarised LN phenotype orchestrated by IFNγ, despite its directional secretion into the synapse. In this setting, dAb targeted against IFNγ may be able to block the intercellular secretion of IFNγ, whereas mAb would only serve to inhibit the cytokines that leak from the synapse. This may enable to inhibition of the response in all cells within a tissue, including those where cytokines are directionally secreted into the synaptic cleft.

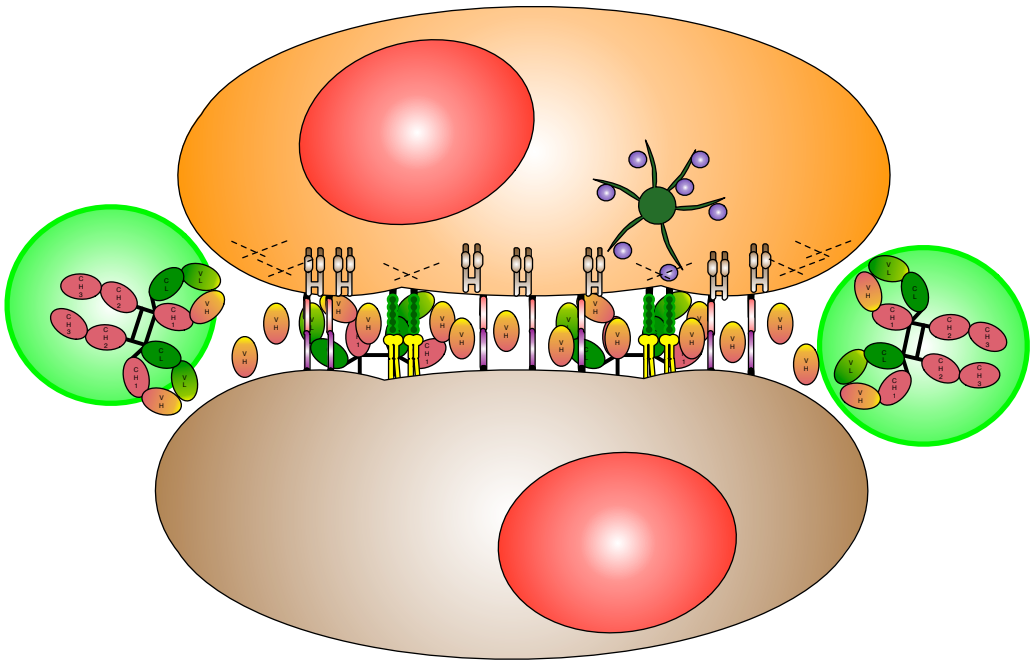


Figure 6.3. NK cell size-dependent exclusion of proteins of various sizes from the activating immune synapse. The activating NK cell immune synapse forms following the ligation of integrin (yellow/green) and activating (red/purple) receptor-ligand complexes. This results in the spreading of the NK cell membrane that clears molecules above a size threshold from the synaptic cleft. The exclusion of dextran is determined by the maintenance of F-actin (dashed lines) at the synapse and the span of the various receptor-ligand complexes that accumulate at the cell-cell interface. Low-density lipoproteins [~24 nm diameter] (green) and immunoglobulin G antibodies [~16 nm diameter] (pink, yellow and green) are excluded from the synapse, whereas $F(ab')_2$ fragments [~9 nm diameter] (pink and green), and to a larger extent domain antibodies [~4 nm diameter] (pink and yellow), are able to access the synaptic cleft. Diagram not to scale.

The exclusion of LDL from the synapse suggests a physiologically relevant role of molecular clearance and exclusion from the synaptic cleft. Previously, LDL has been shown to inhibit the pore-formation of PFN (449, 450). The lipid components of LDL bind to PFN, preventing both membrane insertion and oligomerisation. This has a negative impact on the cytolytic capacity of PFN. Therefore, inclusion of LDL within the IS could inhibit the ability of PFN to puncture the target cell membrane. Therefore, it is possible that clearance and exclusion of LDL from the IS protects PFN secreted across the synapse. LDL was able to access the YTS cell IS to a

greater extent than the synapse formed with target cells and pNK. It is likely that the access of LDL to the YTS synapse could reduce the lytic capacity of these cells, although this is yet to be directly tested. Unlike pNK cells, YTS express fewer activating receptors, which may alter the functional dimensions of the synaptic cleft. Indeed, this was demonstrated by the fact that 32 nm dextran was entirely excluded from the IS of pNK cells (Figure 3.3), but could still be found, to some degree, in the target cell interface with YTS cells (Figure 3.1).

The size threshold of the synapse is consistent with previous measurements of intercellular spaces and receptor-ligand crystal structures at the IS (65, 189, 208, 211, 357). The membrane spacing between an effector and target cell have been shown to be 10 – 30 nm, with some areas of larger span to accommodate larger integrin receptor-ligand complexes, up to 40 – 55 nm. Another possible explanation for the difference in size thresholds of YTS and pNK cells is variation in the density, rather than size, of activating receptors utilised by these cells. YTS cells use the co-stimulatory receptor CD28 as the only activating receptor, hence they are only able to efficiently lyse the target cell line 221 through CD80/86 ligation (20). In contrast, pNK cells possess a range of activating receptors (118), which may be paramount in the establishment of a tight and size restrictive interface/structure. The dense accumulation of these receptors, may create a more selective barrier around the IS. Despite these structural differences in IS formation, dextrans sized 3 or 4 nm and dAb (sized 4 nm in their longest dimension) accessed both the YTS and pNK IS to the greatest extent, demonstrating that molecules of this size are able to freely penetrate the synaptic cleft.

Monoclonal antibodies are unable to access the synapse, and therefore would be unable to block secreted proteins. Therapeutically, this suggests that dAb, and to some extent $F(ab')_2$ fragments, could be administered to bind cytotoxic proteins and/or cytokines secreted at the synapse. It has been demonstrated here that the access of antibodies into the synapse is dependent on physical dimensions. This provides direct evidence as to why previous experiments have failed to block directionally secreted proteins. Importantly, dAb administered as a therapeutic could be used to inhibit aberrant cytolysis or directed cytokine secretion across synapses (Figure 6.4). Furthermore, the evidence that not only NK cells but also T cells are able to exclude molecules above this threshold demonstrates that therapeutics could

be developed to target not only proteins secreted at the NK cell synapse, but also those at the T cell synapse, including cytotoxic proteins and cytokines.

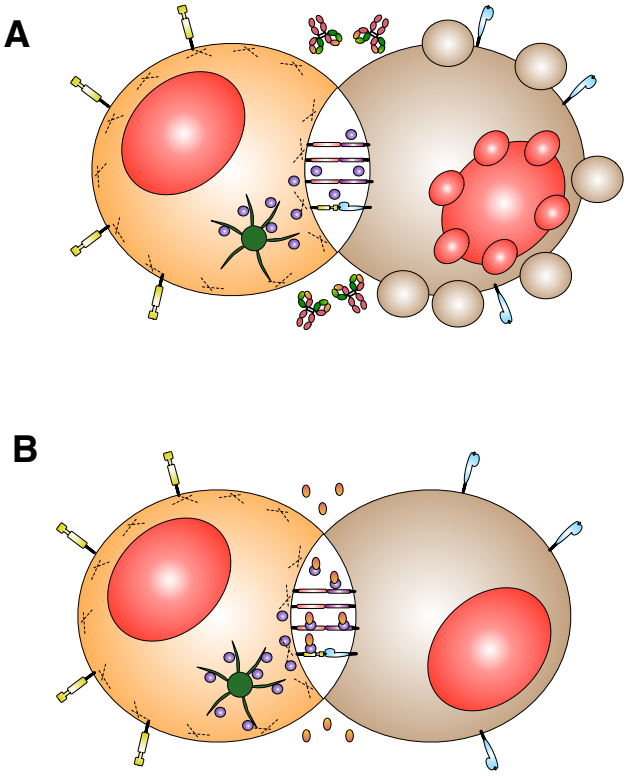


Figure 6.4. Domain antibodies can access the immune synapse and could be used to target proteins secreted across the synaptic cleft. (**A**) Immunoglobulin G antibodies are excluded from the synapse due to their dimensions. As a result, they cannot access directly secreted proteins and have no effect on NK cell effector functions. (**B**) Domain antibodies fall below the size exclusion threshold and the immune synapse and can therefore access the synaptic cleft. Domain antibodies against directionally secreted proteins, such as perforin, would potentially be able to access the regions where they are secreted and block their cytolytic action. Diagram not to scale.

The inhibitory immune synapse does not exclude extracellular molecules

The inhibitory NK cell IS does not result in the secretion of proteins – signalling or cytolytic (9). Therefore, the synaptic penetration of dextran suggests that the retention of secreted proteins or the exclusion of extracellular molecules does not occur at the inhibitory synapse. Despite the similar size of the extracellular domains of inhibitory and activating receptors (83, 84, 124, 210), inhibitory synapses were unable to exclude molecules of any size. Therefore, the clearance and exclusion of extracellular molecules is specific to the activating synapse.

Previous studies have demonstrated that the inhibitory synapse forms asymmetrically without the accumulation of F-actin, as opposed to the F-actin dense, symmetrical structure of the activating synapse (123). Receptors, such as LFA-1, are anchored to F-actin, which accumulates at the activating synapse, for stabilization of the IS structure during sustained signalling. In contrast, signalling at the inhibitory synapse inhibits focal adhesions and lacks this structural integrity (70, 416). This is likely to be the major determining factor in the exclusion of extracellular molecules. As the NK cell contacts its target, the lack of activation may result in little or no spreading and no clearance of dextran from the inhibitory synapse, this could be tested directly using the cell-spreading assay. This theory is supported by the dependency on actin for exclusion of larger dextrans from the activating synapse, demonstrated by actin depolymerisation during effector-target conjugation (Figure 3.25 – 3.29). Whilst actin integrity is required to exclude dextran, the stabilisation of F-actin filaments following synapse formation has no impact on the exclusion of dextran. Therefore, the initial reorganisation of F-actin, not seen in inhibitory synapses, along with cell spreading, are likely to be required to clear dextran. Without these structural changes, molecules remain within the cleft.

6.3 The amount of perforin secreted at the immune synapse is ligand type- and density-dependent

Whilst the mechanisms of PFN secretion have been studied in depth, the effects of different activating signals and repeated stimulation of NK cells on PFN secretion has not yet been directly investigated. NK cell activation is thought to be a binary, or digital, process (476). Whilst a threshold of activating signalling over inhibitory signalling is required for activation of NK cells, once this threshold is reached, it is assumed that NK cells secrete a pre-determined ‘payload’ of cytotoxic proteins towards the target cell (525). Data described here establish that NK cell responses, mediated by the ligation of activating receptors, induces an analogue, metered response, that determine the amount of PFN secreted. In addition, using confocal microscopy of captured proteins, the amounts and concentrations of PFN within the synaptic cleft were estimated for the first time.

Within 3 minutes of exposure to NKG2D or CD16 ligands, in the presence of adhesion molecules, NK cells began to degranulate, evidenced by the presence of PFN spots on the capture assay slide. Indeed, these spots were not as frequent as when cells were incubated for ≥30 minutes, indicating that not all NK cell degranulate this rapidly. This highlights that within a population of NK cells, there exists only a subset that are capable of rapid responses to the ligation of receptors tested here, NKG2D and CD16. This subset may provide an immediate response to a pathogenic agent or transformed cell. Indeed, this response may be faster, or slower, following ligation of other activating receptors not tested in this study. This phenotype may be determined by a specific receptor expression repertoire, gene expression and/or previous encounters with other regulatory or target cells. The phenotypes of NK cell populations, or that of a clonal expansion from a single NK cell, could be assessed prior to the protein capture assay. Determining the PFN secretion kinetics with this information could be correlated to determine the expression profiles that predispose NK cells to a more rapid response. In this study, PFN secretion was initially greater in response to MICA than anti-CD16. However, within 60 minutes, NK cells had secreted similar amounts of PFN on either ligand. This suggests that whilst the initial signalling pathways downstream of NKG2D and CD16 induce different amounts of PFN secretion, activation over a longer period of time results in similar levels of secretion. This may be due to the availability of NKG2D receptors on the NK cell surface, the distribution of signalling proteins within the NK cells or simply the evolution of these pathways that have benefited from a more rapid and greater production of PFN in response to NKG2D stimulation, compared to CD16. Further elucidation of these factors, in relation to secretion kinetics, would further develop our understanding of NK cell PFN secretion.

The amount of perforin secreted is dependent on ligand density

The balance of activating versus inhibitory signalling enables an NK cell to discriminate between healthy and diseased cells (526). Whilst this balance of signals requires a threshold above inhibition in favour of activation to initiate cell-mediated lysis (11, 77, 123), any the effects of further activating receptor ligation have not been addressed. NK cell PFN secretion has previously been described as binary, where an activating signalling threshold is required to initiate cytolysis (525). Indeed, a binary system to initiate NK cell lysis would provide a protective mechanism that

would protect autologous cells from aberrant lysis following the expression of low numbers of ligand on otherwise healthy cells. The data presented here are contradictory to this hypothesis, suggesting that PFN secretion is in fact analogue and can be controlled by ligand density. The data suggest that NK cell signalling is governed by the amount of ligand a cell interacts with. This has functional consequences, with a direct effect on the amount of PFN secreted (Figure 5.4 and 5.5). Analogue signalling allows a metered response to a stimulus, determined by either the amount of receptor expressed or ligand available (Figure 6.5).

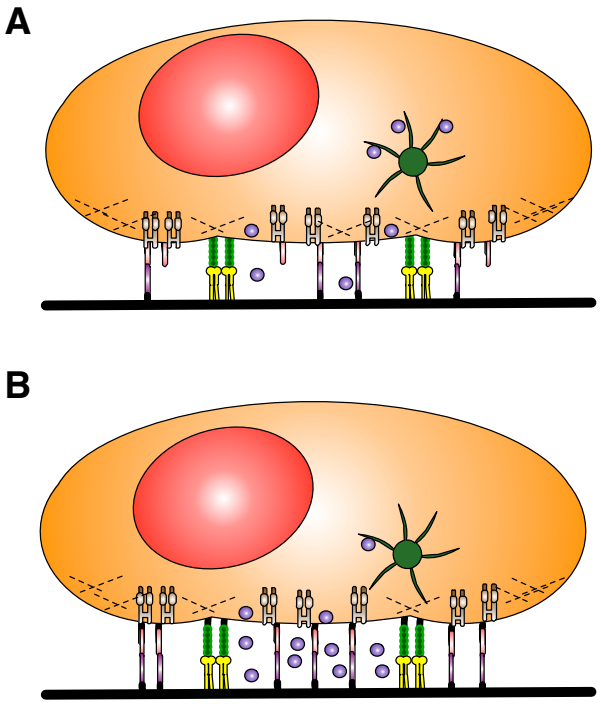


Figure 6.5. NK cells secrete greater amounts of perforin in response to increased ligand density. NK cell ligation of activating receptors results in the secretion of perforin. However, this effector response is analogue, as opposed to digital, and therefore, greater densities of ligand result in greater amounts of perforin secreted. (**A**) A low ligand density causes the secretion of a small amount of perforin. (**B**) A high ligand density results in the secretion of a greater amount of perforin. Diagram not to scale.

NK cell effector responses can be affected by previous encounters with the same or varying ligands

NK cells have been shown to be able to serially lyse target cells (467). However, only a small proportion of NK cells have the ability to serially kill targets. An NK cell would lose stores of PFN following degranulation, but the ability of NK cells to serially lyse target cells suggests that they only lose a certain proportion of stored PFN with each

kill. Serial stimulation through either NKG2D or CD16 caused a decrease in the amount of PFN secreted by NK cells (Figure 3.5.6 and 5.7). This could have been due to either a reduction of PFN stores or the internalisation of receptors. If NK cells internalise their receptors, they would be unable to mount as efficient a response upon further stimulation. The data support this hypothesis, with PFN secretion reduced in response to repeated stimulation with either MICA-Fc proteins or anti-CD16 antibodies (Figure 5.6 and 5.7). However, these data did not address directly whether it was simply a loss of PFN stores that caused the reduction in PFN secretion, or a loss of surface expression of receptors. To address this, NK cells were stimulated sequentially on different ligands to assess if PFN secretion continued to decline, indicating a loss of total PFN stores.

Stimulation through CD16 (ADCC) following initial NKG2D activation triggered PFN secretion at levels seen upon initial activation. However, NKG2D signaling following CD16 activation was insufficient to restore the PFN response (Figure 5.8 – 5.11). This may be due to a downregulation of NKG2D following CD16 ligation. Flow cytometric analysis of NKG2D and CD16 expression showed that NKG2D ligation had little effect on the percentage of cells expressing CD16. However, the level of CD16 expression on the surface of individual NK cells was reduced. CD16 ligation decreased both the proportion of cells expressing NKG2D and the overall levels of NKG2D expressed on the cell surface. The minor reduction in CD16 expression did not seem to be as stark as the dramatic drop in PFN release. Flow cytometric analysis suggested that NK cell size and density was unaffected by the serial stimulation assay, indicating that cell viability was not reduced. This indicates that a decrease in PFN secretion could not be attributed to a reduction in NK cell health, although this can be tested more robustly using a flow stain to directly measure alterations in membrane integrity, such as DAPI. This suggests that whilst receptor expression may influence the ability of NK cells to serially secrete PFN, it is not the only factor. Intracellular signaling is likely to play a role in the degree of PFN secretion. Unfortunately, NK cell signalling was not investigated here. Previous groups have studied the effects of signalling on NK cell-mediated cytolysis, but have yet to show if signalling events are correlated to the amount of PFN secreted. Whilst future work can address these outstanding questions (see below), the data here establish a direct link between serial ligation of activating receptors and the ability of NK cells to secrete PFN.

The desensitisation of NK cells to activating ligands may protect the body from aberrant cell lysis, whilst allowing NK cells to retain the ability to mount a response to opsonised targets. In a tumour setting, repeated stimulation through tumour-expressed ligands for NKG2D (496), causes a downregulation of the receptor on the NK cell surface (504, 527). As a result, NK cells become less efficient, or eventually unable, to lyse tumour cells. B cells have been shown to produce antibodies against both cancer cell-expressed proteins (528) and viral peptides presented on infected cell surfaces (529, 530). Therefore, following the repeated stimulation of NK cells through NKG2D, opsonisation of target cells would result in the ligation of CD16, possibly enabling further lysis of these targets by previously stimulated NK cells. Assessing the NK cell-mediated specific lysis of excess target cells expressing only ICAM1 and a ligand for NKG2D could determine the efficacy of this. During a 6-hour cytotoxic release assay, the addition of IgG targeted to NKG2D ligands, compared to no addition of antibody, would begin to address whether ADCC improved the serial lysis of these target cells. Finally, the inability of NK cells to be re-stimulated following serial activation through CD16 may be a defense mechanism protecting the body from autoimmunity. B cells can produce a number of autoantibodies, during both normal development and in disease (531). The desensitisation of NK cells to ADCC may render them hyporesponsive, protecting the body from further autologous attack.

The fact that NK cells can be activated through CD16 and continue to release PFN following serial stimulation through NKG2D implies that therapeutic antibodies could take advantage of this. Hyporesponsive NK cells within a tumour could lead to decreased specific lysis and the development of a metastatic tumour. Directing antibodies against tumour-specific antigens could reverse NK cell anergy, initiating ADCC against these targets, and leading to an enhanced clearance of transformed cells. Whilst the downregulation of NK cell activating receptors may be a defense mechanism against aberrant autologous cell lysis, the maintained capacity to initiate ADCC of opsonised target cells is likely to be beneficial. Data presented here indicate that NK cell responses to different ligands can have profound effects on their capacity to react to subsequent stimulation. Therefore, therapeutics could take advantage of these systems to induce, or improve, the immune response to viral infection or transformation (Figure 6.6).

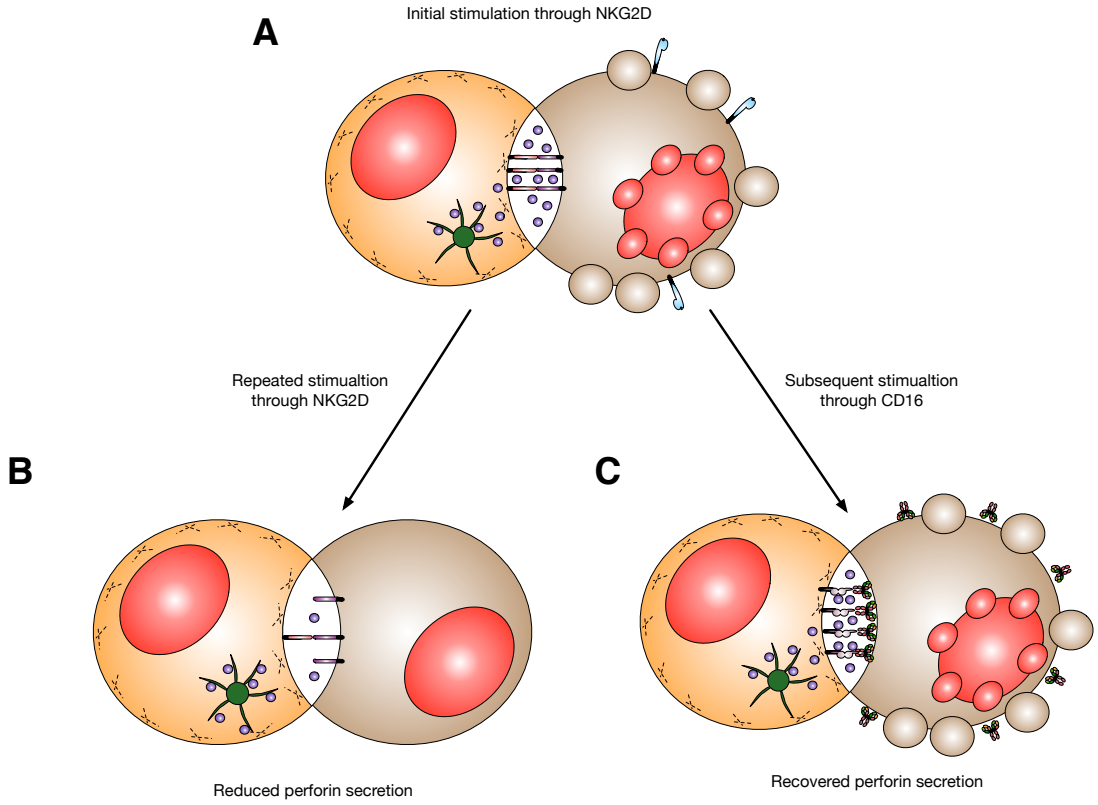


Figure 6.6. ADCC-mediated cytolysis could be used to promote NK cell-mediated serial lysis efficiency. (**A**) The ligation of NKG2D and LFA-1 results in the activation and degranulation of NK cells, causing lysis of the target cell, but also down regulation of NKG2D expression. (**B**) Receptor internalisation results in fewer receptors available to activate the NK cell and therefore less perforin is produced, which may be insufficient to lyse the target cell. (**C**) Following NKG2D ligation, the ligation of CD16 induces a strong effector response where perforin secretion remains high, most likely be sufficient to lyse the target cell. Diagram not to scale.

Estimation of perforin amounts secreted by NK cells

PFN secretion was quantified as a mean integrated intensity per cell. These measurements were used to determine increases or decreases in the amount of PFN secreted by NK cells in response to different stimuli. However, this did not address the actual amounts of PFN, or the number of molecules released by NK cells. To do this, beads coated with known surface densities of antibodies were used to create fluorescent beads that could be imaged and quantified using confocal microscopy. The antibody binding capacities of the beads were used to define the relationship between fluorescence intensity and the number of molecules.

Using previously reported measurements of the dimensions of the synapse to estimate the volume of liquid it contains, these amounts of protein could then be used to estimate the concentration of PFN secreted into the cleft. Following stimulation via NKG2D or CD16, PFN reached concentrations of 13 ± 5.7 µM or 12.2 ± 4.3 µM respectively. However, these values may be an over-estimation. In a physiological cell-cell conjugate setting, PFN binds to the target cell membrane and creates pores that cause endocytosis of the damaged membrane, utilising the membrane repair response (261, 291, 294). Therefore, whilst PFN is secreted constantly at the synapse, the concentration within the synaptic cleft would most likely not exceed 12 µM. Current data shows that NK cell median time to kill is around 10 minutes, and therefore, cytolytic concentrations of PFN may be reached within this time frame. After 12 minutes, the concentration of PFN, via NKG2D or CD16 stimulation, reached 3.6 ± 2.4 µM or 3.3 ± 2.2 µM, respectively. This concentration is consistent with a previous study reporting that 5 µM PFN in solution was able to efficiently lyse cells (261).

The results of this study have investigated the amount of PFN secreted into the IS. PFN secretion varies in response to the density of activating ligand, with increased densities inducing greater PFN secretion. Furthermore, NK cells responsiveness to repeated activation depends on the nature of the activating signal. In conclusion, NK cell signalling and PFN secretion is affected directly by the quality and quantity of ligand binding. Further antibody-based modulation of NK cell responses should account for these factors to modulate the NK cell response.

6.4 Future Perspectives

6.4.1 Clearance and exclusion from the immune synapse

Size-dependent exclusion at the immune synapse

The data presented here show that NK and T cell IS are able to exclude molecules above a size threshold. This is likely due to the dimensions of the extracellular receptors causing nanometer-sized spacing between the two cell membranes. To further investigate this, elongated extracellular domains on the target cell could be used. Köhler *et al* showed that elongating activating or inhibitory ligands abrogated signalling, due to size-dependent segregation at the synapse (124). By using a similar system, the extracellular domains of the activating receptors could be matched to integrin sizes, so that the width of the activating synapse could be increased. If the exclusion of molecules were due to the resultant size of the synaptic cleft, based on receptor-ligand complex dimensions, the increase of intracellular membrane distance would therefore allow larger molecules into the synapse. Sufficient extension to accommodate mAb could also be tested using a cytotoxicity release assay. If the synapse were able to accommodate mAb within the synapse, a mAb against PFN would therefore be able to enter and block killing. This would directly test whether the size exclusions imposed by the synapse are due to extracellular receptor-ligand complex dimensions and the functional ramifications of this.

The inhibitory IS was unable to exclude any of the molecules tested. This suggests that the inhibitory synapse is unable to clear molecules from the cell-cell interface during synapse formation. This may be due to the absence of F-actin accumulation or lack of effector cell spreading, both characteristic of the activating synapse. The addition of dextran to pre-formed inhibitory synapses, as was previously done with activating synapses, is one method that could be used to address the importance of these factors. The formation of inhibitory synapses with target cells or slides coated with inhibitory ligands could be utilised for this. Coupled with fluorescent real-time cytoskeletal markers such as LifeAct (which can be transfected into cells and used to image live actin dynamics), the effect of inhibitory signals on F-actin dynamics, cell

spreading, and dextran clearance could be tested. This would determine whether the structural differences in the formation of inhibitory and activating synapses determines their ability to clear extracellular molecules.

Clearance of molecules from the immune synapse

NK cell spreading, mediated by integrins (532-535), may cause an initial reduction in extracellular molecules within the synapse, but the subsequent ligation of smaller activating receptors may facilitate the complete exclusion of larger molecules. To test whether this is caused by the spreading response initiated by NK cells in contact with activating surfaces, the concentration of both integrins and activating ligands could be titrated. PNK cells could be plated on increasing amounts of activating ligand with a constant amount of ICAM1. This would address whether it is the ligation of activating receptors that induces complete clearance of larger molecules from the synapse.

Alternatively, the TIRF imaging of smaller 4nm dextran, larger 32 nm dextran and actin (using LifeAct) simultaneously could be performed. This would allow imaging of actin cytoskeleton dynamics at the cell-slide interface in the presence of different dextran sizes, allowing correlative analysis of F-actin reorganisation and the clearance of dextran. Furthermore, the use of actin depolymerizing drugs could be used alongside this technique to allow real-time imaging of actin degradation at the synapse, and how this affects the exclusion of larger dextran from the synaptic cleft.

Antibody blockade of directionally secreted proteins

The results have clearly demonstrated that the pNK cell synapse is able to exclude mAb, whereas $F(ab')_2$ fragments and dAb capably penetrate the IS. Thus, smaller sized antibodies would be able to target proteins that are directionally secreted. The production of $F(ab')_2$ fragments and dAb against proteins that are secreted into the synapse, such as PFN, would therefore confirm that exclusion of mAb leads to their failure to inhibit target cell lysis. These antibodies against PFN should be tested using a cytotoxicity release assay in parallel with a degranulation assay (measuring surface expression of CD107a). By analysing the lysis of target cells and the extent

of degranulation, the importance of size for the efficacy of these targeted therapies can be assessed.

The effect of LDL on perforin secreted at the immune synapse

The exclusion of LDL from the pNK cell synapse is consistent with the idea that synapse assembly can clear molecules that would otherwise interfere with secreted proteins. Previous findings have demonstrated the ability of LDL to bind and inhibit PFN and that LDL added to the extracellular solution has little effect on efficient killers (449, 450). The addition of LDL to various effector-target conjugates, formed by CTLs with a range of killing efficiency, showed that 'poorer killers' were more susceptible to the inhibitory effects of LDL.

YTS cells elicit a poorer cytolytic response than pNK cells and this may be due to the inclusion of LDL within the YTS cell synapse. A cytotoxicity release assay in parallel with a degranulation assay in the presence or absence of lipoproteins would address this, with the hypothesis that specific lysis by YTS cells would increase when co-incubation with target cells occurs in lipoprotein-free medium, whereas degranulation would remain the same. This would suggest that the presence of LDL within the synapse is indeed having a direct effect on the cytolytic capacity of YTS cells.

Further to this, elongation of receptors and ligands at the pNK cell synapse could further test this idea. Cytotoxic release assays with targets only expressing ligands with extracellular domain sizes matched to integrin receptor-ligand complexes in normal and LDL-free medium would address the inclusion of LDL could affect the action of secreted PFN.

6.4.2. Perforin secretion at the NK cell immune synapse

NK cell activation and degranulation with different ligands and combinations

Current data addresses how repeated CD16 and NKG2D stimulation alters the capacity of NK cells to secrete PFN. Future experiments should include activation of pNK cells on slides coated with a variety of ligands, including combinations of more than one. This would further elucidate how ligation of different receptors affects NK cell PFN secretion. Further, investigations of PFN secretion from pNK cells has only been addressed under activating conditions. The inclusion of inhibitory ligands on slides would also address impact of inhibitory signals on subsequent PFN secretion. A previous study showed that titrating antibodies against inhibitory receptors had a proportional effect on NK cell-mediated cytolysis (480), which would suggest that PFN secretion is indeed metered by inhibitory receptor ligation. Expansion of the model used in studies detailed here would allow direct assessment of how negative signals alter the PFN response.

Saturation of the capture assay anti-perforin antibodies

Whilst large amounts of anti-PFN antibodies were used to capture PFN, it is possible that the slides were saturated, so not all PFN proteins secreted were captured. By increasing the amounts of anti-PFN antibodies coated on the slide, this could be tested. However, as increasing amounts of PFN was secreted, the proteins would have diffused across the slide, leading to the formation of larger spots of PFN, as seen in the images. The increase in size of the PFN spots arrested 60 minutes after initial stimulation. It could be assumed that no more PFN was secreted, but using increasing amounts of anti-PFN antibody would confirm this.

Replication of a target cell surface on an activating slide

The artificial nature of the PFN capture assay is a drawback of this technique. In this system, only one integrin and one activating receptor are ligated. Whilst this is sufficient to induce a response, the quantity of PFN secreted by the NK cell may differ when co-ligation of different activating and inhibitory receptors occurs. The use of physiologically relevant amounts of activating ligands would better address the

PFN secretion response of NK cells when in contact with a target cell. By flow cytometric analysis of tumour cells, virally-infected cells and common cell lines that are used as NK cell targets, their surface phenotype could be more closely mimicked on a slide. There are other factors, such as cell-cell receptor transfer that are not modeled in this assay. Despite these drawbacks, minor tweaks could provide a more physiological setting to study NK cell signalling and to unravel how various combinations and densities of ligands affect PFN secretion.

The effect of surface tension on perforin secretion

The tension provided by a glass surface is not biomimetic of a cell synapse. Specifically, the high tensile forces generated by interaction with glass may influence NK cell phenotype. This may result in an altered NK cell response, that is less representative of interactions with a conjugated cell, which has a significantly lower modulus. This is a particularly important consideration when attempting to simulate the substrate modulus of tumour cells. It has been shown that tumour tissues are stiffer than non-cancerous tissue (536), and this can enhance their growth (537). It is well known that cells are able to sense and respond to the stiffness of a substrate (538). Migration kinetics on varying substrate moduli have been investigated. These studies demonstrate that increased stiffness is proportionate to increased spreading (539, 540). In contrast, cytokine secretion has been shown to decrease on stiffer substrates (541). Therefore, the use of the protein capture assay on substrates of varying moduli, such as hydrogels (542) or silicone (543), would address how these structures can alter the response of NK cells, not only with PFN but other secreted factors.

The correlation between perforin secretion and NK cell intracellular signalling

The data here show for the first time that NK cells vary the amount of PFN secreted depending on the amount of ligand bound. This may be caused by fluctuations in signalling cascades with a direct impact on the number of LG recruited and fusing at the synapse. What impact NK cell intracellular signalling, and the specific amount of signalling, has on PFN secretion could be directly tested. To do this, propagation of activating signals within NK cells should be assessed. Activating signalling pathways are kinase cascades of tyrosine phosphorylation. Using Western blotting or flow

cytometric analysis, the amounts of phosphorylated proteins, for example Vav1, in response to different ligand densities of activating ligand. This would address whether greater ligand density results in a greater amount of signalling within the NK cell. SiRNA could be used to induce a partial KD of Vav1. These KD cells could then be incubated on increasing densities of activating ligand and PFN secretion compared to untransfected control cells. If signalling through activating receptors is responsible for increased PFN secretion, the KD cells would not be able to release comparable amounts. SiRNA could be used to KD a number of proteins and kinases within the cascade to fully decipher which proteins control the amount of PFN that is released at the synapse.

Comparison of perforin secretion by fresh and IL-2 expanded NK cells

Experiments assessing PFN secretion were performed on pNK cells that had been expanded in IL-2 and 6-day rested prior to use. Co-ligation of LFA1 and CD16 increased the amount of PFN secreted. This is in contrast to a study performed by by Bryceson *et al,* where no change, or even a negative effect, was reported. These differences may be due to the use of IL-2 to activate NK cells, which has a significant impact on NK cells, altering their receptor profiles (544-546) and gene expression (486). To further unravel the effects of IL-2, and how it can alter the responses of NK cells, these experiments could be repeated on freshly isolated NK cells and IL-2-expanded cells from the same donor, providing a direct comparison of how IL-2 stimulation affects PFN secretion.

The effect of cytokine stimulation on serial NK cell PFN secretion

One of the major obstacles to increasing NK cell-mediated lysis in cancer patients is the identification of the most appropriate method to expand NK cells. This can be mediated through the addition of IL-2 or IL-15 (302). Stimulation of NK cells to improve their ability to serially lyse tumours could provide another mechanism to enhance tumour cell clearance. The data presented in this thesis suggest that ADCC-mediated lysis, when preceded by natural cytotoxicity, can still efficiently induce PFN secretion by NK cells. Previous work has shown that IL-15 increases NKG2D-mediated lysis *in vitro* (547), potentially via upregulating components of the cytotoxic machinery. Other studies have also demonstrated the crucial role of IL-15 *in*

vivo. Poly(I:C) activation of NK cells is dependent on interaction with NK cells (548), where IL-15 is trans-presented to NK cells (35, 549). In addition, IL-15-unresponsive NK cells have been shown to induce reduced NKG2D-mediated cytotoxicity (550, 551). Collectively, these data demonstrate an important role for IL-15 in NK cell mediated cytolysis. For this reason, the effect that cytokine stimulation has on NK cell secretion of PFN, and how it may modulate serial secretion of PFN, should be investigated. This could reveal how cytokines could be used to enhance target killing. The protein capture assay could be used for this purpose. Coupling cytokine treatment of NK cells to enhancement of ADCC responses may be a route to enhance cytolysis of tumour cells.

Estimation of perforin secreted by NK cells

The methods used to estimate the concentrations of PFN within the synapse use reported measurements of the synapse to estimate PFN secretion from the data collected following NK cell interaction with an activtaing glass slide. The major drawback of this technique is the requirement for some educated guess work. The ABC of QSC beads were used to estimate the number of antibodies bound at the bead surface. The binding capacity of anti-PFN antibodies and rPFN are assumed to be an average of one. Therefore, to obtain a more accurate reading of PFN, different approaches are required. This could include the use of radioactive isotypes. The measurement of radioactivity is significantly more accurate than fluorescence intensity of a fluorophore. This would significantly reduce the error in the system. By using radioactively labelled antibodies and rPFN, the amounts of PFN that binds to beads and antibodies could be quantified in a step-wise manner. Radioactive anti-PFN antibodies would be incubated with QSC beads then assessed by scintillation. These values could be compared against those obtained with a known number of antibodies in solution to give accurate numbers bound per bead. Once these ABC are known, radioactively labelled rPFN would be incubated with anti-PFN-loaded beads (using the same clone but unlabelled) and measured by scintillation. Again, readings could be compared to known concentrations of rPFN in solution and thus, the amount of PFN bound could be calculated per bead. Finally, the amount of rPFN bound to the beads could be determined by the incubation of radioactively labelled antibodies against the captured PFN. This could be either correlated to previously measured fluorescence intensity or, radioactively labelled anti-PFN could be used to

stain captured PFN in the protein capture assay. This could provide a more accurate estimation of the number of PFN molecules secreted by NK cells.

6.5 Long Term Developments

Blockade of proteins secreted across the immune synapse *in vivo*

The data in this thesis have revealed a novel role of the NK cell IS. Most significantly, the data demonstrate that small domain antibodies, dAbs, are able to penetrate the synaptic cleft. A dAb targeted to proteins directly secreted across the IS could act to block their function. Whilst the effects of specifically targeted dAbs could be tested *in vitro* (cytotoxic release assays, *etc.*), administering them to an model organism would directly address the systemic effects of blocking proteins secreted by NK cells, and would test whether such an antibody-based therapeutic could have an effect physiologically.

The development of the non-obese diabetic (NOD) mouse model (552, 553) has enabled the dissection of many molecular pathways involved in the development of autoimmune diabetes. Within 3 – 4 weeks of neonatal development, T cells, B cells, NK cells and DC infiltrate the islets of Langerhans and attack the tissues, resulting in the development of type 1 DM. Importantly, studies have shown that PFN-deficient NOD mice have a delayed onset of diabetes, suggesting that PFN plays a significant role in disease progression (554). Therefore, the infusion of dAb against PFN could begin to address whether or not such therapies can be used as an alternative to – or in combination with – traditional therapies to reduce destruction of healthy tissues.

The production of dAb against a specific target is both time consuming and complex, requiring a number of stages of affinity maturation (390). However, the use of a phage-display library enables the production of dAb against a large number of antigens. Using this system, a dAb against PFN, or a specific cytokine, could be developed. This dAb could then used to treat a number of conditions. For instance, autoimmunity is initiated by a number of factors, including aberrant signalling and the recognition of ‘self’ antigens as ‘foreign’. This promotes disease onset and progression. This is not only controlled by T cells, but involves interactions between a number of immune cells (555). The progression of these diseases is a combination of both cytokine secretion and autologous cell-mediated lysis. Whilst therapies to bind soluble secreted factors can ameliorate some diseases, these therapies do not target proteins secreted across the IS during intercellular communication. It is in this setting

that dAb may offer a novel treatment, with their ability to access the IS and proteins within it. Targets that conventional therapies are unable to reach.

The data in this thesis have laid groundwork demonstrating that the IS can be accessed by dAb. The development of dAb against proteins directly secreted across the synapse may provide a novel tool to prevent the destruction of autologous tissue. By using such models as the well-established NOD mouse, dAb could be investigated to determine whether or not they are effective and the extent of their efficacy.

Directing the cytolysis of NK cells and promoting serial killing

The data show that NK cells are able to respond to increased ligand density by secreting enhanced amounts of PFN (Figure 5.4 and 5.5). In addition, PFN secretion could be restored to initial amounts by CD16 ligation following serial stimulation through NKG2D (Figure 5.8 and 5.10). This phenomenon may be used to improve NK cell-mediated lysis of tumour cells. Previous work has shown that antibodies can be used to direct the NK cell-mediated lysis of tumour cells (320, 466, 556). This can be done using 'dumbbell' antibodies (such as two dAb connected by a linker peptide chain) that bind both tumour surface targets and NK cell receptors, such as NKG2D (472). Another approach involves redirected NK cell-mediated lysis, binding antibodies against NK cell receptors to the Fc receptors of target cells (557).

Whilst these studies have demonstrated that antibodies can be successfully used to mediate NK cell lysis of tumour cells, the data in this thesis highlight the effects that receptor ligation can have on PFN secretion. Therefore, to develop novel strategies to improve tumour cell clearance, various antibody combinations, or serial binding of antibodies, can be investigated to determine which approach provides the most effective response from NK cells. Specifically, data here show that CD16 ligation can trigger increased PFN secretion after NKG2D ligation. Thus, the application of antibodies that bind tumour-specific targets and trigger lysis through NKG2D could be administered initially. Next, antibodies that bind the same tumour targets, but ligate the ADCC receptor CD16, could then be administered. This may improve the NK cell cytotoxic response to tumour cells, increasing serial lysis of target cells. These experiments could be trialled first *in vitro*; assessing the ability of NK cells to

lyse a number of target cells with an antibody ligating NKG2D, then using a second antibody that targets such as CD16, as used in studies detailed here. A range of antibody combinations in tandem with different activating receptors could be tested to determine the most effective regimen to maintain maximum PFN secretion following serial lysis of tumour cells.

Once the most successful combinations have been determined, these antibodies could be administered to murine cancer models to assess their efficacy *in vivo*. Of course, for these studies murine cells must be first used in the *in vitro* screening process. There are a number of techniques to model cancer in the mouse (*e.g.* microinjection of foreign DNA, endogenous gene locus disruption, Cre-*loxP* inducible, RNA interference and virus-mediated gene delivery) that could be useful in this setting (558). The protein capture assay demonstrated here could be used in combination with *in vivo* mouse studies to determine the efficacy of antibody-based therapies for increasing cell-mediated lysis of tumour cells. These therapies do not have to be restricted to NK cells, as CTL-mediated lysis could also be exploited to increase the clearance of tumour cells further.

Repeated stimulation of NK cells has revealed that the receptors ligated has a profound effect on the ability of an NK cell to serially secrete PFN. These findings can inform future studies using mouse models to study their efficacy *in vivo*. This may lead to the development of novel therapies to increase cell-mediated lysis of tumour cells.

6.6 Concluding Remarks

The NK cell IS is a dynamic cell-cell interface essential for detecting and lysing virally infected or transformed cells. Confocal microscopy has demonstrated the sensitivity of this interaction to receptor-ligand complex formation, during both the secretion of cytotoxic mediators and the clearance of extracellular molecules contained within the synaptic cleft. The development of a range of innovative, multidisciplinary techniques discussed here has facilitated a greater understanding of how NK cells respond to extracellular factors. Future work will further enhance our understanding of the cellular mechanisms, such as structural assembly, and the complex nature of signalling at the IS. This has the potential to contribute to enhanced therapeutic manipulation of NK cell function, providing improved efficacy in the prevention or eradication of disease.

References

1. Kiessling R, Klein E, & Wigzell H (1975) "Natural" killer cells in the mouse. I. Cytotoxic cells with specificity for mouse Moloney leukemia cells. Specificity and distribution according to genotype. *Eur. J. Immunol.* 5(2):112-117.
2. Kiessling R, Klein E, Pross H, & Wigzell H (1975) "Natural" killer cells in the mouse. II. Cytotoxic cells with specificity for mouse Moloney leukemia cells. Characteristics of the killer cell. *Eur. J. Immunol.* 5(2):117-121.
3. Lanier LL, Testi R, Bindl J, & Phillips JH (1989) Identity of Leu-19 (CD56) leukocyte differentiation antigen and neural cell adhesion molecule. *The Journal of experimental medicine* 169(6):2233-2238.
4. Borrego F*, et al.* (1999) NK phenotypic markers and IL2 response in NK cells from elderly people. *Exp. Gerontol.* 34(2):253-265.
5. Sivori S*, et al.* (1997) p46, a novel natural killer cell-specific surface molecule that mediates cell activation. *The Journal of experimental medicine* 186(7):1129-1136.
6. Robertson MJ & Ritz J (1990) Biology and clinical relevance of human natural killer cells. *Blood* 76(12):2421-2438.
7. Moretta L & Moretta A (2004) Unravelling natural killer cell function: triggering and inhibitory human NK receptors. *The EMBO journal* 23(2):255-259.
8. Bryceson YT, March ME, Ljunggren HG, & Long EO (2006) Synergy among receptors on resting NK cells for the activation of natural cytotoxicity and cytokine secretion. *Blood* 107(1):159-166.
9. Davis DM*, et al.* (1999) The human natural killer cell immune synapse. *Proc. Natl. Acad. Sci. U. S. A.* 96(26):15062-15067.
10. Grakoui A*, et al.* (1999) The immunological synapse: a molecular machine controlling T cell activation. *Science* 285(5425):221-227.
11. Bakker AB, Wu J, Phillips JH, & Lanier LL (2000) NK cell activation: distinct stimulatory pathways counterbalancing inhibitory signals. *Hum. Immunol.* 61(1):18-27.
12. Long EO, Kim HS, Liu D, Peterson ME, & Rajagopalan S (2013) Controlling natural killer cell responses: integration of signals for activation and inhibition. *Annu. Rev. Immunol.* 31:227-258.

13. Orange JS*, et al.* (2003) The mature activating natural killer cell immunologic synapse is formed in distinct stages. *Proc. Natl. Acad. Sci. U. S. A.* 100(24):14151-14156.
14. van der Merwe PA (2002) Formation and function of the immunological synapse. *Curr. Opin. Immunol.* 14(3):293-298.
15. Brilot F, Strowig T, Roberts SM, Arrey F, & Munz C (2007) NK cell survival mediated through the regulatory synapse with human DCs requires IL-15Ralpha. *The Journal of clinical investigation* 117(11):3316-3329.
16. Nedvetzki S*, et al.* (2007) Reciprocal regulation of human natural killer cells and macrophages associated with distinct immune synapses. *Blood* 109(9):3776-3785.
17. Schleinitz N, March ME, & Long EO (2008) Recruitment of activation receptors at inhibitory NK cell immune synapses. *PLoS One* 3(9):e3278.
18. Vyas YM*, et al.* (2001) Spatial organization of signal transduction molecules in the NK cell immune synapses during MHC class I-regulated noncytolytic and cytolytic interactions. *J. Immunol.* 167(8):4358-4367.
19. Davis DM & Dustin ML (2004) What is the importance of the immunological synapse? *Trends Immunol.* 25(6):323-327.
20. Chen X*, et al.* (2006) CD28-stimulated ERK2 phosphorylation is required for polarization of the microtubule organizing center and granules in YTS NK cells. *Proc. Natl. Acad. Sci. U. S. A.* 103(27):10346-10351.
21. Lanier LL (2001) On guard--activating NK cell receptors. *Nat. Immunol.* 2(1):23-27.
22. Kalland T (1986) Generation of natural killer cells from bone marrow precursors in vitro. *Immunology* 57(4):493-498.
23. Miller JS, Alley KA, & McGlave P (1994) Differentiation of natural killer (NK) cells from human primitive marrow progenitors in a stroma-based long-term culture system: identification of a CD34+7+ NK progenitor. *Blood* 83(9):2594-2601.
24. Freud AG*, et al.* (2006) Evidence for discrete stages of human natural killer cell differentiation in vivo. *The Journal of experimental medicine* 203(4):1033-1043.
25. Sanchez MJ, Muench MO, Roncarolo MG, Lanier LL, & Phillips JH (1994) Identification of a common T/natural killer cell progenitor in human fetal thymus. *The Journal of experimental medicine* 180(2):569-576.

26. Freud AG*, et al.* (2005) A human CD34(+) subset resides in lymph nodes and differentiates into CD56bright natural killer cells. *Immunity* 22(3):295-304.
27. Vitale M*, et al.* (1998) NKp44, a novel triggering surface molecule specifically expressed by activated natural killer cells, is involved in non-major histocompatibility complex-restricted tumor cell lysis. *The Journal of experimental medicine* 187(12):2065-2072.
28. Lazetic S, Chang C, Houchins JP, Lanier LL, & Phillips JH (1996) Human natural killer cell receptors involved in MHC class I recognition are disulfide-linked heterodimers of CD94 and NKG2 subunits. *J. Immunol.* 157(11):4741-4745.
29. Phillips JH*, et al.* (1996) CD94 and a novel associated protein (94AP) form a NK cell receptor involved in the recognition of HLA-A, HLA-B, and HLA-C allotypes. *Immunity* 5(2):163-172.
30. Mingari MC*, et al.* (1997) Interleukin-15-induced maturation of human natural killer cells from early thymic precursors: selective expression of CD94/NKG2-A as the only HLA class I-specific inhibitory receptor. *Eur. J. Immunol.* 27(6):1374-1380.
31. Toomey JA, Gays F, Foster D, & Brooks CG (2003) Cytokine requirements for the growth and development of mouse NK cells in vitro. *J. Leukocyte Biol.* 74(2):233-242.
32. Mrozek E, Anderson P, & Caligiuri MA (1996) Role of interleukin-15 in the development of human CD56+ natural killer cells from CD34+ hematopoietic progenitor cells. *Blood* 87(7):2632-2640.
33. Barao I, Hudig D, & Ascensao JL (2003) IL-15-mediated induction of LFA-1 is a late step required for cytotoxic differentiation of human NK cells from CD34+Lin- bone marrow cells. *J. Immunol.* 171(2):683-690.
34. Koka R*, et al.* (2003) Interleukin (IL)-15R[alpha]-deficient natural killer cells survive in normal but not IL-15R[alpha]-deficient mice. *The Journal of experimental medicine* 197(8):977-984.
35. Lucas M, Schachterle W, Oberle K, Aichele P, & Diefenbach A (2007) Dendritic cells prime natural killer cells by trans-presenting interleukin 15. *Immunity* 26(4):503-517.
36. Michon JM*, et al.* (1988) Induction of natural killer effectors from human thymus with recombinant IL-2. *J. Immunol.* 140(10):3660-3667.

37. Bajenoff M*, et al.* (2006) Natural killer cell behavior in lymph nodes revealed by static and real-time imaging. *The Journal of experimental medicine* 203(3):619-631.

38. Ferlazzo G*, et al.* (2004) Distinct roles of IL-12 and IL-15 in human natural killer cell activation by dendritic cells from secondary lymphoid organs. *Proc. Natl. Acad. Sci. U. S. A.* 101(47):16606-16611.

39. Baldassarre G*, et al.* (2001) Onset of natural killer cell lymphomas in transgenic mice carrying a truncated HMGI-C gene by the chronic stimulation of the IL-2 and IL-15 pathway. *Proc. Natl. Acad. Sci. U. S. A.* 98(14):7970-7975.

40. Fehniger TA*, et al.* (2001) Fatal leukemia in interleukin 15 transgenic mice follows early expansions in natural killer and memory phenotype CD8+ T cells. *The Journal of experimental medicine* 193(2):219-231.

41. Zimmer J*, et al.* (1998) Activity and phenotype of natural killer cells in peptide transporter (TAP)-deficient patients (type I bare lymphocyte syndrome). *The Journal of experimental medicine* 187(1):117-122.

42. Bix M*, et al.* (1991) Rejection of class I MHC-deficient haemopoietic cells by irradiated MHC-matched mice. *Nature* 349(6307):329-331.

43. Dorfman JR, Zerrahn J, Coles MC, & Raulet DH (1997) The basis for self-tolerance of natural killer cells in beta2-microglobulin- and TAP-1- mice. *J. Immunol.* 159(11):5219-5225.

44. Liao NS, Bix M, Zijlstra M, Jaenisch R, & Raulet D (1991) MHC class I deficiency: susceptibility to natural killer (NK) cells and impaired NK activity. *Science* 253(5016):199-202.

45. Ljunggren HG, Van Kaer L, Ploegh HL, & Tonegawa S (1994) Altered natural killer cell repertoire in Tap-1 mutant mice. *Proc. Natl. Acad. Sci. U. S. A.* 91(14):6520-6524.

46. Anfossi N*, et al.* (2006) Human NK cell education by inhibitory receptors for MHC class I. *Immunity* 25(2):331-342.

47. Fernandez NC*, et al.* (2005) A subset of natural killer cells achieves self-tolerance without expressing inhibitory receptors specific for self-MHC molecules. *Blood* 105(11):4416-4423.

48. Kim S*, et al.* (2005) Licensing of natural killer cells by host major histocompatibility complex class I molecules. *Nature* 436(7051):709-713.

49. Brodin P, Karre K, & Hoglund P (2009) NK cell education: not an on-off switch but a tunable rheostat. *Trends Immunol.* 30(4):143-149.
50. Joncker NT, Fernandez NC, Treiner E, Vivier E, & Raulet DH (2009) NK cell responsiveness is tuned commensurate with the number of inhibitory receptors for self-MHC class I: the rheostat model. *J. Immunol.* 182(8):4572-4580.
51. Akira S, Uematsu S, & Takeuchi O (2006) Pathogen recognition and innate immunity. *Cell* 124(4):783-801.
52. Litman GW, Rast JP, & Fugmann SD (2010) The origins of vertebrate adaptive immunity. *Nat. Rev. Immunol.* 10(8):543-553.
53. Sallusto F, Geginat J, & Lanzavecchia A (2004) Central memory and effector memory T cell subsets: function, generation, and maintenance. *Annu. Rev. Immunol.* 22:745-763.
54. Cooper MA*, et al.* (2009) Cytokine-induced memory-like natural killer cells. *Proc. Natl. Acad. Sci. U. S. A.* 106(6):1915-1919.
55. Fauriat C, Long EO, Ljunggren HG, & Bryceson YT (2010) Regulation of human NK-cell cytokine and chemokine production by target cell recognition. *Blood* 115(11):2167-2176.
56. Perona-Wright G*, et al.* (2009) Systemic but not local infections elicit immunosuppressive IL-10 production by natural killer cells. *Cell host & microbe* 6(6):503-512.
57. Lapaque N, Walzer T, Meresse S, Vivier E, & Trowsdale J (2009) Interactions between human NK cells and macrophages in response to Salmonella infection. *J. Immunol.* 182(7):4339-4348.
58. Costantini C*, et al.* (2010) Neutrophil activation and survival are modulated by interaction with NK cells. *Int. Immunol.* 22(10):827-838.
59. Mendelson M*, et al.* (2010) NKp46 O-glycan sequences that are involved in the interaction with hemagglutinin type 1 of influenza virus. *J. Virol.* 84(8):3789-3797.
60. O'Shea JJ, Weissman AM, Kennedy IC, & Ortaldo JR (1991) Engagement of the natural killer cell IgG Fc receptor results in tyrosine phosphorylation of the zeta chain. *Proc. Natl. Acad. Sci. U. S. A.* 88(2):350-354.
61. Keppel MP, Yang L, & Cooper MA (2013) Murine NK cell intrinsic cytokine-induced memory-like responses are maintained following homeostatic proliferation. *J. Immunol.* 190(9):4754-4762.

62. Norcross MA (1984) A synaptic basis for T-lymphocyte activation. *Ann. Immunol. (Paris)* 135D(2):113-134.

63. Brossard C*, et al.* (2005) Multifocal structure of the T cell - dendritic cell synapse. *Eur. J. Immunol.* 35(6):1741-1753.

64. Alarcon B, Mestre D, & Martinez-Martin N (2011) The immunological synapse: a cause or consequence of T-cell receptor triggering? *Immunology* 133(4):420-425.

65. McCann FE*, et al.* (2003) The size of the synaptic cleft and distinct distributions of filamentous actin, ezrin, CD43, and CD45 at activating and inhibitory human NK cell immune synapses. *J. Immunol.* 170(6):2862-2870.

66. Almeida CR & Davis DM (2006) Segregation of HLA-C from ICAM-1 at NK cell immune synapses is controlled by its cell surface density. *J. Immunol.* 177(10):6904-6910.

67. Huppa JB, Gleimer M, Sumen C, & Davis MM (2003) Continuous T cell receptor signaling required for synapse maintenance and full effector potential. *Nat. Immunol.* 4(8):749-755.

68. Orange JS (2008) Formation and function of the lytic NK-cell immunological synapse. *Nat. Rev. Immunol.* 8(9):713-725.

69. Barber DF, Faure M, & Long EO (2004) LFA-1 contributes an early signal for NK cell cytotoxicity. *J. Immunol.* 173(6):3653-3659.

70. Mace EM, Monkley SJ, Critchley DR, & Takei F (2009) A dual role for talin in NK cell cytotoxicity: activation of LFA-1-mediated cell adhesion and polarization of NK cells. *J. Immunol.* 182(2):948-956.

71. Gismondi A*, et al.* (2000) Cutting edge: functional role for proline-rich tyrosine kinase 2 in NK cell-mediated natural cytotoxicity. *J. Immunol.* 164(5):2272-2276.

72. Gismondi A*, et al.* (2003) Proline-rich tyrosine kinase 2 and Rac activation by chemokine and integrin receptors controls NK cell transendothelial migration. *J. Immunol.* 170(6):3065-3073.

73. Duong LT & Rodan GA (2000) PYK2 is an adhesion kinase in macrophages, localized in podosomes and activated by beta(2)-integrin ligation. *Cell Motil. Cytoskeleton* 47(3):174-188.

74. Besson A, Wilson TL, & Yong VW (2002) The anchoring protein RACK1 links protein kinase Cepsilon to integrin beta chains. Requirements for adhesion and motility. *J. Biol. Chem.* 277(24):22073-22084.

75. Riteau B, Barber DF, & Long EO (2003) Vav1 phosphorylation is induced by beta2 integrin engagement on natural killer cells upstream of actin cytoskeleton and lipid raft reorganization. *J. Exp. Med.* 198(3):469-474.

76. Eriksson M*, et al.* (1999) Inhibitory receptors alter natural killer cell interactions with target cells yet allow simultaneous killing of susceptible targets. *The Journal of experimental medicine* 190(7):1005-1012.

77. Lou Z, Jevremovic D, Billadeau DD, & Leibson PJ (2000) A balance between positive and negative signals in cytotoxic lymphocytes regulates the polarization of lipid rafts during the development of cell-mediated killing. *The Journal of experimental medicine* 191(2):347-354.

78. Fassett MS, Davis DM, Valter MM, Cohen GB, & Strominger JL (2001) Signaling at the inhibitory natural killer cell immune synapse regulates lipid raft polarization but not class I MHC clustering. *Proc. Natl. Acad. Sci. U. S. A.* 98(25):14547-14552.

79. Orange JS & Ballas ZK (2006) Natural killer cells in human health and disease. *Clin. Immunol.* 118(1):1-10.

80. Ghio M*, et al.* (2009) Soluble HLA-I-mediated secretion of TGF-beta1 by human NK cells and consequent down-regulation of anti-tumor cytolytic activity. *Eur. J. Immunol.* 39(12):3459-3468.

81. Chau J*, et al.* (2013) Increased production of IFN-gamma by natural killer cells triggered with bone marrow-derived dendritic cells cultured in the presence of retinoic acid. *Eur. J. Pharmacol.*

82. Cella M*, et al.* (2009) A human natural killer cell subset provides an innate source of IL-22 for mucosal immunity. *Nature* 457(7230):722-725.

83. Barnstable CJ, Jones EA, & Crumpton MJ (1978) Isolation, structure and genetics of HLA-A, -B, -C and -DRw (Ia) antigens. *Br. Med. Bull.* 34(3):241-246.

84. Boyington JC, Motyka SA, Schuck P, Brooks AG, & Sun PD (2000) Crystal structure of an NK cell immunoglobulin-like receptor in complex with its class I MHC ligand. *Nature* 405(6786):537-543.

85. Stewart CA*, et al.* (2005) Recognition of peptide-MHC class I complexes by activating killer immunoglobulin-like receptors. *Proc. Natl. Acad. Sci. U. S. A.* 102(37):13224-13229.

86. Biassoni R*, et al.* (1995) Amino acid substitutions can influence the natural killer (NK)-mediated recognition of HLA-C molecules. Role of serine-77 and

lysine-80 in the target cell protection from lysis mediated by "group 2" or "group 1" NK clones. *The Journal of experimental medicine* 182(2):605-609.

87. Mandelboim O*, et al.* (1997) The binding site of NK receptors on HLA-C molecules. *Immunity* 6(3):341-350.
88. Vales-Gomez M, Reyburn HT, Mandelboim M, & Strominger JL (1998) Kinetics of interaction of HLA-C ligands with natural killer cell inhibitory receptors. *Immunity* 9(3):337-344.
89. Davis DM*, et al.* (1999) The transmembrane sequence of human histocompatibility leukocyte antigen (HLA)-C as a determinant in inhibition of a subset of natural killer cells. *J. Exp. Med.* 189(8):1265-1274.
90. Carlin LM, Eleme K, McCann FE, & Davis DM (2001) Intercellular transfer and supramolecular organization of human leukocyte antigen C at inhibitory natural killer cell immune synapses. *The Journal of experimental medicine* 194(10):1507-1517.
91. Pageon SV*, et al.* (2013) Superresolution microscopy reveals nanometer-scale reorganization of inhibitory natural killer cell receptors upon activation of NKG2D. *Sci Signal* 6(285):ra62.
92. Colonna M & Samaridis J (1995) Cloning of immunoglobulin-superfamily members associated with HLA-C and HLA-B recognition by human natural killer cells. *Science* 268(5209):405-408.
93. Wagtmann N*, et al.* (1995) Molecular clones of the p58 NK cell receptor reveal immunoglobulin-related molecules with diversity in both the extra- and intracellular domains. *Immunity* 2(5):439-449.
94. Wagtmann N, Rajagopalan S, Winter CC, Peruzzi M, & Long EO (1995) Killer cell inhibitory receptors specific for HLA-C and HLA-B identified by direct binding and by functional transfer. *Immunity* 3(6):801-809.
95. Braud VM*, et al.* (1998) HLA-E binds to natural killer cell receptors CD94/NKG2A, B and C. *Nature* 391(6669):795-799.
96. Vance RE, Kraft JR, Altman JD, Jensen PE, & Raulet DH (1998) Mouse CD94/NKG2A is a natural killer cell receptor for the nonclassical major histocompatibility complex (MHC) class I molecule Qa-1(b). *J. Exp. Med.* 188(10):1841-1848.
97. Samaridis J & Colonna M (1997) Cloning of novel immunoglobulin superfamily receptors expressed on human myeloid and lymphoid cells:

structural evidence for new stimulatory and inhibitory pathways. *Eur. J. Immunol.* 27(3):660-665.

98. Cosman D*, et al.* (1997) A novel immunoglobulin superfamily receptor for cellular and viral MHC class I molecules. *Immunity* 7(2):273-282.
99. Markel G*, et al.* (2002) CD66a interactions between human melanoma and NK cells: a novel class I MHC-independent inhibitory mechanism of cytotoxicity. *J. Immunol.* 168(6):2803-2810.
100. Stanietsky N*, et al.* (2009) The interaction of TIGIT with PVR and PVRL2 inhibits human NK cell cytotoxicity. *Proc. Natl. Acad. Sci. U. S. A.* 106(42):17858-17863.
101. Ito M*, et al.* (2006) Killer cell lectin-like receptor G1 binds three members of the classical cadherin family to inhibit NK cell cytotoxicity. *J. Exp. Med.* 203(2):289-295.
102. Meyaard L*, et al.* (1997) LAIR-1, a novel inhibitory receptor expressed on human mononuclear leukocytes. *Immunity* 7(2):283-290.
103. Lanier LL, Chang C, & Phillips JH (1994) Human NKR-P1A. A disulfide-linked homodimer of the C-type lectin superfamily expressed by a subset of NK and T lymphocytes. *J. Immunol.* 153(6):2417-2428.
104. Faure M, Barber DF, Takahashi SM, Jin T, & Long EO (2003) Spontaneous clustering and tyrosine phosphorylation of NK cell inhibitory receptor induced by ligand binding. *J. Immunol.* 170(12):6107-6114.
105. Standeven LJ, Carlin LM, Borszcz P, Davis DM, & Burshtyn DN (2004) The actin cytoskeleton controls the efficiency of killer Ig-like receptor accumulation at inhibitory NK cell immune synapses. *J. Immunol.* 173(9):5617-5625.
106. Stebbins CC*, et al.* (2003) Vav1 dephosphorylation by the tyrosine phosphatase SHP-1 as a mechanism for inhibition of cellular cytotoxicity. *Mol. Cell. Biol.* 23(17):6291-6299.
107. Krzewski K, Chen X, Orange JS, & Strominger JL (2006) Formation of a WIP-, WASp-, actin-, and myosin IIA-containing multiprotein complex in activated NK cells and its alteration by KIR inhibitory signaling. *J. Cell Biol.* 173(1):121-132.
108. Masilamani M, Nguyen C, Kabat J, Borrego F, & Coligan JE (2006) CD94/NKG2A inhibits NK cell activation by disrupting the actin network at the immunological synapse. *J. Immunol.* 177(6):3590-3596.

109. Vales-Gomez M, Erskine RA, Deacon MP, Strominger JL, & Reyburn HT (2001) The role of zinc in the binding of killer cell Ig-like receptors to class I MHC proteins. *Proc. Natl. Acad. Sci. U. S. A.* 98(4):1734-1739.

110. Rajagopalan S & Long EO (1998) Zinc bound to the killer cell-inhibitory receptor modulates the negative signal in human NK cells. *J. Immunol.* 161(3):1299-1305.

111. Burshtyn DN, Shin J, Stebbins C, & Long EO (2000) Adhesion to target cells is disrupted by the killer cell inhibitory receptor. *Current biology : CB* 10(13):777-780.

112. Burshtyn DN*, et al.* (1996) Recruitment of tyrosine phosphatase HCP by the killer cell inhibitor receptor. *Immunity* 4(1):77-85.

113. Tomasello E, Blery M, Vely F, & Vivier E (2000) Signaling pathways engaged by NK cell receptors: double concerto for activating receptors, inhibitory receptors and NK cells. *Semin. Immunol.* 12(2):139-147.

114. Bruhns P, Marchetti P, Fridman WH, Vivier E, & Daeron M (1999) Differential roles of N- and C-terminal immunoreceptor tyrosine-based inhibition motifs during inhibition of cell activation by killer cell inhibitory receptors. *J. Immunol.* 162(6):3168-3175.

115. Andrews DM, Scalzo AA, Yokoyama WM, Smyth MJ, & Degli-Esposti MA (2003) Functional interactions between dendritic cells and NK cells during viral infection. *Nat. Immunol.* 4(2):175-181.

116. Sun JC & Lanier LL (2011) NK cell development, homeostasis and function: parallels with CD8(+) T cells. *Nat. Rev. Immunol.* 11(10):645-657.

117. Brown AC*, et al.* (2011) Remodelling of cortical actin where lytic granules dock at natural killer cell immune synapses revealed by super-resolution microscopy. *PLoS Biol.* 9(9):e1001152.

118. Pegram HJ, Andrews DM, Smyth MJ, Darcy PK, & Kershaw MH (2011) Activating and inhibitory receptors of natural killer cells. *Immunol. Cell Biol.* 89(2):216-224.

119. Wirthmueller U, Kurosaki T, Murakami MS, & Ravetch JV (1992) Signal transduction by Fc gamma RIII (CD16) is mediated through the gamma chain. *The Journal of experimental medicine* 175(5):1381-1390.

120. Lanier LL, Corliss BC, Wu J, Leong C, & Phillips JH (1998) Immunoreceptor DAP12 bearing a tyrosine-based activation motif is involved in activating NK cells. *Nature* 391(6668):703-707.

121. Wu J*, et al.* (1999) An activating immunoreceptor complex formed by NKG2D and DAP10. *Science* 285(5428):730-732.

122. Vivier E, Nunes JA, & Vely F (2004) Natural killer cell signaling pathways. *Science* 306(5701):1517-1519.

123. Culley FJ*, et al.* (2009) Natural killer cell signal integration balances synapse symmetry and migration. *PLoS Biol.* 7(7):e1000159.

124. Kohler K*, et al.* (2010) Matched sizes of activating and inhibitory receptor/ligand pairs are required for optimal signal integration by human natural killer cells. *PLoS One* 5(11):e15374.

125. Houchins JP, Yabe T, McSherry C, & Bach FH (1991) DNA sequence analysis of NKG2, a family of related cDNA clones encoding type II integral membrane proteins on human natural killer cells. *J. Exp. Med.* 173(4):1017-1020.

126. Pende D*, et al.* (1999) Identification and molecular characterization of NKp30, a novel triggering receptor involved in natural cytotoxicity mediated by human natural killer cells. *J. Exp. Med.* 190(10):1505-1516.

127. Cantoni C*, et al.* (1999) NKp44, a triggering receptor involved in tumor cell lysis by activated human natural killer cells, is a novel member of the immunoglobulin superfamily. *J. Exp. Med.* 189(5):787-796.

128. Pessino A*, et al.* (1998) Molecular cloning of NKp46: a novel member of the immunoglobulin superfamily involved in triggering of natural cytotoxicity. *J. Exp. Med.* 188(5):953-960.

129. Spreu J*, et al.* (2010) Interaction of C-type lectin-like receptors NKp65 and KACL facilitates dedicated immune recognition of human keratinocytes. *Proc. Natl. Acad. Sci. U. S. A.* 107(11):5100-5105.

130. Dennehy KM, Klimosch SN, & Steinle A (2011) Cutting edge: NKp80 uses an atypical hemi-ITAM to trigger NK cytotoxicity. *J. Immunol.* 186(2):657-661.

131. Eissmann P*, et al.* (2005) Molecular basis for positive and negative signaling by the natural killer cell receptor 2B4 (CD244). *Blood* 105(12):4722-4729.

132. Bottino C*, et al.* (2003) Identification of PVR (CD155) and Nectin-2 (CD112) as cell surface ligands for the human DNAM-1 (CD226) activating molecule. *J. Exp. Med.* 198(4):557-567.

133. Reth M (1989) Antigen receptor tail clue. *Nature* 338(6214):383-384.

134. Siliciano RF, Pratt JC, Schmidt RE, Ritz J, & Reinherz EL (1985) Activation of cytolytic T lymphocyte and natural killer cell function through the T11 sheep erythrocyte binding protein. *Nature* 317(6036):428-430.

135. Galandrini R, De Maria R, Piccoli M, Frati L, & Santoni A (1994) CD44 triggering enhances human NK cell cytotoxic functions. *J. Immunol.* 153(10):4399-4407.

136. Endt J*, et al.* (2007) Modulation of 2B4 (CD244) activity and regulated SAP expression in human NK cells. *Eur. J. Immunol.* 37(1):193-198.

137. Le Bouteiller P*, et al.* (2002) Engagement of CD160 receptor by HLA-C is a triggering mechanism used by circulating natural killer (NK) cells to mediate cytotoxicity. *Proc. Natl. Acad. Sci. U. S. A.* 99(26):16963-16968.

138. Rabot M*, et al.* (2007) CD160-activating NK cell effector functions depend on the phosphatidylinositol 3-kinase recruitment. *Int. Immunol.* 19(4):401-409.

139. Wilson JL*, et al.* (1999) NK cell triggering by the human costimulatory molecules CD80 and CD86. *J. Immunol.* 163(8):4207-4212.

140. Bauer S*, et al.* (1999) Activation of NK cells and T cells by NKG2D, a receptor for stress-inducible MICA. *Science* 285(5428):727-729.

141. Cosman D*, et al.* (2001) ULBPs, novel MHC class I-related molecules bind to CMV glycoprotein UL16 and stimulate NK cytotoxicity through the NKG2D receptor. *Immunity* 14(2):123-133.

142. Groh V*, et al.* (2001) Costimulation of CD8alphabeta T cells by NKG2D via engagement by MIC induced on virus-infected cells. *Nat. Immunol.* 2(3):255-260.

143. Steinle A*, et al.* (2001) Interactions of human NKG2D with its ligands MICA, MICB, and homologs of the mouse RAE-1 protein family. *Immunogenetics* 53(4):279-287.

144. Gasser S & Raulet DH (2006) Activation and self-tolerance of natural killer cells. *Immunol. Rev.* 214:130-142.

145. Azuma M, Cayabyab M, Buck D, Phillips JH, & Lanier LL (1992) CD28 interaction with B7 costimulates primary allogeneic proliferative responses and cytotoxicity mediated by small, resting T lymphocytes. *J. Exp. Med.* 175(2):353-360.

146. Billadeau DD, Upshaw JL, Schoon RA, Dick CJ, & Leibson PJ (2003) NKG2D-DAP10 triggers human NK cell-mediated killing via a Syk-independent regulatory pathway. *Nat. Immunol.* 4(6):557-564.

147. Mandelboim O*, et al.* (1999) Human CD16 as a lysis receptor mediating direct natural killer cell cytotoxicity. *Proc. Natl. Acad. Sci. U. S. A.* 96(10):5640-5644.

148. Nimmerjahn F & Ravetch JV (2008) Fc gamma receptors as regulators of immune responses. *Nature Reviews Immunology* 8(1):34-47.

149. Cooper MA, Fehniger TA, & Caligiuri MA (2001) The biology of human natural killer-cell subsets. *Trends Immunol.* 22(11):633-640.

150. Chan WK*, et al.* (2012) Antibody-dependent cell-mediated cytotoxicity overcomes NK cell resistance in MLL-rearranged leukemia expressing inhibitory KIR ligands but not activating ligands. *Clin. Cancer Res.* 18(22):6296-6305.

151. Gazit R*, et al.* (2007) NK cytotoxicity mediated by CD16 but not by NKp30 is functional in Griscelli syndrome. *Blood* 109(10):4306-4312.

152. Lanier LL (2003) Natural killer cell receptor signaling. *Curr. Opin. Immunol.* 15(3):308-314.

153. Bryceson YT, Ljunggren HG, & Long EO (2009) Minimal requirement for induction of natural cytotoxicity and intersection of activation signals by inhibitory receptors. *Blood* 114(13):2657-2666.

154. Bryceson YT, March ME, Barber DF, Ljunggren HG, & Long EO (2005) Cytolytic granule polarization and degranulation controlled by different receptors in resting NK cells. *J. Exp. Med.* 202(7):1001-1012.

155. Bustelo XR (2000) Regulatory and signaling properties of the Vav family. *Mol. Cell. Biol.* 20(5):1461-1477.

156. Graham DB*, et al.* (2006) Vav1 controls DAP10-mediated natural cytotoxicity by regulating actin and microtubule dynamics. *J. Immunol.* 177(4):2349-2355.

157. Galea-Lauri J*, et al.* (1999) Expression of a variant of CD28 on a subpopulation of human NK cells: implications for B7-mediated stimulation of NK cells. *J. Immunol.* 163(1):62-70.

158. Topham NJ & Hewitt EW (2009) Natural killer cell cytotoxicity: how do they pull the trigger? *Immunology* 128(1):7-15.

159. Turner CE*, et al.* (1999) Paxillin LD4 motif binds PAK and PIX through a novel 95-kD ankyrin repeat, ARF-GAP protein: A role in cytoskeletal remodeling. *J. Cell Biol.* 145(4):851-863.

160. March ME & Long EO (2011) beta2 integrin induces TCRzeta-Syk-phospholipase C-gamma phosphorylation and paxillin-dependent granule polarization in human NK cells. *J. Immunol.* 186(5):2998-3005.

161. Ostergaard HL, Lou O, Arendt CW, & Berg NN (1998) Paxillin phosphorylation and association with Lck and Pyk2 in anti-CD3- or anti-CD45-stimulated T cells. *J. Biol. Chem.* 273(10):5692-5696.

162. Butler B & Cooper JA (2009) Distinct roles for the actin nucleators Arp2/3 and hDia1 during NK-mediated cytotoxicity. *Curr. Biol.* 19(22):1886-1896.

163. Mace EM, Zhang J, Siminovitch KA, & Takei F (2010) Elucidation of the integrin LFA-1-mediated signaling pathway of actin polarization in natural killer cells. *Blood* 116(8):1272-1279.

164. Katz P, Zaytoun AM, & Lee JH, Jr. (1982) Mechanisms of human cell-mediated cytotoxicity. III. Dependence of natural killing on microtubule and microfilament integrity. *J. Immunol.* 129(6):2816-2825.

165. Orange JS*, et al.* (2002) Wiskott-Aldrich syndrome protein is required for NK cell cytotoxicity and colocalizes with actin to NK cell-activating immunologic synapses. *Proc. Natl. Acad. Sci. U. S. A.* 99(17):11351-11356.

166. Gross CC, Brzostowski JA, Liu D, & Long EO (2010) Tethering of intercellular adhesion molecule on target cells is required for LFA-1-dependent NK cell adhesion and granule polarization. *J. Immunol.* 185(5):2918-2926.

167. Wulfing C, Purtic B, Klem J, & Schatzle JD (2003) Stepwise cytoskeletal polarization as a series of checkpoints in innate but not adaptive cytolytic killing. *Proc. Natl. Acad. Sci. U. S. A.* 100(13):7767-7772.

168. Carpen O, Virtanen I, Lehto VP, & Saksela E (1983) Polarization of NK cell cytoskeleton upon conjugation with sensitive target cells. *J. Immunol.* 131(6):2695-2698.

169. Chen XM*, et al.* (2004) Cdc42 and the actin-related protein/neural Wiskott-Aldrich syndrome protein network mediate cellular invasion by Cryptosporidium parvum. *Infect. Immun.* 72(5):3011-3021.

170. Rohatgi R*, et al.* (1999) The interaction between N-WASP and the Arp2/3 complex links Cdc42-dependent signals to actin assembly. *Cell* 97(2):221-231.

171. Carlin LM*, et al.* (2011) A targeted siRNA screen identifies regulators of Cdc42 activity at the natural killer cell immunological synapse. *Science signaling* 4(201):ra81.

172. Banerjee PP*, et al.* (2007) Cdc42-interacting protein-4 functionally links actin and microtubule networks at the cytolytic NK cell immunological synapse. *J. Exp. Med.* 204(10):2305-2320.

173. Mentlik AN, Sanborn KB, Holzbaur EL, & Orange JS (2010) Rapid lytic granule convergence to the MTOC in natural killer cells is dependent on dynein but not cytolytic commitment. *Mol. Biol. Cell* 21(13):2241-2256.

174. Daniele T*, et al.* (2011) A role for Rab7 in the movement of secretory granules in cytotoxic T lymphocytes. *Traffic* 12(7):902-911.

175. Krzewski K, Gil-Krzewska A, Watts J, Stern JN, & Strominger JL (2011) VAMP4- and VAMP7-expressing vesicles are both required for cytotoxic granule exocytosis in NK cells. *Eur. J. Immunol.* 41(11):3323-3329.

176. Krzewski K, Gil-Krzewska A, Nguyen V, Peruzzi G, & Coligan JE (2013) LAMP1/CD107a is required for efficient perforin delivery to lytic granules and NK-cell cytotoxicity. *Blood* 121(23):4672-4683.

177. Kupfer A, Dennert G, & Singer SJ (1983) Polarization of the Golgi apparatus and the microtubule-organizing center within cloned natural killer cells bound to their targets. *Proc. Natl. Acad. Sci. U. S. A.* 80(23):7224-7228.

178. Chen X, Trivedi PP, Ge B, Krzewski K, & Strominger JL (2007) Many NK cell receptors activate ERK2 and JNK1 to trigger microtubule organizing center and granule polarization and cytotoxicity. *Proc. Natl. Acad. Sci. U. S. A.* 104(15):6329-6334.

179. Tuli A*, et al.* (2013) Arf-like GTPase Arl8b regulates lytic granule polarization and natural killer cell-mediated cytotoxicity. *Mol. Biol. Cell* 24(23):3721-3735.

180. Tolic-Norrelykke IM (2008) Push-me-pull-you: how microtubules organize the cell interior. *Eur. Biophys. J.* 37(7):1271-1278.

181. Laan L*, et al.* (2012) Cortical dynein controls microtubule dynamics to generate pulling forces that position microtubule asters. *Cell* 148(3):502-514.

182. Kanwar N & Wilkins JA (2011) IQGAP1 involvement in MTOC and granule polarization in NK-cell cytotoxicity. *Eur. J. Immunol.* 41(9):2763-2773.

183. Krzewski K, Chen X, & Strominger JL (2008) WIP is essential for lytic granule polarization and NK cell cytotoxicity. *Proc. Natl. Acad. Sci. U. S. A.* 105(7):2568-2573.

184. Stinchcombe JC, Majorovits E, Bossi G, Fuller S, & Griffiths GM (2006) Centrosome polarization delivers secretory granules to the immunological synapse. *Nature* 443(7110):462-465.

185. Campi G, Varma R, & Dustin ML (2005) Actin and agonist MHC-peptide complex-dependent T cell receptor microclusters as scaffolds for signaling. *J. Exp. Med.* 202(8):1031-1036.

186. Mace EM & Orange JS (2012) Dual channel STED nanoscopy of lytic granules on actin filaments in natural killer cells. *Commun. Integr. Biol.* 5(2):184-186.

187. Rak GD, Mace EM, Banerjee PP, Svitkina T, & Orange JS (2011) Natural killer cell lytic granule secretion occurs through a pervasive actin network at the immune synapse. *PLoS Biol.* 9(9):e1001151.

188. Mace EM*, et al.* (2012) NK cell lytic granules are highly motile at the immunological synapse and require F-actin for post-degranulation persistence. *J. Immunol.* 189(10):4870-4880.

189. Alakoskela JM*, et al.* (2011) Mechanisms for size-dependent protein segregation at immune synapses assessed with molecular rulers. *Biophys. J.* 100(12):2865-2874.

190. Stinchcombe JC*, et al.* (2001) Rab27a is required for regulated secretion in cytotoxic T lymphocytes. *The Journal of cell biology* 152(4):825-834.

191. Alter G, Malenfant JM, & Altfeld M (2004) CD107a as a functional marker for the identification of natural killer cell activity. *J. Immunol. Methods* 294(1-2):15-22.

192. Liu D, Martina JA, Wu XS, Hammer JA, 3rd, & Long EO (2011) Two modes of lytic granule fusion during degranulation by natural killer cells. *Immunol. Cell Biol.* 89(6):728-738.

193. Bertrand F*, et al.* (2013) An initial and rapid step of lytic granule secretion precedes microtubule organizing center polarization at the cytotoxic T lymphocyte/target cell synapse. *Proc. Natl. Acad. Sci. U. S. A.* 110(15):6073-6078.

194. Kupfer H, Monks CR, & Kupfer A (1994) Small splenic B cells that bind to antigen-specific T helper (Th) cells and face the site of cytokine production in the Th cells selectively proliferate: immunofluorescence microscopic studies of Th-B antigen-presenting cell interactions. *J. Exp. Med.* 179(5):1507-1515.

195. Kupfer A, Swain SL, Janeway CA, Jr., & Singer SJ (1986) The specific direct interaction of helper T cells and antigen-presenting B cells. *Proc. Natl. Acad. Sci. U. S. A.* 83(16):6080-6083.

196. Monks CR, Freiberg BA, Kupfer H, Sciaky N, & Kupfer A (1998) Three-dimensional segregation of supramolecular activation clusters in T cells. *Nature* 395(6697):82-86.

197. Bousso P, Bhakta NR, Lewis RS, & Robey E (2002) Dynamics of thymocyte-stromal cell interactions visualized by two-photon microscopy. *Science* 296(5574):1876-1880.

198. Stoll S, Delon J, Brotz TM, & Germain RN (2002) Dynamic imaging of T cell-dendritic cell interactions in lymph nodes. *Science* 296(5574):1873-1876.

199. Miller MJ, Wei SH, Parker I, & Cahalan MD (2002) Two-photon imaging of lymphocyte motility and antigen response in intact lymph node. *Science* 296(5574):1869-1873.

200. Carson RT, Vignali KM, Woodland DL, & Vignali DA (1997) T cell receptor recognition of MHC class II-bound peptide flanking residues enhances immunogenicity and results in altered TCR V region usage. *Immunity* 7(3):387-399.

201. Garcia KC*, et al.* (1996) CD8 enhances formation of stable T-cell receptor/MHC class I molecule complexes. *Nature* 384(6609):577-581.

202. Cronin SJ & Penninger JM (2007) From T-cell activation signals to signaling control of anti-cancer immunity. *Immunol. Rev.* 220:151-168.

203. Freiberg BA*, et al.* (2002) Staging and resetting T cell activation in SMACs. *Nat. Immunol.* 3(10):911-917.

204. Bunnell SC*, et al.* (2002) T cell receptor ligation induces the formation of dynamically regulated signaling assemblies. *J. Cell Biol.* 158(7):1263-1275.

205. Bunnell SC*, et al.* (2006) Persistence of cooperatively stabilized signaling clusters drives T-cell activation. *Mol. Cell. Biol.* 26(19):7155-7166.

206. Varma R, Campi G, Yokosuka T, Saito T, & Dustin ML (2006) T cell receptor-proximal signals are sustained in peripheral microclusters and terminated in the central supramolecular activation cluster. *Immunity* 25(1):117-127.

207. Yokosuka T*, et al.* (2005) Newly generated T cell receptor microclusters initiate and sustain T cell activation by recruitment of Zap70 and SLP-76. *Nat. Immunol.* 6(12):1253-1262.

208. Yin Y, Wang XX, & Mariuzza RA (2012) Crystal structure of a complete ternary complex of T-cell receptor, peptide-MHC, and CD4. *Proc. Natl. Acad. Sci. U. S. A.* 109(14):5405-5410.

209. Garcia KC*, et al.* (1996) An alphabeta T cell receptor structure at 2.5 A and its orientation in the TCR-MHC complex. *Science* 274(5285):209-219.

210. Fan QR, Long EO, & Wiley DC (2001) Crystal structure of the human natural killer cell inhibitory receptor KIR2DL1-HLA-Cw4 complex. *Nat. Immunol.* 2(5):452-460.

211. Li P*, et al.* (2001) Complex structure of the activating immunoreceptor NKG2D and its MHC class I-like ligand MICA. *Nat. Immunol.* 2(5):443-451.

212. Qu A & Leahy DJ (1995) Crystal structure of the I-domain from the CD11a/CD18 (LFA-1, alpha L beta 2) integrin. *Proc. Natl. Acad. Sci. U. S. A.* 92(22):10277-10281.

213. Davis SJ & van der Merwe PA (2006) The kinetic-segregation model: TCR triggering and beyond. *Nat. Immunol.* 7(8):803-809.

214. Williams AF & Beyers AD (1992) T-cell receptors. At grips with interactions. *Nature* 356(6372):746-747.

215. Kaizuka Y, Douglass AD, Varma R, Dustin ML, & Vale RD (2007) Mechanisms for segregating T cell receptor and adhesion molecules during immunological synapse formation in Jurkat T cells. *Proc. Natl. Acad. Sci. U. S. A.* 104(51):20296-20301.

216. Bratke K, Kuepper M, Bade B, Virchow JC, Jr., & Luttmann W (2005) Differential expression of human granzymes A, B, and K in natural killer cells and during CD8+ T cell differentiation in peripheral blood. *Eur. J. Immunol.* 35(9):2608-2616.

217. Bade B*, et al.* (2005) Differential expression of the granzymes A, K and M and perforin in human peripheral blood lymphocytes. *Int. Immunol.* 17(11):1419-1428.

218. Kawasaki A, Shinkai Y, Yagita H, & Okumura K (1992) Expression of perforin in murine natural killer cells and cytotoxic T lymphocytes in vivo. *Eur. J. Immunol.* 22(5):1215-1219.

219. Lowin B, Beermann F, Schmidt A, & Tschopp J (1994) A null mutation in the perforin gene impairs cytolytic T lymphocyte- and natural killer cell-mediated cytotoxicity. *Proc. Natl. Acad. Sci. U. S. A.* 91(24):11571-11575.

220. Solomou EE*, et al.* (2007) Perforin gene mutations in patients with acquired aplastic anemia. *Blood* 109(12):5234-5237.

221. Davis JE, Sutton VR, Smyth MJ, & Trapani JA (2000) Dependence of granzyme B-mediated cell death on a pathway regulated by Bcl-2 or its viral homolog, BHRF1. *Cell Death Differ.* 7(10):973-983.

222. Smyth MJ*, et al.* (1999) Perforin is a major contributor to NK cell control of tumor metastasis. *J. Immunol.* 162(11):6658-6662.

223. Burkhardt JK, Hester S, Lapham CK, & Argon Y (1990) The lytic granules of natural killer cells are dual-function organelles combining secretory and pre-lysosomal compartments. *The Journal of cell biology* 111(6 Pt 1):2327-2340.

224. Peters PJ*, et al.* (1991) Cytotoxic T lymphocyte granules are secretory lysosomes, containing both perforin and granzymes. *The Journal of experimental medicine* 173(5):1099-1109.

225. Blott EJ & Griffiths GM (2002) Secretory lysosomes. *Nat. Rev. Mol. Cell Biol.* 3(2):122-131.

226. Ham H & Billadeau DD (2014) Human Immunodeficiency Syndromes Affecting Human Natural Killer Cell Cytolytic Activity. *Front. Immunol.* 5:2.

227. Kurowska M*, et al.* (2012) Terminal transport of lytic granules to the immune synapse is mediated by the kinesin-1/Slp3/Rab27a complex. *Blood* 119(17):3879-3889.

228. Peters PJ*, et al.* (1989) Molecules relevant for T cell-target cell interaction are present in cytolytic granules of human T lymphocytes. *Eur. J. Immunol.* 19(8):1469-1475.

229. Matti U*, et al.* (2013) Synaptobrevin2 is the v-SNARE required for cytotoxic T-lymphocyte lytic granule fusion. *Nature communications* 4:1439.

230. Kaplan J, De Domenico I, & Ward DM (2008) Chediak-Higashi syndrome. *Curr. Opin. Hematol.* 15(1):22-29.

231. Clark R & Griffiths GM (2003) Lytic granules, secretory lysosomes and disease. *Curr. Opin. Immunol.* 15(5):516-521.

232. Griscelli C*, et al.* (1978) A syndrome associating partial albinism and immunodeficiency. *Am. J. Med.* 65(4):691-702.

233. Griffiths GM (2002) Albinism and immunity: what's the link? *Curr. Mol. Med.* 2(5):479-483.

234. Cichocki F*, et al.* (2014) Transcriptional regulation of Munc13-4 expression in cytotoxic lymphocytes is disrupted by an intronic mutation associated with a primary immunodeficiency. *J. Exp. Med.*

235. Menager MM*, et al.* (2007) Secretory cytotoxic granule maturation and exocytosis require the effector protein hMunc13-4. *Nat. Immunol.* 8(3):257-267.

236. Marks MS, Heijnen HF, & Raposo G (2013) Lysosome-related organelles: unusual compartments become mainstream. *Curr. Opin. Cell Biol.* 25(4):495-505.

237. Pattu V*, et al.* (2013) In the Crosshairs: Investigating Lytic Granules by High-Resolution Microscopy and Electrophysiology. *Front. Immunol.* 4:411.

238. Neighbour PA, Huberman HS, & Kress Y (1982) Human large granular lymphocytes and natural killing ultrastructural studies of strontium-induced degranulation. *Eur. J. Immunol.* 12(7):588-595.

239. Grujic M*, et al.* (2005) Serglycin-deficient cytotoxic T lymphocytes display defective secretory granule maturation and granzyme B storage. *J. Biol. Chem.* 280(39):33411-33418.

240. Masson D & Tschopp J (1987) A family of serine esterases in lytic granules of cytolytic T lymphocytes. *Cell* 49(5):679-685.

241. Masson D, Nabholz M, Estrade C, & Tschopp J (1986) Granules of cytolytic T-lymphocytes contain two serine esterases. *EMBO J.* 5(7):1595-1600.

242. Voskoboinik I, Dunstone MA, Baran K, Whisstock JC, & Trapani JA (2010) Perforin: structure, function, and role in human immunopathology. *Immunol. Rev.* 235(1):35-54.

243. Voskoboinik I, Smyth MJ, & Trapani JA (2006) Perforin-mediated target-cell death and immune homeostasis. *Nat. Rev. Immunol.* 6(12):940-952.

244. Nakata M*, et al.* (1992) Expression of perforin and cytolytic potential of human peripheral blood lymphocyte subpopulations. *Int. Immunol.* 4(9):1049-1054.

245. Salcedo TW, Azzoni L, Wolf SF, & Perussia B (1993) Modulation of perforin and granzyme messenger RNA expression in human natural killer cells. *J. Immunol.* 151(5):2511-2520.

246. Rochel N & Cowan J (1996) Negative cooperativity exhibited by the lytic amino-terminal domain of human perforin: implications for perforin-mediated cell lysis. *Chem. Biol.* 3(1):31-36.

247. Shatursky O*, et al.* (1999) The mechanism of membrane insertion for a cholesterol-dependent cytolysin: a novel paradigm for pore-forming toxins. *Cell* 99(3):293-299.

248. Voskoboinik I*, et al.* (2005) Calcium-dependent plasma membrane binding and cell lysis by perforin are mediated through its C2 domain: A critical role for aspartate residues 429, 435, 483, and 485 but not 491. *The Journal of biological chemistry* 280(9):8426-8434.

249. Slade DJ*, et al.* (2008) Crystal structure of the MACPF domain of human complement protein C8 alpha in complex with the C8 gamma subunit. *J. Mol. Biol.* 379(2):331-342.

250. Tschopp J, Masson D, & Stanley KK (1986) Structural/functional similarity between proteins involved in complement- and cytotoxic T-lymphocyte-mediated cytolysis. *Nature* 322(6082):831-834.

251. Rosado CJ*, et al.* (2008) The MACPF/CDC family of pore-forming toxins. *Cell. Microbiol.* 10(9):1765-1774.

252. Brennan AJ*, et al.* (2011) Protection from endogenous perforin: glycans and the C terminus regulate exocytic trafficking in cytotoxic lymphocytes. *Immunity* 34(6):879-892.

253. van der Spoel A, Bonten E, & d'Azzo A (1998) Transport of human lysosomal neuraminidase to mature lysosomes requires protective protein/cathepsin A. *EMBO J.* 17(6):1588-1597.

254. Uellner R*, et al.* (1997) Perforin is activated by a proteolytic cleavage during biosynthesis which reveals a phospholipid-binding C2 domain. *EMBO J.* 16(24):7287-7296.

255. Fraser SA, Karimi R, Michalak M, & Hudig D (2000) Perforin lytic activity is controlled by calreticulin. *J. Immunol.* 164(8):4150-4155.

256. Metkar SS*, et al.* (2002) Cytotoxic cell granule-mediated apoptosis: perforin delivers granzyme B-serglycin complexes into target cells without plasma membrane pore formation. *Immunity* 16(3):417-428.

257. Portales P*, et al.* (2003) Interferon-alpha restores HIV-induced alteration of natural killer cell perforin expression in vivo. *AIDS* 17(4):495-504.

258. Bradley M, Zeytun A, Rafi-Janajreh A, Nagarkatti PS, & Nagarkatti M (1998) Role of spontaneous and interleukin-2-induced natural killer cell activity in the cytotoxicity and rejection of Fas+ and Fas- tumor cells. *Blood* 92(11):4248-4255.

259. Walsh CM*, et al.* (1994) Immune function in mice lacking the perforin gene. *Proc. Natl. Acad. Sci. U. S. A.* 91(23):10854-10858.

260. Simon MM*, et al.* (1997) In vitro- and ex vivo-derived cytolytic leukocytes from granzyme A x B double knockout mice are defective in granule-mediated apoptosis but not lysis of target cells. *J. Exp. Med.* 186(10):1781-1786.

261. Keefe D*, et al.* (2005) Perforin triggers a plasma membrane-repair response that facilitates CTL induction of apoptosis. *Immunity* 23(3):249-262.

262. Brennan AJ, Chia J, Trapani JA, & Voskoboinik I (2010) Perforin deficiency and susceptibility to cancer. *Cell Death Differ.* 17(4):607-615.

263. Grossman WJ*, et al.* (2003) The orphan granzymes of humans and mice. *Curr. Opin. Immunol.* 15(5):544-552.

264. Poe M*, et al.* (1991) Human cytotoxic lymphocyte granzyme B. Its purification from granules and the characterization of substrate and inhibitor specificity. *J. Biol. Chem.* 266(1):98-103.

265. Edwards KM, Kam CM, Powers JC, & Trapani JA (1999) The human cytotoxic T cell granule serine protease granzyme H has chymotrypsin-like (chymase) activity and is taken up into cytoplasmic vesicles reminiscent of granzyme B-containing endosomes. *J. Biol. Chem.* 274(43):30468-30473.

266. Kam CM, Hudig D, & Powers JC (2000) Granzymes (lymphocyte serine proteases): characterization with natural and synthetic substrates and inhibitors. *Biochim. Biophys. Acta* 1477(1-2):307-323.

267. Griffiths GM & Isaaz S (1993) Granzymes A and B are targeted to the lytic granules of lymphocytes by the mannose-6-phosphate receptor. *The Journal of cell biology* 120(4):885-896.

268. Meade JL*, et al.* (2006) A family with Papillon-Lefevre syndrome reveals a requirement for cathepsin C in granzyme B activation and NK cell cytolytic activity. *Blood* 107(9):3665-3668.

269. D'Angelo ME*, et al.* (2010) Cathepsin H is an additional convertase of pro-granzyme B. *J. Biol. Chem.* 285(27):20514-20519.

270. Raja SM*, et al.* (2002) Cytotoxic cell granule-mediated apoptosis. Characterization of the macromolecular complex of granzyme B with serglycin. *J. Biol. Chem.* 277(51):49523-49530.

271. Lord SJ, Rajotte RV, Korbutt GS, & Bleackley RC (2003) Granzyme B: a natural born killer. *Immunol. Rev.* 193:31-38.

272. Bleackley RC & Heibein JA (2001) Enzymatic control of apoptosis. *Nat. Prod. Rep.* 18(4):431-440.

273. Darmon AJ, Nicholson DW, & Bleackley RC (1995) Activation of the apoptotic protease CPP32 by cytotoxic T-cell-derived granzyme B. *Nature* 377(6548):446-448.

274. Darmon AJ, Ley TJ, Nicholson DW, & Bleackley RC (1996) Cleavage of CPP32 by granzyme B represents a critical role for granzyme B in the induction of target cell DNA fragmentation. *J. Biol. Chem.* 271(36):21709-21712.

275. Adrain C, Murphy BM, & Martin SJ (2005) Molecular ordering of the caspase activation cascade initiated by the cytotoxic T lymphocyte/natural killer (CTL/NK) protease granzyme B. *J. Biol. Chem.* 280(6):4663-4673.

276. Kothakota S*, et al.* (1997) Caspase-3-generated fragment of gelsolin: effector of morphological change in apoptosis. *Science* 278(5336):294-298.

277. Enari M*, et al.* (1998) A caspase-activated DNase that degrades DNA during apoptosis, and its inhibitor ICAD. *Nature* 391(6662):43-50.

278. Andrade F*, et al.* (1998) Granzyme B directly and efficiently cleaves several downstream caspase substrates: implications for CTL-induced apoptosis. *Immunity* 8(4):451-460.

279. Barry M*, et al.* (2000) Granzyme B short-circuits the need for caspase 8 activity during granule-mediated cytotoxic T-lymphocyte killing by directly cleaving Bid. *Mol. Cell. Biol.* 20(11):3781-3794.

280. Heibein JA*, et al.* (2000) Granzyme B-mediated cytochrome c release is regulated by the Bcl-2 family members bid and Bax. *J. Exp. Med.* 192(10):1391-1402.

281. Froelich CJ*, et al.* (1996) Granzyme B/perforin-mediated apoptosis of Jurkat cells results in cleavage of poly(ADP-ribose) polymerase to the 89-kDa apoptotic fragment and less abundant 64-kDa fragment. *Biochem. Biophys. Res. Commun.* 227(3):658-665.

282. Zhu P*, et al.* (2006) Granzyme A, which causes single-stranded DNA damage, targets the double-strand break repair protein Ku70. *EMBO Rep* 7(4):431-437.

283. Beresford PJ*, et al.* (2001) Granzyme A activates an endoplasmic reticulum-associated caspase-independent nuclease to induce single-stranded DNA nicks. *J. Biol. Chem.* 276(46):43285-43293.

284. Hurley JH & Misra S (2000) Signaling and subcellular targeting by membrane-binding domains. *Annu. Rev. Biophys. Biomol. Struct.* 29:49-79.

285. Shin OH*, et al.* (2010) Munc13 C2B domain is an activity-dependent Ca2+ regulator of synaptic exocytosis. *Nat. Struct. Mol. Biol.* 17(3):280-288.

286. Law RH*, et al.* (2010) The structural basis for membrane binding and pore formation by lymphocyte perforin. *Nature* 468(7322):447-451.

287. J Thiery DK, S. Saffarian, D. Martinvalet, M. Walch, E. Boucrot, T. Kirchhausen, and J. Lieberman (2010) Perforin activated clathrin- and dynamin-dependent endocytosis, which is required for plasma membrane repeair and delivery of granzyme B for granzyme-mediated apoptosis. *Blood* 115(8):1582-1593.

288. Praper T*, et al.* (2011) Human perforin employs different avenues to damage membranes. *J. Biol. Chem.* 286(4):2946-2955.

289. Dourmashkin RR, Deteix P, Simone CB, & Henkart P (1980) Electron microscopic demonstration of lesions in target cell membranes associated with antibody-dependent cellular cytotoxicity. *Clin. Exp. Immunol.* 42(3):554-560.

290. Gross C, Koelch W, DeMaio A, Arispe N, & Multhoff G (2003) Cell surface-bound heat shock protein 70 (Hsp70) mediates perforin-independent apoptosis by specific binding and uptake of granzyme B. *J. Biol. Chem.* 278(42):41173-41181.

291. Lopez JA*, et al.* (2013) Perforin forms transient pores on the target cell plasma membrane to facilitate rapid access of granzymes during killer cell attack. *Blood* 121(14):2659-2668.

292. Froelich CJ*, et al.* (1996) New paradigm for lymphocyte granule-mediated cytotoxicity. Target cells bind and internalize granzyme B, but an endosomolytic agent is necessary for cytosolic delivery and subsequent apoptosis. *J. Biol. Chem.* 271(46):29073-29079.

293. Thiery J*, et al.* (2010) Perforin activates clathrin- and dynamin-dependent endocytosis, which is required for plasma membrane repair and delivery of granzyme B for granzyme-mediated apoptosis. *Blood* 115(8):1582-1593.

294. J. Thiery DK, S. Boulant, E. Boucrot, M. Walch, D. Martinvalet, I. S. Goping, R. C. Bleackley, T. Kirchhausen, and J. Leiberman (2011) Perforin pores in the endosomal membrane trigger the release of endocytosed granzyme B into the cytosol of target cells. *Nat. Immunol.* 12(8):770-777.

295. Doubrovina ES*, et al.* (2003) Evasion from NK cell immunity by MHC class I chain-related molecules expressing colon adenocarcinoma. *J. Immunol.* 171(12):6891-6899.

296. Reiners KS*, et al.* (2013) Soluble ligands for NK cell receptors promote evasion of chronic lymphocytic leukemia cells from NK cell anti-tumor activity. *Blood* 121(18):3658-3665.

297. Mamessier E*, et al.* (2011) Human breast cancer cells enhance self tolerance by promoting evasion from NK cell antitumor immunity. *J. Clin. Invest.* 121(9):3609-3622.

298. Odom CI, Gaston DC, Markert JM, & Cassady KA (2012) Human herpesviridae methods of natural killer cell evasion. *Adv. Virol.* 2012:359869.

299. Jonjic S, Babic M, Polic B, & Krmpotic A (2008) Immune evasion of natural killer cells by viruses. *Curr. Opin. Immunol.* 20(1):30-38.

300. Mao H*, et al.* (2009) Influenza virus directly infects human natural killer cells and induces cell apoptosis. *J. Virol.* 83(18):9215-9222.

301. Koehl U*, et al.* (2004) IL-2 activated NK cell immunotherapy of three children after haploidentical stem cell transplantation. *Blood Cells Mol. Dis.* 33(3):261-266.

302. Iliopoulou EG*, et al.* (2010) A phase I trial of adoptive transfer of allogeneic natural killer cells in patients with advanced non-small cell lung cancer. *Cancer Immunol. Immunother.* 59(12):1781-1789.

303. Berg M*, et al.* (2009) Clinical-grade ex vivo-expanded human natural killer cells up-regulate activating receptors and death receptor ligands and have enhanced cytolytic activity against tumor cells. *Cytotherapy* 11(3):341-355.

304. Guma SR*, et al.* (2014) Natural killer cell therapy and aerosol interleukin-2 for the treatment of osteosarcoma lung metastasis. *Pediatr. Blood Cancer* 61(4):618-626.

305. Miller JS*, et al.* (2005) Successful adoptive transfer and in vivo expansion of human haploidentical NK cells in patients with cancer. *Blood* 105(8):3051-3057.

306. Foley B, De Santis D, Lathbury L, Christiansen F, & Witt C (2008) KIR2DS1-mediated activation overrides NKG2A-mediated inhibition in HLA-C C2-negative individuals. *Int. Immunol.* 20(4):555-563.

307. Cooley S*, et al.* (2009) Donors with group B KIR haplotypes improve relapse-free survival after unrelated hematopoietic cell transplantation for acute myelogenous leukemia. *Blood* 113(3):726-732.

308. Venstrom JM*, et al.* (2012) HLA-C-dependent prevention of leukemia relapse by donor activating KIR2DS1. *N. Engl. J. Med.* 367(9):805-816.

309. Fehniger TA, Cooper MA, & Caligiuri MA (2002) Interleukin-2 and interleukin-15: immunotherapy for cancer. *Cytokine Growth Factor Rev.* 13(2):169-183.

310. Rodella L*, et al.* (2001) Interleukin 2 and interleukin 15 differentially predispose natural killer cells to apoptosis mediated by endothelial and tumour cells. *Br. J. Haematol.* 115(2):442-450.

311. Waldmann TA, Dubois S, & Tagaya Y (2001) Contrasting roles of IL-2 and IL-15 in the life and death of lymphocytes: implications for immunotherapy. *Immunity* 14(2):105-110.

312. Kobayashi H*, et al.* (2005) Role of trans-cellular IL-15 presentation in the activation of NK cell-mediated killing, which leads to enhanced tumor immunosurveillance. *Blood* 105(2):721-727.

313. Moretta L*, et al.* (2006) Effector and regulatory events during natural killer-dendritic cell interactions. *Immunol. Rev.* 214:219-228.

314. Hamerman JA, Ogasawara K, & Lanier LL (2005) NK cells in innate immunity. *Curr. Opin. Immunol.* 17(1):29-35.

315. Cooper MA, Fehniger TA, Fuchs A, Colonna M, & Caligiuri MA (2004) NK cell and DC interactions. *Trends Immunol.* 25(1):47-52.

316. Trinchieri G (2003) Interleukin-12 and the regulation of innate resistance and adaptive immunity. *Nat. Rev. Immunol.* 3(2):133-146.

317. Sinkovics JG & Horvath JC (2005) Human natural killer cells: a comprehensive review. *Int. J. Oncol.* 27(1):5-47.

318. Chiou SH, Sheu BC, Chang WC, Huang SC, & Hong-Nerng H (2005) Current concepts of tumor-infiltrating lymphocytes in human malignancies. *J. Reprod. Immunol.* 67(1-2):35-50.

319. Smyth MJ*, et al.* (2006) CD4+CD25+ T regulatory cells suppress NK cell-mediated immunotherapy of cancer. *J. Immunol.* 176(3):1582-1587.

320. Seidel UJ, Schlegel P, & Lang P (2013) Natural killer cell mediated antibody-dependent cellular cytotoxicity in tumor immunotherapy with therapeutic antibodies. *Front. Immunol.* 4:76.

321. Maloney DG*, et al.* (1994) Phase I clinical trial using escalating single-dose infusion of chimeric anti-CD20 monoclonal antibody (IDEC-C2B8) in patients with recurrent B-cell lymphoma. *Blood* 84(8):2457-2466.

322. van Oers MH*, et al.* (2010) Rituximab maintenance treatment of relapsed/resistant follicular non-Hodgkin's lymphoma: long-term outcome of the EORTC 20981 phase III randomized intergroup study. *J. Clin. Oncol.* 28(17):2853-2858.

323. Wu J*, et al.* (1997) A novel polymorphism of FcgammaRIIIa (CD16) alters receptor function and predisposes to autoimmune disease. *J. Clin. Invest.* 100(5):1059-1070.

324. Rudnicka D*, et al.* (2013) Rituximab causes a polarization of B cells that augments its therapeutic function in NK-cell-mediated antibody-dependent cellular cytotoxicity. *Blood* 121(23):4694-4702.

325. Kohrt HE*, et al.* (2012) Stimulation of natural killer cells with a CD137-specific antibody enhances trastuzumab efficacy in xenotransplant models of breast cancer. *J. Clin. Invest.* 122(3):1066-1075.

326. Lundin J*, et al.* (2002) Phase II trial of subcutaneous anti-CD52 monoclonal antibody alemtuzumab (Campath-1H) as first-line treatment for patients with B-cell chronic lymphocytic leukemia (B-CLL). *Blood* 100(3):768-773.

327. Jonker DJ*, et al.* (2007) Cetuximab for the treatment of colorectal cancer. *N. Engl. J. Med.* 357(20):2040-2048.

328. Romagne F*, et al.* (2009) Preclinical characterization of 1-7F9, a novel human anti-KIR receptor therapeutic antibody that augments natural killer-mediated killing of tumor cells. *Blood* 114(13):2667-2677.

329. Wu L*, et al.* (2008) lenalidomide enhances natural killer cell and monocyte-mediated antibody-dependent cellular cytotoxicity of rituximab-treated CD20+ tumor cells. *Clin. Cancer. Res.* 14(14):4650-4657.

330. Watanabe M*, et al.* (2010) Interleukin-21 can efficiently restore impaired antibody-dependent cell-mediated cytotoxicity in patients with oesophageal squamous cell carcinoma. *Br. J. Cancer* 102(3):520-529.

331. Lehmann D*, et al.* (2014) IL-12 directs further maturation of ex vivo differentiated NK cells with improved therapeutic potential. *PLoS One* 9(1):e87131.

332. Nguyen QH*, et al.* (1998) Enhancement of antibody-dependent cellular cytotoxicity of neonatal cells by interleukin-2 (IL-2) and IL-12. *Clin. Diagn. Lab. Immunol.* 5(1):98-104.

333. Roberti MP*, et al.* (2011) IL-15 and IL-2 increase Cetuximab-mediated cellular cytotoxicity against triple negative breast cancer cell lines expressing EGFR. *Breast Cancer Res. Treat.* 130(2):465-475.

334. Schleinitz N, Vely F, Harle JR, & Vivier E (2010) Natural killer cells in human autoimmune diseases. *Immunology* 131(4):451-458.

335. Arbuckle MR*, et al.* (2003) Development of autoantibodies before the clinical onset of systemic lupus erythematosus. *New Engl. J. Med.* 349(16):1526-1533.

336. Dotta F*, et al.* (2007) Coxsackie B4 virus infection of beta cells and natural killer cell insulitis in recent-onset type 1 diabetic patients. *Proc. Natl. Acad. Sci. U. S. A.* 104(12):5115-5120.

337. Ito T*, et al.* (2008) Maintenance of hair follicle immune privilege is linked to prevention of NK cell attack. *J. Invest. Dermatol.* 128(5):1196-1206.

338. Pachman LM*, et al.* (1998) Studies of muscle biopsies (MBx) from DQA1*0501 untreated children with juvenile dermatomyositis (JDM) very early in their disease course: evidence of a TCR V beta 8 motif and increased CD56+ NK cells. *Arthritis Rheum.* 41(9):S203-S203.

339. Willcox A, Richardson SJ, Bone AJ, Foulis AK, & Morgan NG (2009) Analysis of islet inflammation in human type 1 diabetes. *Clin. Exp. Immunol.* 155(2):173-181.

340. Mistry AR & O'Callaghan CA (2007) Regulation of ligands for the activating receptor NKG2D. *Immunology* 121(4):439-447.

341. Jonsen A*, et al.* (2007) Association between SLE nephritis and polymorphic variants of the CRP and Fc gamma RIIIa genes. *Rheumatology* 46(9):1417-1421.

342. Yabuhara A*, et al.* (1996) A killing defect of natural killer cells as an underlying immunologic abnormality in childhood systemic lupus erythematosus. *J. Rheumatol.* 23(1):171-177.

343. Aramaki T*, et al.* (2009) A significantly impaired natural killer cell activity due to a low activity on a per-cell basis in rheumatoid arthritis. *Modern Rheumatology* 19(3):245-252.

344. Park YW*, et al.* (2009) Impaired Differentiation and Cytotoxicity of Natural Killer Cells in Systemic Lupus Erythematosus. *Arthritis Rheum.* 60(6):1753-1763.

345. Carrega P & Ferlazzo G (2012) Natural killer cell distribution and trafficking in human tissues. *Front. Immunol.* 3:347.

346. Dalbeth N & Callan MF (2002) A subset of natural killer cells is greatly expanded within inflamed joints. *Arthritis Rheum.* 46(7):1763-1772.

347. Jiang W, Chai NR, Maric D, & Bielekova B (2011) Unexpected role for granzyme K in CD56bright NK cell-mediated immunoregulation of multiple sclerosis. *J. Immunol.* 187(2):781-790.

348. Morse RH, Seguin R, McCrea EL, & Antel JP (2001) NK cell-mediated lysis of autologous human oligodendrocytes. *J. Neuroimmunol.* 116(1):107-115.

349. Saikali P*, et al.* (2007) NKG2D-mediated cytotoxicity toward oligodendrocytes suggests a mechanism for tissue injury in multiple sclerosis. *J. Neurosci.* 27(5):1220-1228.

350. Bielekova B*, et al.* (2006) Regulatory CD56(bright) natural killer cells mediate immunomodulatory effects of IL-2Ralpha-targeted therapy (daclizumab) in multiple sclerosis. *Proc. Natl. Acad. Sci. U. S. A.* 103(15):5941-5946.

351. Bielekova B*, et al.* (2009) Effect of anti-CD25 antibody daclizumab in the inhibition of inflammation and stabilization of disease progression in multiple sclerosis. *Arch. Neurol.* 66(4):483-489.

352. Yuan D, Thet S, Zhou XJ, Wakeland EK, & Dang T (2011) The role of NK cells in the development of autoantibodies. *Autoimmunity* 44(8):641-651.

353. Takeda K & Dennert G (1993) The development of autoimmunity in C57BL/6 lpr mice correlates with the disappearance of natural killer type 1-positive cells: evidence for their suppressive action on bone marrow stem cell proliferation, B cell immunoglobulin secretion, and autoimmune symptoms. *J. Exp. Med.* 177(1):155-164.

354. Hervier B*, et al.* (2011) Phenotype and function of natural killer cells in systemic lupus erythematosus: excess interferon-gamma production in patients with active disease. *Arthritis Rheum.* 63(6):1698-1706.

355. Schubert DA*, et al.* (2012) Self-reactive human CD4 T cell clones form unusual immunological synapses. *J. Exp. Med.* 209(2):335-352.

356. Casasnovas JM, Stehle T, Liu JH, Wang JH, & Springer TA (1998) A dimeric crystal structure for the N-terminal two domains of intercellular adhesion molecule-1. *Proc. Natl. Acad. Sci. U. S. A.* 95(8):4134-4139.

357. Li P, McDermott G, & Strong RK (2002) Crystal structures of RAE-1beta and its complex with the activating immunoreceptor NKG2D. *Immunity* 16(1):77-86.

358. Trapani JA, Jans DA, & Sutton VR (1998) Lymphocyte granule-mediated cell death. *Springer Semin. Immunopathol.* 19(3):323-343.

359. Lieberman J (2003) The ABCs of granule-mediated cytotoxicity: new weapons in the arsenal. *Nature reviews. Immunology* 3(5):361-370.

360. Stinchcombe JC & Griffiths GM (2003) The role of the secretory immunological synapse in killing by CD8+ CTL. *Semin. Immunol.* 15(6):301-305.

361. Sigal LH (2005) Basic science for the clinician 30: The immunologic synapse. *Journal of clinical rheumatology : practical reports on rheumatic & musculoskeletal diseases* 11(4):234-239.

362. Williams GS*, et al.* (2007) Membranous structures transfer cell surface proteins across NK cell immune synapses. *Traffic* 8(9):1190-1204.

363. Benninger RK*, et al.* (2009) Live cell linear dichroism imaging reveals extensive membrane ruffling within the docking structure of natural killer cell immune synapses. *Biophys. J.* 96(2):L13-15.

364. Lieberman J (2010) Granzyme A activates another way to die. *Immunol. Rev.* 235(1):93-104.

365. Stinchcombe JC, Bossi G, Booth S, & Griffiths GM (2001) The immunological synapse of CTL contains a secretory domain and membrane bridges. *Immunity* 15(5):751-761.

366. Schlesinger BC & Cheng L (1994) Characterization of a novel monoclonal antibody against human perforin using transfected cell lines. *Immunology* 81(2):291-295.

367. Semino C, Angelini G, Poggi A, & Rubartelli A (2005) NK/iDC interaction results in IL-18 secretion by DCs at the synaptic cleft followed by NK cell activation and release of the DC maturation factor HMGB1. *Blood* 106(2):609-616.

368. Poggi A & Zocchi MR (2014) NK cell autoreactivity and autoimmune diseases. *Front. Immunol.* 5:27.

369. Batista FD, Iber D, & Neuberger MS (2001) B cells acquire antigen from target cells after synapse formation. *Nature* 411(6836):489-494.

370. Blanchard N, Di Bartolo V, & Hivroz C (2002) In the immune synapse, ZAP-70 controls T cell polarization and recruitment of signaling proteins but not formation of the synaptic pattern. *Immunity* 17(4):389-399.

371. Rossy J, Owen DM, Williamson DJ, Yang Z, & Gaus K (2013) Conformational states of the kinase Lck regulate clustering in early T cell signaling. *Nat. Immunol.* 14(1):82-89.

372. Cremer C & Cremer T (1978) Considerations on a laser-scanning-microscope with high resolution and depth of field. *Microsc. Acta* 81(1):31-44.

373. Borlinghaus RT, Birk H, & Schreiber F (*Detectors for Sensitive Detection: HyD* (Mendez-Vilas A (ed.)).

374. Brakenhoff GJ, van der Voort HT, van Spronsen EA, Linnemans WA, & Nanninga N (1985) Three-dimensional chromatin distribution in neuroblastoma nuclei shown by confocal scanning laser microscopy. *Nature* 317(6039):748-749.

375. Shimomura O, Johnson FH, & Saiga Y (1962) Extraction, purification and properties of aequorin, a bioluminescent protein from the luminous hydromedusan, Aequorea. *J. Cell. Comp. Physiol.* 59:223-239.

376. Mattheyses AL, Simon SM, & Rappoport JZ (2010) Imaging with total internal reflection fluorescence microscopy for the cell biologist. *J. Cell Sci.* 123(Pt 21):3621-3628.

377. Axelrod D (2008) Chapter 7: Total internal reflection fluorescence microscopy. *Methods Cell Biol.* 89:169-221.

378. Yoneda N*, et al.* (1992) Detection of Epstein-Barr virus genome in natural-killer-like cell line, YT. *Leukemia* 6(2):136-141.

379. Schneider U, Schwenk HU, & Bornkamm G (1977) Characterization of EBV-genome negative "null" and "T" cell lines derived from children with acute lymphoblastic leukemia and leukemic transformed non-Hodgkin lymphoma. *Int. J. Cancer* 19(5):621-626.

380. Cohen GB*, et al.* (1999) The selective downregulation of class I major histocompatibility complex proteins by HIV-1 protects HIV-infected cells from NK cells. *Immunity* 10(6):661-671.

381. Shimizu Y, Geraghty DE, Koller BH, Orr HT, & DeMars R (1988) Transfer and expression of three cloned human non-HLA-A,B,C class I major

histocompatibility complex genes in mutant lymphoblastoid cells. *Proc. Natl. Acad. Sci. U. S. A.* 85(1):227-231.

382. Klein G (1975) The Epstein-Barr virus and neoplasia. *N. Engl. J. Med.* 293(26):1353-1357.
383. Lozzio CB & Lozzio BB (1975) Human chronic myelogenous leukemia cell-line with positive Philadelphia chromosome. *Blood* 45(3):321-334.
384. Pulvertaft JV (1964) Cytology of Burkitt's Tumour (African Lymphoma). *Lancet* 1(7327):238-240.
385. Goodman A, Weil RM, & Stern KG (1955) On the mechanism of dextran formation; chromatographic studies with C14-labeled sugars. *J. Biol. Chem.* 217(2):977-985.
386. Armstrong JK, Wenby RB, Meiselman HJ, & Fisher TC (2004) The hydrodynamic radii of macromolecules and their effect on red blood cell aggregation. *Biophys. J.* 87(6):4259-4270.
387. Thorne RG & Nicholson C (2006) In vivo diffusion analysis with quantum dots and dextrans predicts the width of brain extracellular space. *Proc. Natl. Acad. Sci. U. S. A.* 103(14):5567-5572.
388. Rousseaux J, Rousseaux-Prevost R, & Bazin H (1983) Optimal conditions for the preparation of Fab and F(ab')2 fragments from monoclonal IgG of different rat IgG subclasses. *J. Immunol. Methods* 64(1-2):141-146.
389. Harmsen MM & De Haard HJ (2007) Properties, production, and applications of camelid single-domain antibody fragments. *Appl. Microbiol. Biotechnol.* 77(1):13-22.
390. Walker A*, et al.* (2009) Single domain antibodies against the collagen signalling receptor glycoprotein VI are inhibitors of collagen induced thrombus formation. *Platelets* 20(4):268-276.
391. Goldstein JL, Brown MS, Anderson RG, Russell DW, & Schneider WJ (1985) Receptor-mediated endocytosis: concepts emerging from the LDL receptor system. *Annu. Rev. Cell Biol.* 1:1-39.
392. Davis DM (2006) Intrigue at the immune synapse. *Sci. Am.* 294(2):48-55.
393. Gibbons RJ & Fitzgerald RJ (1969) Dextran-induced agglutination of Streptococcus mutans, and its potential role in the formation of microbial dental plaques. *J. Bacteriol.* 98(2):341-346.
394. Pasteur L (1861) On the viscous fermentation and the butyrous fermentation. *Bull. Soc. Chim. Fr.* 11:30-31.

395. Riva FM*, et al.* (2012) The outcome of prostaglandin-E1 and dextran-40 compared to no antithrombotic therapy in head and neck free tissue transfer: analysis of 1,351 cases in a single center. *Microsurgery* 32(5):339-343.

396. Wang Q, Perez JM, & Webster TJ (2013) Inhibited growth of Pseudomonas aeruginosa by dextran- and polyacrylic acid-coated ceria nanoparticles. *Int J Nanomedicine* 8:3395-3399.

397. Kaplan HR & Murthy VS (1975) Hemoglobin solution: a potential oxygen transporting plasma volume expander. *Fed. Proc.* 34(6):1461-1465.

398. Fisher KA, Huddersman KD, & Taylor MJ (2003) Comparison of micro- and mesoporous inorganic materials in the uptake and release of the drug model fluorescein and its analogues. *Chemistry (Easton)* 9(23):5873-5878.

399. Pecora R (2000) Dynamic light scattering measurement of nanometer particles in liquids. *J Nanopart Res* 2(2):123-131.

400. Xiao F, Nicholson C, Hrabe J, & Hrabetova S (2008) Diffusion of flexible random-coil dextran polymers measured in anisotropic brain extracellular space by integrative optical imaging. *Biophys. J.* 95(3):1382-1392.

401. Shimizu Y & DeMars R (1989) Production of human cells expressing individual transferred HLA-A,-B,-C genes using an HLA-A,-B,-C null human cell line. *J. Immunol.* 142(9):3320-3328.

402. Kupfer A, Mosmann TR, & Kupfer H (1991) Polarized expression of cytokines in cell conjugates of helper T cells and splenic B cells. *Proc. Natl. Acad. Sci. U. S. A.* 88(3):775-779.

403. Barcia C*, et al.* (2008) In vivo polarization of IFN-gamma at Kupfer and non-Kupfer immunological synapses during the clearance of virally infected brain cells. *J. Immunol.* 180(3):1344-1352.

404. Huse M, Lillemeier BF, Kuhns MS, Chen DS, & Davis MM (2006) T cells use two directionally distinct pathways for cytokine secretion. *Nat. Immunol.* 7(3):247-255.

405. James JR & Vale RD (2012) Biophysical mechanism of T-cell receptor triggering in a reconstituted system. *Nature* 487(7405):64-69.

406. Davis SJ*, et al.* (2003) The nature of molecular recognition by T cells. *Nat. Immunol.* 4(3):217-224.

407. Yarmola EG, Somasundaram T, Boring TA, Spector I, & Bubb MR (2000) Actin-latrunculin A structure and function. Differential modulation of actin-binding protein function by latrunculin A. *J. Biol. Chem.* 275(36):28120-28127.

408. Visegrady B, Lorinczy D, Hild G, Somogyi B, & Nyitrai M (2004) The effect of phalloidin and jasplakinolide on the flexibility and thermal stability of actin filaments. *FEBS Lett.* 565(1-3):163-166.

409. Brzostek J*, et al.* (2010) Ligand dimensions are important in controlling NK-cell responses. *Eur. J. Immunol.* 40(7):2050-2059.

410. Pageon SV*, et al.* (2013) Dynamics of natural killer cell receptor revealed by quantitative analysis of photoswitchable protein. *Biophys. J.* 105(9):1987-1996.

411. Springer TA (1990) Adhesion receptors of the immune system. *Nature* 346(6283):425-434.

412. Davis DM (2009) Mechanisms and functions for the duration of intercellular contacts made by lymphocytes. *Nat. Rev. Immunol.* 9(8):543-555.

413. Poggi A, Panzeri MC, Moretta L, & Zocchi MR (1996) CD31-triggered rearrangement of the actin cytoskeleton in human natural killer cells. *Eur. J. Immunol.* 26(4):817-824.

414. Ham H*, et al.* (2013) Dedicator of cytokinesis 8 interacts with talin and Wiskott-Aldrich syndrome protein to regulate NK cell cytotoxicity. *J. Immunol.* 190(7):3661-3669.

415. Mizesko MC*, et al.* (2013) Defective actin accumulation impairs human natural killer cell function in patients with dedicator of cytokinesis 8 deficiency. *J. Allergy Clin. Immunol.* 131(3):840-848.

416. Hemmings L*, et al.* (1996) Talin contains three actin-binding sites each of which is adjacent to a vinculin-binding site. *J. Cell Sci.* 109 (Pt 11):2715-2726.

417. Litman GW*, et al.* (1993) Phylogenetic diversification of immunoglobulin genes and the antibody repertoire. *Mol. Biol. Evol.* 10(1):60-72.

418. Harris LJ, Larson SB, Hasel KW, & McPherson A (1997) Refined structure of an intact IgG2a monoclonal antibody. *Biochemistry* 36(7):1581-1597.

419. Huber R, Deisenhofer J, Colman PM, Matsushima M, & Palm W (1976) Crystallographic Structure Studies of an Igg Molecule and an Fc Fragment. *Nature* 264(5585):415-420.

420. Beale D & Feinstein A (1976) Structure and function of the constant regions of immunoglobulins. *Q. Rev. Biophys.* 9(2):135-180.

421. Wysocki L, Manser T, & Gefter ML (1986) Somatic evolution of variable region structures during an immune response. *Proc. Natl. Acad. Sci. U. S. A.* 83(6):1847-1851.

422. Wang AZ*, et al.* (2008) Biofunctionalized targeted nanoparticles for therapeutic applications. *Expert Opin. Biol. Ther.* 8(8):1063-1070.

423. Tanha J*, et al.* (2001) Optimal design features of camelized human single-domain antibody libraries. *J. Biol. Chem.* 276(27):24774-24780.

424. Vincke C*, et al.* (2009) General strategy to humanize a camelid single-domain antibody and identification of a universal humanized nanobody scaffold. *J. Biol. Chem.* 284(5):3273-3284.

425. Vranken W*, et al.* (2002) Solution structure of a llama single-domain antibody with hydrophobic residues typical of the VH/VL interface. *Biochemistry* 41(27):8570-8579.

426. Ghahroudi MA, Desmyter A, Wyns L, Hamers R, & Muyldermans S (1997) Selection and identification of single domain antibody fragments from camel heavy-chain antibodies. *FEBS Lett.* 414(3):521-526.

427. Schwaber J & Cohen EP (1973) Human x mouse somatic cell hybrid clone secreting immunoglobulins of both parental types. *Nature* 244(5416):444-447.

428. Riechmann L, Clark M, Waldmann H, & Winter G (1988) Reshaping human antibodies for therapy. *Nature* 332(6162):323-327.

429. Jolliffe LK (1993) Humanized antibodies: enhancing therapeutic utility through antibody engineering. *Int. Rev. Immunol.* 10(2-3):241-250.

430. Waldmann TA (2003) Immunotherapy: past, present and future. *Nat. Med.* 9(3):269-277.

431. Rutgeerts P*, et al.* (2005) Infliximab for induction and maintenance therapy for ulcerative colitis. *N. Engl. J. Med.* 353(23):2462-2476.

432. Sandborn WJ & Hanauer SB (2002) Infliximab in the treatment of Crohn's disease: a user's guide for clinicians. *Am. J. Gastroenterol.* 97(12):2962-2972.

433. Hanauer SB*, et al.* (2002) Maintenance infliximab for Crohn's disease: the ACCENT I randomised trial. *Lancet* 359(9317):1541-1549.

434. Meroni PL & Valesini G (2014) Tumour Necrosis Factor alpha Antagonists in the Treatment of Rheumatoid Arthritis: An Immunological Perspective. *Biodrugs* 28 Suppl 1:5-13.

435. Kahan BD, Rajagopalan PR, & Hall M (1999) Reduction of the occurrence of acute cellular rejection among renal allograft recipients treated with basiliximab, a chimeric anti-interleukin-2-receptor monoclonal antibody. United States Simulect Renal Study Group. *Transplantation* 67(2):276-284.

436. Sievers EL*, et al.* (2001) Efficacy and safety of gemtuzumab ozogamicin in patients with CD33-positive acute myeloid leukemia in first relapse. *J. Clin. Oncol.* 19(13):3244-3254.

437. Corbacioglu S, Eber S, Gungor T, Hummerjohann J, & Niggli F (2003) Induction of long-term remission of a relapsed childhood B-acute lymphoblastic leukemia with rituximab chimeric anti-CD20 monoclonal antibody and autologous stem cell transplantation. *J. Pediatr. Hematol. Oncol.* 25(4):327-329.

438. Beutler B, Milsark IW, & Cerami AC (1985) Passive immunization against cachectin/tumor necrosis factor protects mice from lethal effect of endotoxin. *Science* 229(4716):869-871.

439. Keffer J*, et al.* (1991) Transgenic mice expressing human tumour necrosis factor: a predictive genetic model of arthritis. *EMBO J.* 10(13):4025-4031.

440. Elliott MJ*, et al.* (1994) Randomised double-blind comparison of chimeric monoclonal antibody to tumour necrosis factor alpha (cA2) versus placebo in rheumatoid arthritis. *Lancet* 344(8930):1105-1110.

441. Wang W, Singh S, Zeng DL, King K, & Nema S (2007) Antibody structure, instability, and formulation. *J. Pharm. Sci.* 96(1):1-26.

442. Baud FJ*, et al.* (1995) Brief report: treatment of severe colchicine overdose with colchicine-specific Fab fragments. *N. Engl. J. Med.* 332(10):642-645.

443. Figini M*, et al.* (1998) Panning phage antibody libraries on cells: isolation of human Fab fragments against ovarian carcinoma using guided selection. *Cancer Res.* 58(5):991-996.

444. Lu J*, et al.* (2006) Passive immunotherapy for influenza A H5N1 virus infection with equine hyperimmune globulin F(ab')2 in mice. *Respir. Res.* 7:43.

445. Ramisse F, Binder P, Szatanik M, & Alonso JM (1996) Passive and active immunotherapy for experimental pneumococcal pneumonia by polyvalent human immunoglobulin or F(ab')2 fragments administered intranasally. *J. Infect. Dis.* 173(5):1123-1128.

446. Harmsen MM, van Solt CB, van Zijderveld-van Bemmel AM, Niewold TA, & van Zijderveld FG (2006) Selection and optimization of proteolytically stable llama single-domain antibody fragments for oral immunotherapy. *Appl. Microbiol. Biotechnol.* 72(3):544-551.

447. Wesolowski J*, et al.* (2009) Single domain antibodies: promising experimental and therapeutic tools in infection and immunity. *Med. Microbiol. Immunol.* 198(3):157-174.

448. Behar G*, et al.* (2008) Isolation and characterization of anti-FcgammaRIII (CD16) llama single-domain antibodies that activate natural killer cells. *Protein Eng. Des. Sel.* 21(1):1-10.

449. Tschopp J, Masson D, & Schafer S (1986) Inhibition of the lytic activity of perforin by lipoproteins. *J. Immunol.* 137(6):1950-1953.

450. Young JD, Damiano A, DiNome MA, Leong LG, & Cohn ZA (1987) Dissociation of membrane binding and lytic activities of the lymphocyte pore-forming protein (perforin). *J. Exp. Med.* 165(5):1371-1382.

451. Rajman I, Eacho PI, Chowienczyk PJ, & Ritter JM (1999) LDL particle size: an important drug target? *Br. J. Clin. Pharmacol.* 48(2):125-133.

452. Kumar V*, et al.* (2011) Three-Dimensional cryoEM Reconstruction of Native LDL Particles to 16 angstrom Resolution at Physiological Body Temperature. *PLoS One* 6(5).

453. Schumaker VN, Phillips ML, & Chatterton JE (1994) Apolipoprotein-B and Low-Density-Lipoprotein Structure - Implications for Biosynthesis of Triglyceride-Rich Lipoproteins. *Advances in Protein Chemistry, Vol 45* 45:205-248.

454. Bahr GF, Bloom G, & Friberg U (1957) Volume changes of tissues in physiological fluids during fixation in osmium tetroxide or formaldehyde and during subsequent treatment. *Exp. Cell Res.* 12(2):342-355.

455. Hevonoja T, Pentikainen MO, Hyvonen MT, Kovanen PT, & Ala-Korpela M (2000) Structure of low density lipoprotein (LDL) particles: Basis for understanding molecular changes in modified LDL. *Biochimica Et Biophysica Acta-Molecular and Cell Biology of Lipids* 1488(3):189-210.

456. Steim JM, Edner OJ, & Bargoot FG (1968) Structure of human serum lipoproteins: nuclear magnetic resonance supports a micellar model. *Science* 162(3856):909-911.

457. Prassl R & Laggner P (2009) Molecular structure of low density lipoprotein: current status and future challenges. *European Biophysics Journal with Biophysics Letters* 38(2):145-158.

458. Segrest JP, Jones MK, De Loof H, & Dashti N (2001) Structure of apolipoprotein B-100 in low density lipoproteins. *J. Lipid Res.* 42(9):1346-1367.

459. Brown MS, Kovanen PT, & Goldstein JL (1981) Regulation of plasma cholesterol by lipoprotein receptors. *Science* 212(4495):628-635.

460. Fiers W, Beyaert R, Declercq W, & Vandenabeele P (1999) More than one way to die: apoptosis, necrosis and reactive oxygen damage. *Oncogene* 18(54):7719-7730.

461. Yoshiike Y, Kayed R, Milton SC, Takashima A, & Glabe CG (2007) Pore-forming proteins share structural and functional homology with amyloid oligomers. *Neuromolecular Med.* 9(3):270-275.

462. Gurcel L, Abrami L, Girardin S, Tschopp J, & van der Goot FG (2006) Caspase-1 activation of lipid metabolic pathways in response to bacterial pore-forming toxins promotes cell survival. *Cell* 126(6):1135-1145.

463. Pross HF, Baines MG, Rubin P, Shragge P, & Patterson MS (1981) Spontaneous Human Lymphocyte-Mediated Cyto-Toxicity against Tumor Target-Cells .9. The Quantitation of Natural-Killer Cell-Activity. *J. Clin. Immunol.* 1(1):51-63.

464. Long EO (2008) Negative signaling by inhibitory receptors: the NK cell paradigm. *Immunol. Rev.* 224:70-84.

465. Choi PJ & Mitchison TJ (2013) Imaging burst kinetics and spatial coordination during serial killing by single natural killer cells. *Proc. Natl. Acad. Sci. U. S. A.* 110(16):6488-6493.

466. Bhat R & Watzl C (2007) Serial killing of tumor cells by human natural killer cells--enhancement by therapeutic antibodies. *PLoS One* 2(3):e326.

467. Vanherberghen B*, et al.* (2013) Classification of human natural killer cells based on migration behavior and cytotoxic response. *Blood* 121(8):1326-1334.

468. Alsmadi O & Tilley SA (1998) Antibody-dependent cellular cytotoxicity directed against cells expressing human immunodeficiency virus type 1 envelope of primary or laboratory-adapted strains by human and chimpanzee

monoclonal antibodies of different epitope specificities. *J. Virol.* 72(1):286-293.

469. Laoprasopwattana K*, et al.* (2007) Antibody-dependent cellular cytotoxicity mediated by plasma obtained before secondary dengue virus infections: potential involvement in early control of viral replication. *J. Infect. Dis.* 195(8):1108-1116.
470. Torisu-Itakura H*, et al.* (2011) Redirected lysis of human melanoma cells by a MCSP/CD3-bispecific BiTE antibody that engages patient-derived T cells. *J. Immunother.* 34(8):597-605.
471. Liddy N*, et al.* (2012) Monoclonal TCR-redirected tumor cell killing. *Nat. Med.* 18(6):980-987.
472. Germain C*, et al.* (2008) Redirecting NK cells mediated tumor cell lysis by a new recombinant bifunctional protein. *Protein Engineering Design & Selection* 21(11):665-672.
473. Deguine J, Breart B, Lemaitre F, & Bousso P (2012) Cutting edge: tumor-targeting antibodies enhance NKG2D-mediated NK cell cytotoxicity by stabilizing NK cell-tumor cell interactions. *J. Immunol.* 189(12):5493-5497.
474. Sandusky MM, Messmer B, & Watzl C (2006) Regulation of 2B4 (CD244)-mediated NK cell activation by ligand-induced receptor modulation. *Eur. J. Immunol.* 36(12):3268-3276.
475. Debanne D, Bialowas A, & Rama S (2013) What are the mechanisms for analogue and digital signalling in the brain? *Nat. Rev. Neurosci.* 14(1):63-69.
476. Das J (2010) Activation or tolerance of natural killer cells is modulated by ligand quality in a nonmonotonic manner. *Biophys. J.* 99(7):2028-2037.
477. Tkach KE*, et al.* (2014) T cells translate individual, quantal activation into collective, analog cytokine responses via time-integrated feedbacks. *Elife* 3:e01944.
478. Fadok VA*, et al.* (1998) Macrophages that have ingested apoptotic cells in vitro inhibit proinflammatory cytokine production through autocrine/paracrine mechanisms involving TGF-beta, PGE2, and PAF. *J. Clin. Invest.* 101(4):890-898.
479. Sanborn KB & Orange JS (2010) Navigating barriers: the challenge of directed secretion at the natural killer cell lytic immunological synapse. *J. Clin. Immunol.* 30(3):358-363.

480. Regunathan J, Chen Y, Wang D, & Malarkannan S (2005) NKG2D receptor-mediated NK cell function is regulated by inhibitory Ly49 receptors. *Blood* 105(1):233-240.

481. Martinez E, Brzostowski JA, Long EO, & Gross CC (2011) Cutting Edge: NKG2D-Dependent Cytotoxicity Is Controlled by Ligand Distribution in the Target Cell Membrane. *J. Immunol.* 186(10):5538-5542.

482. Raffaghello L*, et al.* (2004) Downregulation and/or release of NKG2D ligands as immune evasion strategy of human neuroblastoma. *Neoplasia* 6(5):558-568.

483. Salih HR, Rammensee HG, & Steinle A (2002) Cutting edge: down-regulation of MICA on human tumors by proteolytic shedding. *J. Immunol.* 169(8):4098-4102.

484. Hanna J*, et al.* (2004) Novel APC-like properties of human NK cells directly regulate T cell activation. *J. Clin. Invest.* 114(11):1612-1623.

485. Stinchcombe JC & Griffiths GM (1999) Regulated secretion from hemopoietic cells. *J. Cell Biol.* 147(1):1-6.

486. Dybkaer K*, et al.* (2007) Genome wide transcriptional analysis of resting and IL2 activated human natural killer cells: gene expression signatures indicative of novel molecular signaling pathways. *BMC Genomics* 8:230.

487. Raucher D & Sheetz MP (2000) Cell spreading and lamellipodial extension rate is regulated by membrane tension. *J. Cell Biol.* 148(1):127-136.

488. Coombs D, Dembo M, Wofsy C, & Goldstein B (2004) Equilibrium thermodynamics of cell-cell adhesion mediated by multiple ligand-receptor pairs. *Biophys. J.* 86(3):1408-1423.

489. Burroughs NJ & Wulfing C (2002) Differential segregation in a cell-cell contact interface: the dynamics of the immunological synapse. *Biophys. J.* 83(4):1784-1796.

490. Dustin ML*, et al.* (1998) A novel adaptor protein orchestrates receptor patterning and cytoskeletal polarity in T-cell contacts. *Cell* 94(5):667-677.

491. Donnadieu E, Revy P, & Trautmann A (2001) Imaging T-cell antigen recognition and comparing immunological and neuronal synapses. *Immunology* 103(4):417-425.

492. Roda-Navarro P & Reyburn HT (2007) Intercellular protein transfer at the NK cell immune synapse: mechanisms and physiological significance. *FASEB J.* 21(8):1636-1646.

493. Togo T, Krasieva TB, & Steinhardt RA (2000) A decrease in membrane tension precedes successful cell-membrane repair. *Mol. Biol. Cell* 11(12):4339-4346.

494. Yun CH*, et al.* (2005) Natural killer cells and Helicobacter pylori infection: bacterial antigens and interleukin-12 act synergistically to induce gamma interferon production. *Infect. Immun.* 73(3):1482-1490.

495. Lindgren A, Pavlovic V, Flach CF, Sjoling A, & Lundin S (2011) Interferon-gamma secretion is induced in IL-12 stimulated human NK cells by recognition of Helicobacter pylori or TLR2 ligands. *Innate Immun.* 17(2):191-203.

496. Nausch N & Cerwenka A (2008) NKG2D ligands in tumor immunity. *Oncogene* 27(45):5944-5958.

497. Spear P, Wu MR, Sentman ML, & Sentman CL (2013) NKG2D ligands as therapeutic targets. *Cancer Immun.* 13:8.

498. Groh V*, et al.* (1996) Cell stress-regulated human major histocompatibility complex class I gene expressed in gastrointestinal epithelium. *Proc. Natl. Acad. Sci. U. S. A.* 93(22):12445-12450.

499. Eagle RA, Jafferji I, & Barrow AD (2009) Beyond Stressed Self: Evidence for NKG2D Ligand Expression on Healthy Cells. *Curr. Immunol. Rev.* 5(1):22-34.

500. Kim U, Baumler A, Carruthers C, & Bielat K (1975) Immunological escape mechanism in spontaneously metastasizing mammary tumors. *Proc. Natl. Acad. Sci. U. S. A.* 72(3):1012-1016.

501. Vasmel WL, Sijts EJ, Leupers CJ, Matthews EA, & Melief CJ (1989) Primary virus-induced lymphomas evade T cell immunity by failure to express viral antigens. *J. Exp. Med.* 169(4):1233-1254.

502. Maeurer MJ*, et al.* (1996) Tumor escape from immune recognition: lethal recurrent melanoma in a patient associated with downregulation of the peptide transporter protein TAP-1 and loss of expression of the immunodominant MART-1/Melan-A antigen. *J. Clin. Invest.* 98(7):1633-1641.

503. Garcia-Iglesias T*, et al.* (2009) Low NKp30, NKp46 and NKG2D expression and reduced cytotoxic activity on NK cells in cervical cancer and precursor lesions. *BMC Cancer* 9:186.

504. Groh V, Wu J, Yee C, & Spies T (2002) Tumour-derived soluble MIC ligands impair expression of NKG2D and T-cell activation. *Nature* 419(6908):734-738.

505. Romee R, *et al.* (2013) NK cell CD16 surface expression and function is regulated by a disintegrin and metalloprotease-17 (ADAM17). *Blood* 121(18):3599-3608.

506. Mace EM, *et al.* (2014) Cell biological steps and checkpoints in accessing NK cell cytotoxicity. *Immunol. Cell Biol.* 92(3):245-255.

507. Zompi S, *et al.* (2003) NKG2D triggers cytotoxicity in mouse NK cells lacking DAP12 or Syk family kinases. *Nat. Immunol.* 4(6):565-572.

508. Cella M, *et al.* (2004) Differential requirements for Vav proteins in DAP10- and ITAM-mediated NK cell cytotoxicity. *J. Exp. Med.* 200(6):817-823.

509. Jiang K, *et al.* (2000) Pivotal role of phosphoinositide-3 kinase in regulation of cytotoxicity in natural killer cells. *Nat. Immunol.* 1(5):419-425.

510. Tassi I, *et al.* (2005) Phospholipase C-gamma 2 is a critical signaling mediator for murine NK cell activating receptors. *J. Immunol.* 175(2):749-754.

511. Caraux A, *et al.* (2006) Phospholipase C-gamma2 is essential for NK cell cytotoxicity and innate immunity to malignant and virally infected cells. *Blood* 107(3):994-1002.

512. Regunathan J, *et al.* (2006) Differential and nonredundant roles of phospholipase Cgamma2 and phospholipase Cgamma1 in the terminal maturation of NK cells. *J. Immunol.* 177(8):5365-5376.

513. Bonnema JD, Karnitz LM, Schoon RA, Abraham RT, & Leibson PJ (1994) Fc receptor stimulation of phosphatidylinositol 3-kinase in natural killer cells is associated with protein kinase C-independent granule release and cell-mediated cytotoxicity. *J. Exp. Med.* 180(4):1427-1435.

514. Andrin C, *et al.* (1998) Interaction between a Ca2+-binding protein calreticulin and perforin, a component of the cytotoxic T-cell granules. *Biochemistry* 37(29):10386-10394.

515. Garg S, *et al.* (2013) Calcium-dependent permeabilization of erythrocytes by a perforin-like protein during egress of malaria parasites. *Nature communications* 4:1736.

516. Kataoka T, Togashi K, Takayama H, Takaku K, & Nagai K (1997) Inactivation and proteolytic degradation of perforin within lytic granules upon neutralization of acidic pH. *Immunology* 91(3):493-500.

517. Li Y, Wang Q, & Mariuzza RA (2011) Structure of the human activating natural cytotoxicity receptor NKp30 bound to its tumor cell ligand B7-H6. *J. Exp. Med.* 208(4):703-714.

518. Piguet V & Sattentau Q (2004) Dangerous liaisons at the virological synapse. *The Journal of clinical investigation* 114(5):605-610.

519. Chowdhury D & Lieberman J (2008) Death by a thousand cuts: Granzyme pathways of programmed cell death. *Annu. Rev. Immunol.* 26:389-420.

520. Kelso A*, et al.* (2002) The genes for perforin, granzymes A-C and IFN-gamma are differentially expressed in single CD8(+) T cells during primary activation. *Int. Immunol.* 14(6):605-613.

521. Ishiura S*, et al.* (1990) Calcium is essential for both the membrane binding and lytic activity of pore-forming protein (perforin) from cytotoxic T-lymphocyte. *Mol. Immunol.* 27(8):803-807.

522. Ealick SE*, et al.* (1991) Three-dimensional structure of recombinant human interferon-gamma. *Science* 252(5006):698-702.

523. Sanderson NS*, et al.* (2012) Cytotoxic immunological synapses do not restrict the action of interferon-gamma to antigenic target cells. *Proc. Natl. Acad. Sci. U. S. A.* 109(20):7835-7840.

524. Perona-Wright G, Mohrs K, & Mohrs M (2010) Sustained signaling by canonical helper T cell cytokines throughout the reactive lymph node. *Nat. Immunol.* 11(6):520-526.

525. Holmes TD*, et al.* (2011) A human NK cell activation/inhibition threshold allows small changes in the target cell surface phenotype to dramatically alter susceptibility to NK cells. *J. Immunol.* 186(3):1538-1545.

526. Lanier LL (2008) Up on the tightrope: natural killer cell activation and inhibition. *Nat. Immunol.* 9(5):495-502.

527. Pietra G*, et al.* (2012) Melanoma cells inhibit natural killer cell function by modulating the expression of activating receptors and cytolytic activity. *Cancer Res.* 72(6):1407-1415.

528. Punt CJ*, et al.* (1994) Anti-tumor antibody produced by human tumor-infiltrating and peripheral blood B lymphocytes. *Cancer Immunol. Immunother.* 38(4):225-232.

529. Isaguliants MG*, et al.* (2002) Antibody responses against B-cell epitopes of the hypervariable region 1 of hepatitis C virus in self-limiting and chronic human hepatitis C followed-up using consensus peptides. *J. Med. Virol.* 66(2):204-217.

530. Luther SA, Gulbranson-Judge A, Acha-Orbea H, & MacLennan IC (1997) Viral superantigen drives extrafollicular and follicular B cell differentiation leading to virus-specific antibody production. *J. Exp. Med.* 185(3):551-562.

531. Wardemann H*, et al.* (2003) Predominant autoantibody production by early human B cell precursors. *Science* 301(5638):1374-1377.

532. Gruda R*, et al.* (2012) Loss of kindlin-3 alters the threshold for NK cell activation in human leukocyte adhesion deficiency-III. *Blood* 120(19):3915-3924.

533. Lee MS*, et al.* (2006) Integrin signaling and cell spreading mediated by phorbol 12-myristate 13-acetate treatment. *J. Cell. Biochem.* 99(1):88-95.

534. D'Souza-Schorey C, Boettner B, & Van Aelst L (1998) Rac regulates integrin-mediated spreading and increased adhesion of T lymphocytes. *Mol. Cell. Biol.* 18(7):3936-3946.

535. Somersalo K*, et al.* (1995) Activation of natural killer cell migration by leukocyte integrin-binding peptide from intracellular adhesion molecule-2 (ICAM-2). *J. Biol. Chem.* 270(15):8629-8636.

536. Li J*, et al.* (2014) Tumour biomechanical response to the vascular disrupting agent ZD6126 in vivo assessed by magnetic resonance elastography. *Br. J. Cancer* 110(7):1727-1732.

537. Mouw JK*, et al.* (2014) Tissue mechanics modulate microRNA-dependent PTEN expression to regulate malignant progression. *Nat. Med.* 20(4):360-367.

538. Discher DE, Janmey P, & Wang YL (2005) Tissue cells feel and respond to the stiffness of their substrate. *Science* 310(5751):1139-1143.

539. Li J, Han D, & Zhao YP (2014) Kinetic behaviour of the cells touching substrate: the interfacial stiffness guides cell spreading. *Sci. Rep.* 4:3910.

540. Yeung T*, et al.* (2005) Effects of substrate stiffness on cell morphology, cytoskeletal structure, and adhesion. *Cell Motil. Cytoskeleton* 60(1):24-34.

541. Irwin EF*, et al.* (2008) Modulus-dependent macrophage adhesion and behavior. *J. Biomater. Sci. Polym. Ed.* 19(10):1363-1382.

542. Aydin D*, et al.* (2010) Polymeric substrates with tunable elasticity and nanoscopically controlled biomolecule presentation. *Langmuir* 26(19):15472-15480.

543. Simmons CS, Ribeiro AJ, & Pruitt BL (2013) Formation of composite polyacrylamide and silicone substrates for independent control of stiffness and strain. *Lab Chip* 13(4):646-649.

544. de Rham C*, et al.* (2007) The proinflammatory cytokines IL-2, IL-15 and IL-21 modulate the repertoire of mature human natural killer cell receptors. *Arthrit. Res. Ther.* 9(6).

545. Huenecke S*, et al.* (2010) IL-2-driven Regulation of NK Cell Receptors With Regard to the Distribution of CD16(+) and CD16(-) Subpopulations and In Vivo Influence After Haploidentical NK Cell Infusion. *J. Immunother.* 33(2):200-210.

546. Voskens CJ*, et al.* (2010) Ex-vivo expanded human NK cells express activating receptors that mediate cytotoxicity of allogeneic and autologous cancer cell lines by direct recognition and antibody directed cellular cytotoxicity. *J. Exp. Clin. Cancer Res.* 29.

547. Horng T, Bezbradica JS, & Medzhitov R (2007) NKG2D signaling is coupled to the interleukin 15 receptor signaling pathway. *Nat. Immunol.* 8(12):1345-1352.

548. Beuneu H*, et al.* (2009) Dynamic behavior of NK cells during activation in lymph nodes. *Blood* 114(15):3227-3234.

549. Mortier E, Woo T, Advincula R, Gozalo S, & Ma A (2008) IL-15Ralpha chaperones IL-15 to stable dendritic cell membrane complexes that activate NK cells via trans presentation. *The Journal of experimental medicine* 205(5):1213-1225.

550. Minagawa M*, et al.* (2002) Enforced expression of Bcl-2 restores the number of NK cells, but does not rescue the impaired development of NKT cells or intraepithelial lymphocytes, in IL-2/IL-15 receptor beta-chain-deficient mice. *J. Immunol.* 169(8):4153-4160.

551. Imada K*, et al.* (1998) Stat5b is essential for natural killer cell-mediated proliferation and cytolytic activity. *J. Exp. Med.* 188(11):2067-2074.

552. Makino S*, et al.* (1980) Breeding of a non-obese, diabetic strain of mice. *Jikken Dobutsu* 29(1):1-13.

553. Kikutani H & Makino S (1992) The murine autoimmune diabetes model: NOD and related strains. *Adv. Immunol.* 51:285-322.

554. Kagi D*, et al.* (1997) Reduced incidence and delayed onset of diabetes in perforin-deficient nonobese diabetic mice. *J. Exp. Med.* 186(7):989-997.

555. Shi FD & Zhou Q (2011) Natural killer cells as indispensable players and therapeutic targets in autoimmunity. *Autoimmunity* 44(1):3-10.

556. Zamai L*, et al.* (2007) NK cells and cancer. *J. Immunol.* 178(7):4011-4016.

557. Corral L, Takizawa H, Hanke T, Jamieson AM, & Raulet DH (1999) A new monoclonal antibody reactive with several Ly49 NK cell receptors mediates redirected lysis of target cells. *Hybridoma* 18(4):359-366.

558. Cheon DJ & Orsulic S (2011) Mouse models of cancer. *Annu. Rev. Pathol.* 6:95-119.